AD NUMBER

AD815481

LIMITATION CHANGES

TO:

Approved for public release; distribution is unlimited.

FROM:

Distribution authorized to U.S. Gov't. agencies and their contractors; Critical Technology; FEB 1967. Other requests shall be referred to Office of Naval Research, Attn: Code 421, One Liberty Center, 875 North Randolph Street, Arlington, VA 22203-1995. This document contains export-controlled technical data.

AUTHORITY

ONR ltr dtd 28 Aug 1968

IRIA State-of-the-Art Report

BAND-MODEL METHODS FOR COMPUTING ATMOSPHERIC SLANT-PATH MOLECULAR ABSORPTION

DAVID ANDING

February 1967 NAVSO P-2499-1

INFRARED AND OPTICAL SENSOR LABORATORY
Willow Run Laboratories
THE INSTITUTE OF SCIENCE AND TECHNOLOGY

Contract NOnr 1224(52)

7142-21-T

IRIA State-of-the-Art Report

BAND-MODEL METHODS FOR COMPUTING ATMOSPHERIC SLANT-PATH MOLECULAR ABSORPTION

DAVID ANDING

February 1967

Infrared and Optical Sensor Laboratory
Willow Run Laboratories
THE INSTITUTE OF SCIENCE AND TECHNOLOGY
THE UNIVERSITY OF MICHIGAN
Ann Arbor, Michigan

ACKNOWLEDGMENTS

The author wishes to acknowledge the assistance of Harvey M. Rose, who provided first-draft versions of sections 4, 5, and 6, and who contributed largely to the many computational and plotting labors encountered in the writing of this report. I am particularly indebted to George Oppel for his technical advice and suggestions, and for providing the necessary information for section 2.3.

The author is also indebted to William L. Wolfe of the Radiation Center of Honeywell, Inc., and Thomas Limperis of the Willow Run Laboratories for their advice and comments.

PREFACE

The IRIA (Infrared Information and Analysis) Center, a part of the Willow Run Laboratories of The University of Michigan's Institute of Science and Technology, is responsible for collecting, analyzing, and disseminating to authorized recipients all information concerning military infrared research and development. To this end, IRIA prepares annotated bibliographies, request subject bibliographies, state-of-the-art reports, The Proceedings of IRIS, and other special publications. IRIA also sponsors symposiums and maintains a staff of specialists in infrared technology to assist and advise visitors. The consulting services offered by IRIA are available to qualified requesters without charge.

For its first ten years IRIA was supported by a tri-service contract, NOnr 1224(12), and reports were issued under Project 2389. Effective March 1965, IRIA is being supported by a new tri-service contract, NOnr 1224(52), and reports will be issued under Project 7142. The contract is administered by the Office of Naval Research, Physics Branch; a steering committee consisting of representatives of the three military services assists in the technical direction of the work.

The quarterly IRIA Annotated Bibliographies and The Proceedings of IRIS are sent to all those on the IRIS distribution list. In addition to receiving these publications, those on the IRIS distribution list are notified of all other IRIA publications. To be added to the list send a request via appropriate security channels to Mr. T. B. Dowd, Office of Naval Research, 495 Summer St., Boston, Massachusetts 02210.

ABSTRACT

The general transmissivity equation for computing slant-path molecular absorption spectra is developed and two methods for evaluating this equation, the direct integration and that which assumes a model of the band structure, are discussed. Five band models are discussed and twelve methods for computing molecular absorption based on these band models are presented. Spectra computed by band-model methods are compared with spectra calculated by direct integration of the general transmissivity equation and with open-air field measurements of absorption spectra. Conclusions concerning the capability of band-model methods for predicting slant-path absorption spectra are stated and recommendations for future research are outlined. A summary of open-air field measurements of absorption spectra and laboratory measurements of absorption spectra for homogeneous paths is presented and a computer program for computing the equivalent sea-level path, the Curtis-Godson equivalent pressure, and the absorber concentration for atmospheric slant paths for any model atmosphere is given in appendix I.

CONTENTS

FIGURES

TABLES

BAND-MODEL METHODS FOR COMPUTING ATMOSPHERIC SLANT-PATH MOLECULAR ABSORPTION

1 INTRODUCTION

The literature devoted to the development and presentation of methods for computing atmospheric slant-path molecular absorption based on assuming models of the band structure is extensive. This state-of-the-art report summarizes the literature, discusses the advantages and limitations of such methods, and demonstrates the degree of correctness with which absorption spectra computed by band-model methods can predict the true absorption spectra for an atmospheric slant path.

In recent years there has been considerable interest in predicting the amount of atmospheric attenuation of electromagnetic radiation for a wavelength range extending from the visible to the far infrared. Knowledge of the amount of radiation which will be transmitted by the atmosphere between a heat source and a detector is required for the design of infrared equipment. Other concerns are the amount of sky-background radiation a detector will see and problems of radiation transfer in the atmosphere. These diverse problems require values of attenuation spectra ranging from mere approximate values of attenuation for broad spectral intervals to fairly accurate, high-resolution attenuation spectra.

In order to fulfill such diverse requirements, extensive research has been done in the past decade with the objective, first, of specifying and defining the problem of atmospheric attenuation, and second, of developing methods for predicting the attenuation for arbitrary atmospheric slant paths for assumed model atmospheres.

In general, there are five attenuating mechanisms which may be associated with the atmosphere:

(1) Absorption by the ozone in the Hartley continuum
(2) Rayleigh scattering by molecular nitrogen and oxygen
(3) Particulate or Mie scattering
(4) Resonance atomic absorption
(5) Molecular band absorption

In the spectral range from 0.2 to 0.32 μ, photo-absorption associated with the decomposition of ozone plays a dominant role in attenuation. In this range, attenuation is very sensitive to wavelength and the ozone density. Unfortunately, the ozone density is a complex function of altitude, the functional relationship being variable with time and geographic location.

Rayleigh scattering by molecular nitrogen and oxygen must be considered in the ultraviolet and visible regions. From the standpoint of both the distribution of the scattering matter and the wavelength dependence of the absorption coefficients, this is the simplest of the attenuating mechanisms to be considered here.

The presence of haze or trace distributions of particulate matter in the atmosphere causes Mie scattering—a phenomenon of particular importance to ground-based observations. This scattering problem becomes less acute as reasonable altitudes are achieved since the particulate matter is generally confined to lower altitudes. It is a rather complex problem, however, because the wavelength dependence of the absorption coefficient is a function of particle size. The spatial distribution of particulate matter is fairly complex and still relatively unknown.

The most complicated and difficult attenuation problem arises from molecular band absorption. The molecules in the atmosphere which have vibration-rotation resonance frequencies in the infrared, and hence give rise to absorption, are water vapor (H_2O), carbon dioxide (CO_2), ozone (O_3), nitrous oxide (N_2O), methane (CH_4), and carbon monoxide (CO). H_2O, CO_2, and O_3 cause the greatest amount of absorption because they have strong absorption bands and exist in the atmosphere at relatively high concentration. The molecular species CO, N_2O, and CH_4 demonstrate significant amounts of absorption only when the line of sight passes through a large number of air masses.

To completely specify the amount of attenuation of some source of radiation as it traverses an atmospheric slant path, it would be necessary to consider each of the five mechanisms. However, each attenuation mechanism constitutes a complex problem warranting separate treatment. In this report we consider only the problem of molecular absorption, and place particular emphasis on band-model methods of computing the absorption caused by an atmospheric slant path.

The problem of calculating the molecular absorption by any one of the absorbing species mentioned above is extremely complex because of the many variables that must be known before the computation can be performed. In general, it is necessary to specify the meteorological conditions that exist at each point along the path, including pressure, temperature, and the concentration of each absorber. Also, for a given wavelength interval, the location, intensity, and shape of each absorption line must be specified as well as the functional relationships between these parameters and meteorological conditions. If all of the above quantities are known, then the absorption spectra for any desired resolution can be determined by summing the contribution to absorption of each spectral line throughout a given wavelength interval. This method is most easily applied to homogeneous paths but can be extended to slant paths by performing a direct pressure integration along the path.

The method of summing the contribution of each spectral line is the most rigorous way of determinlng atmospheric absorption since it involves a direct integration of the generai transmissivity function which specifies the absorption of an atmospheric slant path. Although rigorous, this method has not received general application for all absorbing species and all spectral regions since the necessary line parameters are known fairly accurately for only a small portion of the spectrum for the major absorbing species and are almost unknown for the minor constituents. Because knowledge of the band parameters is limited and because the direct integration involves such extensive computational labor, almost all of the currently available methods for computing absorption use approximations which reduce the general transmissivity function to a form which expresses the transmission averaged over some interval, in terms of elementary functions. The simplified equation is then used in conjunction with laboratory homogeneous-path data to predict absorption for other homogeneous paths. This last restriction necessitates the reduction of a slant path to an equivalent homogeneous path. The standard approach used in performing the simplification of the general transmissivity function is to use a model of the band structure, that is, to assume that the line positions and strengths are distributed in a way that can be presented by a mathematical model.

It should be pointed out that both the rigorous calculations and the band-model methods require laboratory data, but with this difference: the rigorous calculations depend upon high-resolution spectra to obtain the necessary line parameters prior to performing the direct integration. Band model methods involve empirically fitting the integrated transmissivity function to laboratory spectra to specify equivalent line parameters.

The rigorous calculations would appear to yield results that are more exact since the line positions are not simulated. However, the model calculations are more accurate at the present time for some molecules in some spectral regions. The reason for this is related to the inaccuracies in the shape, intensity, and half-width of the spectral lines. The great advantage of using a direct integration is the ability to extrapolate over extreme ranges of pressure, temperature, and absorber concentration and the fact that much higher resolution is obtainable than from band-model calculations.

In section 2 of this report, the general transmissivity function for determining atmospheric slant-path absorption is derived and the simplification of this function through the use of band models is performed. The equations for determining an equivalent homogeneous path for an atmospheric slant path are also derived and methods of empirically fitting band-model absorption equations to homogeneous-path absorption spectra are presented.

2
GENERAL THEORY OF ATMOSPHERIC ABSORPTION

The atoms of any molecule not at absolute zero are constantly oscillating about their positions of equilibrium. The amplitudes of these oscillations are extremely minute and their frequencies are high. Since these frequencies are of the same orders of magnitude as are infrared radiations, some direct relationship might be expected between motions of the atoms within molecules and their effects on infrared radiation incident upon the atoms. Actually, those molecular vibrations which are accompanied by a change of dipole moment, so-called "infrared-active" vibrations, absorb by resonance all or part of the incident radiation, provided the frequencies of the latter coincide exactly with those of the intramolecular vibrations. Thus, if a sample of molecules of a single absorbing species is irradiated in succession by a series of monochromatic bands of infrared, and the percentage of radiation transmitted is plotted as a function of either wavelength or frequency, the resulting graph will show regions of absorption centered at each of the resonant frequencies. The percentage transmission is generally different for each resonant frequency, depending upon the energy of the molecular transition. These regions of absorption are known as spectral lines. If the sample of molecules being irradiated is at a pressure so low that there is a minimal amount of molecular interaction and at a temperature so low that there is little relative molecular motion, then each of the spectral lines would be extremely narrow and in the limit would have an infinitesimal width. For atmospheric conditions the pressures are such that there is a significant molecular interaction giving rise to spectral lines which absorb over a range of frequencies. Although asymmetrical lines have been observed for some molecules under some conditions, for the most part the absorption of a spectral line is a maximum at the resonant frequency and decreases to zero asymptotically at smaller and greater frequencies in a symmetrical manner.

Because the spectral lines of atmospheric gases are generally clustered in bands of frequencies, there are certain broad regions where no absorption exists and other regions where the absorption is almost continuous. For example, water vapor has two absorption bands near 2.7 μ containing approximately 4000 spectral lines. Figure 1 shows the near-infrared solar spectrum of atmospheric air and laboratory absorption spectra for each of the infrared-active atmospheric gases. In order of presentation, carbon monoxide has one fairly weak band at approximately 4.8 μ. Methane has two regions of absorption at 3.2 and 7.8 μ. The second methane band is almost completely obscured by nitrous oxide which also absorbs at 7.8 μ. The strongest of the two nitrous oxide bands is centered at approximately 4.7 μ. Ozone has two bands, one at 9.6 μ and the other at 14 μ. The two remaining gases, carbon dioxide and water vapor, are the

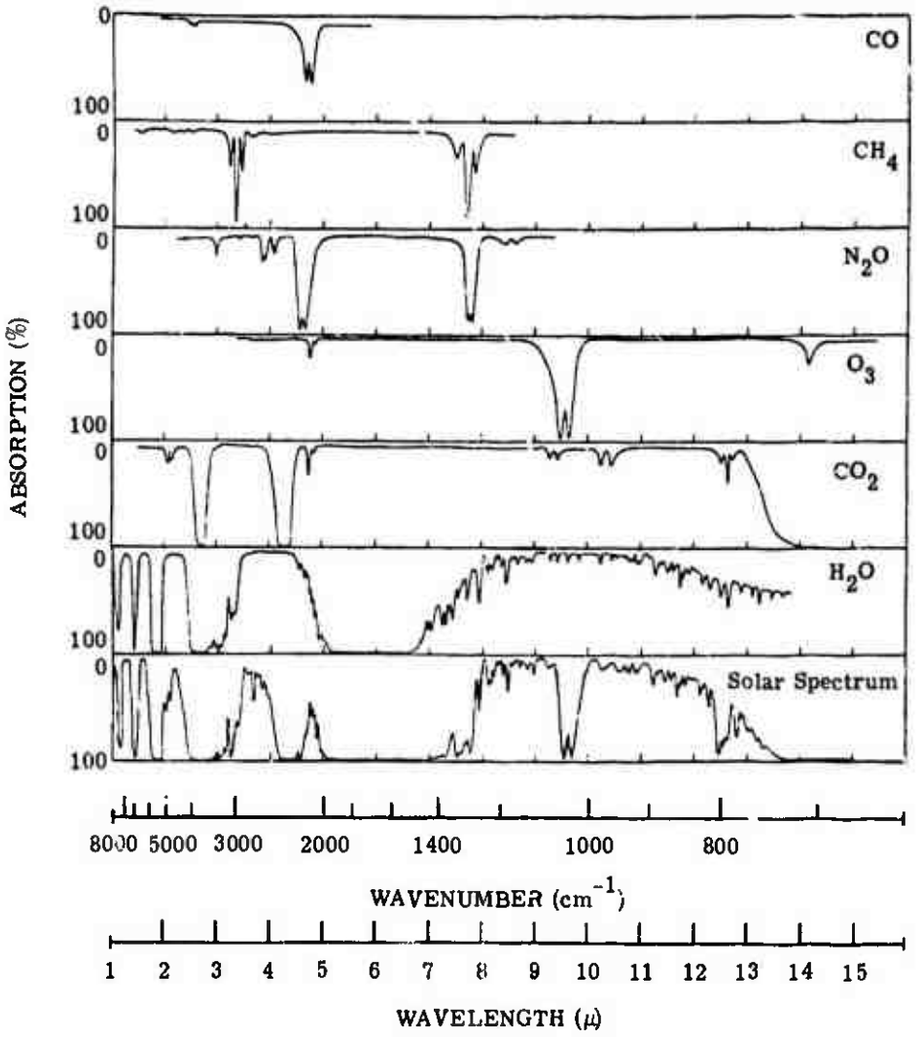

FIGURE 1. THE NEAR-INFRARED SPECTRA OF SOLAR IRRADIATION AND OF CO, CH_4, N_2O, O_3, CO_2, AND H_2O

most significant contributors to atmospheric absorption. Carbon dioxide has three strong bands at 2.7, 4.3, and 15 μ. Water vapor has a greater number of absorption bands than any other absorbing species with bands at 1.14, 1.38, 1.88, 2.7, 3.2, and 6.3 μ.

The absorption of infrared radiation by atmospheric gases is then characterized by discrete bands consisting of a large number of overlapping spectral lines of various strengths which are distributed throughout the band. The degree of overlapping depends upon the line half-width, and the distribution of lines throughout an absorption band depends upon the absorbing molecule. For example, the line positions for water vapor are distributed unevenly, in contrast to carbon dioxide, which displays a relatively regular spectral-line distribution.

2.1. GENERAL EQUATION FOR SLANT-PATH ABSORPTION

The general equation which specifies the molecular absorption of an atmospheric slant path composed of a single absorbing gas may be derived by considering the Lambert-Beer law. This law is rigorous when the absorption coefficient does not vary over the spectral bandwidth under consideration. It states that the decrease in spectral intensity $dI(x, \nu)$ which is caused by absorption in a (thin) differential section of path dx, is proportional to dx, to the intensity $I(x, \nu)$ of the radiation incident on the front face, and to the concentration $\rho(x)$ of the absorbing molecule. The proportionality constant is designated $k(x, \nu)$. Mathematically,

$$dI(x, \nu) = -I(x, \nu)k(x, \nu)\rho(x)\,dx$$

Integration gives the transmission τ over a path from $x = 0$ to $x = X$.

$$\tau(X, \nu) = \exp\left[-\int_0^X k(x, \nu)\rho(x)\,dx\right]$$

To determine the transmission over a finite frequency interval the average is taken:

$$\overline{\tau(X, \nu)} = \frac{1}{\Delta\nu}\int_{\Delta\nu}\left\{\exp\left[-\int_0^X k(x, \nu)\rho(x)\,dx\right]\right\}d\nu$$

Rewriting in terms of absorption, we have the average absorption for the frequency interval $\Delta\nu$ given by

$$A = \frac{1}{\Delta\nu}\int_{\Delta\nu}\left\{1 - \exp\left[\int_0^X k(x, \nu)\rho(x)\,dx\right]\right\}d\nu \qquad (1)$$

where $\rho(x)$ is the density of the absorbing gas

x is the distance along the path

$k(x, \nu)$ is the absorption coefficient

The absorption and its functional form with respect to the path therefore depend upon the form of the absorption coefficient within the interval $\Delta\nu$. Let us assume that the interval $\Delta\nu$ contains a single spectral line and let us specify the various forms of $k(x, \nu)$, where each form depends upon the environmental conditions of the absorbing gas.

If only one molecule of gas were present, the form of $k(x, \nu)$ would simply be a constant having a value only at ν_0, the center frequency of the spectral line. In general, there are many gas molecules present and the fact that gas molecules collide gives rise to the Lorentz pressure-broadened line which is considered fundamental for the whole theory of atmospheric transmission. The form of $k(x, \nu)$ as given by the Lorentz theory is

$$k(x, \nu) = \frac{S}{\pi} \frac{\alpha_L}{(\nu - \nu_0)^2 + \alpha_L^2} \tag{2}$$

In this equation, ν_0 is the frequency at the line center and S is the line strength which depends upon temperature according to

$$S = S_0(T_0/T)^{3/2} \exp\left(\frac{-E''}{k}\frac{T_0 - T}{TT_0}\right)$$

where E'' is the vibration-rotation energy of the initial state. The half-width of the line (α_L) depends upon pressure and temperature in the following manner:

$$\alpha_L = \alpha_{L0}\left(\frac{P}{P_0}\right)\left(\frac{T_0}{T}\right)^n$$

where P is the effective broadening pressure. It is different from the total pressure because the absorbing gas molecules are more effective in broadening than are the foreign gas molecules. Burch et al. [1] have shown for CO_2 that P equals the total pressure plus 0.3 times the partial pressure of CO_2. T is the absolute temperature, and n depends upon the nature of the broadening gas and line center frequency. For nitrogen-water vapor collisions, Benedict and Kaplan [2] show n = 0.62 to be a good representative value. Here S_0 and α_{L0} refer to the strength and half-width, respectively, calculated at a reference temperature T_0.

A study by Winters et al. [3] of an isolated CO_2 spectral line showed that the intensity in the wings of the line decreased more rapidly than predicted by the Lorentz expression. On the

basis of this study Benedict proposed the following empirical expression for the spectral line shape of CO_2:

$$k(x, \nu) = \frac{S}{\pi} \frac{\alpha_L}{(\nu - \nu_0)^2 + \alpha_L^2}, \qquad |\nu - \nu_0| \leqq d$$

$$= \frac{S}{\pi} \frac{A\alpha_L \exp\left(-a|\nu - \nu_0|^b\right)}{(\nu - \nu_0)^2 + \alpha_L^2}, \qquad |\nu - \nu_0| \geqq d$$

where d is the average spacing between spectral lines

$a = 0.0675$

$b = 0.7$

$d = 2.5\ cm^{-1}$

The value of A is chosen to make the two forms continuous at $|\nu - \nu_0| = d = 2.5\ cm^{-1}$.

There is a second cause of line broadening known as the Doppler effect which is related to the relative motions of the molecules. The pure Doppler broadened line [4] is given by

$$k(x, \nu) = k_0 e^{-y^2} \tag{3}$$

where

$$k_0 = \frac{S}{\alpha_D}\left(\frac{\ell n\, 2}{\pi}\right)^{1/2}$$

$$y = \frac{(\nu - \nu_0)}{\alpha_D}(\ell n\, 2)^{1/2}$$

and α_D, the Doppler half-width at half maximum, is given by

$$\alpha_D = 3.58 \times 10^{-7}\left(\frac{T}{M}\right)^{1/2} \nu_0$$

where M = molecular weight.

For lower altitudes where the atmospheric pressure is high, the Lorentz half-width, α_L, is dominant. As the atmospheric pressure decreases, the Lorentz half-width decreases and the influence of Doppler broadening becomes more marked. For the 15-μ CO_2 band, the Doppler and Lorentz half-widths are equal at about 10 mb [5] and at lower pressures the Doppler

half-width is greater. Thus, over a wide range of atmospheric pressures it is necessary to consider the mixed Doppler-Lorentz line shape to be completely accurate. The absorption coefficient for the mixed broadening is given by reference 6:

$$k(x, \nu) = \frac{k_0 u}{\pi} \int_{-\infty}^{\infty} \frac{e^{-t^2}}{u^2 + (Y - t)^2} dt \tag{4}$$

where k_0, Y are as before and

$$u = \frac{\alpha_L}{\alpha_D} (\ln 2)^{1/2}$$

Four different forms for $k(x, \nu)$ have been stated, each form accurately representing the shape of a spectral line if the appropriate conditions are satisfied. Therefore, to completely specify the absorption as given by equation 1 it is necessary to substitute the appropriate form of $k(x, \nu)$.

Let us assume that the spectral interval over which equation 1 is defined contains many spectral lines. Then we have

$$A\Delta\nu = \int_{\Delta\nu} \left\{ 1 - \exp \left[-\frac{1}{\pi} \sum_{i=1}^{N} \int_0^X k(x, \nu) \rho(x) \, dx \right] \right\} \tag{5}$$

Equation 5 is the general equation for specifying the absorption of a given species over an atmospheric slant path, the range of pressures encompassed by the path defining the specific form for the absorption coefficient $k(x, \nu)$.

To better understand the parameters that must be specified before equation 5 can be evaluated let us assume that the slant path is such that the Lorentz line shape is valid. Then equation 5 becomes

$$A\Delta\nu = \int_{\Delta\nu} \left\{ 1 - \exp \left[-\frac{1}{\pi} \sum_{i=1}^{N} \int_0^X \frac{S_i \alpha_i \rho(x)}{(\nu - \nu_{0_i})^2 + \alpha_i^2} dx \right] \right\} d\nu \tag{6}$$

The summation is over the total number of lines in the spectral interval and S_n is the strength of the nth line, α_n is the half-width of the nth line, and ν_{0_n} is the center frequency of the nth line.

The problem of determining slant-path transmission spectra is then to evaluate equation 6 for each frequency within the spectral interval of interest. To perform this evaluation, the following four parameters must be specified:

(1) The shape of each spectral line

(2) The location of each spectral line

(3) The intensity and half-width of each line and their variations with temperature and pressure

(4) The density of the absorber at each point in the path

In theory, if all of these parameters were known exactly for all absorption bands and for all absorbing species, the infinity-resolved transmittance could be determined simply by summing the contribution to absorption of each spectral line at each wavelength. Unfortunately, although the line positions are documented, the line parameters such as intensity and half-width are known fairly accurately for only the 2.7-μ H_2O band and the 15-μ CO_2 band. Drayson [5] has evaluated equation 6 for the 15-μ CO_2 band for 200 paths ranging from sea level to the limit of the atmosphere for zenith angles extending from the horizontal to the vertical. Some representative spectra are presented in section 7 of this report. Gates et al. [7] have also evaluated equation 6 for the 2.7-μ H_2O band for homogeneous paths. Samples of their spectra are also presented.

The method for computing absorption by the direct integration shown in equation 6 is classified as the rigorous method since it sums the contribution of each spectral line* after first determining its position and intensity. This is in contrast to the method which assumes that the positions and intensities obey some mathematical model. The rigorous method requires a great amount of computational labor and the process must be completely repeated for each slant path. The advantages of this method are its ability to extrapolate over extreme conditions and that any resolution is obtainable since $\Delta\nu$ in equation 6 may be made as small as desired.

2.2. BAND MODELS FOR COMPUTING SPECTRAL ABSORPTION

2.2.1. INTRODUCTION TO THE BAND-MODEL CONCEPT. Many applications do not require a highly accurate determination of the absorption spectra, but only a first-order approximation to the true spectra, and in many cases the spectra may have relatively low resolution. Therefore, almost all of the available methods for computing atmospheric absorption use approximations which reduce equation 6 to a form which expresses the transmission, averaged

*All spectral lines are not necessarily included, but only those having an intensity greater than a certain minimum value.

over some interval, in terms of elementary functions. The simplified equation is then used with laboratory homogeneous-path data to predict absorption for other homogeneous paths.

The classical approach used in performing the simplification of equation 6 is that of using a model of the band structure. That is, it is assumed that the line positions and strengths are distributed in a way that can be represented by a simple mathematical model. The most commonly used band models are listed here.*

(1) The Elsasser or regular model [8-10] assumes spectral lines of equal intensity, equal spacing, and identical half-widths. The transmission function is averaged over an interval equal to the spacing between the line centers.

(2) The statistical or random model, originally developed for water vapor assumes that the positions and strengths of the lines are given by a probability function. The statistical model was suggested by Telles and worked out by Mayer [11] and (independently) Goody [12].

(3) The random-Elsasser model [10] is a generalization of the Elsasser model and the statistical model. It assumes a random superposition of any number of Elsasser bands of different intensities, spacings, and half-widths. Therefore, as the number of bands ranges from one of infinity, the band model extends, respectively, from the Elsasser model to the purely statistical model. This generalization, therefore, yields an infinite set of absorption curves between those of the Elsasser and statistical models.

(4) The best available model is the quasi-random model [13]. It is capable of fairly accurate representation of the band provided the averaging interval is made sufficiently small. However, of the five models, it requires the greatest amount of computation.

(5) The King model [14] consists of an infinite array of lines, either random or regular, which is modulated by a band envelope whose intensity falls off exponentially from the band center.

2.2.2. A SINGLE LORENTZ LINE. Let us consider the absorption caused by a single spectral line of a homogeneous path of a single absorbing gas. Let us assume that the shape of this line is represented by the Lorentz equation. For these conditions the absorption is given by

*Other band models have been developed and are discussed in detail by R. M. Goody (Atmospheric Radiation, Oxford University Press, 1964). The models listed here are those that have received general application.

$$A\Delta\nu = \int_{\Delta\nu} \left\{ 1 - \exp\left[-\frac{1}{\pi} \int_0^X \frac{S\alpha\rho}{(\nu - \nu_0)^2 + \alpha^2} dx \right] \right\} d\nu \tag{7}$$

For a homogeneous path S, α and ρ are constant; equation 7 further reduces to

$$A\Delta\nu = \int_{\Delta\nu} \left\{ 1 - \exp\left[-\frac{S}{\pi} \frac{\alpha W}{(\nu - \nu_0)^2 + \alpha^2} \right] \right\} d\nu \tag{8}$$

where $W = \int_0^X \rho dx = \rho X$ and is defined as the optical path length.

A plot of absorption versus frequency is shown in figure 2 for different path lengths, or for different values of W. The absorption caused by this line for a path of length X_1 would be considered a weak line since the absorption is small even at the line center. For a path of length X_3 the center of the line is completely absorbed away and any further increase in path length would only change the absorption in the wings of the line. Absorption by paths of length equal to or greater than X_3 would, therefore, be considered strong-line absorption.

In equation 8, if it is assumed that the interval $\Delta\nu$ is such that the entire line is included, then the limits of integration can be taken from $-\infty$ to ∞ without introducing a significant error. When these limits are used, equation 8 can be solved exactly for the total absorption. Ladenburg and Reiche [15] have solved the integral to obtain

$$A\Delta\nu = 2\pi\alpha\psi e^{-\psi}[I_0(\psi) + I_1(\psi)] \tag{9}$$

where $\psi = SW/2\pi\alpha$ and I_0 and I_1 are Bessel functions of imaginary argument. Examining equation 9 under conditions of weak-line and strong-line absorption, we have for weak-line absorption $\psi << 1$; equation 9 reduces to

$$A\Delta\nu = 2\pi\alpha\psi = SW \tag{10}$$

and absorption is linear with the optical path length W. Under conditions of strong-line absorption ψ is large and equation 9 reduces to

$$A\Delta\nu = 2\sqrt{S\alpha W} \tag{11}$$

which is known as the square-root approximation. The above derivations are for a single spectral line but are also valid for absorption when many spectral lines are present but do not

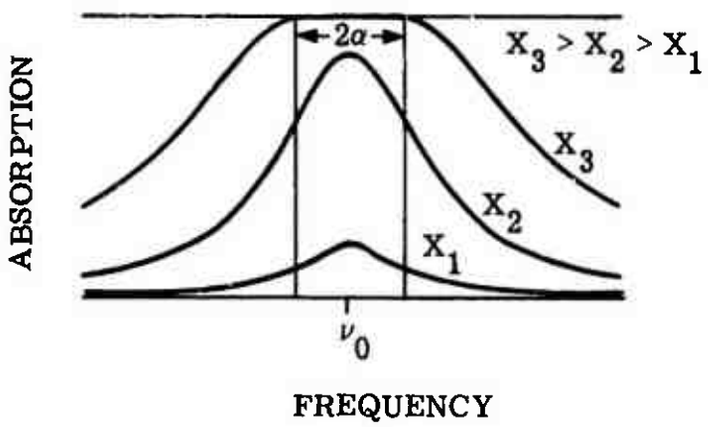

FIGURE 2. ABSORPTION VS. FREQUENCY FOR A SINGLE LINE

overlap. Therefore, for the nonoverlapping approximation the absorption is simply given by equation 9, 10, or 11, depending upon the value of ψ.

2.2.3. ELSASSER MODEL. The Elsasser model of an absorption band is formed by allowing a single Lorentz line to repeat itself periodically throughout the interval $\Delta\nu$. This gives rise to a series of lines that are equally spaced and that have a constant intensity and half-width throughout the interval. This arrangement of spectral lines was first proposed by Elsasser [8] and his derivation is presented here. The absorption coefficient for a periodic band is given by

$$k(\nu) = \sum_{n=-\infty}^{\infty} \frac{S}{\pi} \frac{\alpha}{(\nu - nd)^2 + \alpha^2} \tag{12}$$

It is possible to express equation 12 in terms of an analytical function owing to the fact that if such a function has only single poles, it is uniquely defined by these poles. Therefore, equation 12 is equivalent to

$$k(\nu) = \frac{S}{d} \frac{\sinh \beta}{\cosh \beta - \cos s} \tag{13}$$

where $\beta = 2\pi\alpha/d$

$s = 2\pi\nu/d$

If the averaging interval $\Delta\nu$ is taken as one period of the band ($\Delta\nu = 2\pi$), then equation 6 becomes

$$A = \frac{1}{2\pi} \int_{-\pi}^{\pi} \{1 - \exp[-Wk(\beta, s)]\}\, ds \tag{14}$$

This integral has been evaluated by Elsasser [16] to give the general expression for absorption by an Elsasser band, namely

$$A = \sinh \beta \int_0^Y I_0(Y) \exp(-Y \cosh \beta)\, dY \tag{15}$$

where $\beta = 2\pi\alpha/d$

$Y = \beta\psi/\sinh \beta$

$\psi = SW/2\pi\alpha$

d = mean spacing between spectral lines

A plot of this function for various values of β is given in figure 3. Because the function in its present form is difficult to evaluate, considerable effort has been expended comparing

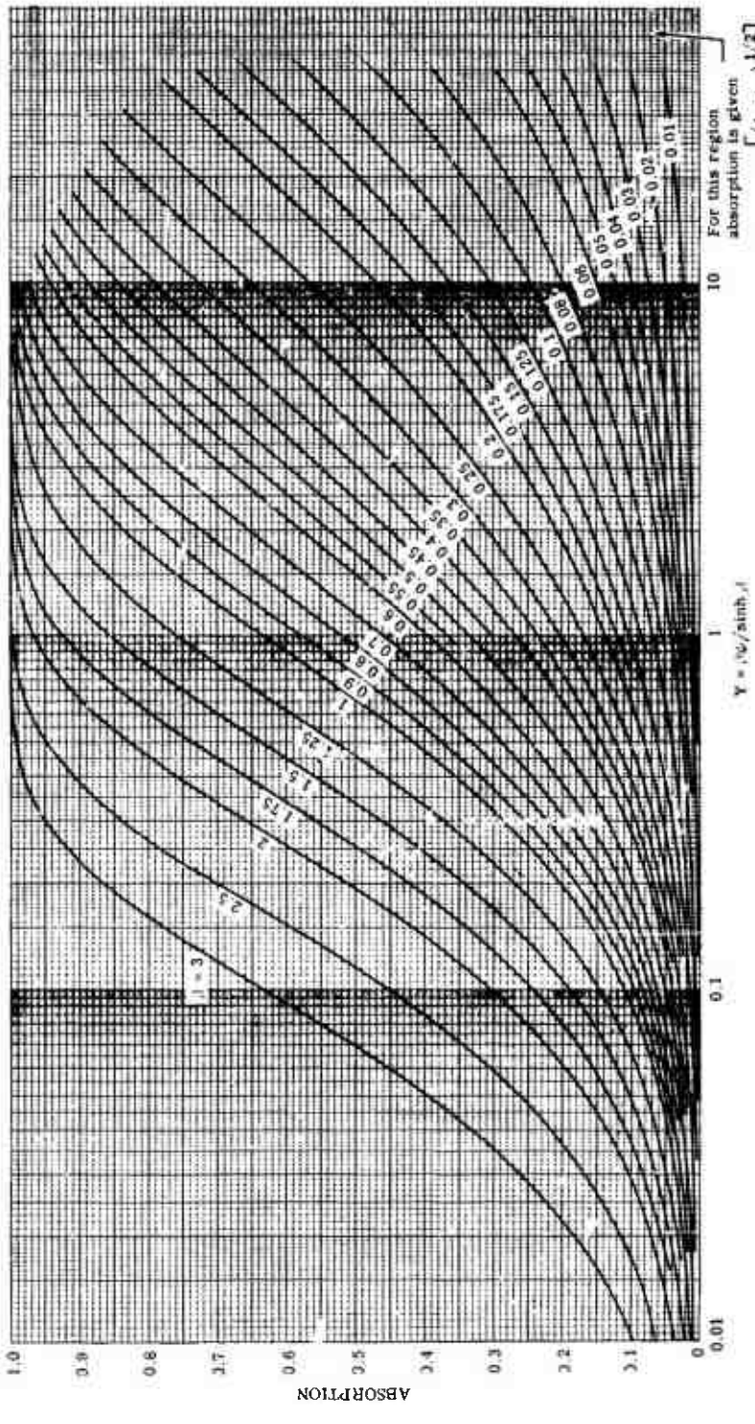

FIGURE 3. ABSORPTION BY A SINGLE ELSASSER BAND. For $\beta > 3$, $A \cong 1 - \exp\left(-\frac{S}{d}W\right)$.

approximate formulae and evaluating the integral. Kaplan [17] has expanded the integral into a series which is convergent only for values of β less than 1.76. D. Lundholm [18] derived an algorithm for the Elsasser integral which is convergent for all values of β and ψ. The algorithm and a computer program, written by Oppel, for the evaluation of the Elsasser integral based on this algorithm are presented in appendix E. However, it is frequently desirable to work with approximations to the function which are valid for certain conditions.

2.2.3.1. Weak-Line Approximation. In figure 4 the absorption given by equation 15 is plotted as a function of the product $\beta\psi = SW/d$ for four values of β. It is noted for $\beta \leqq 1$ that the absorption curves become superimposed for all values of ψ. Since the parameter β measures the ratio of line width to the distance of neighboring line, $\beta \leqq 1$ implies that the spectral lines are strongly overlapped and spectral line structure is not observable. This condition corresponds to large pressures which would be realistic for atmospheric paths at low altitudes. For $\beta \leqq 1$, equation 15 can be approximated by

$$A = 1 - e^{-\beta\psi} \tag{16}$$

Further, equation 16 is a good approximation to equation 15 whenever the absorption is small at the line centers (small ψ) regardless of the value of β. Therefore, this approximation is referred to as the weak-line approximation, and, as will be shown later, is independent of the position of the spectral lines within the band. Table 1 summarizes the regions of β and ψ for which the weak-line approximation is valid with an error of less than 10%. This approximation is particularly useful in extrapolating the absorption to small values of ψ and to large values of pressure. Note that the weak-line approximation reduces to the linear approximation when the absorption is small even if the lines overlap.

2.2.3.2. Strong-Line Approximation. Of increasing interest are the long atmospheric paths at high altitudes which give rise to large values of W and small values of pressure. Under these conditions the absorption at the line centers is usually complete (large ψ), the half-widths are narrow, and the lines do not overlap strongly (small β). For large ψ and small β, equation 15 may be approximated by

$$A = \operatorname{erf}\left(\frac{1}{2}\beta^2\psi\right)^{1/2} \tag{17}$$

where

$$\operatorname{erf}(t) = \frac{2}{\sqrt{\pi}}\int_0^t e^{-t^2}\,dt$$

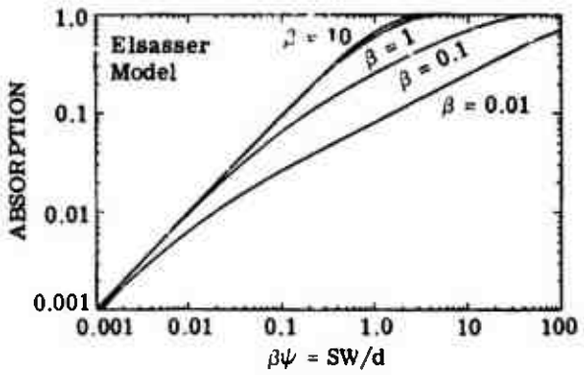

FIGURE 4. ABSORPTION AS A FUNCTION OF $\beta\psi = SW/d$ FOR THE ELSASSER MODEL. The weak-line approximation is the uppermost curve.

TABLE I. REGIONS OF VALIDITY OF VARIOUS APPROXIMATIONS FOR BAND ABSORPTION*

Approximation	$\beta = 2\pi\alpha/d$	Elsasser Model	Statistical Model; All Lines Equally Intense	Statistical Model; Exponential Line Intensity Distribution
Strong-line approximation:	0.001	$\psi > 1.63$	$\psi > 1.63$	$\psi_0 > 2.4$
	0.01	$\psi > 1.63$	$\psi > 1.63$	$\psi_0 > 2.4$
	0.1	$\psi > 1.63$	$\psi > 1.63$	$\psi_0 > 2.3$
Equations 17 and 25:	1	$\psi > 1.35$	$\psi > 1.1$	$\psi_0 > 1.4$
	10	$\psi > 0.24$	$\psi > 0.24$	$\psi_0 > 0.27$
	100	$\psi > 0.024$	$\psi > 0.024$	$\psi_0 > 0.24$
Weak-line approximation:	0.001	$\psi < 0.20$	$\psi < 0.20$	$\psi_0 < 0.10$
	0.01	$\psi < 0.20$	$\psi < 0.20$	$\psi_0 < 0.10$
	0.1	$\psi < 0.20$	$\psi < 0.20$	$\psi_0 < 0.10$
Equation 16:	1	$\psi < \infty$	$\psi < 0.23$	$\psi_0 < 0.11$
	10	$\psi < \infty$	$\psi < \infty$	$\psi_0 < \infty$
	100	$\psi < \infty$	$\psi < \infty$	$\psi_0 < \infty$
Nonoverlapping-line approximation:	0.001	$\psi < 600{,}000$	$\psi < 63{,}000$	$\psi_0 < 80{,}000$
	0.01	$\psi < 6000$	$\psi < 630$	$\psi_0 < 800$
	0.1	$\psi < 60$	$\psi < 6.3$	$\psi_0 < 8$
	1	$\psi < 0.7$	$\psi < 0.22$	$\psi_0 < 0.23$
Equations 26 and 33:	10	$\psi < 0.02$	$\psi < 0.020$	$\psi_0 < 0.020$
	100	$\psi < 0.002$	$\psi < 0.0020$	$\psi_0 < 0.0020$

*When $\psi = SW/2\pi\alpha$ satisfies the given inequalities, the indicated approximation for the absorption is valid with an error of less than 10%. For the exponential line intensity distribution, $\psi_0 = S_0 W/2\pi\alpha$, where $P(S) = S_0^{-1} \exp(-S/S_0)$.

which is known as the strong-line approximation to the Elsasser band model. Figure 5 is a plot of equation 15 with absorption as a function of $\beta^2\psi$. For $\beta \leq 0.01$, equations 15 and 17 are superimposed for $\beta^2\psi > 0.0003$. Clearly, given small β and large ψ, equation 17 is a particularly good approximation for representing the absorption when $\beta \leq 1$. If $\beta \leq 1$, then equation 17 is valid whenever $0.1 \leq A \leq 1$. This includes most values of absorption that are usually of interest. This case differs from the square-root approximation in that it is not necessary that the lines do not overlap. For overlapping spectral lines (larger β), the values of ψ for which the approximation is valid are simply restricted to large values of ψ. The specific regions of validity are given in table 1.

2.2.3.3. Nonoverlapping Approximation. The third approximation to the Elsasser band model is known as the nonoverlapping approximation. The regions of validity for the strong- and weak-line approximations depend only upon the value of absorption at the frequency of the line centers and do not depend upon the degree of overlapping of the spectral lines. On the other hand, the only requirement for the validity of the nonoverlapping-line approximation is that the spectral lines do not overlap appreciably. It is valid regardless of the value of the absorption at the line centers. This approximation is particularly useful for extrapolating the absorption to small values of W and small values of pressure which correspond to short paths at high altitudes. Under these conditions equation 15 reduces to

$$A = \beta\psi e^{-\psi}[I_0(\psi) + I_1(\psi)] \tag{18}$$

which is exactly the same expression as that obtained for the absorption by a single spectral line. This is an expected result, for if the lines do not overlap there will be only one line that contributes to the absorption at a given frequency.

In figure 6, A/β is given as a function of ψ. The uppermost curve is the nonoverlapping approximation. For $\psi << 1$, the curve has a slope of 1 (i.e., a region where the weak-line approximation is valid) and for $\psi >> 1$ the curve has a slope of one-half (i.e., a region where the strong-line approximation is valid). The region of validity for various values of β and ψ are given in table 1.

The general expression for absorption by an Elsasser band given by equation 15 and the strong-line approximation (eq. 17) are useful for determining absorption by CO_2 since the bands consist of fairly regularly spaced lines. However, the bands of H_2O and O_3 have a highly irregular fine structure and cannot be well described by equation 15. To develop an analytical expression for the transmissivity function for H_2O and O_3 we must employ statistical methods.

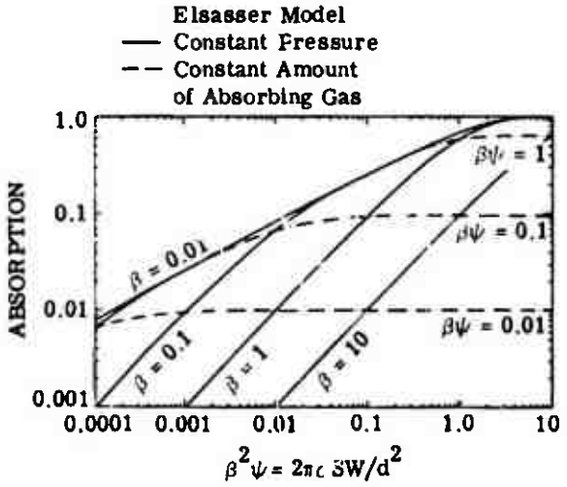

FIGURE 5. ABSORPTION AS A FUNCTION OF $\beta^2\psi = 2\pi\alpha SW/d^2$ FOR THE ELSASSER MODEL. Curves are shown for constant pressure (β = constant) and for constant amount of the absorbing gas ($\beta\psi$ = constant). The strong-line approximation is the uppermost curve.

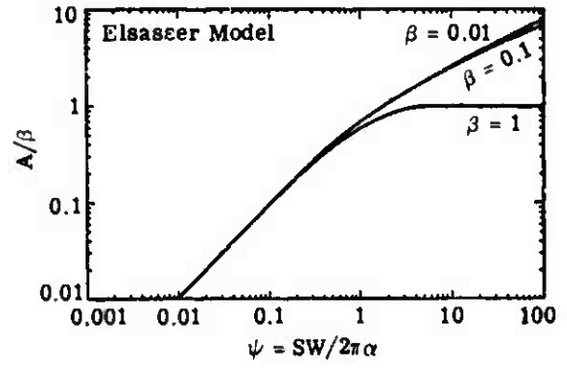

FIGURE 6. ABSORPTION DIVIDED BY β AS A FUNCTION OF $\psi = SW/2\pi\alpha$ FOR THE ELSASSER MODEL. The nonoverlapping-line approximation is the uppermost curve.

2.2.4. STATISTICAL BAND MODEL. Let $\Delta\nu$ be a spectral interval in which there are n lines of mean distance d:

$$\Delta\nu = nd \tag{19}$$

Let $P(S_i)$ be the probability that the ith line will have an intensity S_i and let P be normalized; then

$$\int_0^\infty P(S)\,dS = 1 \tag{20}$$

We assume that any line has equal probability of being anywhere in the interval $\Delta\nu$. The mean absorption clearly does not depend upon ν provided we are far enough away from the edges of the interval. We shall, therefore, determine it for $\nu = 0$, the center of the interval. If we let the center of the ith line be at $\nu_0 = \nu_i$, then the absorption coefficient becomes

$$k_i(S_i, \nu_i) = k(\nu = \nu_i, \nu_0 = 0)$$

The mean transmissivity is found by averaging over all positions and all intensities of the lines; thus

$$\tau = \frac{1}{(\Delta\nu)^n}\int_{\Delta\nu} d\nu_1 \cdots \int_{\Delta\nu} d\nu_n \int_0^\infty P(S_1)e^{-kW}dS_1 \cdots \int_0^\infty P(S_n)e^{-kW}dS_n$$

But since all integrals are alike,

$$\tau = \left[\frac{1}{\Delta\nu}\int d\nu \int P(S)e^{-kW}dS\right]^n = \left[1 - \frac{1}{\Delta\nu}\int d\nu \int P(S)(1 - e^{-kW})\,dS\right]^n$$

Since $\Delta\nu = nd$, when n becomes large the last expression approaches an exponential; therefore,

$$\tau = \exp\left[-\frac{1}{d}\int P(S)(A_1\Delta\nu)\,dS\right] \tag{21}$$

where

$$[A_1\Delta\nu] = \int_{\Delta\nu}(1 - e^{-kW})\,d\nu$$

A_1 is the absorptivity of a single line taken over the interval $\Delta\nu$.

2.2.4.1. Equal Intensity Lines. Equation 21 can be evaluated for two special cases. First, when all the lines have equal intensities equation 21 reduces to

$$\tau = e^{-A_1 \Delta\nu/d} = \exp\left\{-\beta\psi e^{-\psi}[I_0(\psi) + I_1(\psi)]\right\}$$

Rewriting in terms of absorption, we have

$$A = 1 - \exp\left\{-\beta\psi e^{-\psi}[I_0(\psi) + I_1(\psi)]\right\} \tag{22}$$

If each of the lines absorbs weakly so that ψ is small, then equation 16 reduces to

$$A = 1 - \exp(-\beta\psi) \tag{23}$$

This is the weak-line approximation to the statistical model with all lines equally intense. If the lines absorb strongly then equation 22 reduces to

$$A = 1 - \exp(-2\sqrt{S\alpha W}/d) \tag{24}$$

In terms of β and ψ,

$$A = 1 - \exp\left[-\left(\frac{2}{\pi}\beta^2\psi\right)^{1/2}\right] \tag{25}$$

This is the strong-line approximation to the statistical model in which all lines are equally intense.

The nonoverlapping approximation to equation 22 is obtained from the first term in the expansion of the exponential, so that

$$A = \beta\psi e^{-\psi}[I_0(\psi) + I_1(\psi)] \tag{26}$$

This is the same expression as that obtained for the nonoverlapping approximation to the Elsasser model, equation 18.

2.2.4.2. Line Strength by Poisson Distribution. Next let us consider the case where the lines are of different strength and the distribution for the probability of their strength is a simple Poisson distribution, namely,

$$P(S) = \frac{1}{S_0} e^{-S/S_0} \tag{27}$$

By letting k = KS in equation 21, we obtain

$$\tau = \exp\left(-\frac{1}{d}\int_{\Delta\nu}\frac{KWS_0}{1 + KWS_0}\,d\nu\right) \tag{28}$$

We now introduce the Lorentz line shape

$$K = \frac{\alpha}{\pi(\nu^2 + \alpha^2)}$$

This vanishes fast enough for large $\Delta\nu$ that we can extend the integration in equation 28 from $-\infty$ to ∞, giving

$$\tau = \exp\left[-\frac{WS_0\alpha}{d\sqrt{\alpha^2 + (WS_0\alpha)/\pi}}\right] \tag{29}$$

Rewriting in terms of absorption and β and ψ, we have

$$A = 1 - \exp\left[-\beta\psi_0/(1 + 2\psi_0)^{1/2}\right] \tag{30}$$

where $\psi_0 = S_0W/2\pi\alpha$. This is the formula first developed by Goody and is therefore referred to as the Goody band model.

The weak-line approximation to equation 30 is obtained when $\psi_0 << 1$. Under these conditions equation 30 becomes

$$A = 1 - \exp(-\beta\psi_0) \tag{31}$$

The strong-line approximation to the statistical model with an exponential distribution of line strengths is obtained when $\psi_0 >> 1$. Under these conditions equation 30 becomes

$$A = 1 - \exp\left[-\left(\frac{1}{2}\beta^2\psi\right)^{1/2}\right] \tag{32}$$

The nonoverlapping approximation is obtained from equation 30 when the exponent is small and is therefore given by the first two terms of the expansion, or

$$A = \beta\psi_0/(1 + 2\psi_0)^{1/2} \tag{33}$$

2.2.4.3. Strong-Line, Weak-Line, and Nonoverlapping Approximations. The three approximations to the two statistical models will be discussed concurrently because they are so

closely related. First, we shall consider the weak-line approximation. Recall for this case that absorption was given by $A = 1 - \exp(-\beta\psi)$, which is exactly the expression obtained for the weak-line approximation to the Elsasser band model. The same expression results when an exponential distribution of line intensities is assumed with ψ replaced by ψ_0. This confirms our earlier statement that under weak-line absorption, absorption is independent of the arrangement of the spectral lines within the band. Absorption versus $\beta\psi$ is plotted for equation 22 in figure 7. The solid curves give the absorption for the statistical model for the case in which all lines are equally intense. The dashed curves give the absorption for the statistical model with an exponential distribution of line strengths. The uppermost solid and dashed curves represent the weak-line approximations for those intensity distributions. The regions of validity are given in table 1. For the case in which all lines are equally intense, the weak-line approximation is always valid within 10% when $\psi < 0.2$. It is valid for the exponential intensity distribution when $\psi < 0.1$. If 1% accuracy is required, these values of ψ should be divided by 10.

The strong-line approximation to the statistical model for all lines of equal intensity and for an exponential distribution of line strengths are given respectively by equations 25 and 32. The absorption for these models as a function of $\beta^2\psi$ is shown in figure 8. The strong-line approximation is the uppermost curve in the figure. The absorption can even become greater than the limiting values given by this curve. It is evident that the distribution of line intensities in a band only slightly influences the shape of the absorption curve. As for the strong-line approximation to the Elsasser model, the strong-line approximation to the statistical model for either distribution of line strengths is always valid when $\beta \leq 1$ and $0.1 \leq A \leq 1$. The complete regions of validity are given in table 1.

The last approximation to be discussed for the statistical model is the nonoverlapping approximation. For all lines of equal intensity the absorption is given by the expression used for the nonoverlapping approximation to the Elsasser model, namely,

$$A = \beta\psi e^{-\psi}[I_0(\psi) + I_1(\psi)]$$

For an exponential distribution of line strengths the absorption is given by equation 33. Therefore, the intensity distribution, but not the regular or random spacing of the spectral lines, influences the absorption curve in this approximation. In figure 9, A/β is plotted as a function of ψ for the statistical model Note that if this figure is compared with the corresponding one for the Elsasser model the nonoverlapping approximation to the Elsasser model has a considerably larger region of validity. This is because the spectral lines begin to overlap at considerably larger path lengths for the Elsasser model than for the statistical model (cf. table 1).

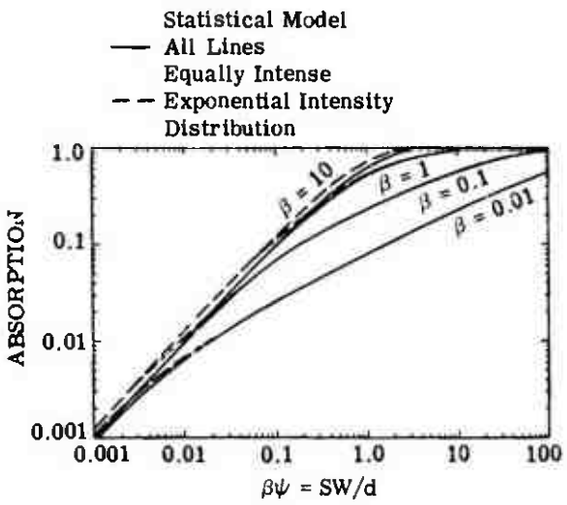

FIGURE 7. ABSORPTION AS A FUNCTION OF $\beta\psi$ = SW/d FOR THE STATISTICAL MODEL. The absorption for a model in which the spectral lines are all of equal intensity is compared with that for a model in which the spectral lines have an exponential intensity-distribution function. The weak-line approximation is the uppermost curve.

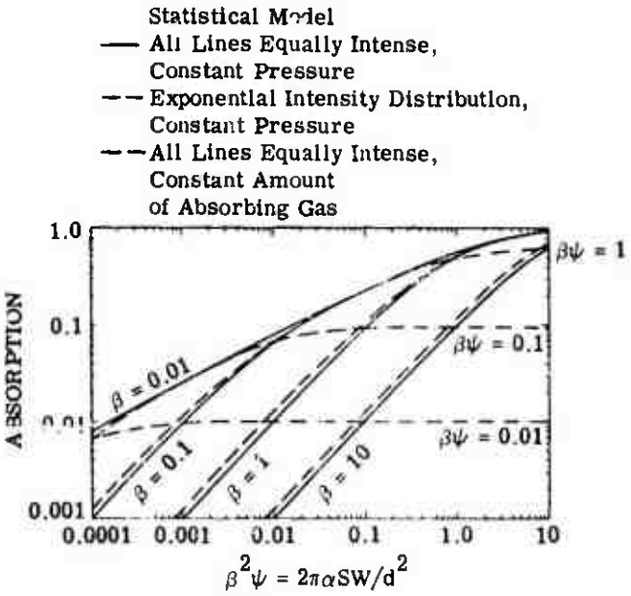

FIGURE 8. ABSORPTION AS A FUNCTION OF $\beta^2\psi = 2\pi\alpha SW/d^2$ FOR THE STATISTICAL MODEL. Curves are shown for constant pressure (β = constant) and for constant amount of the absorbing gas ($\beta\psi$ = constant). The absorption is shown when all the spectral lines have equal intensity and when there is an exponential intensity-distribution function. The strong-line approximation is the uppermost curve.

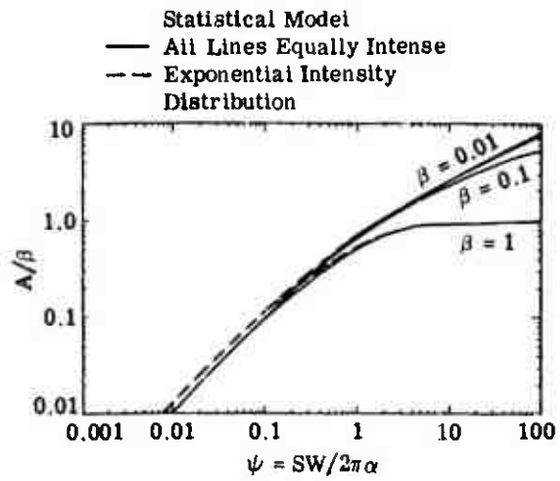

FIGURE 9. ABSORPTION DIVIDED BY β AS A FUNCTION OF $\psi = SW/2\pi\alpha$ FOR THE STATISTICAL MODEL. The absorption for a model in which the spectral lines are all of equal intensity is compared with that for a model in which the spectral lines have an exponential intensity-distribution function. The nonoverlapping-line approximation is the uppermost curve.

Three important approximations to the band models of Elsasser and Goody have been discussed above. These three approximations provide a reliable means for the extrapolation of laboratory absorption data to values of the pressure and path length that cannot easily be reproduced in the laboratory. For example, the absorption for large values of pressure can be obtained from the strong- and weak-line approximations, depending upon whether W is relatively large or small. For extrapolation to small values of pressure all three approximations may be used in their respective regions of validity; however, the nonoverlapping-line approximation is valid over the largest range of values of W. For extrapolation to large values of W, either the strong- or weak-line approximation may be used, but the former approximation is valid over a much wider range of pressure than the latter. For extrapolation to small values of W, all three approximations may be used in their respective regions of validity; however the nonoverlapping-line approximation is valid over a wider range of pressure. In general, atmospheric slant paths that are of interest to the systems engineer contain relatively large amounts of absorber and the range of pressures are such that the strong-line approximation to any of the models is applicable. As will be seen in section 3, almost all researchers used only the strong-line approximations to the various band models to develop equations for predicting absorption over a specified frequency band.

2.2.5. RANDOM-ELSASSER BAND MODEL. At small values of ψ the same absorption is predicted by the statistical and Elsasser models, and is determined by the total strength of all the absorbing lines. However, as ψ increases the results calculated from these two models begin to diverge; the Elsasser theory always gives more absorption than does the statistical model for a given value of ψ. The reason for this is that there is always more overlapping of spectral lines with the statistical model than with the regular arrangement of lines in the Elsasser model; thus, for a given path length and pressure, the total line strength is not used as effectively for absorption in the statistical model.

An actual band has its spectral lines arranged neither completely at random nor at regular intervals. The actual pattern is formed by the superposition of many systems of lines. Therefore, for some gases and some spectral regions the absorption can be represented more accurately by the random Elsasser band model than by either the statistical or Elsasser model alone. The random Elsasser band model is a natural generalization of the original models which assumes that the absorption can be represented by the random superposition of Elsasser bands. The individual bands may have different line spacings, half-widths, and intensities. As the number of superposed Elsasser bands becomes large, the predicted absorption approaches that of the usual statistical model.

The absorption for N randomly superposed Elsasser bands with equal intensities, half-widths, and line spacings is given by

$$A = 1 - \left[1 - \mathrm{erf}\left(\frac{1}{2}\beta^2\psi/N^2\right)\right]^N$$

The derivation of this equation and the more general equation for different intensities, half-widths, and line spacings is discussed in detail by Plass [10]. The more general result is not presented here since the result given above is the only function which has received application.

2.2.6. QUASI-RANDOM MODEL. The fourth band model that has been developed [13, 19]—the quasi-random band model—reportedly presents a more realistic model of the absorption bands of water vapor and carbon dioxide. It does not require that the lines be uniformly nor randomly spaced, but can represent any type of spacing which may occur. It also accurately simulates the intensity distribution of the spectral lines including as many of the weaker lines as actually contribute to the absorption. Furthermore, it provides a means of accurately calculating the effect of wing absorption from spectral lines whose centers are outside the given frequency interval. The quasi-random model allows for more accurate prediction of absorption than do the other three models but sacrifices simplicity in the process. When this model is used the general transmissivity function cannot be expressed in terms of elementary functions. Moreover, to determine accurate absorption spectra by this method, a priori knowledge of the band structure is required, as it is in the rigorous method.

The quasi-random model is characterized by the following features:

(1) The frequency interval $\Delta\nu$ for which the transmission is desired is divided into a set of subintervals of width D. Within the small interval D the lines are assumed to be arranged at random. The transmission over $\Delta\nu >> D$ is then calculated by averaging the results from the smaller intervals.

(2) The interval $\Delta\nu$ is divided into subintervals D in an arbitrary manner. The transmission is first calculated for one mesh, which defines a certain set of frequency intervals. The calculation is repeated for another mesh which is shifted in frequency by D/2 relative to the first set. In principle, the mesh can be shifted n times by an amount D/n. The final calculation is then the average of the results for each of these meshes.

(3) The transmission for each subinterval D is calculated from expressions which are valid for a finite and possibly small number of spectral lines in the interval. The expression is not used which is valid in the limit as the number of lines becomes large.

(4) The spectral lines in each frequency interval are divided into intensity subgroups which are fine enough to simulate the actual intensity distribution. In the calculation, the average intensity of all the lines in each subgroup is used with the actual number of lines.

(5) The contribution from the wings of the spectral lines whose centers are outside a given interval is included. The wing effect is treated in the same detailed manner used for evaluating the contribution from the lines within an interval.

Let us consider one interval D_k of a given mesh. If there are n_k lines in the interval with their line centers at the frequencies ν_i ($i = 1, 2, \ldots, n_k$), then the transmission at the frequency ν is affected by these n_k lines so that

$$\tau_{n_K}(\nu) = \frac{1}{D_k^{n_k}} \prod_{i=1}^{n_K} \int_{D_k} \exp\left[-Wk(\nu, \nu_i)\right] d\nu_1 \qquad (34)$$

where W is the amount of absorber and $k(\nu, \nu_1)$ may be expressed as $k(\nu, \nu_i) = S_i b(\nu, \nu_i)$, $b(\nu, \nu_i)$ is called the line-shape factor (Lorentz, Doppler, etc.), and S_i is the intensity of the ith line. The transmission is calculated at some frequency ν which for convenience is usually taken at the center of the interval D_k. Since this transmission corresponds to the average of all permutations of the positions of the spectral lines within the interval, it is also assumed to represent the most probable transmission for the interval.

To be completely rigorous the transmission of each spectral line should be calculated from its intensity and position and then substituted into equation 34. This procedure would require a computation time analogous to that required for the rigorous method and hence would defeat the purpose of employing a band model. Thus, a method is used which simulates the actual intensity distribution.

The procedure adopted for intensity simulation is to divide the lines in each frequency interval into subgroups by intensity decades. When the line intensities are calculated, the results are grouped according to these intensity decades. The average intensity $\overline{S_i}$ of the lines in each decade is then calculated.

Wyatt, Stull, and Plass [19] have found that only the first five intensity decades for each frequency interval influence the value of transmission. Thus only the data for the five strongest

intensity decades need be retained for each frequency interval. It should be emphasized that the numerical range of the intensity decades retained is quite different for a frequency interval which contains strong lines than for one which has weak lines. The criterion is applied separately to each frequency interval.

Thus, the transmission can be calculated by the following equation from the average value of the intensity $\overline{S}_i$ together with the number of lines n in each intensity decade:

$$T_{n_k}(\nu) = \prod_{i=1}^{5} \left(\frac{1}{D} \int_{D_k} e^{-\overline{S}_i W_b(\nu,\nu_i)} \, d\nu_i \right)^{n_i} \tag{35}$$

The number of lines n_k in the frequency interval is given by

$$n_k = \sum_{i=1}^{5} n_i \tag{36}$$

Equation 35 represents the transmission at a frequency ν for the interval D_k as affected by n_k spectral lines whose centers are within the interval D_k. The integral in equation 35 represents the transmission over the finite interval D_k of a single line representative of the average intensity of the decade.

The transmission at a frequency ν is also influenced by the wings of the spectral lines whose centers lie in intervals outside the interval D_k, denoted by D_l. The wing transmission, T_{n_i}, from each of these intervals D_i is calculated by assuming a random distribution of the lines within the interval D_i. Thus, by the random hypothesis, the transmission at the frequency ν is the product of all transmissions calculated for the lines with centers in intervals, outside D_k, taken with the transmission for the interval D_k. Therefore

$$T(\nu) = \prod_{i=1}^{\infty} T_{n_i}(\nu) \tag{37}$$

where the subscript n_i indicates that there are n_i lines in the frequency interval D_i. The transmission for the lines whose centers are in the interval D_l are given by equation 35. The lines in distant intervals from the particular frequency ν have a negligible effect on the transmission, so that in practice the product (eq. 37) usually needs to be evaluated over only a few terms.

It is clear that the quasi-random model can reproduce the actual line structure fairly accurately if the chosen interval D_k is small enough. However, the smaller the interval the

greater the amount of computation required. The tradeoff between the two has not been discussed by the authors, but such an investigation would indeed be of interest since any particular application has a tolerable error which might be used to establish the frequency interval and hence the degree of computation.

2.2.7. KING MODEL. All previous models generate expressions which can be used to calculate absorption averaged over spectral intervals in the order of 5 to 10 wavenumbers. To calculate total-band absorption using any one of these models one would necessarily calculate the narrowband absorption at each wavelength throughout an absorption band and then evaluate the integral $\int A_\nu d_\nu$, where A_ν is the absorption averaged over some Δ_ν which is very small compared to the total band. King [14] sought an expression which would yield the total band absorption directly by performing the frequency integration prior to the empirical fitting procedure. He first assumed the band structure was described by the statistical or Elsasser models. Since each of these models assumes an infinite spectrum and absorption bands are finite, the frequency integration cannot be performed without some modification of the model.

Every absorption band contains many spectral lines of varying intensities. Those near the center of the band are more intense than those near the wings of the band. This distribution of line strengths gives rise to a band envelope that King assumed to be approximately exponential. That is, the line strengths decrease exponentially from the band center. From this assumption, King used an exponential envelope to modulate the spectral-line arrays as given by the statistical or Elsasser model. Either modulated array was then integrated to yield an expression for the total-band absorption.

Recall that the narrowband transmittance as given by the statistical model is

$$\bar{\tau}_\nu = \exp\left\{-\frac{SW/d}{[1 + (SW/\pi\alpha)]^{1/2}}\right\}$$

where S, d, and α are all taken within the band element.

In the opaque line-center approximation (strong-line approximation), $SW/\pi\alpha \gg 1$. Therefore, the band-element transmittance becomes

$$\bar{\tau}_\nu = \exp\left[-(\pi\alpha SW/d^2)^{1/2}\right] = \exp\left[-(2k_n W)^{1/2}\right] \tag{36}$$

where we have defined the harmonic mean absorption coefficient k_n by

$$\frac{1}{k_n} = \int_0^\infty \bar{\tau}_\nu dW = \int_0^\infty \exp\left[-\left(\frac{\pi\alpha SW}{d^2}\right)^{1/2}\right] dW = \frac{2d^2}{\pi\alpha S} \tag{37}$$

Let us assume that these elements are modulated by a band profile whose shape is given by

$$k_n = (k_n)_{max} \exp(-|\nu|/\nu_e) \tag{38}$$

leading to

$$dk_n/d\nu = -k_n/\nu_e \tag{39}$$

where ν_e is the band scale-width and is a measure of the steepness of the band profile.

The total band transmittance is the average of the narrowband transmittance over the finite bandwidth $\Delta\nu$. So

$$\tau = \frac{1}{\Delta\nu}\int_{-\Delta\nu/2}^{\Delta\nu/2} \exp\left[-(2k_n W)^{1/2}\right] d\nu \tag{40}$$

By changing the dummy variable of integration from ν to the harmonic mean-absorption coefficient k_n, one can express the transmittance as a Laplace-like transform. Thus

$$\tau = -\frac{2}{\Delta\nu}\int_{k_{n_{max}}}^{k_{n_{min}}} \exp\left[(-2k_n W)^{1/2}\right]\frac{d\nu}{dk_n}dk_n \tag{41}$$

Substituting equation 39 into equation 41, we have

$$\tau = \frac{\nu_e}{\Delta\nu/2}\int_{k_{n_{max}}}^{k_{n_{min}}} \exp\left[(-2k_n W)^{1/2}\right]\frac{dk_n}{k_n}$$

$$= 2\left(\frac{\nu_e}{\Delta\nu/2}\right)\left\{E_1\left[(2k_{min}W)^{1/2}\right] - E_1\left[(2k_{max}W)^{1/2}\right]\right\} \tag{42}$$

where E_1 is the first exponential integral and is given by.

$$E_1(x) = \int_1^\infty \frac{e^{-tx}}{t}dt$$

For the strong line approximation, $k_{n_{min}} \ll 1$ and $k_{n_{max}} W \gg 1$. By expanding the exponential integral, one obtains an expression for the total-band absorption. Thus

$$A = 1 - \tau = 2\left(\frac{\nu_e}{\Delta\nu/2}\right)\left[\frac{1}{2}\ln\frac{2k_{n_{max}}}{2k_{n_{min}}} + \alpha + \frac{1}{2}\ln 2k_{n_{min}}W\right]$$

and

$$A\Delta\nu = \int A_\nu d\nu = 2\nu_e\left[\ln W + \ln 2k_{n_{max}} + 2\alpha\right] \tag{43}$$

where $\alpha = 0.5772156$ is the Euler-Mascheroni constant. For the weak-line approximation, $k_{n_{min}}W \ll 1$ and $k_{n_{max}} < 1$, and equation 42 can be approximated by

$$A = 2\left(\frac{\nu_e}{\Delta\nu/2}\right)\left(2k_{n_{max}}W\right)^{1/2}$$

and

$$A\Delta\nu = \int A_\nu d\nu = 4\nu_e\left(2k_{n_{max}}W\right)^{1/2} \tag{44}$$

Expressions 43 and 44 then represent the total-band absorption for the strong- and weak-line approximations, respectively, if one assumes that the ordering of the line array in the band elements is statistical.

If we assume that the lines in the subset are spaced regularly, we have, from the Elsasser model in the opaque line-center approximation,

$$\bar{\tau} = \text{erf}\,(\pi cSW/d^2)^{1/2} = \text{erf}\,(k_n W/2)^{1/2}$$

Using a procedure parallel to that used in the development of equation 42, this equation leads directly to the following expression for transmittance:

$$\tau = \frac{\nu_e}{\Delta\nu/2}\int_{k_{n_{min}}}^{k_{n_{max}}} \text{erf}\left(\frac{k_n W}{2}\right)^{1/2}\frac{dk_n}{k_n}$$

$$= 2\left(\frac{\nu_e}{\Delta\nu/2}\right)\left[F_1\left(\frac{k_{n_{min}}W}{2}\right)^{1/2} - F_1\left(\frac{k_{n_{max}}W}{2}\right)^{1/2}\right]$$

where an error-function integral is defined by analogy to the exponential integral by

$$F_1(x) = \int_x^\infty \operatorname{erf} t \frac{dt}{t}$$

The expansion of $F_1(x)$ for small argument is given by

$$F_1(x) = -\delta - \ln x + 2x/\pi^{1/2} - 2x^3/9\pi^{1/2} + \ldots$$

where $\delta = 0.981$.

Similiarly, the strong-fit expression is obtained by analogy with equation 43:

$$A\Delta\nu = 2\nu_e\left(\ln W + 1/2 \ln k_{n_{max}} + 2\delta\right) \tag{45}$$

The weak fit is obtained using the expansion for $F_1(x)$ and a procedure similar to that used in equation 44.

$$A\Delta\nu = 8\nu_e\pi^{-1/2}\left(\frac{k_{n_{max}} W}{2}\right)^{1/2} \tag{46}$$

Four expressions have been derived which express total integrated-band absorption under conditions of strong and weak absorption in terms of three parameters ν_e, W, and $k_{n_{max}}$. These parameters can be determined by empirically fitting the respective functions to laboratory homogeneous-path data. Once these parameters are specified these expressions can be used to predict total-band absorption for other homogeneous paths. It is emphasized that one should reduce the laboratory data to standard temperature and pressure (STP) before one empirically evaluates the band parameter. The absorber concentration at STP is denoted by W^* and is given by $W^* = W\frac{P}{P_0}\left(\frac{T}{T_0}\right)^n$, where P = effective broadening pressure and n is a function of the absorbing molecule. Then the respective equations can be used to calculate absorption for atmospheric slant paths by first reducing the absorber concentration in the path to an equivalent sea-level concentration W^*. The procedures for evaluating W^* are discussed later.

2.2.8. BAND-MODEL LIMITATIONS. In the preceding paragraphs, five models of the band structure were discussed, four of which led to the derivation of closed-form expressions which can be used to calculate absorption spectra. Although the use of these models greatly reduces

the amount of computation required by the method of summing the contribution of each spectral line, their use is subject to several limitations:

(1) By their very nature the models are such that they can only simulate the actual line intensities and distribution. Since the different absorbers have different line structures, a model that may be applicable to one gas may be inapplicable to another. Also, the model may be reasonably accurate for one spectral interval but very inaccurate for another.

(2) The solutions lose their simplicity when a mixed-line shape is used rather than the pure pressure-broadened Lorentz line shape. Therefore, models are applicable only for a range of pressure for which the Lorentz shape is valid.

(3) The spectral resolution for most models is limited. For the quasi-random model this is not the case if the averaging interval is small enough, but under these conditinns the simplicity of the model is sacrificed.

(4) A band model can be used only to predict absorption for homogeneous naths. Therefore, atmospheric slant paths must be reduced to equivalent sea-level paths or to equivalent homogeneous paths, both of which involve the use of the Curtis-Godson approximation. This approximation is valid only for constant-temperature paths under conditions of strong-line absorption.

(5) The use of band models is further limited by the accuracy of the laboratory data upon which the final solution is based.

These limitations may sound rather severe, but for the range of atmospheric paths for which the systems engineer wishes to determine absorption spectra the restrictions imposed by the band models are satisfied. It has been shown by Plass [20] that for altitudes below 50 km (a category encompassing most paths of interest) under conditions of strong- or weak-line absorption, the absorption can be represented by the Lorentz equation. Also, the slant paths of interest are usually long enough that strong line conditions are present and therefore the Curtis-Godson approximation is usually applicable. It is emphasized that before a band-model method is used to compute the absorption spectra for an atmospheric slant path, it should be verified that the approximations inherent in the band-model methods are satisfied. This is done by, first, approximating the values of β and ψ and then comparing the results with the information in table 1.

2.2.9. TEMPERATURE AND FREQUENCY DEPENDENCE OF BAND-MODEL PARAMETERS. A summary of the band models that yield closed-form expressions for spectral-band

absorption is presented in table 2. All of these expressions are functions of two parameters, β and ψ, which are functions of temperature, pressure, absorber concentration, and frequency. Recall that

$$\beta = \frac{2\pi\alpha}{d} = \frac{2\pi\alpha_0}{d}\frac{P}{P_0}\left(\frac{T_0}{T}\right)^n$$

and

$$\psi = \frac{SW}{2\pi\alpha} = \frac{SW}{2\pi\alpha_0}\frac{P_0}{P}\left(\frac{T}{T_0}\right)^n$$

including the dependence of line half-width on pressure and temperature. Also, the line strength is a function of temperature and frequency and is given by

$$S = S_0\left(\frac{T_0}{T}\right)^{3/2} \exp\left[-\frac{E(\nu)''}{k}\left(\frac{T_0 - T}{TT_0}\right)\right]$$

where S_0 is the line strength at standard temperature and E" is the ground-level energy of a given spectral line. Because E" varies from line to line, the variation of line strength with temperature is different for each spectral line. Figure 10 clearly demonstrates this temperature dependence. As the temperature decreases, the line strengths near the center of the band increase and the line strengths in the wings of the band decrease; the area under the curve decreases slightly. If two homogeneous paths having different temperatures were compared, the integrated absorption for the lower temperature path would be less than the integrated absorption for the higher temperature path. Drayson et al. [5] have shown that for two identical slant paths having temperature profiles that differ by a constant amount of 10°K the transmission varies as much as 10% in the wings of the band and somewhat less nearer the center of the band. They also concluded that the effect of temperature on line half-width has a secondary effect on transmission.

Since the variation of line strength with temperature is different for each spectral line, it would be impossible to include the effect of temperature on line strength and still retain the band-model expressions in closed form. For this reason, the band-model expressions in their present form can be used only to predict absorption for homogeneous paths that are at standard temperature. Further, since Drayson et al. [5] have shown that the effect of temperature on

TABLE 2. SUMMARY OF CLOSED-FORM EXPRESSIONS FOR SPECTRA BAND ABSORPTION

Band Model	Approximation	Equation
1. Single Lorentz line	None	$A = \frac{1}{\Delta\nu} 2\pi\alpha\psi^{-\psi}[I_0(\psi) + I_1(\psi)]$
2. Single Lorentz line	Linear	$A = SW/\Delta\nu$
3. Single Lorentz line	Square root	$A = 2\sqrt{S\alpha W/\Delta\nu}$
4. Elsasser band	None	$A = \sinh\beta\int_0^Y I_0(Y)\exp(-Y\cos h\beta)dY$
5. Elsasser band	Weak	$A = 1 - e^{-\beta\psi}$
6. Elsasser band	Strong	$A = \text{erf}\,(1/2\beta^2\psi)^{1/2}$
7. Statistical band (Poisson)	None	$A = 1 - \exp\left[-\beta\psi_0/(1 + 2\psi_0)^{1/2}\right]$
8. Statistical band	None	$A = 1 - \exp-\left\{\beta\psi\, e^{-\psi}\,[I_0(\psi) + I_1(\psi)]\right\}$
9. Statistical band (Poisson)	Weak	$A = 1 - e^{-\beta\psi}$
10. Statistical band (Poisson and equal)	Strong	$A = 1 - \exp\left[-\left(\frac{1}{2}\beta^2\psi_0\right)^{1/2}\right]$
11. Statistical band (equal)	Strong	$A = 1 - \exp\left[-\left(\frac{2}{\pi}\beta^2\psi\right)^{1/2}\right]$
12. Random Elsasser band	Strong	$A = 1 - \left[1 - \text{erf}\left(\frac{1}{2}\beta^2\psi/N^2\right)^{1/2}\right]^N$

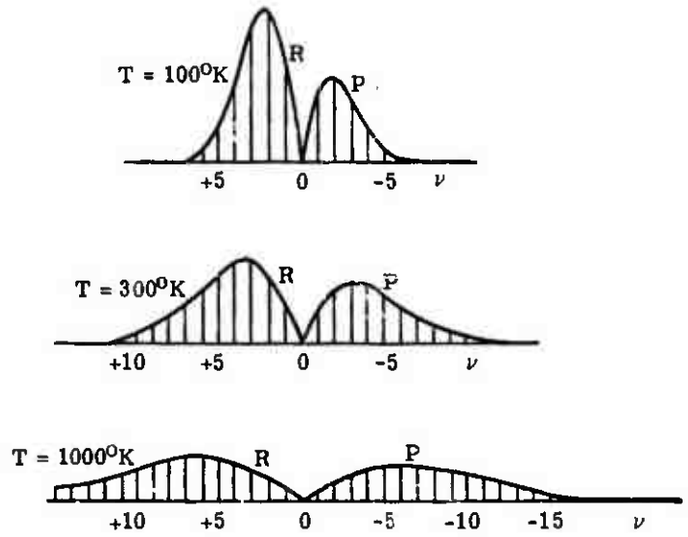

FIGURE 10. THE EFFECT OF TEMPERATURE ON THE DISTRIBUTION OF LINE STRENGTH

line half-width has a secondary effect on absorption, this dependence is neglected also. Therefore, if we let $T = T_0$, the expressions for β and ψ become

$$\beta = \frac{2\pi\alpha_0}{d}\frac{P}{P_0} = \frac{2\pi\alpha_0'}{d}P \tag{47}$$

and

$$\psi = \frac{S_0 W P_0}{2\pi\alpha_0}\frac{P}{P} = \frac{S}{2\pi\alpha_0'}\frac{W}{P} \tag{48}$$

where α_0' is the half-width at standard temperature, per unit pressure.

The expressions listed in table 2 are of the following general form:

(1) $A = A(\beta, \psi)$ when no approximation to the model is assumed

(2) $A = A(\beta^2, \psi)$ for the strong-line approximation

(3) $A = A(\beta, \psi)$ for the weak-line approximation

Substituting equations 47 and 48 into 1, 2, and 3, we have the first expression as a function of two frequency-dependent parameters, $2\pi\alpha_0'/d$ and $S/2\pi\alpha_0'$, and two path parameters, W and P. The second expression gives absorption as a function of one frequency-dependent parameter, $2\pi\alpha_0' S/d^2$ and two path parameters, W and P. The last is a function of S/d and W, being independent of pressure.

The next problem in completely specifying the absorption expressions is that of evaluating the frequency-dependent parameters by empirically fitting the respective equations to laboratory homogeneous absorption spectra. The empirical procedure is the most involved when no approximations to the model are assumed since, in this case, two parameters must be evaluated, rather than only one for both the strong- and weak-line approximations. After the frequency-dependent parameters have been specified and the values of W and P have been determined for a given slant path, it becomes a simple matter to generate absorption spectra.

2.3. DETERMINATION OF FREQUENCY-DEPENDENT PARAMETERS BY EMPIRICAL PROCEDURES

The determination of the frequency-dependent parameters is undoubtedly the most critical aspect of developing a function for use in computing homogeneous-path spectral absorption. The theory of band models is reasonably well defined and the resulting functions should be capable of specifying spectral absorption to a good approximation if, first, the conditions inherent in the band-model development are satisfied, and second, rigorous empirical proce-

dures are applied to high-quality laboratory homogeneous-path data to specify the absorption constants.

It has been stated that the first conditional restrictions are satisfied by most atmospheric slant paths of interest. Therefore, it seems hopeful that usable transmissivity functions could be developed if the second procedural restrictions are satisfied.

Oppel [21] has postulated and employed certain rules for selecting laboratory data and performing an empirical fit. His approach is sound and is analogous to that suggested by Plass [22]. Hence, the methods of Oppel are those which are recommended for the determination of the spectral absorption constants and are stated below.

It has been found by most researchers that the quality and the reduction of the laboratory data have constituted the most critical step in determining the absorption constants. In order to insure satisfactory results from an empirical fitting procedure the following rules should be observed.

(1) The data should be consistent from one run to another; that is, all runs for a particular spectral interval should have the same resolution and spectral calibration. The absolute spectral calibration is not nearly as important as the relative spectral position from run to run, because the absorption constants can be determined for relative frequency units. Also, the spectrum can later be shifted if necessary.

(2) Only data with absorption between 5% and 95% should be used. Usually the data for very high or very low absorption values are questionable because of the uncertainty of the 0% and 100% levels, and relatively small differences may have an inordinately great effect on the determination of the unknown parameters.

(3) It is desirable to have spectra obtained over a range of paths and pressures which is wide enough that the function can be properly fitted to the data. Ideally, for each frequency, one would like to have data which would give absorptions between 5% and 95% and which include the following conditions:

(a) Pressure and absorption path are sufficiently small that there is negligible overlapping of the spectral lines.

(b) Pressure is high and absorption path is small so that there is heavy overlapping of the spectral lines.

(c) Pressure is low and absorption path is large so that the spectral lines are opaque at their centers and the transmission is achieved only in the wings of the lines.

(4) Measurements for which pressure self-broadening is predominant, that is, where the absorbing-gas pressure is an appreciable part of the total pressure, should be discarded. This is necessary since self-broadened spectral lines need not be evaluated under real atmospheric conditions.

(5) In general, better results are obtained if spectral frequencies are selected at which absorption achieves a local maximum, minimum, or inflection point. Thus, the absorption constants should not necessarily be selected at uniform intervals but for spectral positions that are more easily measured. It has been frequently observed that published spectra are hand plotted and that their author will tend to be more exact on the maxima, minima, and inflection points than he will be on any other part of the curve.

Atmospheric paths that are of greatest interest to the infrared researcher are long paths through an atmosphere of relatively low pressure. Such paths give rise to large values of W and small values of equivalent pressure $\bar{P}$. The dominant spectral lines, those which account for 95% of the absorption, are opaque at their centers but do not display a significant amount of overlapping. Therefore, for such paths β is small ($\beta < 1$) and ψ is large ($\psi >> 1$) and the strong-line conditions are valid. It has been stated that strong-line absorption must be present for an atmospheric path to be reduced to an equivalent homogeneous path. For these reasons most researchers assume that absorption is represented by the strong-line approximation, $A = A(\beta^2\psi)$, and empirically fit this function to laboratory data. When such a procedure is used, if the data used do not satisfy strong-line absorption conditions erroneous constants will be determined.

After selecting the laboratory homogeneous-path spectra according to the above rules and the appropriate model for representing absorption for a given absorption band, one has the proper foundation for performing an empirical fit which will yield a valid closed-form expression for predicting absorption for other homogeneous paths.

Basically, the absorption coefficients are determined by minimizing the sums of the squares of the errors between measured and calculated values of absorption. Before the least-squares iteration can begin, an initial estimate of the two parameters $2\pi\alpha_0'/d$ and $S/2\pi\alpha_0'$ must be made. The method of determination and the accuracy of these initial parameters does not affect the final accuracy except that poorly chosen estimates will considerably increase the iteration time. The method suggested is based on the fact that the three approximations to the Elsasser integral, described in section 2 always show greater absorption than that given by the complete Elsasser integral and approach the complete expression in the limit. This method can be described as follows:

(1) Three master graphs are drawn on log-log paper. The first graph (fig. 11), is a plot of Beers' law, given by

$$A = 1 - \exp(-\beta\psi);\ \beta\psi = \frac{S}{d}\frac{W}{P}$$

The second master graph (fig. 12) gives the strong-line approximation to the Elsasser integral:

$$A = \operatorname{erf}\left[\left(\frac{1}{2}\beta^2\psi\right)^{1/2}\right];\ \beta^2\psi = \frac{2\pi\alpha_0' S}{d^2}WP$$

The third master graph (fig. 13) gives the nonoverlapping-line approximation:

$$A = \beta\psi[I_0(\psi) + I_1(\psi)]\ \exp(-\psi)$$

$$\beta = \frac{2\pi\alpha_0'}{d}P,\ \psi = \frac{S}{2\pi\alpha_0'}\frac{W}{P}$$

(2) Three working graphs are plotted for each spectral frequency for which absorption constants are to be determined.

(a) In the first working graph (fig. 14) fractional absorption A is plotted as a function of the absorption path W (atm cm).

(b) The second graph (fig. 15) gives fractional absorption versus absorption path times effective broadening pressure WP_e (atm cm × mm Hg).

(c) The third working graph (fig. 16) is a plot of the ratio of fractional absorption to effective broadening pressure, A/P (mm Hg^{-1}) versus absorption path/effective broadening pressure W/P (atm cm/mm Hg).

(3) The six graphs are now paired off in the following order: figure 11 is superposed over figure 14, figure 12 over figure 15, and figure 13 over figure 16. With a good spread of data, it now becomes apparent that the several approximations are limiting functions and all points on the graphs will fall below the limiting curve. Figure 11 is adjusted in the W direction until all plotted points of figure 14 fall below and to the right of the curve drawn on figure 11. Thus, the curve of figure 11 forms the limiting continuum for the points of figure 14. The relative positions yield the approximate value

$$(S/d) = (\beta\psi/W)$$

Similarly, figure 12 is superposed over figure 15 and adjusted along the axis until the limiting continuum is found, yielding the approximate value

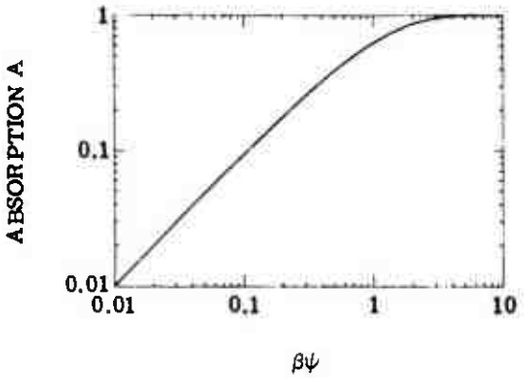

FIGURE 11. WEAK-LINE APPROXIMATION TO THE ELSASSER MODEL. $A = 1 - \exp(-\beta\psi)$; $\beta\psi = SW'/d$.

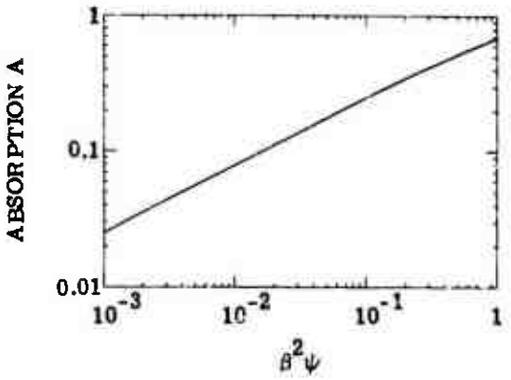

FIGURE 12. STRONG-LINE APPROXIMATION TO THE ELSASSER MODEL. $A = \mathrm{erf}\left[\left(\frac{1}{2}\beta^2\psi\right)^{1/2}\right]$; $\beta^2\psi = \left(2\pi\sigma_0' S/d^2\right)WP$.

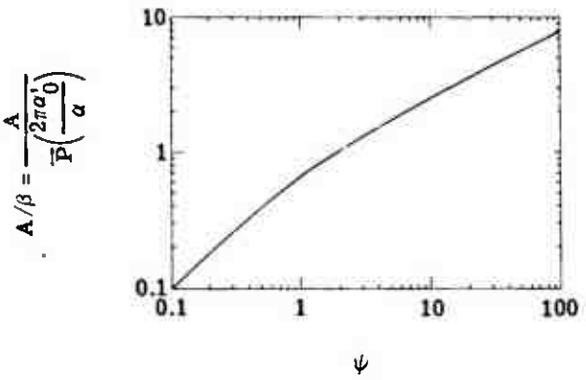

FIGURE 13. NONOVERLAPPING-LINE APPROXIMATION TO THE ELSASSER MODEL. $A/\beta = \psi\left[I_0(\psi) + I_1(\psi)\right]\exp -\psi$; $\psi = (S/2\pi\alpha_0')(W/P)$.

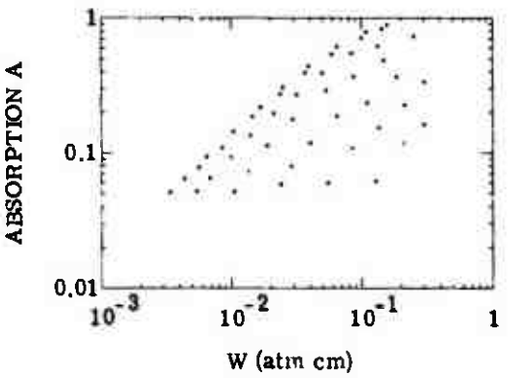

FIGURE 14. WORKING GRAPH FOR ESTIMATING S/d. For these data $S/d \cong 15$.

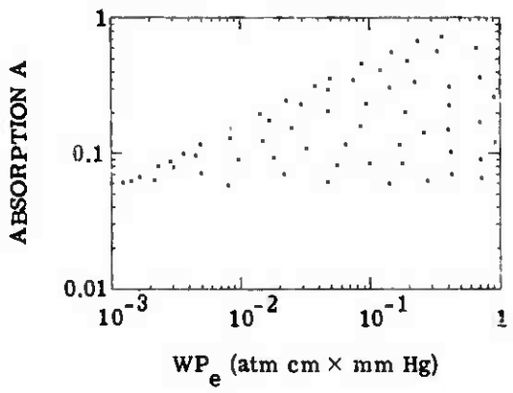

FIGURE 15. WORKING GRAPH FOR ESTIMATING $2\pi\alpha_0' S/d^2$. For these data $2\pi\alpha_0' S/d^2 \cong 4.5$.

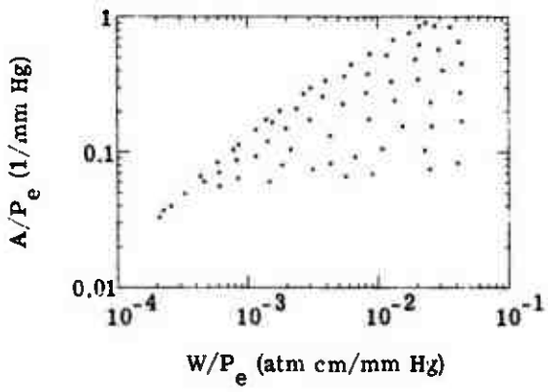

FIGURE 16. WORKING GRAPH FOR ESTIMATING $2\pi\alpha_0'/d$ and $S/2\pi\alpha_0'$. For these data $2\pi\alpha_0'/d \cong 0.3$ and $S/2\pi\alpha_0' \cong 500$.

$$\left(\frac{2\pi a_0' S}{d^2}\right) = \frac{(\beta^2 \psi)}{(W P_e)}$$

The third pair (figs. 13 and 16) can be adjusted in both directions to give approximations to two parameters:

$$\left(\frac{2\pi a_0'}{d}\right) = \frac{A/P_e}{(A/\beta)}$$

and

$$\left(\frac{S}{2\pi a_0'}\right) = \frac{\psi}{(W/P_e)}$$

The three plots indicated above are not all necessary if sufficient data are available since only two constants are necessary to evaluate the Elsasser integral; however, experience has shown that sufficient spread of data is usually not available to adequately construct all of the graphs. For this reason, the best graphs should be chosen. In the event that the nonoverlapping approximation gives a good continuum, then it may be used alone for both approximations to the unknown parameters.

At this point it is assumed that the initial estimates of the parameters have been made and the laboratory data have been properly chosen. Beginning with the first estimates, the absorption is calculated for each value of absorber concentration and each value of equivalent pressure and compared with the measured value. The parameters are adjusted until the sums of the squared residuals between computed and measured absorption values are minimized.

A computer program has been written by Baumelster and Marquardt and distributed as a SHARE program [23]. This program, when coupled with the Elsasser-model alogorithm described in section 2, will optimize the parameters for the Elsasser function.

The procedure described above is that which should be used when fitting the complete Elsasser integral to laboratory data. It is emphasized that if the strong-line or weak-line approximation to the Elsasser model is used to represent atmospheric absorption, then the laboratory data must be such that these conditions are satisfied. This can be determined by using the initial estimates of $2\pi a_0'/d$ and $S/d\pi a_0'$ and the values of W and P to calculate β and ψ. These results can then be compared with the values in table 2.

A completely analogous procedure should be used when fitting the Goody model to a set of laboratory data. That is, all three equations should be fitted to the data to obtain a set of

frequency-dependent parameters. Parameters obtained in this manner will give valid results whether the absorption is strong, weak, or of some intermediate value.

The method described above for performing an empirical fit of a band model to laboratory data is the suggested procedure. However, it has been used by only two of the many researchers that have developed functions for calculating atmospheric absorption. Of the various methods that have been employed, some are similar to it and others are very different; in section 3 each of the empirical functions developed by the various researchers is presented and the empirical procedures employed by each of these researchers are discussed.

Empirically fitting a band-model expression to homogeneous data generates coefficients that represent the best value for all available data. The absorption constants then do not actually represent the strengths, widths, and spacings of the spectral lines but can be interpreted as a set of lines giving equivalent absorption. It can be expected that calculations should be satisfactory for conditions bounded by the laboratory data. However, for extreme cases the results may be rather poor. It is difficult to theoretically analyze the accuracy with which a band model can be used to predict absorption, so the approach used here is simply to compare the results with field measurements. Such comparisons are presented and discussed in section 7.

2.4. CONVERSION OF SLANT-PATH TO EQUIVALENT-PATH PARAMETERS

Since the band-model expressions can be applied only to homogeneous paths at standard temperature, any real atmospheric slant path must be reduced to an equivalent homogeneous path at standard temperature or an equivalent sea-level path which is a homogeneous path at standard temperature and pressure. In the discussions that follow, the methods for determining the equivalent paths are derived for various types of absorption and the assumptions and approximations used are discussed.

The absorption spectra for any homogeneous path, assuming a constant temperature, is defined by the absorber concentration W of each gas and the equivalent broadening pressure $\overline{P}$ which determines the half-width of the spectral lines. Therefore, to determine an equivalent homogeneous path for an atmospheric slant path, it is necessary to determine a value of W and $\overline{P}$ for each absorbing species such that the slant path will absorb exactly as does the homogeneous path. Although this cannot be achieved exactly, since the intensities and half-widths are continually changing from point to point along a slant path, under certain conditions the concept of an equivalent path is a reasonable approximation.

Recall that the general equation for absorption over an atmospheric slant path is given by

$$A_S\Delta\nu = \int_{\Delta\nu}\left\{1 - \exp\left[-\frac{1}{\pi}\sum_{i=1}^{N}\int_0^X \frac{S_i\alpha_i\rho}{\left(\nu - \nu_{0_i}\right)^2 + \alpha_i^2}dx\right]\right\}d\nu \tag{49}$$

The absorption of a homogeneous path is given by

$$A_h\Delta\nu = \int_{\Delta\nu}\left\{1 - \exp\left[-\frac{1}{\pi}\sum_{i=1}^{N}\frac{S_{h_i}\alpha_{h_i}W_h}{\left(\nu - \nu_{0_i}\right)^2 + \alpha_{h_i}^2}\right]\right\}d\nu \tag{50}$$

2.4.1. WEAK-LINE NONOVERLAPPING CONDITION. Let us consider the case where every spectral line in the interval $\Delta\nu$ is a weak absorber and the spectral lines do not overlap strongly. This will be true in general for short paths at high altitudes. Under these conditions the pressures are low and the half-widths are narrow. If the absorption is small at the line center for each spectral line within the interval $\Delta\nu$, the slant-path absorption may be approximated by taking the first two terms in the expansion of the exponential. Thus equation 49 reduces to

$$A_S\Delta\nu = \int_{\Delta\nu}\left[\frac{1}{\pi}\sum_{i=1}^{N}\int_0^X \frac{S_i\alpha_i\rho}{\left(\nu - \nu_{0_i}\right)^2 + \alpha_i^2}dx\right]d\nu \tag{51}$$

Further, for each ν_{0_i} within $\Delta\nu$ the entire spectral line is within $\Delta\nu$, so the order of integration may be interchanged, giving

$$A_S\Delta\nu = \int_0^X \frac{1}{\pi}\sum_{i=1}^{N}S_i\left[\int_{\Delta\nu}\frac{\alpha_i}{\left(\nu - \nu_{0_i}\right)^2 + \alpha_i^2}d\nu\right]\rho dx \tag{52}$$

Since $\Delta\nu$ encompasses the entire spectral line, the limits may be taken as $-\infty$ to ∞ with no loss in generality. Now

$$\int_{-\infty}^{\infty}\frac{\alpha_i}{\left(\nu - \nu_{0_i}\right)^2 + \alpha_i^2}d\nu = \pi$$

so equation 52 becomes

$$A_S{}^{\Delta\nu} = \int_0^X \sum_{i=1}^N S_i \rho \, dx \tag{53}$$

or

$$A_S{}^{\Delta\nu} = \sum_{i=1}^N \int_0^X S_i \rho \, dx \tag{54}$$

If it is further assumed that the line strengths S_i are independent of the path, then

$$A_S{}^{\Delta\nu} = \sum_{i=1}^N S_i \int_0^X \rho \, dx \tag{55}$$

If we perform an analogous development for a homogeneous path, we obtain

$$A_h{}^{\Delta\nu} = \sum_{i=1}^N S_i \rho X = \sum_{i=1}^N S_i W_h \tag{56}$$

So under conditions of weak-line nonoverlapping absorption with the line strengths independent of path, the slant path will absorb approximately the same as a homogeneous path with the absorber concentration of the homogeneous path given by

$$W_h = \int_0^X \rho \, dx \tag{57}$$

Under these conditions the absorption is independent of pressure and is completely specified by W_h.

2.4.2. STRONG-LINE EQUIVALENT PRESSURE $\overline{P}$. Recall that the absorption for conditions other than weak-line absorption is defined by the weak-line absorber concentration W and the equivalent path pressure $\overline{P}$. That is,

$$A = A(2\pi a_0'/d,\ S/2\pi a_0', W,\ \overline{P}) \text{ (no approximation)}$$

$$A = A(2\pi a_0' S/d^2,\ W\overline{P}) \text{ (strong-line approximation)}$$

$$A = A(S/d,\ W) \text{ (weak-line approximation)}$$

To develop an expression for the equivalent pressure for a slant path, let us consider the case in which all of the lines within $\Delta\nu$ are strong-line absorbers. This characteristic implies that absorption is complete to wavenumbers that are in excess of the line half-width. Therefore, a further increase in path length simply increases the absorption in the wings of a spectral line and has no affect on the absorption at the line center. For the Lorentz line shape this means that $\left(\nu - \nu_{0_i}\right)^2 >> \alpha_i^2$ for all lines. Using this approximation, we may write equation 49 as

$$A_S \Delta\nu = \int_{\Delta\nu} \left\{ 1 - \exp\left[-\frac{1}{\pi} \sum_{i=1}^{N} \int_0^X \frac{S_i \alpha_i \rho_S}{\left(\nu - \nu_{0_i}\right)^2} dx \right] \right\} d\nu \tag{58}$$

For a homogeneous path, we have

$$A_h \Delta\nu = \int_{\Delta\nu} \left\{ 1 - \exp\left[-\frac{1}{\pi} \sum_{i=1}^{N} \frac{S_{h_i} \alpha_{h_i} W_h}{\left(\nu - \nu_{0_i}\right)^2} \right] \right\} d\nu \tag{59}$$

If it is assumed as before that S_i does not vary along the slant path, then the slant path will absorb approximately as a homogeneous path with

$$\alpha_{h_i} W_h = \int_0^X \alpha_i \rho_S \, dx \tag{60}$$

Recall that

$$\alpha_{h_i} = \alpha_{0_{h_i}} \frac{P_h}{P_0} \left(\frac{T_0}{T_h} \right)^n \tag{61}$$

Also,

$$\alpha_i = \alpha_{0_i} \frac{P_S}{P_0} \left(\frac{T_0}{T_S} \right)^n \tag{62}$$

As was mentioned previously, the value of pressure used in equation 62 should be the effective broadening pressure. However, the partial pressure of any absorbing gas is very small compared to atmospheric pressure, so the error involved in assuming P_S to be total atmospheric pressure is assumed to be negligible. Substituting these expressions into equation 60, we obtain

$$W_h \frac{P_h}{P_0}\left(\frac{T_0}{T_h}\right)^n = \int_0^X \frac{P_S}{P_0}\left(\frac{T_0}{T}\right)^n \rho_S \, dx \tag{63}$$

Substituting in the slant-path integral expression for W_h, we have

$$\frac{P_h}{P_0}\left(\frac{T_0}{T_h}\right)^n = \frac{\int_0^X \frac{P}{P_0}\left(\frac{T_0}{T}\right)^n \rho \, dx}{\int_0^X \rho \, dx} \tag{64}$$

The assumptions imposed thus far have been strong-line absorption and line strength independent of path. If we further assume that the path is isothermal and equal to T_h, which in effect completely neglects the effect of temperature on half-width, then the pressure of the homogeneous path, such that the homogeneous and slant paths absorb the same, is given by

$$\bar{P}_h = \frac{\int_0^X P_S \rho_S \, dx}{\int_0^X \rho_S \, dx} \tag{65}$$

Equation 65 is then the expression for obtaining the equivalent path pressure. This pressure will be denoted by $\bar{P}$. This concept was first considered by Curtis and Godson [24, 25] and is therefore referred to as the Curtis-Godson approximation.

The equivalent-path parameters are given by equations 57 and 65. Equation 57 is valid under any conditions of absorption, assuming only that the line strengths are independent of path. Equation 65 is valid only for those conditions of strong-line absorption in which the effect of temperature on the spectral-line half-width and line strength are neglected.

2.4.3. EQUIVALENT SEA-LEVEL ABSORBER CONCENTRATION W^*. Some authors have empirically determined their frequency-dependent parameters from laboratory data that are at standard pressure as well as standard temperature. Therefore, their methods can only be used to predict absorption for other homogeneous paths that are at standard conditions. To apply such methods to atmospheric slant paths, the paths would have to be reduced to equivalent homogeneous paths at STP. Such paths have been defined as equivalent sea-level paths and are denoted by W^*.

Returning to equation 60, a slant path will absorb approximately as a homogeneous path with

$$\alpha_{h_i} W_h = \int_0^X \alpha_i \rho_S \, dx \tag{66}$$

As was stated previously, this expression is valid only for strong-line absorption with S_i independent of path.

For this case the homogeneous path is at STP so $\alpha_{h_i} = \alpha_{0_i}$ and equation 66 becomes

$$\alpha_{0_i} W_h = \int_0^X \alpha_{0_i} \frac{P_S}{P_0} \left(\frac{T_0}{T_S}\right)^n \rho_S \, dx$$

and, finally, the equivalent sea-level absorber concentration is given by

$$W^* = W_h = \int_0^X \frac{P_S}{P_0} \left(\frac{T_0}{T_S}\right)^n \rho_S \, dx \tag{67}$$

It is useful to note that under conditions of strong-line absorption (neglecting the effect of temperature on half-width and line strength) the equivalent sea-level concentration is equal to the product of the weak-line nonoverlapping absorber concentration and the equivalent-path pressure normalized to standard pressure. Or

$$W^* = W \frac{\overline{P}}{P_0} \tag{68}$$

2.4.4. GENERAL COMMENTS ON W, $\overline{P}$, AND W^*. Three expressions have been derived which will be used throughout the remainder of the report. First is the weak-line nonoverlapping absorber concentration W, which is simply the grams of absorber in the slant path. Second is the Curtis-Godson equivalent pressure $\overline{P}$. The concept of an equivalent slant-path pressure is valid only under conditions of strong-line absorption and isothermal slant paths. Also, this concept requires that the effect of temperature on half-width be neglected. The last quantity which was derived is the "equivalent sea-level path," W^*. This equivalent concentration is effectively the grams of absorber in the slant path adjusted in accordance with the dependence of half-width on temperature and pressure. This concept is valid only under conditions of strong-line absorption and for isothermal slant paths.

To develop closed-form band-model expressions for absorption it was necessary to neglect the effect of temperature on line strength and line half-width. Such approximations were also required to determine the equivalent-path parameters. Although this assumption does, of course, introduce errors in the final result, Drayson has shown that such errors are not large. Also, there is an added fact which further reduces the error introduced hy this assumption. Consider the integrated absorption for an entire spectral band. It has been stated previously that as the temperature decreased the integrated absorption decreases. However, the line half-widths become larger for smaller temperatures and thus give rise to increased absorption. Therefore, rather than being additive the errors tend to cancel each other.

The integral expressions for W and W^* given by equations 57 and 67 yield, respectively, the grams per square centimeter and effective grams per square centimeter for a slant path. The accepted practice is to normalize these quantities by dividing by the density of the absorbing gas at standard temperature and pressure. For the gases CO_2, O_3, N_2O, CO, and CH_4, W and W^* will have units of centimeters since for each of these gases ρ_{STP} is expressed in grams per cubic centimeter. Actually, W represents the length of a column of pure gas (1 cm^2 in cross section) at STP which contains the same number of grams as the slant path. For W^* the length is adjusted in accordance with the variation of half-width with pressure and temperature. According to this definition, the units of W and W^* are commonly referred to as atmospheric centimeters.

The units of W and W^* are defined somewhat differently for water vapor. For a given slant path the amount of water vapor is reduced to an equivalent amount of liquid water at STP or precipitable centimeters of water. The normalizing factor is, therefore, the density of liquid water rather than water vapor. There is no justification for using different units for the two cases; it has simply been the accepted practice since transmission work began.

2.4.5. A GENERALIZED CALCULATION OF W, $\overline{P}$ AND W^*. To clarify the exact technique for evaluating W, W^*, and $\overline{P}$ for each absorbing species for a slant path, consider a path that begins at the earth's surface and extends outward to the limits of the atmosphere. As a result of the refracting characteristics of the atmosphere, the line of sight will be slightly curved rather than straight, and the amount of curvature will increase as the path becomes more horizontal. The first step in determining the reduced optical path is to determine the actual refractive path through the atmosphere. A computer program has been written in FORTRAN which performs this computation. The analytical procedures and computer program are discussed in

detail in appendix I. After the refracted path is determined, the values of pressure and temperature and the mixing ratio of each absorbing species can be expressed as functions of distance along the path. These are represented by P(x), T(x), and M(x), respectively. For the computation of W we have from equation 67:

$$W^* = \frac{1}{\left(\frac{M_{gas} P_0}{RT_0}\right)} \int_0^X M(x) \frac{P(x)}{P_0} \left(\frac{T_0}{T(x)}\right)^n \frac{M_{air} P(x)}{RT(x)} dx \tag{69}$$

where P_0 = surface pressure
T_0 = surface temperature
M_{gas} = molecular weight of absorbing gas
M_{air} = molecular weight of air
R = gas constant
$M(x)$ = mixing ratio in grams of gas per gram of air
X = path length in centimeters

Since the mixing ratio for gases is usually given in moles of gas per mole of air, the mixing ratio must be converted to grams of gas per gram of air by multiplying by the ratio of their molecular weights. The equation for determining W^* for a slant path becomes

$$W^* = \int_0^X M(x) \left(\frac{P(x)}{P_0}\right)^2 \left(\frac{T_0}{T(x)}\right)^{n+1} dx \tag{70}$$

where M(x) is the mixing ratio in moles of gas per mole of air.

The equation for computing the equivalent slant-path precipitable centimeters of water differs slightly from equation 70 since the mixing ratio for water is given in grams of H_2O per kilogram of air, and the density of H_2O at STP is used as the normalizing factor. For this case it is easily shown that the precipitable centimeters of H_2O in the slant path are given by

$$W^* = 1.225 \times 10^{-6} \int_0^X M(x) \left(\frac{P(x)}{P_0}\right)^2 \left(\frac{T_0}{T(x)}\right)^{n+1} dx \tag{71}$$

where M(x) is the mixing ratio in g/kg.

In summary, equation 70 is used to compute atmospheric centimeters for gases for which the mixing ratio is given in moles of gas per moles of air. Equation 71 is used to compute

precipitable centimeters of water vapor if the mixing ratio is given in grams of H_2O per kilogram of air. To compute the respective values of W, simply let the exponents of the pressure and temperature terms in equations 70 and 71 be unity. To determine $\overline{P}$ for a slant path, first compute the appropriate value of W^*, letting n = 0. Next, compute the value of W as stated above. Then $\overline{P}$ will be given by

$$\overline{P} = \frac{[W^*]_{n=0} P_0}{W}$$

In conjunction with the refractive-path computer program, programs for computing W^*, W, and $\overline{P}$ have been written in FORTRAN for the IBM 7090. These programs are also included and discussed in appendix I.

The use of a computer program to evaluate the quantities W, W^*, and $\overline{P}$ for each absorbing gas for an atmospheric slant path is a rigorous yet practical method for determining the equivalent-path parameters. Many researchers [26-28] have proposed methods for evaluating equations 70 and 71 without the aid of a computer by approximating the mixing ratio, pressure, and temperature profiles with analytical functions and thus allow the integrals to be evaluated by direct interpretation. Such methods yield adequate results for a fixed set of atmospheric conditions, but are not capable of handling variable meteorological conditions. This can be a rather severe limitation in the case of water vapor and ozone. Therefore, it is recommended that these methods not be used unless only first-order approximations to the path parameters are required.

The computer program is simple to apply and performs an exact numerical integration. Therefore, it is felt that there is no need to introduce approximations to a problem that already has a relatively simple solution.

2.5. SUMMARY

In this section four basic methods for computing atmospheric-slant-path molecular absorption have been discussed. The first involved a direct-pressure integration over the slant path, summing the contribution of each spectral line, including the effect of temperature and pressure on line strength and half-width. This method requires complete a priori knowledge of the band parameters, including line strength, line half-width, and line location. The absorption spectra are computed by direct integration of the general transmissivity function.

The second method employed the use of the quasi-random model of the band structure. This model simulates the band structure in a prescribed way such that the absorption spectra

for any homogeneous path may be determined. This method requires some a priori knowledge of the band parameters (as does the rigorous method), but once the absorption spectra are determined for one homogeneous path, a set of coefficients is generated so that the summing procedure need not be repeated to determine the absorption for a different homogeneous path. Homogeneous laboratory spectra are not a prerequisite for the use of this method but are usually employed to normalize the absorption coefficients.

The third method assumed models of the band structure which allowed for the derivation of closed-form analytical expressions that could be used in conjunction with laboratory homogeneous-path data to predict spectral absorption for other homogeneous paths. The models assumed were the Elsasser, statistical, and random-Elsasser models.

The fourth method assumed models of the band structure and then modulated these line arrays with an exponential envelope. The resulting band model was integrated directly to obtain expressions for the total integrated band absorption, $A_\nu d\nu$. These expressions, in conjunction with laboratory homogeneous-path data, could then be used to predict integrated-band absorption values for atmospheric slant paths.

In order to use the closed-form expressions derived by methods three and four to predict absorption for slant paths, the slant paths need first be reduced to equivalent homogeneous paths. Some of the expressions require that the equivalent path need only be homogeneous and express absorption in terms of W and $\overline{P}$. Others require that the path be reduced to standard conditions and therefore express the absorption in terms of W^*.

The reason for developing methods for computing absorption based on band models was to generate a method that required a minimal amount of computation yet would give results that were at least a first-order approximation to the true results. Later in the report absorption spectra as computed by the various methods are compared both with one another and with field measurements; the results of these comparisons are analyzed and discussed.

3
METHODS FOR COMPUTING MOLECULAR ABSORPTION SPECTRA BASED UPON BAND MODELS

3.1. INTRODUCTION

In section 2, the general theory for computing atmospheric slant-path molecular absorption was formulated. The most useful results developed from the theory were the closed-form band-model functions. These functions express absorption as a function of one or two frequency-dependent parameters which are determined by empirically fitting the band-model expressions to homogeneous-path laboratory data. Because many researchers have made such empirical fits, no two methods for computing absorption are exactly the same. This inconsistency results from the fact that different researchers selected different band models (or different forms of the same model), had different collections of laboratory data, and employed differing procedures to achieve the desired empirical fit.

In this section those methods which are considered most representative of the state of the art are represented. Each method will be discussed separately, and the band models, laboratory data, and empirical procedures used by each author will be stated.

3.2. METHOD OF W. M. ELSASSER

Elsasser [9] developed transmissivity functions for the absorption bands of carbon dioxide, ozone, and water vapor using a method which is a simple extension of the band-model procedures discussed in section 2.2.

The strong-line approximation to the Elsasser and Goody models can be expressed as

$$\tau = \tau(k(\lambda)\cdot W^*)$$

where $k(\lambda)$ is defined as a generalized absorption coefficient and the functional form of τ is given by either the Elsasser or the Goody model. The empirical procedure outlined in section 2.3 was to assume the appropriate form for τ, which depended upon the absorbing gas under consideration. The laboratory homogeneous-path data were used to evaluate the frequency-dependent parameter or parameters for each wavelength throughout the band. Elsasser did not assume that the functional form of τ was given by either model, but used the laboratory data to define both the functional form of τ and the absorption coefficient $k(\lambda)$. The procedure he used is described here:

The homogeneous-path laboratory data were reduced to equivalent W* values using the expression

$$W^* = W_h \frac{P_e}{P_0}\left(\frac{T_0}{T}\right)^{1/2}$$

The absorption band was then divided into subintervals approximately 10 wavenumbers wide and for each subinterval the mean transmission for the interval was plotted as a function of W*. Elsasser found that each of the curves obtained for the various intervals had approximately the same functional form. Therefore, a standard transmissivity curve (the functional form of τ) was adopted which expressed the transmission as a function of the product $W^* \cdot k(\lambda)$. Therefore, Elsasser proceeded ... the inherent assumption that an absorption band may be represented by a strong-line band-model expression, but determined the functional form of this expression empirically rather than analytically. The empirically derived transmissivity function undergoes a shift along the W* scale as one passes from one interval in the spectrum to an adjacent interval. Elsasser plotted this shift as a function of wavelength and fitted a curve to the data using a least-squares procedure. This curve defines the generalized absorption coefficient, $k(\lambda)$.

Elsasser's results are presented in the form of tables which represent the two functions, $\tau(k(\lambda))$ and $k(\lambda)$. Since the concept of strong-line absorption was utilized in the development of these functions, the method should be applied only to slant paths for which this condition is satisfied.

3.2.1. TRANSMISSIVITY FUNCTION: CARBON DIOXIDE. Elsasser developed transmissivity functions for only the 15-μ absorption band of CO_2. The laboratory data upon which the empirical procedures were based were taken from the work of Cloud [29]. Elsasser later considered the work of Howard, Burch, and Williams [30], Kaplan and Eggers [31], and Yamamoto and Sasamori [32] and proposed modifications to the original transmissivity functions to obtain functions that are in agreement with all three sets of laboratory data.

The transmissivity function obtained is shown in figure 17, and the generalized absorption coefficient derived from the shift in the τ curves is shown in figure 18. For convenience in determining atmospheric-transmission values, both the transmissivity curve and the generalized absorption coefficient curve are tabulated. The results are given in table 3.

Using the transmissivity curve shown in figure 17 and the absorption coefficient shown in figure 18, Elsasser reconstructed the absorption-band contours for various values of W* which

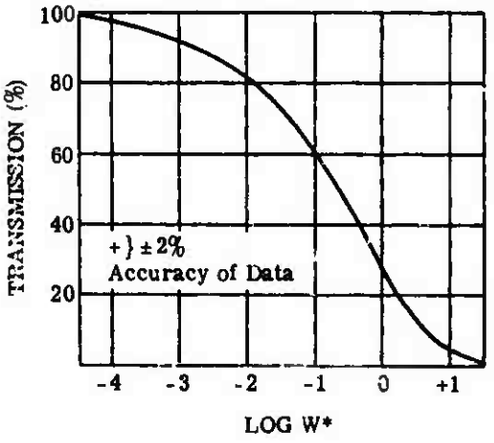

FIGURE 17. TRANSMISSIVITY CURVE FOR CARBON DIOXIDE

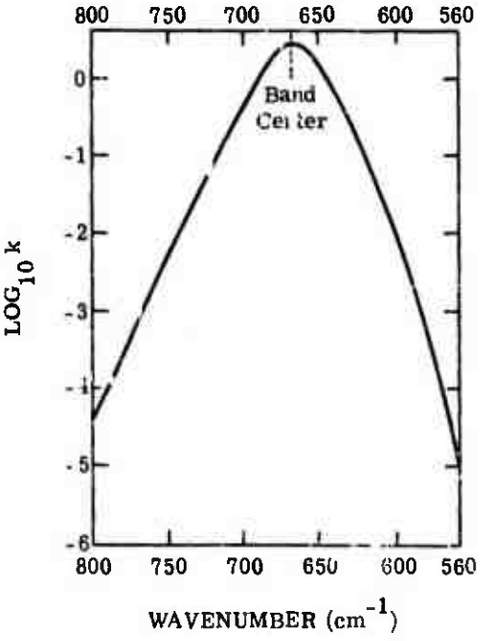

FIGURE 18. GENERALIZED ABSORPTION COEFFICIENT FOR 15-μ CARBON DIOXIDE BAND

TABLE 3. TRANSMISSIVITY FUNCTION AND ABSORPTION COEFFICIENTS FOR CARBON DIOXIDE

λ (μ)	ν (cm^{-1})	k	$\tau(k \cdot W^*)$ (%)	$k \cdot W^*$
11.77	850	1.59 E-7	100.00	6.31 E-6
11.95	837.5	5.01 E-7	99.97	7.94 E-6
12.13	825	3.16 E-6	99.91	1.00 E-5
12.35	810	1.48 E-5	99.82	1.26 E-5
12.50	800	4.07 E-5	99.70	1.59 E-5
12.66	790	1.17 E-4	99.55	1.99 E-5
12.82	780	3.02 E-4	99.37	2.51 E-5
12.99	770	8.32 E-4	99.16	3.16 E-5
13.16	760	2.14 E-3	98.92	3.98 E-5
13.33	750	5.37 E-3	98.65	5.01 E-5
13.51	740	1.32 E-2	98.35	6.31 E-5
13.70	730	3.16 E-2	98.02	7.94 E-5
13.89	720	8.32 E-2	97.66	1.00 E-4
14.08	710	1.91 E-1	97.27	1.26 E-4
14.29	700	4.57 E-1	96.85	1.59 E-4
14.49	690	1.00	96.39	1.99 E-4
14.71	680	2.09	95.90	2.51 E-4
14.93	670	2.69	95.38	3.16 E-4
15.15	660	2.40	94.82	3.98 E-4
15.38	650	1.45	94.22	5.01 E-4
15.63	640	6.17 E-1	93.58	6.31 E-4
15.87	630	2.45 E-1	92.90	7.94 E-4
16.13	620	8.91 E-2	92.18	1.00 E-3
16.39	610	3.16 E-2	91.41	1.26 E-3
16.67	600	8.17 E-3	90.59	1.59 E-3
16.95	590	2.34 E-3	89.72	1.99 E-3
17.24	580	5.01 E-4	88.79	2.51 E-3
17.54	570	8.91 E-5	87.80	3.16 E-3
17.86	560	1.07 E-5	86.74	3.98 E-3
18.2	550	1.26 E-6	85.61	5.01 E-3
			84.40	6.31 E-3
			83.10	7.94 E-1
			81.70	1.00 E-2
			80.19	1.26 E-2
			78.56	1.59 E-2
			76.80	1.99 E-2
			74.91	2.51 E-2
			72.88	3.16 E-2
			70.71	3.98 E-2
			68.39	5.01 E-2
			65.92	6.31 E-2
			63.30	7.94 E-2
			60.53	1.00 E-1
			57.62	1.26 E-1
			54.58	1.59 E-1

TABLE 3. TRANSMISSIVITY FUNCTION AND ABSORPTION COEFFICIENTS FOR CARBON DIOXIDE (Continued)

$\frac{\lambda}{(\mu)}$	$\frac{\nu}{(cm^{-1})}$	k	$\tau(k \cdot W^*)$ (%)	$k \cdot W^*$
			51.42	1.99 E-1
			48.15	2.51 E-1
			44.78	3.16 E-1
			41.33	3.98 E-1
			37.82	5.01 E-1
			34.26	6.31 E-1
			30.75	7.94 E-1
			27.27	1.00
			23.89	1.26
			20.66	1.59
			17.63	1.99
			14.84	2.51
			12.30	3.16
			10.02	3.98
			8.01	5.01
			6.27	6.31
			4.80	7.94
			3.60	1.00
			2.66	1.26
			1.96	1.59
			1.47	1.99
			1.13	2.51
			0.89	3.16
			0.71	3.98
			0.56	5.01
			0.42	6.31
			0.28	7.94
			0.14	1.00
			0.00	1.26

are shown in figure 19. In order to compare the results using Cloud's data with the results of Howard, Yamamoto, and Kaplan and Eggers, Elsasser planimetered the curves shown in figure 19 to obtain values of the band area for each value of W^*. This procedure evaluates the integral $\int A d\nu$ for each value of W^*. The band area as a function of W^* was then plotted and compared with the results obtained by other authors. The results are shown in figure 20. It is noted that Elsasser proposed a method of adjusting his absorption coefficients so that the curve of figure 20 would be in agreement with other existing data. This method involved various steps. First, a curve (labeled "adopted") was drawn which most closely approximated the composite set of data given in figure 20. The difference between this curve and the curve marked "trial" along the W^* scale was used to relabel the curves of figure 19. For example, for $W^* = 1$, the band area is approximately 85 cm^{-1}. From figure 20, using the "adopted" curve, the new value of W^* is approximately 0.4. After all the curves shown in figure 19 are relabeled, they may be used in conjunction with the transmissivity curve of figure 17 to find new values for the absorption coefficients.

Since the method outlined above for modifying the absorption coefficients was not applied to Elsasser's original data, the data presented in this section are the result of Elsasser's original work on Cloud's data. The amount of computation labor required to perform the suggested modification would be comparable to that required to perform the initial empirical fit, and such a modification appears to be impractical. It is suggested that the present absorption coefficients be used and the results obtained be adjusted according to figure 20.

3.2.2. TRANSMISSIVITY FUNCTION: OZONE. Because the procedure used to develop the transmissivity function and absorption coefficients for ozone is completely analogous in all details to the one used for carbon dioxide, the description in this section will be brief. The transmissivity function and absorption coefficients for ozone were first developed from the laboratory data of Summerfield [33]. The results of the empirical fit are shown in figures 21 and 22. The transmissivity curve differs clearly from the corresponding curve for CO_2 (fig. 17) not only in shape but also in that there is a much larger scatter of the observed points. Using the transmissivity curve and the absorption coefficients, Elsasser computed band spectra for various values of W^* (as was done for CO_2). These curves were planimetered and plotted as W^* versus band area and compared with the experimental results of Walshaw [34]. The results are shown in figure 23.

Note that Elsasser's curve is below Walshaw's curve for every value of band area. Elsasser proposed that this a result of the nature of the pressure correction used in reducing the laboratory

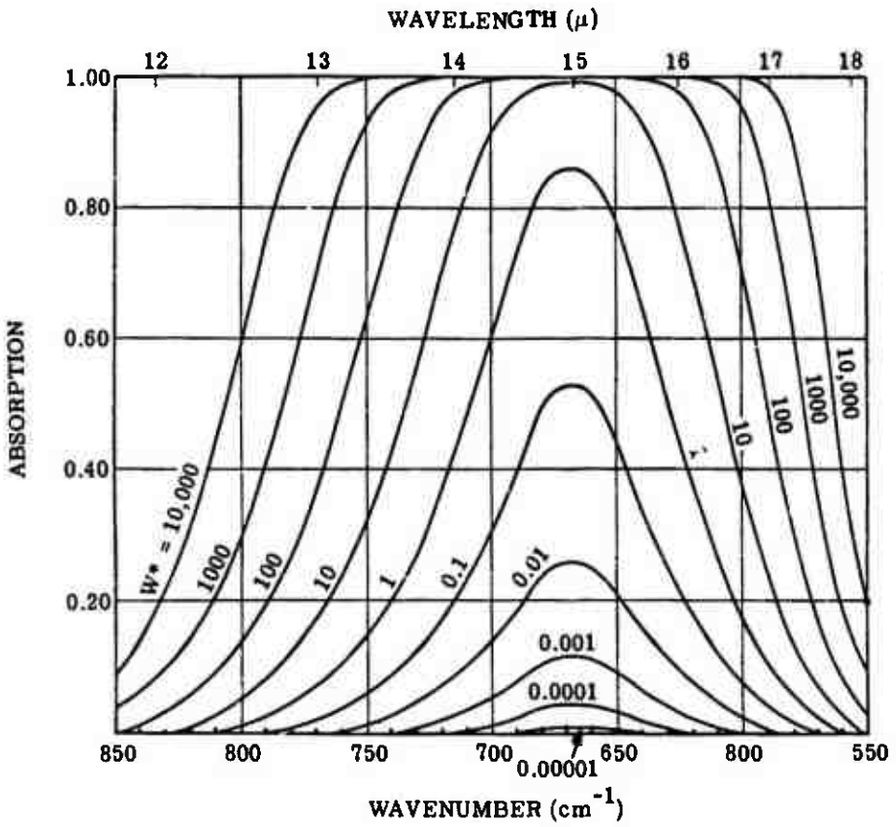

FIGURE 19. ACTUAL ABSORPTION OF 15-μ CARBON DIOXIDE BAND. Corresponds to trial curve in figure 20.

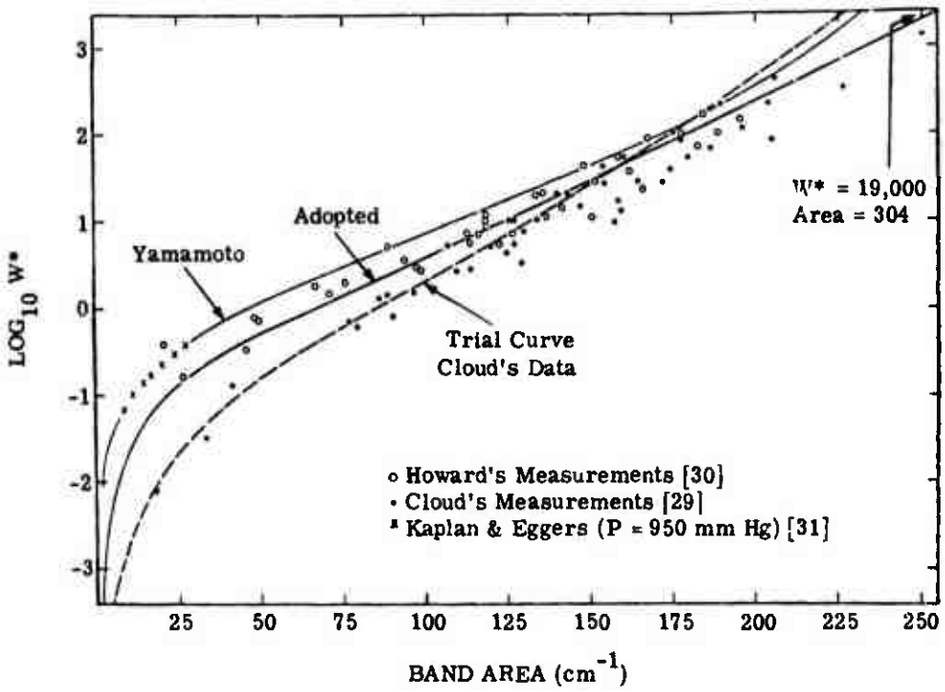

FIGURE 20. COMPUTED AND MEASURED BAND AREAS FOR 15-μ CARBON DIOXIDE BAND

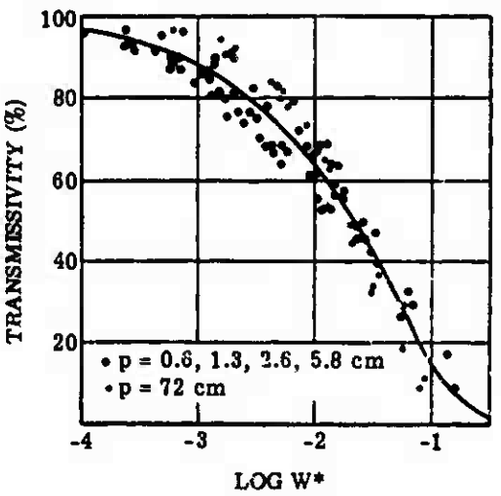

FIGURE 21. TRANSMISSIVITY CURVE FOR OZONE

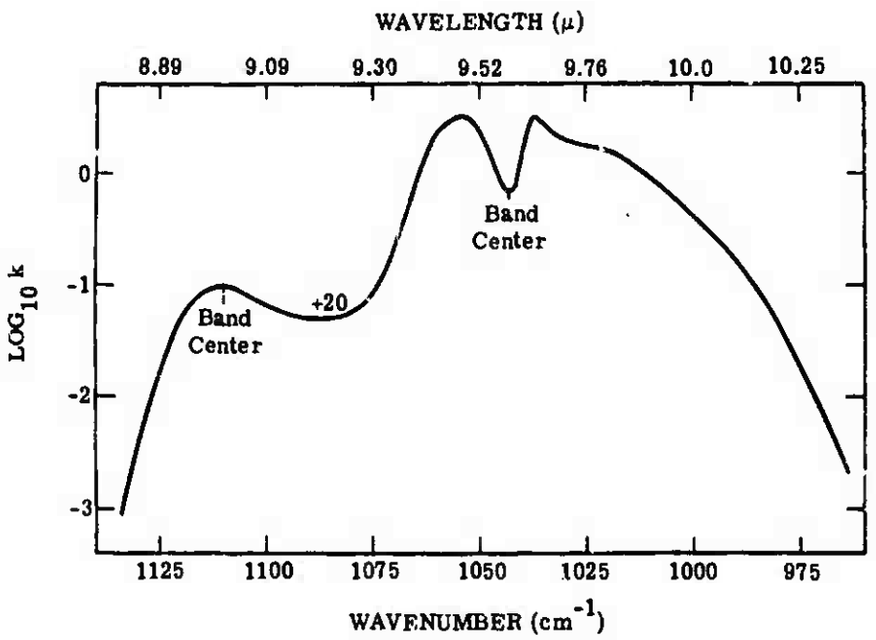

FIGURE 22. GENERALIZED ABSORPTION COEFFICIENT FOR 9.6-μ AND 9-μ OZONE BANDS

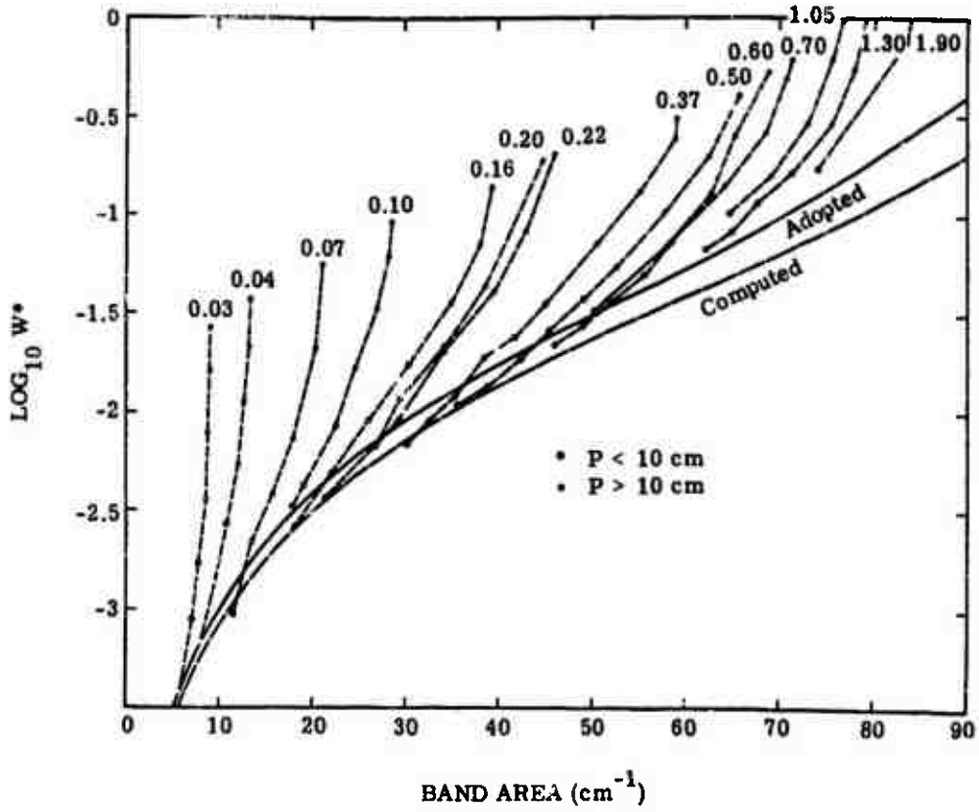

FIGURE 23. COMPUTED AND OBSERVED BAND AREAS FOR 9.6-μ OZONE BAND

data. Recall that $W^* = W_h \frac{P_e}{P}\left(\frac{T_0}{T}\right)^n$, where P_e is the effective broadening pressure. Elsasser assumed a linear pressure correction for CO_2 and O_3 when reducing the W values to equivalent W^* values. He felt that this assumption was valid for CO_2, although it gave poor results for O_3. Elsasser further suggested that had he used a pressure correction of approximately 0.8, his original data would have been in close agreement with Walshaw's data. However, since he did not make any corrections to his original data, it is recommended that these original data be used for transmission calculations; the user should remember, however, that the final values will overpredict absorption by approximately 10%.

As for CO_2, the transmissivity function and the generalized absorption coefficients for O_3 are tabulated. The results are given in table 4.

3.2.3. TRANSMISSIVITY FUNCTION: WATER VAPOR. Elsasser considered only the far-infrared spectrum of H_2O; that is, he considered the 6.3-μ vibration-rotation band and the purely rotational band at the long-wave end of the spectrum. The transmissivity curves developed by Howard et al. [30] were used for both the 6.3-μ band and the rotational water band. Their two curves, representing a total pressure of 740 mm Hg and 125 mm Hg are plotted in figure 24, together with the curves derived by Yamamoto [35] and Daw [36]. All curves were shifted along the abscissa so they would coincide at the point of 50% absorption. Elsasser adopted the curve of Howard et al. which corresponds to a pressure of 125 mm Hg. This is the pressure to which the laboratory data were reduced before the empirical fit was made. It seems that the curve for 740 mm Hg would be more realistic for absorption calculations since that is the pressure for which the "equivalent sea-level path" is defined. However, since Elsasser desired the greatest accuracy for high-altitude slant paths, he chose 125 mm Hg. The differences between any two of the curves is small enough that the selection of any one of the transmissivity curves would not produce an appreciable difference in the final absorption calculation.

Elsasser adopted a curve for the generalized absorption coefficient for the 6.3-μ band using a trial-and-error procedure based on the work of Daw [36], Yamamoto [35], and Howard [30]. Daw and Yamamoto separately constructed curves of the generalized absorption coefficient for the 6.3-μ band; their results are shown in figure 25. A plot of band area versus W^* for Howard's data is shown in figure 26. Elsasser assumed that the shape of Daw's curve was correct but that the curve was high; he shifted Daw's curve (the top of which is sketched in fig. 25) downward by an amount which would produce a satisfactory fit to the band areas shown in figure 26. The final curves for the generalized absorption coefficient are shown in figure 27.

TABLE 4. TRANSMISSIVITY FUNCTION AND ABSORPTION COEFFICIENTS FOR OZONE

λ (μ)	ν (cm^{-1})	k	$\tau(k \cdot W^*)$ (%)	$k \cdot W^*$
8.85	1130	3.16 E-3	100.0	5.01 E-5
8.93	1120	5.01 E-2	99.2	8.31 E-5
9.01	1110	1.00 E-1	98.4	7.94 E-5
9.09	1100	8.31 E-2	97.8	1.00 E-4
9.17	1090	5.01 E-2	98.8	1.28 E-4
9.26	1080	5.62 E-2	98.0	1.59 E-4
9.35	1070	2.00 E-1	95.2	1.99 E-4
9.43	1060	2.24	94.4	2.51 E-4
9.51	1052	3.18	93.6	3.16 E-4
9.57	1045	7.94 E-1	92.7	3.98 E-4
9.84	1037	3.16	91.7	5.01 E-4
9.71	1030	2.00	90.6	8.31 E-4
9.80	1020	1.59	89.4	7.94 E-4
9.90	1010	8.91 E-1	88.1	1.00 E-3
10.00	1000	3.98 E-1	86.6	1.26 E-3
10.10	990	1.59 E-1	84.9	1.59 E-3
10.20	980	3.98 E-2	83.0	1.99 E-3
10.31	970	6.31 E-3	80.9	2.51 E-3
10.42	960	6.31 E-4	78.8	3.18 E-3
10.47	955	5.01 E-5	76.1	3.98 E-3
			73.4	5.01 E-3
12.00			70.5	6.31 E-3
12.20	820	6.31 E-5	67.3	7.94 E-3
12.50	800	3.98 E-4	63.8	1.00 E-2
12.82	780	1.59 E-3	60.0	1.28 E-2
13.16	760	3.98 E-3	55.9	1.59 E-2
13.51	740	7.94 E-2	51.5	1.99 E-2
13.79	725	1.00 E-2	46.8	2.51 E-2
14.08	710	5.01 E-3	41.8	3.16 E-2
14.49	690	7.94 E-3	36.6	3.98 E-2
14.93	670	5.01 E-3	31.2	5.01 E-2
15.38	650	1.99 E-3	25.7	6.31 E-2
15.87	630	5.01 E-4	20.2	7.94 E-2
16.39	610	2.51 E-5	15.1	1.00 E-1
			10.8	1.26 E-1
			7.4	1.59 E-1
			4.8	1.99 E-1
			2.9	2.51 E-1
			1.5	3.16 E-1
			0.5	3.98 E-1
			0.0	5.01 E-1

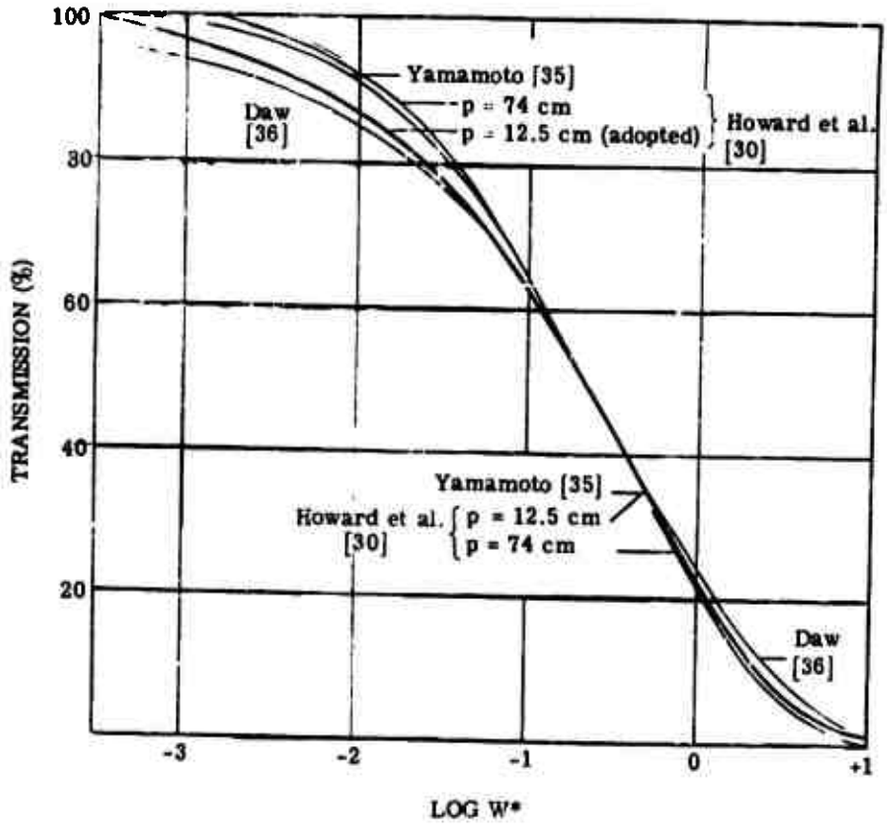

FIGURE 24. TRANSMISSIVITY CURVES FOR WATER VAPOR

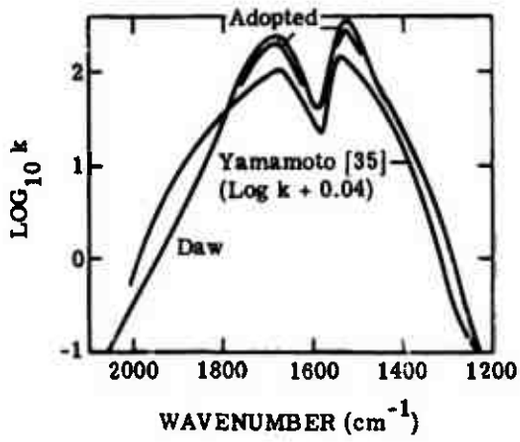

FIGURE 25. COMPARISON OF CONTOURS FOR 6.3-μ WATER VAPOR BAND

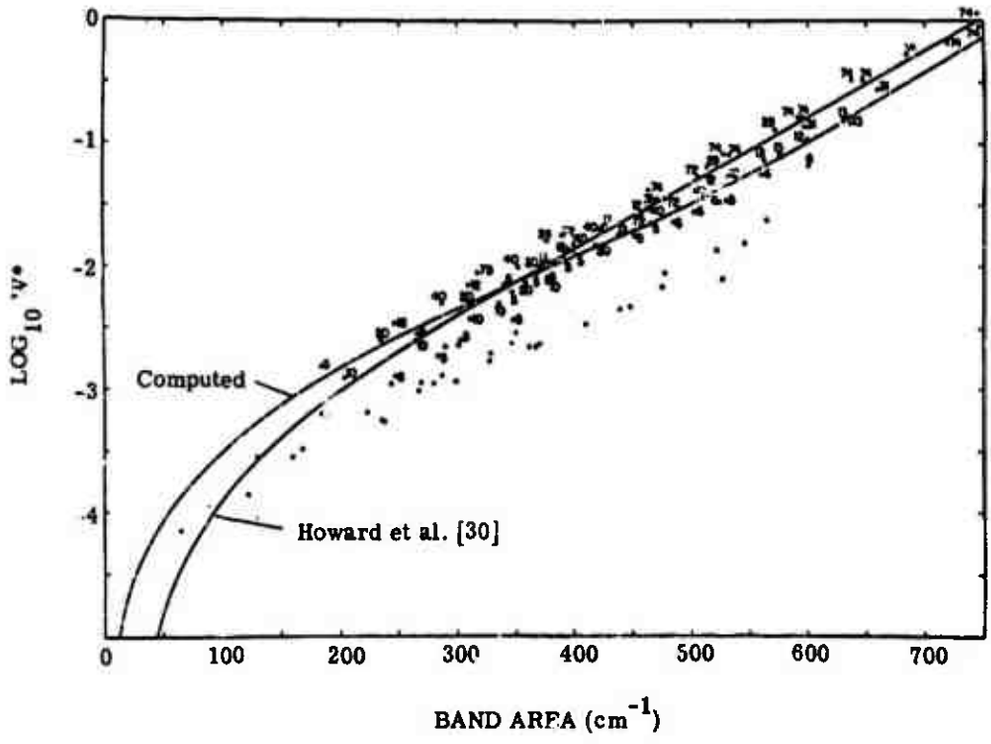

FIGURE 26. COMPUTED AND MEASURED BAND AREAS FOR 6.3-μ WATER VAPOR BAND. Numbers indicate approximate pressure in centimeters of mercury. Where there is no number, P ≦ 3 cm Hg.

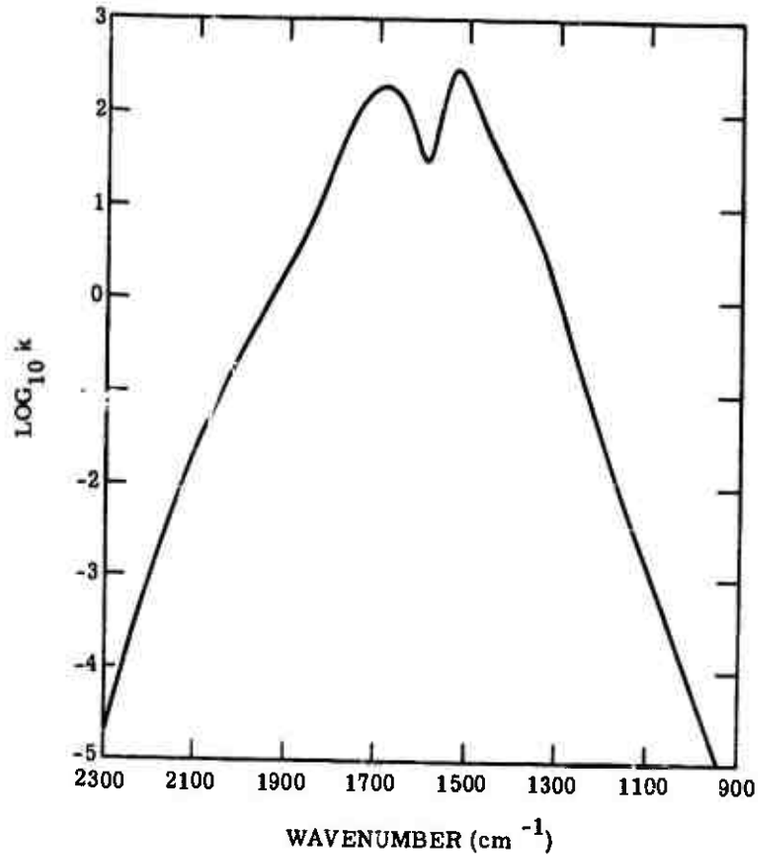

FIGURE 27. GENERALIZED ABSORPTION COEFFICIENT FOR 6.3-μ WATER VAPOR BAND

As for CO_2 and O_3, band areas for a series of reduced optical paths were calculated and plotted. The results are represented by the "computed curve" shown in figure 26. Elsasser obtained the heavy curve by making a best fit to Howard's data [30], disregarding the values for $P \geq 30$ mm Hg. Note that the two curves compare closely for band areas greater than 200 cm^{-1}. This value of band area corresponds to values at absorption less than 20%. For absorption values less than 20% Elsasser's data will yield values of absorption that are lower than Howard's by approximately 10%.

For the rotational band Elsasser used the same transmissivity curve as for the 6.3-μ band and used Yamamoto's absorption coefficients [35] for the rotational band. The results are shown in figure 28. Yamamoto determined these coefficients by summing the contributions from all of the spectral lines. The line intensities were computed only from the measurements of the electrostatic dipole movement of the water molecule. Yamamoto's results are compared with the experimental results of Palmer [37] and Bell [38] in figure 29. Elsasser considered the comparison sufficiently close to justify the use of Yamamoto's data without modification.

The region between the two bands is known as the window; absorption there is weak. It is known that there are a number of weak lines within this interval and also that a certain amount of the total absorption is caused by the wings of the very strong lines concentrated at the peak of the rotational band and the 6.3-μ band. Recall that the absorption coefficient for the Lorentz line shape is given by

$$k(\nu) = \frac{S_i \alpha_i}{\pi\left[\left(\nu - \nu_{0_i}\right) + \alpha_i^2\right]}$$

We see that at large distances from the line centers the term α_i^2 in the denominator may be neglected compared to $\left(\nu - \nu_{0_i}\right)^2$. The net effect of the wings of all the distant lines is then a continuous absorption with

$$k(\nu) = \sum_i \frac{S_i \alpha_i}{\pi\left(\nu - \nu_{0_i}\right)^2}$$

where the summation extends over all distant lines. This quantity for the window has been determined by Roach and Goody [39] from atmospheric observations and the results of their work used by Elsasser. To determine the total absorption for the window region Elsasser proposes the following technique. As seen in figure 29, the extrapolated generalized absorption coefficients

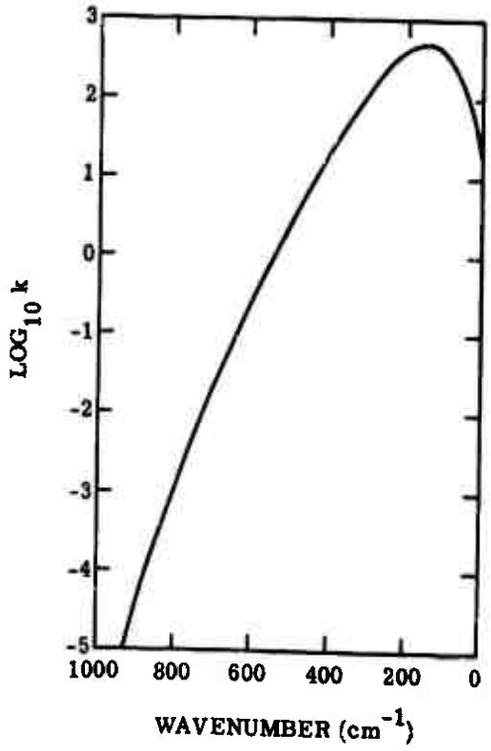

FIGURE 28. GENERALIZED ABSORPTION COEFFICIENT FOR ROTATIONAL WATER VAPOR BAND

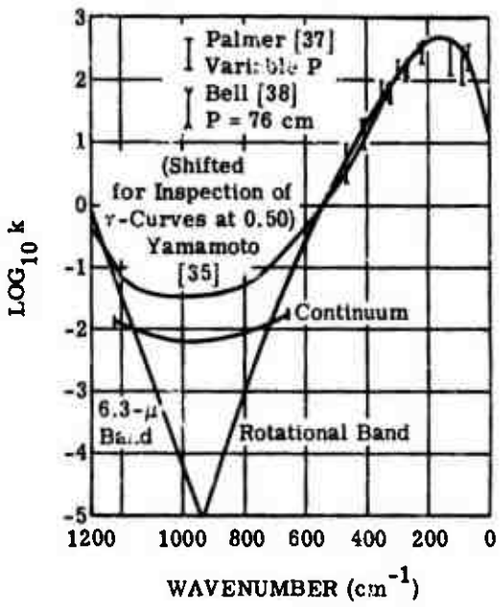

FIGURE 29. GENERALIZED ABSORPTION COEFFICIENT OF ROTATIONAL WATER VAPOR BAND AND WINDOW

for the two main bands are shown together with the absorption coefficients of the continuum. For the spectral region from 660 cm^{-1} to 1220 cm^{-1} the absorption is first computed from the extrapolated values and then by the values given by the continuum. The total absorption throughout the region is then given by

$$\tau_{total} = \tau_{continuum} \cdot \tau_{band}$$

An equation such as the one above is rigorously correct if two continuous transmission spectra are superimposed. Therefore, Elsasser assumed it should be a reasonable approximation if one of the components were a continuum.

As for the previous gases, the transmissivity function and the absorption coefficients are tabulated and the results are given in table 5. Note that for the spectral region from 8.33 to 14.7 μ the two absorption coefficients k_{band} and $k_{continuum}$, respectively, are tabulated.

3.3. METHOD OF T. L. ALTSHULER

The method Altshuler developed for computing slant-path absorption [26] is extremely compact and simple to use. The absorption functions and the generalized absorption coefficients are presented in the form of curves which allow for fast computation of spectral absorption for four different atmospheric gases, namely H_2O, CO_2, O_3, and N_2O. Altshuler's method is basically applicable to only those paths which give rise to strong-line absorption. However, he also proposed a method for computing absorption for weak-line nonoverlapping conditions, which is based upon the strong-line absorption functions.

The laboratory data used in performing the empirical fits and the method of empirical fit will be discussed for each of the absorbing species and the exact procedure to be followed when computing transmission will be outlined. Table 6 is a listing of the laboratory data and the values of the many parameters used in obtaining the empirical fits for each gas.

3.3.1. TRANSMISSIVITY FUNCTION: WATER VAPOR. The strong-line approximation to the statistical model with an exponential distribution of line strengths was used as the transmissivity function for H_2O. This function, expressed in terms of W*, is given by

$$A = 1 - \exp\left(\frac{\pi \alpha_0 S W^*}{d^2}\right)^{1/2} \qquad (72)$$

Note in table 6 this equation was fitted to the data of Howard, Burch, and Williams [30] for the wavelength region from 1.0 to 9.1 μ, the data of Yates and Taylor [42] for the wavelength

TABLE 5. TRANSMISSIVITY FUNCTION AND ABSORPTION COEFFICIENTS FOR WATER VAPOR

λ (μ)	(ν) (cm^{-1})	k Band	k Continuum	$\tau(k \cdot W^*)$ (%)	$k \cdot W^*$
4.39	2280	3.89 E-5		100.00	1.99 E-4
4.46	2240	2.04 E-4		99.90	2.51 E-4
4.55	2200	9.33 E-4		99.67	3.16 E-4
4.62	2160	3.80 E-3		99.32	3.98 E-4
4.72	2120	1.32 E-2		98.87	5.01 E-4
4.81	2080	3.98 E-2		98.33	8.31 E-4
4.90	2040	1.10 E-1		97.72	7.94 E-4
5.00	2000	2.57 E-1		97.05	1.00 E-3
5.10	1960	6.17 E-1		96.33	1.26 E-3
5.21	1920	1.38		95.58	1.59 E-3
5.32	1880	3.16		94.75	1.99 E-3
5.43	1840	8.13		93.89	2.51 E-3
5.56	1800	2.40 E 1		92.98	3.16 E-3
5.68	1760	7.24 E 1		92.00	3.98 E-3
5.81	1720	1.48 E 2		90.94	5.01 E-3
5.95	1680	1.95 E 2		89.78	6.31 E-3
6.10	1640	1.20 E 2		88.51	7.94 E-3
6.25	1600	3.63 E 1		87.11	1.00 E-2
6.29	1590	3.09 E 1		85.56	1.26 E-2
6.41	1560	1.02 E 2		83.84	1.59 E-2
6.58	1520	2.89 E 2		81.94	1.99 E-2
8.76	1480	1.12 E 2		79.84	2.51 E-2
6.94	1440	4.37 E 1		77.53	3.16 E-2
7.14	1400	1.86 E 1		75.00	3.98 E-2
7.35	1360	7.08		72.25	5.01 E-2
7.58	1320	2.24		69.28	6.31 E-2
7.81	1280	5.50 E-1		66.10	7.94 E-2
8.06	1240	1.17 E-1		62.72	1.00 E-1
8.33	1200	2.35 E-2	1.18 E-2	59.15	1.28 E-1
8.62	1160	8.51 E-3	9.55 E-3	55.41	1.59 E-1
8.93	1120	2.40 E-3	8.13 E-3	51.52	1.99 E-1
9.26	1080	7.08 E-4	7.08 E-3	47.50	2.51 E-1
9.62	1040	2.04 E-4	6.76 E-3	43.38	3.16 E-1
10.00	1000	5.89 E-5	6.61 E-3	39.19	3.98 E-1
10.42	960	1.78 E-5	6.61 E-3	34.97	5.01 E-1
10.87	920	1.58 E-5	6.76 E-3	30.76	6.31 E-1
11.36	880	6.31 E-5	7.24 E-3	26.61	7.94 E-1
11.90	840	2.57 E-4	7.76 E-3	22.58	1.00
12.50	800	1.00 E-3	8.71 E-3	18.74	1.26
13.16	760	3.63 E-2	1.05 E-2	15.18	1.59
13.89	720	1.20 E-2	1.32 E-2	11.98	1.99
14.70	680	3.80 E-2	1.66 E-2	9.20	2.51
15.63	640	1.07 E-1		6.87	3.61

TABLE 5. TRANSMISSIVITY FUNCTION AND ABSORPTION COEFFICIENTS FOR WATER VAPOR (Continued)

λ (μ)	(ν) (cm^{-1})	k Band	k Continuum	$\tau(k \cdot W^*)$ (%)	$k \cdot W^*$
16.67	600	2.82 E-1		5.00	3.98
17.86	580	7.08 E-1		3.57	5.01
19.23	520	1.70		2.50	8.31
20.83	480	3.99		1.88	7.94
22.72	440	8.91		1.03	1.00 E-1
25.00	400	2.00 E 1		0.49	1.26 E-1
27.78	360	4.47 E 1		0.0	1.59 E-1
31.25	320	9.12 E 1			
35.71	280	1.70 E 2			
41.67	240	2.82 E 2			
50.00	200	4.07 E 2			
62.50	160	4.90 E 2			
83.33	120	4.68 E 2			
125.00	80	2.95 E 2			
250.00	40	1.10 E 2			

TABLE 6. SUMMARY OF LABORATORY DATA AND PATH PARAMETERS

Gas or Vapor	λ	ν	P	p	P_e	T	W (atm-cm)	n	W* (atm-cm)	Ref.
CO_2	1.3-1.7	6000-7000	760	50.0	777	285	8100	0.80	8200	30
	1.8-2.1	4600-5400	760	50.0	777	295	8330	0.78	8700	30
	2.5-3.1	3500-3700	737	1.0	738	285	22	0.88	21	30
	2.5-3.1	3500-3700	755	10.0	758	295	1818	0.86	1614	30
	4.0-5.4	1800-2500	1.0	1.0	1.3	285	18	0.80	0.11	30
	4.0-5.4	1800-2500	734	8.8	737	295	1043	0.80	1018	30
	8.0-11	910-1100	760	608	842	295	5600	0.60	6580	40
	8.0-11	810-1100	6080	6080	7900	295	8000	0.27	15,100	41
	12-19	550-850	750	0.25	750	285	3	0.88	2.9	30
	12-19	550-850	745	4.0	746	295	173	0.88	168	30
							(pr cm)		(pr cm)	
H_2O	1.0-1.05	95-10,000								
	1.05-1.2	8200-8500			750	285	3	0.52	2.9	30
	1.05-2.2	4600-8500			740	295	50	0.80	48	30
	1.05-2.2	4600-9500			740	285	0.05	0.60	0.048	30
	1.2-2.2	4600-8250			740	285	0.71	0.60	0.70	30
	2.3-3.65	2800-4400	740	16.3	821	295	1.68	0.62	1.75	30
	2.3-3.65	2800-4400	740	16.3	821	295	0.140	0.62	0.147	30
	2.3-3.65	2800-4400	740	2	750	285	0.017	0.82	0.017	30
	3.65-4.5	2200-2800								
	4.5-8.1	1100-2200			748	285	1.03	0.60	1.02	30
	4.5-9.1	1100-2200			746	285	0.047	0.60	0.046	30
	4.5-8.1	1100-2200	123	2.5	136	295	0.021	0.70	0.006	30
	9.1-13	1100-770			760	291	4.18	1.0	4.18	42
	9.1-13	1100-770			760	285	6.7	1.0	6.7	42(run 61)
	9.1-13	1100-770			760	288	0.57	1.0	0.57	42(run 60)
	13-16	625-770								
	18-20	500-625			760	298	0.57	1.0	0.57	42(run 60)
	20-30	333-500	606	4.0	626	290	0.074	1.0	0.061	43
	20-30	333-500	600	1.6	808	280	0.0325	1.0	0.026	43
	20-30	333-500	580	0.2	591	290	0.0050	1.0	0.0038	43
	30-40	250-333	603	0.15	604	283	0.00318	1.0	0.00255	43
	40-2500	4-250			780	295	0.0104	1.0	0.0103	44
Gas							(atm cm)		(atm cm)	
O_3	4.4-5.1	1960-2270	230	230	370	285	9.98	0.3	7.38	45, 46
	8.0-8.3	1075-1250	160	160	257	285	6.32	0.3	4.58	45
	8.3-10.2	980-1075					0.31		0.13	47
	12.0-16.5	606-833	160	160	257	295	6.32	0.3	4.58	46
							(atm cm)		(atm cm)	
N_2O	3.8-4.1	2240-2630							0.062	48, 49
	4.24-4.36	2290-2360	400	400	448	300	12.6	0.8	8.1	50
	4.4-4.7	2130-2270			750	295	5.8	0.7	5.7	51
	4.4-4.7	2130-2270			759	285	0.0101	0.7	0.0100	51
	7.6-8.1	1235-1315	100	100	112	288	0.78	0.8	0.17	52
	8.5-9.1	1100-1175	240	240	269	288	1.8	0.8	0.83	52
	16.0-18.0	555-625	160	160	179	288	5.5	0.8	1.73	52

P = total pressure
p = partial gas pressure
P_e = equivalent pressure
T = temperature
W = actual quantity of gas in path
W^* = equivalent sea-level path
n = exponent for P and T correction

region from 9.1 to 20 μ, that of Palmer [43] for the region from 20 to 40 μ, and the Yaroslavsky and Stanevich [44] data for the region from 40 to 2500 μ.

The empirical procedure used to evaluate the absorption coefficient was as follows. The laboratory data cited in table 6 were reduced to equivalent W* values from the equation

$$W^* = W_h \left[\frac{P_e}{P_0} \left(\frac{T_0}{T} \right)^{1/2} \right]^n$$

The values of n are given in table 6. The spectral interval from 1.0 to 2000 μ was divided into equal wavelength increments on a logarithmic scale and for each value of W* a mean absorption coefficient was evaluated for each wavelength increment, assuming the transmission for each wavelength interval obeys equation 72. The absorption coefficients for each wavelength increment were plotted as a function of wavelength and a curve was fitted to the data using a least-squares fitting procedure. The resulting curve was a plot of the generalized absorption coefficient $a_0 S\pi/d^2$ as a function of wavelength. This curve was then used to calculate values of transmission versus wavelength for certain values of W* The curves for water vapor are given in figure 30. Note that each curve is a plot of transmission versus wavelength for a single value of W*. To determine the absorption for a different value of W*, simply shift the curve by an amount indicated by the index on the right. The transmission data for all of the gases are presented in the same format, and examples of computation are given in section 3.3.4.

3.3.2. TRANSMISSIVITY FUNCTION: CARBON DIOXIDE. The transmissivity function for this gas was developed by a purely empirical technique and is, therefore, given by a curve of transmission versus the product of the generalized absorption coefficient and the equivalent sea-level path W* or $\tau = \tau(kW^*)$. This curve is shown in figure 31. Since the procedure used in obtaining this curve is exactly that which was used by Elsasser, the reader is referred to section 3.2 where the specific details of this form of empirical fitting are discussed. In general, when performing a purely empirical fit to a set of absorption data one finds that one function will be determined for one absorption band and another for a different absorption band. However, Altshuler fitted the same curve (fig. 31) for the entire interval from 1.3 to 19 μ to the data of Howard et al. [30] and King [14]. Therefore, one function represents the CO_2 data for the entire interval. Using this transmissivity function he determined the absorption coefficients exactly as those for H_2O and the results are plotted in the same format. The curves are represented by figure 32. The units of W* for CO_2 are atmospheric centimeters, but the units on the curves

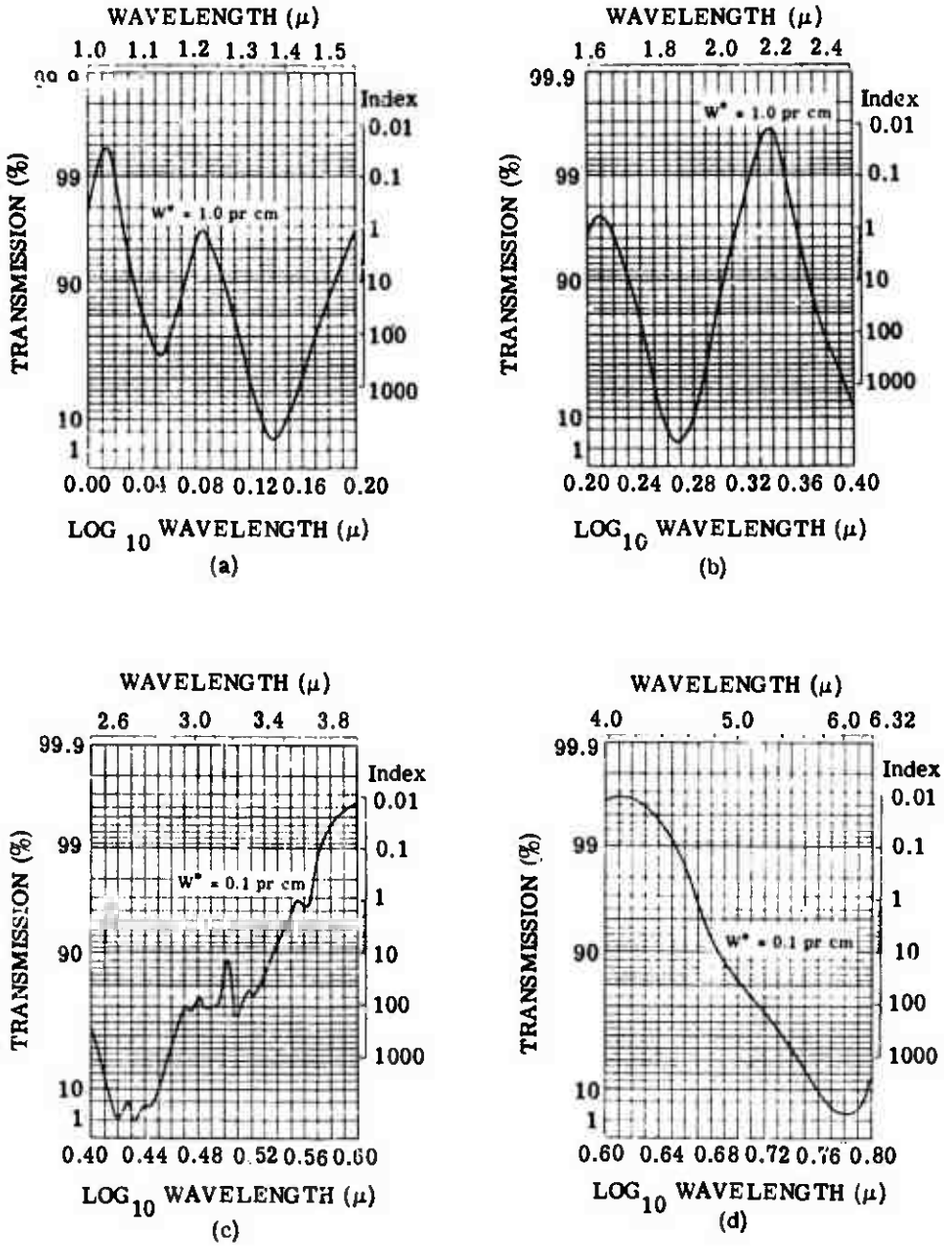

FIGURE 30. TRANSMISSION VS. WAVELENGTH FOR WATER VAPOR

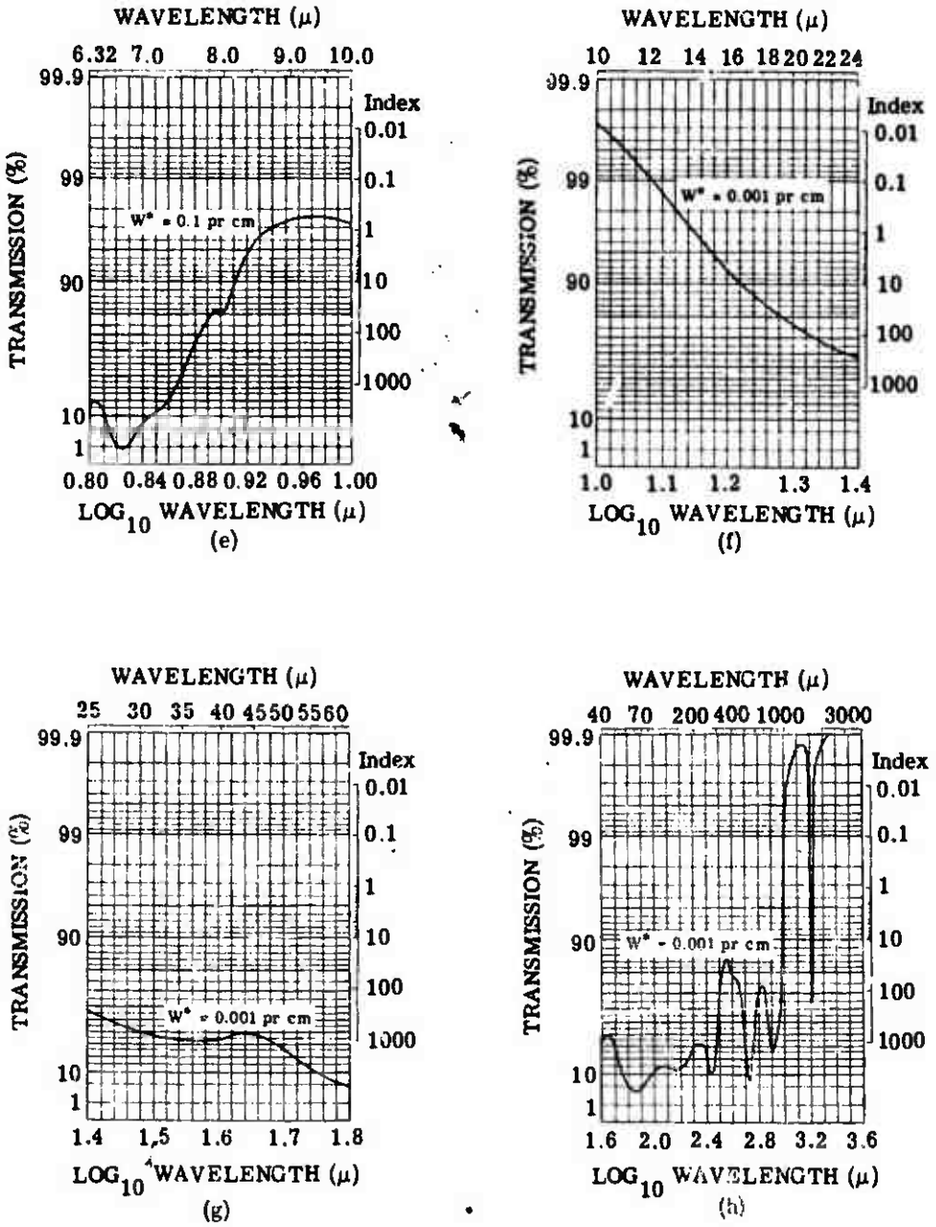

FIGURE 30. TRANSMISSION VS. WAVELENGTH FOR WATER VAPOR (Continued)

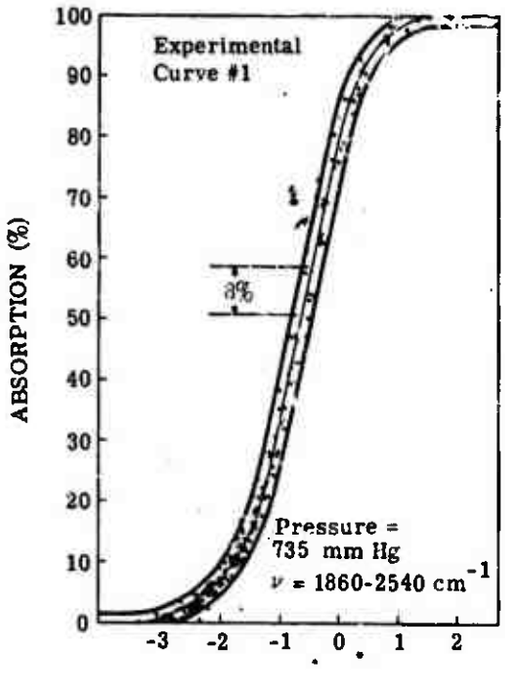

FIGURE 31. TRANSMISSIVITY CURVE FOR CARBON DIOXIDE

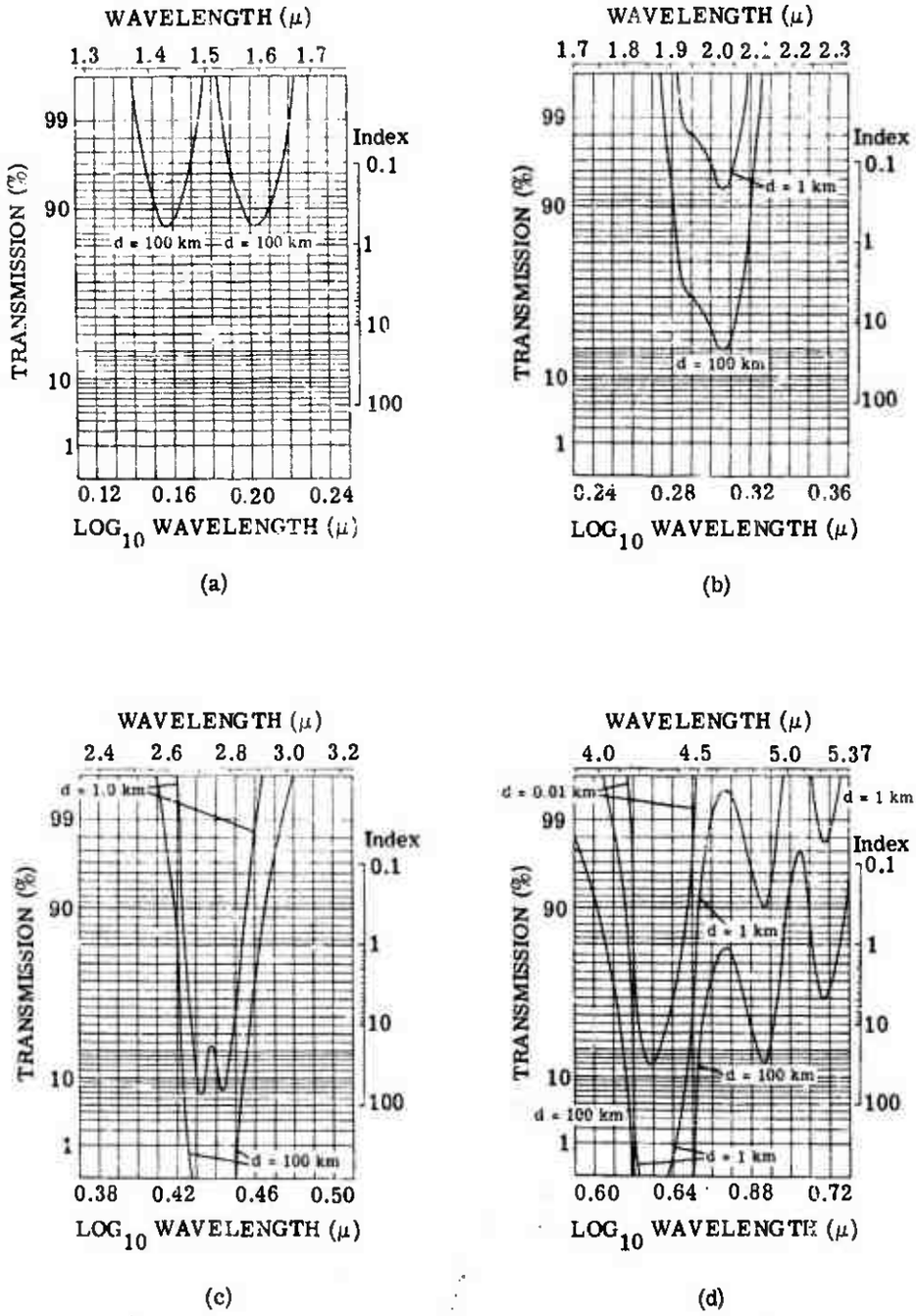

FIGURE 32. TRANSMISSION VS. WAVELENGTH FOR CARBON DIOXIDE

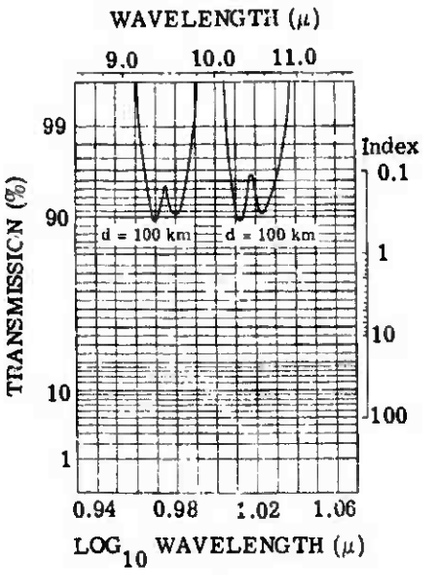

(e)

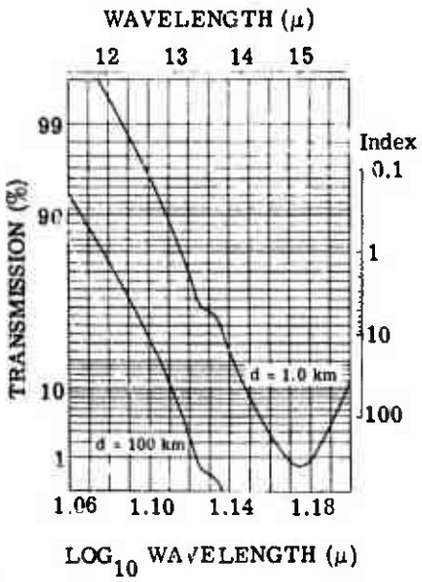

(f)

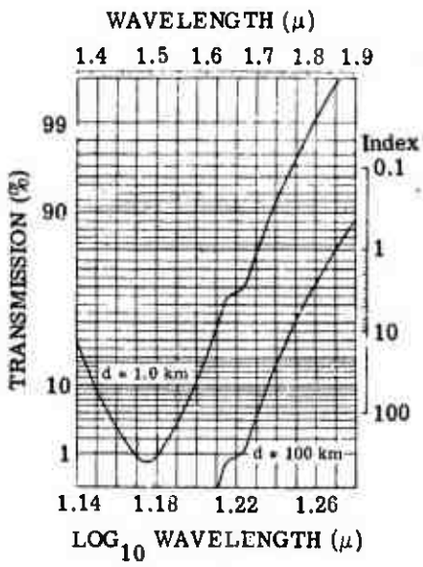

(g)

FIGURE 32. TRANSMISSION VS. WAVELENGTH FOR CARBON DIOXIDE (Continued)

are kilometers of dry air. Therefore, to use the curves, convert atmospheric centimeters to kilometers of dry air by recalling that 1 km of dry air equals approximately 32 atm cm of CO_2.

3.3.3. TRANSMISSIVITY FUNCTION: OZONE AND NITROUS OXIDE. The strong-line approximation to the Elsasser model which was used as the transmissivity function for both O_3 and N_2O is given by

$$\tau = 1 - \operatorname{erf}\left(\frac{\pi S \alpha_0}{d^2} W^*\right)^{1/2}$$

This equation was fitted to the data in table 6 by the same procedure used for H_2O. The resulting absorption curves are given in figure 33. The curves for N_2O use the same units as do those for CO_2 and can be converted to atmospheric centimeters by recalling that 1 km of dry air contains 0.028 atm cm of N_2O. Because the curves for O_3 are given directly in atmospheric centimeters, no conversion is necessary.

3.3.4. PROCEDURE FOR CALCULATING ABSORPTION. Figures 30, 32, and 33 represent all of Altshuler's absorption data. The computation of transmission becomes a trivial matter once the amount of each absorbing species in the slant path is determined. The technique for reducing a slant path to an equivalent sea-level path W* has been previously discussed and the results are given by equation 67 (sec. 2.4.3). Altshuler, however, suggests that W* be computed by an equation which is a slight modification of equation 67:

$$W^* = \int_0^X \left[\left(\frac{P}{P_0}\right)\left(\frac{T_0}{T}\right)^{1/2}\right]^n \rho \, dx \qquad (73)$$

where n = 1.0 for CO_2
n = 1.0 for H_2O
n = 0.3 for O_3
n = 1.0 for N_2O

For CO_2, H_2O, and N_2O the two equations are identical since n = 1. However, for O_3 Altshuler suggests a pressure correction on half-width, that is, 0.3 rather than linear. Altshuler determined this value empirically from Walshaw's [34] laboratory data. There is some controversy concerning the correct pressure correction which should be used when reducing laboratory data to equivalent W* values. Theory indicates that half-width varies linearly with the effective

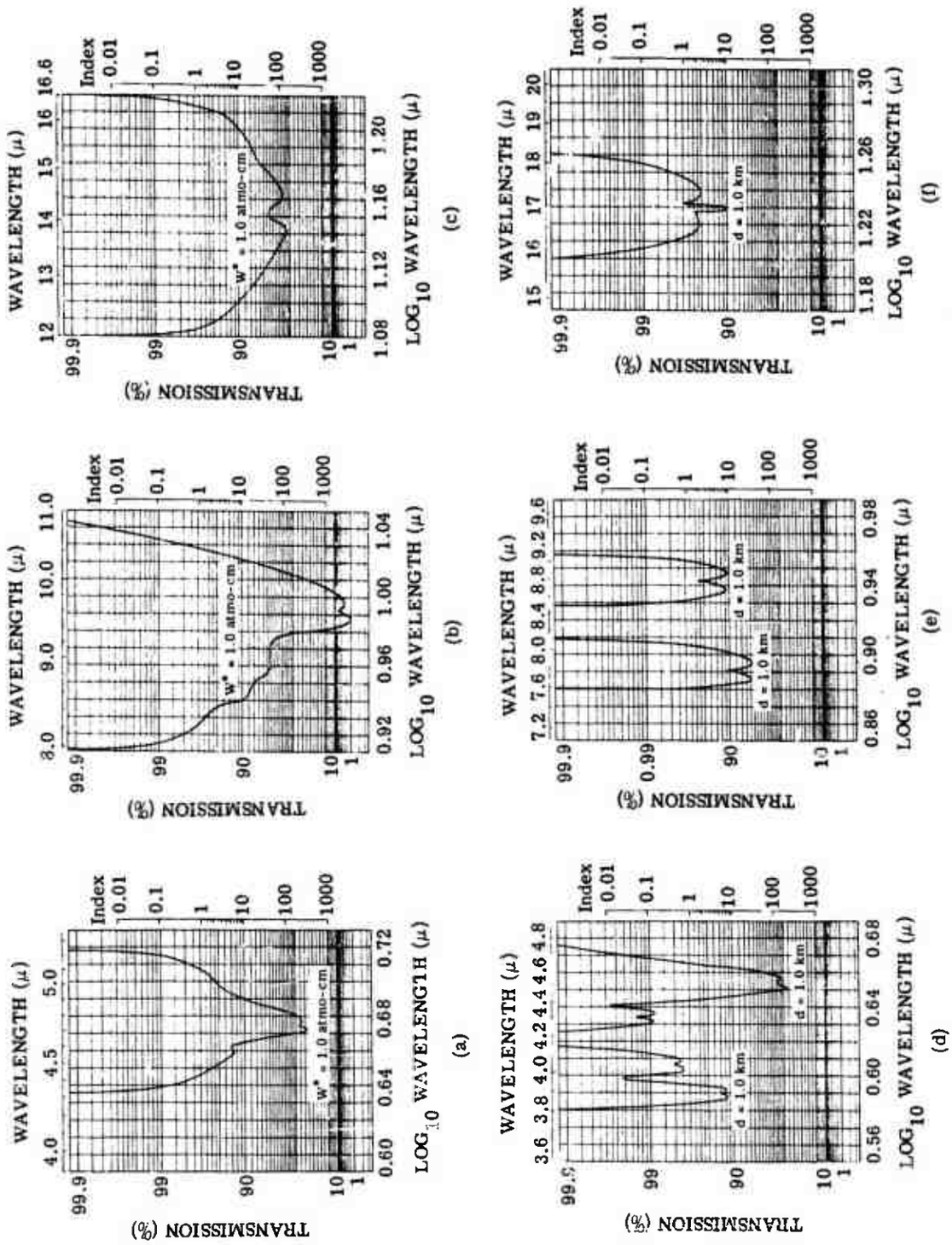

FIGURE 33. TRANSMISSION VS. WAVELENGTH FOR OZONE

broadening pressure P_e; this does not seem to be supported by laboratory data. A possible solution, particularly for O_3, would be to perform all empirical fits with W and $\bar{P}$ as parameters and not use the equivalent sea-level path concept. Under these conditions a pressure correction would not be required.

The technique described in appendix I may be used to evaluate equation 73. The output of the program will yield values of W* in precipitable centimeters for H_2O and in atmospheric centimeters for O_3 which may be used directly on the curves. However, values of W* for CO_2 and N_2O must be converted to an equivalent length of dry air, d. For CO_2, d = W*/32 and for N_2O, d = W*/0.028. After the appropriate values of W* and d have been computed the following procedure is used to compute transmission:

(1) With the use of dividers, mark off on the "index" the amount of absorbing gas present in the slant path, i.e., W* or d. Use the fine scale between 1 and 10 on the index for interpolating between the major divisions on the index.

(2) Locate the major division on the index corresponding to the values of W* or d identifying the curve on the figure.

(3) The transmission is obtained by displacing the transmission curve by the same amount and direction that the entry value differs from the curve.

(4) Read the transmission τ for each gas at the same wavelength and calculate

$$\tau(\lambda) = \left[\tau_{H_2O}(\lambda)\right]\left[\tau_{CO_2}(\lambda)\right]\left[\tau_{O_3}(\lambda)\right]\left[\tau_{N_2O}(\lambda)\right]$$

(5) Repeat (1)-(4) for each wavelength through the interval of interest.

Atshuler's method for computing transmission is valid only when there is enough absorbing gas that strong-line conditions are present. Recall that when the quantities of gases and vapors are small and the pressures are low, absorption is such that the weak-line nonoverlapping approximation is valid and absorption varies linearly with W*. This occurs for values of absorption less than approximately 10%, regardless of which absorption model applies, the Elsasser model, the statistical model, or the experimental model. Examining figure 34 one may note that all band models overpredict absorption for small quantities of gas. It is necessary, therefore, to correct these values of absorption to bring them in to agreement with the actual absorption.

Figure 35 shows the linear absorption region for various gases and vapors. Absorption is plotted versus the altitude of a horizontal path. This figure demonstrates the fact that at higher altitudes the maximum absorption for weak-line conditions becomes less and less owing to the

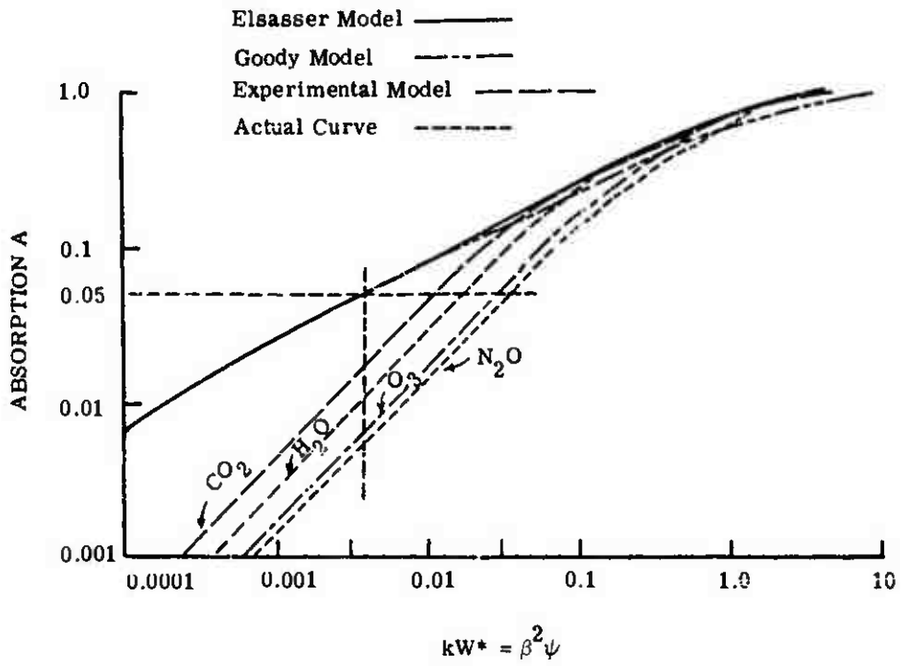

FIGURE 34. TRANSMISSIVITY CURVES SHOWING THE DIVERGENCE OF ABSORPTION FROM THAT PREDICTED BY THE ELSASSER, GOODY, AND EXPERIMENTAL BAND MODELS. For gases at sea level.

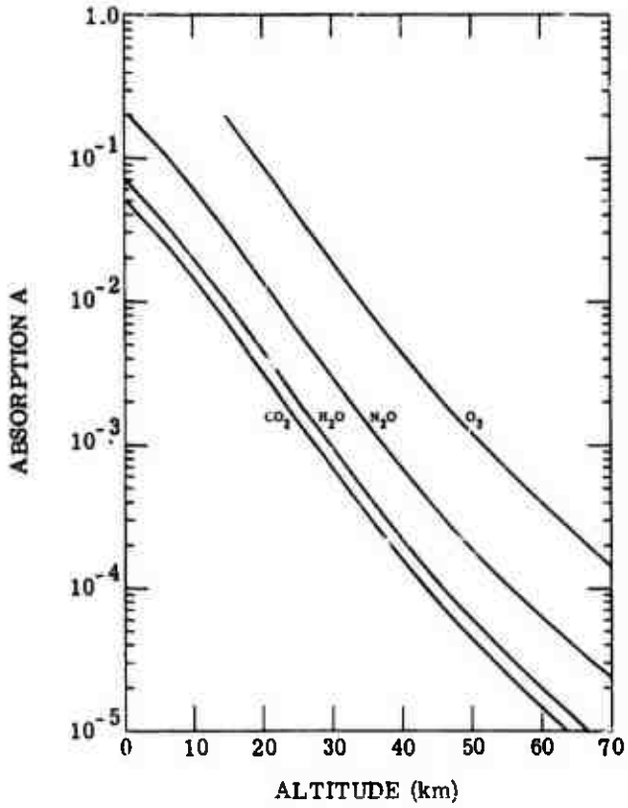

FIGURE 35. REGIONS OF LINEAR ABSORPTION FOR HORIZONTAL ATMOSPHERIC PATHS AT VARIOUS ALTITUDES. Areas below the curves are linear absorption regions, i.e., where maximum error in A is less than 10%.

decrease in spectral-line width with decreasing pressure. In order to apply this figure to an actual calculation, simply determine the absorption for a given path and if it lies below the curve of figure 35 the use of the weak-line approximation is valid. If the path is not horizontal, the mean attitude of the path may be used to a good approximation.

In order to compute transmission for weak-line conditions, first compute the amount of absorber that will yield a value of absorption equal to 5%. Then, using the values of W* for each gas, determine the absorption from the following equations (taken from figure 34 by inspection).

$$A_{H_2O} = 0.012 \frac{W^*_{H_2O}}{W^*_{H_2O}(95\%)} \tag{74}$$

$$A_{CO_2} = 0.0016 \frac{W^*_{CO_2}}{d_{CO_2}(95\%)} \tag{75}$$

$$A_{O_3} = 0.07 \frac{W^*_{O_3}}{W^*_{O_3}(95\%)} \tag{76}$$

$$A_{N_2O} = 0.22 \frac{W^*_{N_2O}}{d_{N_2O}(95\%)} \tag{77}$$

$W^*_{H_2O}$, $W^*_{CO_2}$, $W^*_{O_3}$, and $W^*_{N_2O}$ are the reduced equivalent paths for each gas and $W^*_{H_2O}(95\%)$ and $W^*_{O_3}(95\%)$ are the equivalent paths that will yield a value of transmission equal to 95%. $d_{CO_2}(95\%)$ and $d_{N_2O}(95\%)$ are the dry-air path lengths that give a transmission of 95%. The values of absorption obtained from these equations are compared with the curves of figure 35 to test the validity of calculation.

3.4. METHOD OF A. ZACHOR

Zachor [27] used four different functions based on the band models of Elsasser and the homogeneous laboratory data of Howard, Bursh, and Williams [30] and Walshaw [34] to develop transmissivity functions which can be used to calculate absorption versus wavelength for the spectral interval from 1.03 to 10.80 μ for CO_2 and O_3. Zachor also included in reference 27 a method for computing absorption caused by H_2O for the same spectral interval. However, the method presented was taken directly from the results of Howard et al. (see sec. 3.5,

ref. 30). Therefore, this section presents only the results of Zachor's original contribution: methods for computing absorption caused by CO_2 and O_3.

3.4.1. OZONE. Zachor made an empirical fit to the laboratory data of Walshaw [34] for the 9.6-μ ozone band using a modification of the Elsasser band model. Recall that the absorption as given by the Elsasser model is

$$A = \sinh \beta \int_0^Y I_0(Y) \exp(-Y \cosh \beta)\, dY$$

where $\beta = \frac{2\pi\alpha_0}{d}\frac{P}{P_0} = \beta_0 \frac{P}{P_0}$

$$Y = \frac{S}{d}\frac{W}{\sinh \beta}$$

According to this model, the mean half-width α of a spectral line, is a linear function of the effective broadening pressure. Zachor found that this linear relationship was not supported by Walshaw's data and that β was more accurately described by

$$\beta = \beta_0 \left(\frac{P}{P_0}\right)^c$$

where c is a parameter that depends upon wavelength. Therefore, Zachor used this modification of the Elsasser model to describe absorption by O_3. The Elsasser model is plotted for different values of β in figure 36. The values of β and Y for which the weak- and strong-line approximations may be used are noted on the figure. The constants β_0, S/d, and c are listed in table 7.

3.4.2. CARBON DIOXIDE. Zachor analyzed the laboratory data of Howard et al. [30] and found that a single model could not be used to accurately describe the absorption by CO_2 for the entire spectral region from 1.03 to 10.80 μ. Therefore, Zachor used four different models, each model being used to describe the absorption over only a portion of the total spectral interval. The four models used are listed below.

Model 1: The exact Elsasser band model

$$A = \sinh \beta \int_0^Y I_0(Y) \exp(-Y \cosh \beta)\, dY \qquad (78)$$

$$Y = \frac{S}{d}\frac{W}{\sinh \beta}$$

$$\beta = \beta_0 \left(\frac{P}{P_0}\right)^c$$

$$\beta_0 = \frac{2\pi\alpha_0}{d}$$

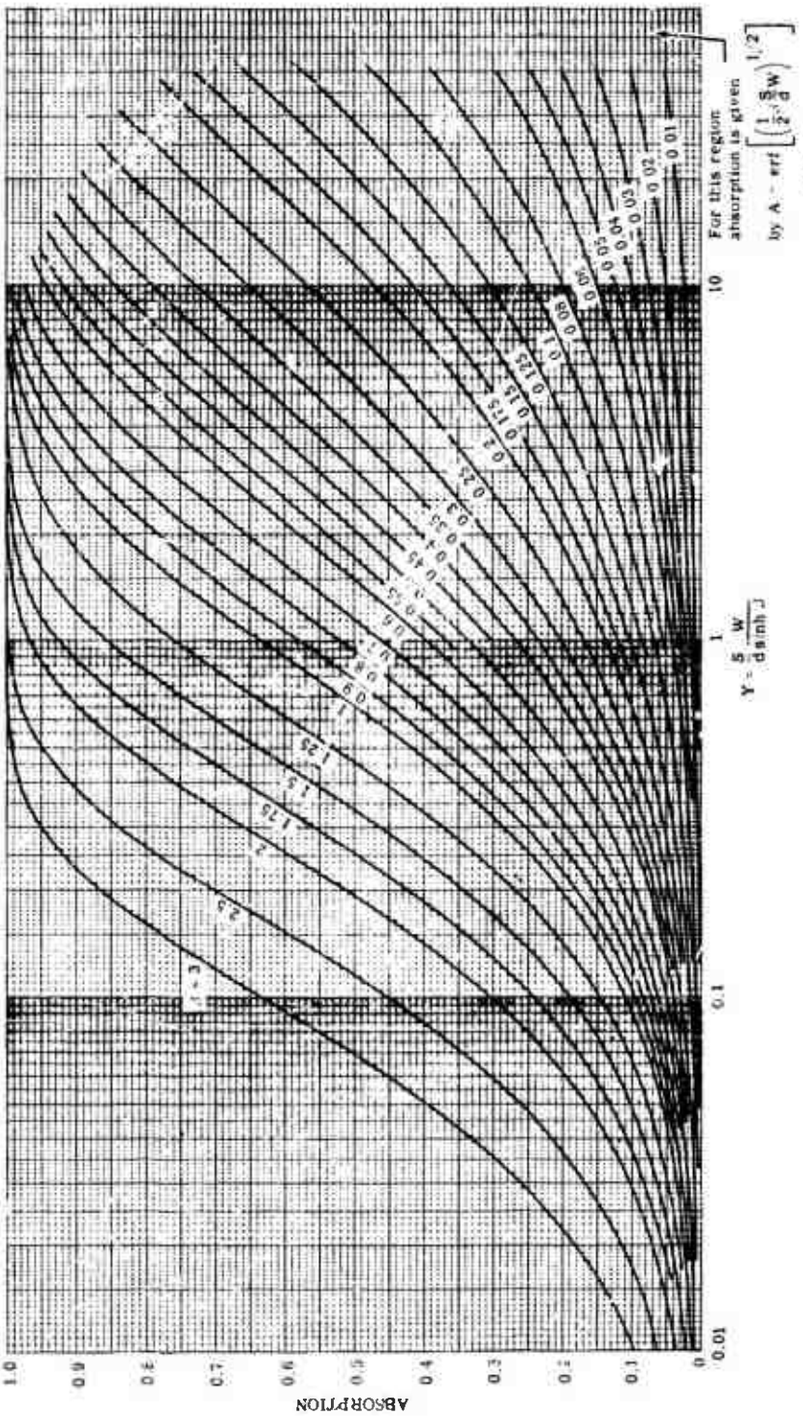

FIGURE 36. ABSORPTION BY A SINGLE ELSASSER BAND. For $\beta > 3$, $A = 1 - \exp\left(-\frac{S}{d}W\right)$.

TABLE 7. EMPIRICAL CONSTANTS FOR OZONE

λ (μ)	S/d	β_0	c
9.335	0.555	0.678	0.602
9.398	0.476	0.712	0.477
9.463	10.0	1.70	0.854
9.494	14.3	1.48	0.648
9.526	9.43	2.07	0 899
9.590	4.58	1.38	0.602
9.652	7.15	2.03	0.802
9.713	8.34	1.49	0.648
9.773	8.00	1.67	0.699
9.834	7.14	1.88	0.756
9.893	5.20	1.74	0.725
9.953	3.22	1.82	0.748
10.07	0.944	2.27	0.745
10.19	0.318	0.554	0.301

Model 2: The strong-line approximation to the Elsasser band model

$$A = \text{erf}\,(KW^a p^{c/2}) \tag{79}$$

Model 3: The strong-line approximation to two overlapping Elsasser bands with equal line spacing and intensity

$$A = 1[1 - \text{erf}\,(KW^a p^{c/2})]^2 \tag{80}$$

Model 4: The strong-line approximation to the statistical band model

$$A = 1 - \exp\,(-KW^a p^{c/2}) \tag{81}$$

Each of these models is a modification of one of the original models discussed in section 2.2. If the values a = 1/2 and c = 1 were used for every wavelength the models would be identical. Although there is no theoretical reason for employing such modifications, Zachor justified their use by the fact that the modified models allowed for better empirical fits to the laboratory data. The wavelength-dependent parameters K, a, and c and the model to be used to compute absorption for each wavelength are given in table 8.

Let us consider the actual procedure used by Zachor to fit the empirical relations for O_3 and CO_2 to the absorption data. A number of discrete wavelengths were picked in each of the absorption bands studied. These were picked to accurately describe the Howard, Burch, and Williams spectral data; that is, given measured absorption at each of these wavelengths, the band spectra could be duplicated almost exactly by simply sketching a curve through these measured values. For each of the chosen wavelengths, values of absorption corresponding to different (effective) pressures and concentrations were read from the spectra and plotted in the form A vs. log W for different constant values of P. Figure 37 shows plots of the data for the wavelengths 4.85, 2.76, and 2.70 μ. The plotted data were compared to the master plot of equations 78-81 by placing the plots of the equations, one over the other, on a light table; the plot of the data was shifted to the right or left until the curves best matching the data points were found. These curves were then traced directly onto the data plot as indicated by the solid curves of figure 37. This procedure established the form of the empirical equation, and led into the problem of determining the values of the three constants.

Figure 37a demonstrates that the absorption data at $\lambda = 4.85\ \mu$ is accurately described by equation 78. The shape of the absorption curve given by equation 78 is taken directly from the labeled curves of the master plot after they are traced through the data points. The value of c is determined by comparing the β's for any two of the curves; that is, $P_1/P_2 = (\beta_1/\beta_2)^c$. As would be expected, the values of c obtained from different pairs were usually not consistent on the first attempt. The value of c for which all the curves simultaneously fit the data points with

TABLE 8. EMPIRICAL CONSTANTS FOR CARBON DIOXIDE

λ (μ)	Model	k	a	c/2	S/d	β/0	c
1.37	2	1.29×10^{-6}	0.500	0.500			
1.38	2	7.8×10^{-6}	0.500	0.500			
1.39	2	1.71×10^{-5}	0.500	0.500			
1.40	2	1.42×10^{-4}	0.500	0.264			
1.41	2	2.02×10^{-4}	0.500	0.295			
1.42	4	6.38×10^{-4}	0.399	0.358			
1.44	4	1.02×10^{-3}	0.399	0.292			
1.46	2	2.30×10^{-4}	0.500	0.286			
1.48	2	2.40×10^{-5}	0.500	0.500			
1.50	2	2.54×10^{-6}	0.500	0.500			
1.52	2	3.62×10^{-7}	0.500	0.500			
1.54	2	1.24×10^{-5}	0.500	0.500			
1.56	2	4.07×10^{-5}	0.500	0.491			
1.58	2	2.00×10^{-4}	0.500	0.366			
1.60	4	3.62×10^{-4}	0.446	0.399			
1.63	2	1.61×10^{-4}	0.500	0.336			
1.65	2	3.04×10^{-5}	0.500	0.500			
1.67	2	1.1×10^{-5}	0.500	0.500			
1.68	2	3.27×10^{-6}	0.500	0.500			
1.69							
	$\tau \cong 1$						
1.88							
1.90	2	2.92×10^{-5}	0.500	0.500			
1.92	2	8.66×10^{-5}	0.500	0.542			
1.94	2	1.03×10^{-3}	0.500	0.332			
1.95	2	1.39×10^{-3}	0.46	0.35			
1.96	2	1.29×10^{-3}	0.500	0.387			
1.97	2	9.9×10^{-4}	0.528	0.356			
1.98	2	7.92×10^{-4}	0.500	0.383			
1.99	2	2.32×10^{-4}	0.676	0.402			
2.00	4	1.83×10^{-4}	0.717	0.572			
2.01	4	5.35×10^{-3}	0.446	0.399			
2.02	4	2.64×10^{-2}	0.358	0.177			

TABLE 8. EMPIRICAL CONSTANTS FOR CARBON DIOXIDE (Continued)

λ (μ)	Model	k	a	c/2	S/d	β_0	c
2.03	4	7.44×10^{-3}	0.447	0.213			
2.04	2	1.99×10^{-3}	0.500	0.276			
2.05	2	1.35×10^{-3}	0.500	0.363			
2.06	2	1.46×10^{-3}	0.500	0.377			
2.07	2	3.64×10^{-3}	0.415	0.303			
2.08	4	3.6×10^{-3}	0.399	0.292			
2.10	2	5.0×10^{-5}	0.500	0.207			
2.12							
	$\tau \cong 1$						
2.62							
2.64	4	1.04×10^{-3}	0.446	0.424			
2.66	4	1.38×10^{-2}	0.375	0.316			
2.68	4	2.31×10^{-2}	0.448	0.378			
2.70	4	3.29×10^{-2}	0.446	0.435			
2.72	4	2.36×10^{-2}	0.414	0.455			
2.74	4	1.07×10^{-2}	0.500	0.493			
2.76	3	5.87×10^{-3}	0.500	0.485			
2.78	4	1.82×10^{-2}	0.500	0.490			
2.80	4	2.89×10^{-2}	0.399	0.380			
2.82	4	3.07×10^{-2}	0.292	0.344			
2.84	4	3.25×10^{-2}	0.216	0.257			
2.86	4	2.25×10^{-2}	0.189	0.217			
2.88	4	8.87×10^{-3}	0.292	0.141			
2.90							
	$\tau \cong 1$						
3.96							
4.00							
4.05	2	2.11×10^{-6}	0.500	1.17			
4.10	1				2×10^{-3}	0.212	1.81
4.15	1				2.5×10^{-2}	0.103	1.00
4.20	2	1.0×10^{-2}	0.500	0.363			
4.25	---						
4.30	--						

TABLE 8. EMPIRICAL CONSTANTS FOR CARBON DIOXIDE (Continued)

λ (μ)	Model	k	a	c/2	S/d	β_0	c
4.35	4	1.12×10^{-1}	0.446	0.372			
4.40	4	4.81×10^{-2}	0.500	0.367			
4.45	4	1.77×10^{-2}	0.500	0.380			
4.50	1				7.5×10^{-3}	0.409	0.675
4.55	2	1.48×10^{-3}	0.500	0.193			
4.60	2	1.12×10^{-4}	0.500	0.500			
4.65	2	8.94×10^{-5}	0.500	0.500			
4.70	2	1.74×10^{-4}	0.500	0.500			
4.75	1				1.3×10^{-3}	0.103	1.00
4.80	1				2.41×10^{-3}	0.207	1.00
4.85	1				4.17×10^{-3}	0.205	0.742
4.90	1				1.89×10^{-3}	0.102	0.440
4.95	1				7.40×10^{-5}	0.203	0.433
5.00	--						
5.05	$\tau \equiv 1$						
5.10	1				1.08×10^{-4}	0.021	1.00
5.15	2	9.9×10^{-5}	0.500	0.500			
5.20	1				5.56×10^{-4}	0.314	1.30
5.25	1				2.25×10^{-4}	1.19	1.00
5.30	$\tau \equiv 1$						

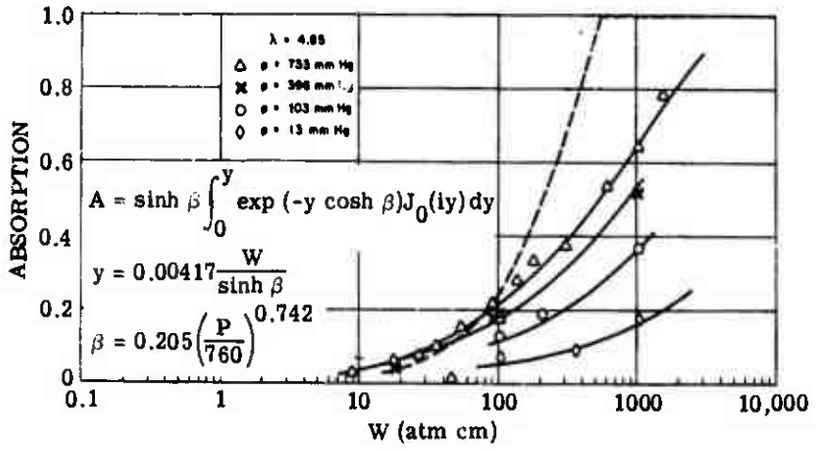

(a) 4.85 μ

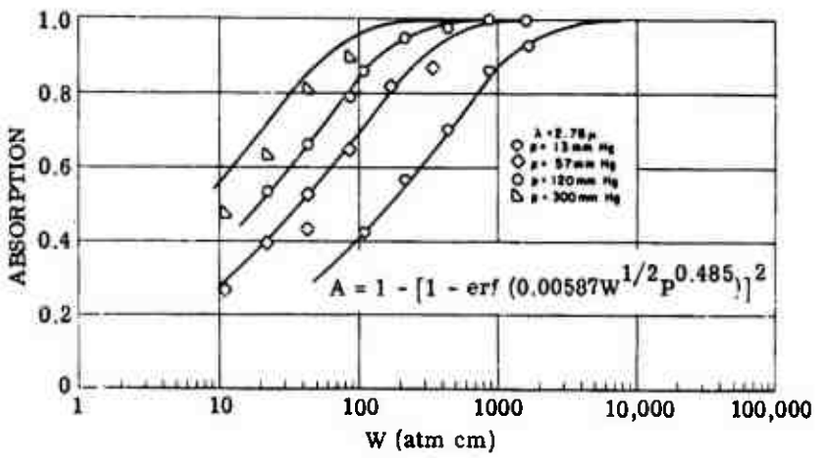

(b) 2.76 μ

FIGURE 37. FRACTIONAL ABSORPTION

minimum scatter can eventually be determined by retracing the curves several times. From the determined values of c and of any one of the β's the value of β_0 can be calculated from the relation $\beta = \beta_0(P/P_0)^c$. Since the abscissa of the master plot is $\beta\psi = (S/d)W$, as in figure 36, the value of S/d is determined as soon as the curves are traced through the data points by dividing the value of (S/d)W on the abscissa of the master plot by the corresponding value of concentration W on data plot.

Figures 37a and 37b show, except for the uppermost curve in figure 37b, that the absorption at 2.76 and 2.70 μ is described by equations 80 and 81, respectively. The procedure in determining the appropriate values of K, k, and c in either of these equations is much the same as the procedure used to make the empirical fit of equation 78 to the 4.85-μ data. The value of k was determined by tracing the curves of the master plot through the data points. The value of c/2 could have been found in the same manner, by plotting A vs. log P = for constant W and using the master plot again; the usual process, however, was to equate the values of $W^k P^{c/2}$, which give the same absorption for two different pressures. If $A(W_1, P_1) = A(W_2, P_2)$, then $(W_1/W_2)^k = (P_2/P_1)^{c/2}$, which gives c/2 when k is known. By substituting the known values of k and c and the absorption corresponding to any P and W into the absorption equation one can determine the value of K.

Zachor's method for computing absorption is unique in that he is the only author that incorporated a pressure correction on half-width that is nonlinear and a function of frequency. Such a pressure correction implies that a change in pressure affects the average line half-width differently, depending upon the frequency interval. Although such effects are not supported by theory, they were observed by Zachor upon examining the laboratory data and were, therefore, incorporated into the fitting procedure. It seems to the author that the observed anomalies should have been attributed to experimental error rather than to a new physical phenomenon and that a linear correction should be used (at least one that was constant with frequency) rather than the one employed. This would result in an empirical fit that had a tendency to average out the errors rather than emphasizing them.

Zachor's method for computing slant-path transmission is quite straight-forward. First, the values of W and P are determined for each absorbing gas. To compute absorption caused by O_3, calculate Y and β for each wavelength, using the constants given in table 7. The values of Y and β can then be used to determine the spectral absorption from figure 36 or equation 78. The strong-line and weak-line approximations to the exact Elsasser model should not be used unless the values of Y and β are satisfied by the conditions noted on figure 36.

To calculate absorption for CO_2, one of four models is used: table 8 gives the appropriate model to use for a given wavelength. These models in conjunction with the constants k, a, c/2, S/d, β_0 and c, also given in table 8, are then used to calculate slant-path absorption spectra.

3.5. METHOD OF J. HOWARD, D. BURCH, AND D. WILLIAMS

The major contribution of Howard, Burch, and Williams to the field of atmospheric absorption has been the measurement of low- and high-resolution absorption spectra for homogeneous paths under laboratory conditions. The major results of their efforts are published in two reports [1, 30] which include a wealth of data. The earlier of these reports contained spectra measured at relatively low resolution compared to the resolution obtained from their more recent measurements.

WATER VAPOR. In an effort to contribute further to the field of atmospheric transmission, Howard et al. made an empirical fit of the Goody band model to their low-resolution absorption spectra [30]. Let us consider the empirical procedures which were employed.

Recall that the Goody model is given by

$$A = 1 - \exp\left[\frac{-\frac{S}{d}\alpha W}{\left(\alpha^2 + \frac{S\alpha}{\pi}W\right)^{1/2}}\right] \tag{82}$$

Equation 82 expresses the absorption averaged over a narrow spectral interval in terms of the mean line intensity S for that interval as well as the mean line half-width and the absorber concentration. It was assumed by Howard et al. that the average intensity for a subinterval varied across an absorption band according to the relation $S = k/W_0$, where k is a constant and W_0 is the value of absorber concentration, at some pressure which yields a value of absorption equal to 50%. Substituting this expression into equation 82 and simplifying, we reduce that equation to

$$A = 1 - \exp\left\{\frac{-\frac{k}{d}\left(\frac{W}{W_0}\right)}{\left[1 + \frac{k}{\pi\alpha_0}\frac{P_0}{P}\left(\frac{W}{W_0}\right)\right]^{1/2}}\right\} \tag{83}$$

Before equation 83 can be used to predict absorption the various parameters must be evaluated. W_0 is the only frequency-dependent parameter and has been evaluated as follows: a number of homogeneous absorption spectra were selected covering a broad range of absorber concentrations, each concentration reduced to an equivalent value at some common pressure. The absorption band was divided into subintervals and for each subinterval the absorption was plotted as a function of absorber concentration. A curve was fitted to these points and the value

of absorber corresponding to an absorption of 50% defines W_0 for that subinterval. This process was continued until W_0 was determined for the entire band. The values of W_0 are given in table 9.

The next step in performing the empirical fit was to determine the values of k/d and k/α_0. This was done simply by plotting A vs. $\frac{P_0}{P}\left(\frac{W}{W_0}\right)$ for all of the homogeneous laboratory spectra and adjusting the two constants until equation 83 gave a best fit to the data. The resulting expression for absorption as determined by Howard et al. is given by

$$A = 1 - \exp\left\{\frac{-1.97\left(\frac{W}{W_0}\right)}{\left[1 + 6.57\frac{P_0}{P}\left(\frac{W}{W_0}\right)\right]^{1/2}}\right\} \tag{84}$$

Equation 84 in conjunction with the values of W_0 presented in table 9 can be used to compute H_2O absorption for any path for which values of W and P are known.

3.6. METHOD OF G. LINDQUIST

Lindquist [53] made an empirical fit of the Goody band-model absorption equation to the laboratory data of Howard, et al. to develop a transmissivity function for H_2O for the wavelength region from 1.06 to 9.2 μ.

The form of the absorption equation used by Lindquist is

$$A = 1 - \exp\left[\frac{-C_3 W^*}{(1 + C_4 W^*)^{1/2}}\right] \tag{85}$$

where W^* is the equivalent sea-level path and C_3 and C_4 are empirically derived constants. The procedure used to evaluate the constants was as follows: The Howard spectral data were reduced to equivalent W^* values by the equation

$$W^* = W\frac{P_e}{P_0}\left(\frac{T_0}{T}\right)^{0.62}$$

Equation 85 was then fitted to the reduced data, determining C_3 and C_4 such that the error between measured and calculated values of absorption was minimized in a least-squares sense. The resulting values of C_3 and C_4 are given in table 10.

TABLE 9. w_0 Vs. WAVELENGTH FOR WATER VAPOR

λ (μ)	w_0	λ (μ)	w_0	λ (μ)	w_0	λ (μ)	w_0
1.03	3.6×10^{3}	1.38	6.2×10^{-2}	1.97	2.15	2.72	4.75×10^{-3}
1.04	1.62×10^{3}	1.39	7.5×10^{-2}	1.98	3.45	2.74	8.00×10^{-3}
1.05	7.2×10^{2}	1.40	9.5×10^{-2}	1.99	5.55	2.76	9.6×10^{-3}
1.06	3.0×10^{2}	1.41	1.3×10^{-1}	2.00	8.6	2.78	1.1×10^{-2}
1.07	1.14×10^{2}	1.42	1.85×10^{-1}	2.01	1.37×10	2.80	1.29×10^{-2}
1.08	3.75×10	1.44	4.3×10^{-1}	2.02	2.1×10	2.82	1.65×10^{-2}
1.09	1.45×10	1.46	1.08	2.03	3.3×10	2.84	2.45×10^{-2}
1.10	6.8	1.48	2.55	2.04	4.95×10	2.86	4.00×10^{-2}
1.11	3.15	1.50	5.9	2.05	7.6×10	2.88	7.00×10^{-2}
1.12	1.91	1.52	1.59×10	2.06	1.1×10^{2}	2.90	1.23×10^{-1}
1.13	1.42	1.54	5.1×10	2.07	1.6×10^{2}	2.92	2.14×10^{-1}
1.14	1.62	1.56	1.86×10^{2}	2.08	2.35×10^{2}	2.94	3.00×10^{-1}
1.15	2.65	1.58	7.7×10^{2}	2.10	4.8×10^{2}	2.96	3.47×10^{-1}
1.16	4.8	1.60	3.5×10^{3}	2.12	9.2×10^{2}	2.98	3.75×10^{-1}
1.17	8.4	1.63	1.6×10^{3}	2.14	1.68×10^{3}	3.00	3.83×10^{-1}
1.18	1.5×10	1.65	6.0×10^{2}	2.16	2.8×10^{3}	3.02	3.65×10^{-1}
1.19	2.8×10	1.67	2.15×10^{2}	2.18	2.1×10^{3}	3.04	3.22×10^{-1}
1.20	5.8×10	1.68	1.25×10^{2}	2.20	1.17×10^{3}	3.06	2.92×10^{-1}
1.21	1.45×10^{2}	1.69	7.2×10	2.24	2.6×10^{2}	3.08	2.93×10^{-1}
1.22	5.6×10^{2}	1.70	4.1×10	2.28	6.4×10	3.10	3.65×10^{-1}
1.23	1.7×10^{3}	1.72	1.3×10	2.32	1.75×10	3.12	6.2×10^{-1}
1.24	5.3×10^{2}	1.74	4.2	2.36	5.5	3.14	1.2
1.25	1.85×10^{2}	1.76	1.3	2.40	1.95	3.16	1.7
1.26	6.6×10	1.78	4.25×10^{-1}	2.44	7×10^{-1}	3.18	1.0
1.27	2.5×10	1.80	1.52×10^{-1}	2.48	2×10^{-1}	3.20	3.4×10^{-1}
1.28	1.0×10	1.82	5.6×10^{-2}	2.52	5×10^{-2}	3.22	2.25×10^{-1}
1.29	4.45	1.84	2.6×10^{-2}	2.54	2.25×10^{-2}	3.24	2.27×10^{-1}
1.30	2.08	1.86	2.35×10^{-2}	2.56	1.12×10^{-2}	3.26	2.8×10^{-1}
1.31	1.0	1.88	3.95×10^{-2}	2.58	8.5×10^{-3}	3.28	3.5×10^{-1}
1.32	5.05×10^{-1}	1.90	8.7×10^{-2}	2.60	7.1×10^{-3}	3.30	4.5×10^{-1}
1.33	2.65×10^{-1}	1.92	2.2×10^{-1}	2.62	5.6×10^{-3}	3.32	5.8×10^{-1}
1.34	1.5×10^{-1}	1.94	5.5×10^{-1}	2.64	3.85×10^{-3}	3.34	7.6×10^{-1}
1.35	9.2×10^{-2}	1.95	8.6×10^{-1}	2.66	2.6×10^{-3}	3.36	1.0
1.36	6.5×10^{-2}	1.96	1.37	2.68	2.2×10^{-3}	3.40	1.80
1.37	5.7×10^{-2}			2.70	2.37×10^{-3}	3.44	3.35

TABLE 9. w_0 Vs. WAVELENGTH FOR WATER VAPOR (Continued)

λ (μ)	w_0	λ (μ)	w_0	λ (μ)	w_0
3.48	6.40				
3.52	1.23×10	5.10	8.9×10^{-1}	6.90	2.75×10^{-3}
3.56	2.3×10	5.15	6.4×10^{-1}	6.95	3.5×10^{-3}
3.60	4.4×10	5.20	4.7×10^{-1}	7.00	4.3×10^{-2}
3.64	8.5×10	5.25	3.4×10^{-1}	7.10	6.8×10^{-3}
3.68	1.59×10^{2}	5.30		7.20	1.1×10^{-2}
3.72	3.0×10^{2}	5.35	1.78×10^{-1}	7.40	2.75×10^{-2}
3.76	5.7×10^{2}	5.40	1.25×10^{-1}	7.60	7.3×10^{-2}
3.80	1.06×10^{3}	5.45	8.8×10^{-2}	7.80	1.9×10^{-1}
3.84	1.95×10^{3}	5.50	6.3×10^{-2}	8.00	4.7×10^{-1}
3.88	3.68×10^{3}	5.50	3.0×10^{-2}	8.20	1.0
3.92	6.9×10^{3}	5.70	1.4×10^{-2}	8.40	2.0
3.96	↑	5.80	7.2×10^{-3}	8.60	3.85
4.00	|	5.85	5.1×10^{-3}	8.80	6.9
4.05	|	5.90	3.5×10^{-3}	9.00	1.21×10
4.10	|	5.95	2.65×10^{-3}	9.20	2.17×10
4.15	$\tau \cong 1$	6.00	2.1×10^{-3}	9.40	3.95×10
4.20	|	6.05	1.97×10^{-3}	9.60	7.4×10
4.25	|	6.10	2.15×10^{-3}	9.80	1.43×10^{2}
4.30	|	6.15	2.95×10^{-3}	10.00	3.00×10^{2}
4.35	|	6.20	4.15×10^{-3}	10.20	6.8×10^{2}
4.40	4.45×10^{3} ↓	6.25	5.8×10^{-3}	10.40	1.65×10^{3}
4.45	1.7×10^{3}	6.30	7.7×10^{-3}	10.60	4.65×10^{3}
4.50	8.0×10^{2}	6.35	8.05×10^{-3}	10.80	$\tau \cong 1$
4.55	3.6×10^{2}	6.40	7.1×10^{-3}		
4.60	1.85×10^{2}	8.45	4.8×10^{-3}		
4.65	8.8×10	6.50	3.1×10^{-3}		
4.70	4.5×10	6.55	2.05×10^{-3}		
4.75	2.3×10	6.60	1.5×10^{-3}		
4.90	1.2×10	6.65	1.35×10^{-3}		
4.85	6.8	6.70	1.37×10^{-3}		
4.90	4.15	6.75	1.52×10^{-3}		
4.95	2.7	6.80	1.8×10^{-3}		
5.00		6.85	2.2×10^{-3}		
5.05	1.26				

TABLE 10. ABSORPTION COEFFICIENTS FOR WATER VAPOR

λ (μ)	C_3	C_4	λ (μ)	C_3	C_4
1.06	0.000	0.000	1.41	13.371	43.401
1.07	0.000	0.000	1.42	9.311	30.223
1.08	0.3615	0.1173	1.44	4.186	13.589
1.09	0.1010	0.328	1.46	2.077	6.742
1.10	0.3062	0.994	1.48	0.9289	3.015
1.11	0.6318	2.051	1.50	0.4572	1.848
1.12	1.0075	3.271	1.52	0.1661	0.5392
1.13	1.331	4.321	1.54	0.09148	0.297
1.14	1.365	4.432	1.56	0.04348	0.1411
1.15	1.0687	3.469	1.58	0.03715	0.1206
1.16	0.7635	2.478	1.63	0.04	0.130
1.17	0.5117	1.661	1.65	0.0370	0.1201
1.18	0.2954	0.9587	1.67	0.1360	0.4415
1.19	0.142	0.4608	1.68	0.06592	0.214
1.20	0.08026	0.2605	1.69	0.1570	0.510
1.21	0.000	0.000	1.70	0.1378	0.4472
1.22	0.000	0.000	1.72	0.423	1.373
1.23	0.000	0.000	1.74	0.7224	2.345
1.24	0.01616	0.0524	1.76	2.137	6.936
1.25	0.05153	0.1673	1.78	6.117	19.857
1.26	0.0915	0.2970	1.80	20.11	65.278
1.27	0.1529	0.4964	1.82	41.56	134.89
1.28	0.2789	0.9054	1.84	55.26	179.38
1.29	0.4497	1.460	1.86	46.45	150.78
1.30	0.7576	2.459	1.88	32.83	106.58
1.31	1.2486	4.053	1.90	18.45	59.903
1.32	2.2946	7.448	1.92	8.121	26.36
1.33	4.4518	14.451	1.94	2.678	8.693
1.34	9.1296	29.635	1.95	1.526	4.955
1.35	17.389	58.446	1.96	0.9034	2.932
1.36	26.884	87.267	1.97	0.5233	1.699
1.37	32.454	105.35	1.98	0.3867	1.255
1.38	30.6415	99.464	1.99	0.2939	0.954
1.39	24.83	80.792	2.00	0.2375	0.7708
1.40	18.712	60.741	2.01	0.1674	0.5434

TABLE 10. ABSORPTION COEFFICIENTS FOR WATER VAPOR (Continued)

$\frac{\lambda}{(\mu)}$	C_3	C_4	$\frac{\lambda}{(\mu)}$	C_3	C_4
2.02	0.1674	0.5434	3.00	4.420	14.349
2.03	0.1037	0.3366	3.02	5.453	17.701
2.04	0.1037	0.3366	3.04	6.360	20.646
2.05	0.000	0.000	3.06	6.503	21.109
2.24	0.000	0.000	3.08	6.199	20.123
2.28	0.0225	0.07329	3.10	4.879	15.838
2.32	0.08951	0.2906	3.12	2.909	9.444
2.38	0.2732	0.8869	3.14	1.373	4.458
2.40	0.7837	0.2544	3.18	1.364	4.429
2.44	1.885	6.120	3.18	4.094	13.291
2.48	8.687	21.64	3.20	7.542	24.482
2.52	29.31	95.15	3.22	5.897	19.141
2.54	55.51	180.20	3.24	4.581	14.889
2.58	118.0	383.15	3.26	3.845	12.481
2.58	281.4	913.48	3.28	3.813	11.729
2.60	554.3	1799.3	3.30	3.464	11.245
2.62	778.8	2528.0	3.32	3.205	10.404
2.64	583.7	1894.7	3.34	2.831	9.187
2.66	533.5	1731.9	3.36	2.259	7.331
2.68	700.5	2274.0	3.40	1.219	3.957
2.70	814.1	2642.8	3.44	0.8888	2.171
2.72	644.2	2091.2	3.48	0.3885	1.190
2.74	588.6	1910.7	3.52	0.1851	0.6007
2.76	561.4	1822.3	3.56	0.08803	0.2858
2.78	469.0	1522.6	3.60	0.05465	0.1774
2.80	207.1	872.36	3.64	0.03957	0.1284
2.82	101.4	329.01	3.88	0.03918	0.1272
2.84	53.89	174.93	3.72	0.000	0.000
2.86	33.11	107.47	4.50	0.000	0.000
2.88	18.51	60.081	4.55	0.000	0.000
2.90	11.94	38.758	4.80	0.01122	0.03642
2.92	8.446	27.416	4.85	0.08547	0.2125
2.94	6.795	22.058	4.70	0.1508	0.4887
2.96	5.818	18.885	4.75	0.2620	0.8505
2.98	4.8400073	15.71	4.80	0.3935	1.277

TABLE 10. ABSORPTION COEFFICIENTS FOR WATER VAPOR (Continued)

λ (μ)	C_3	C_4	λ (μ)	C_3	C_4
4.85	0.5686	1.846	6.50	1126.8	3857.8
4.90	0.7842	2.545	6.55	1503.2	4879.4
4.95	1.064	3.454	6.60	1825.6	5925.9
5.00	1.431	4.644	6.65	1243.3	4035.8
5.05	1.906	6.189	6.70	866.9	2814.1
5.10	2.580	8.373	6.75	616.2	2000.3
5.15	3.567	11.578	6.80	461.35	1497.6
5.20	4.986	16.183	6.85	459.23	1490.7
5.25	6.961	22.597	6.90	327.42	1062.8
5.30	9.634	31.274	6.95	256.58	832.87
5.35	13.38	43.422	7.00	198.02	642.78
5.40	18.64	60.492	7.10	135.98	441.35
5.45	25.97	84.287	7.20	78.93	258.21
5.50	35.78	116.14	7.40	32.719	108.21
5.60	68.97	223.87	7.60	10.851	35.223
5.70	138.8	450.58	7.80	3.997	12.980
5.80	420.2	1383.8	8.00	2.584	8.389
5.85	619.4	2010.6	8.20	1.278	4.1487
5.90	825.9	2681.02	8.40	0.5465	1.7739
5.95	991.1	3217.3	8.60	0.2764	0.8971
6.00	1249.	4055.7	8.80	0.1778	0.5772
6.05	1218.	3954.3	9.00	0.0977	0.3172
6.10	954.5	3098.4	9.20	0.085775	0.2135
6.15	556.98	1808.0			
6.20	370.86	1203.8			
6.25	275.68	894.87			
6.30	241.40	783.60			
6.35	309.1	1003.4			
6.40	434.13	1409.2			
6.45	702.05	2278.9			

To predict H_2O absorption by the method of Lindquist, the amount of H_2O in an atmospheric slant path is reduced to an equivalent sea level concentration, W*. This value and the constants C_3 and C_4 are substituted in equation 85.

3.7. METHOD OF G. E. OPPEL

Oppel [18, 21, 54] has applied the absorption band models of Elsasser and Goody to the laboratory data of Burch, Williams, Gryvnak, Singleton, and France [1] and the calculated homogeneous-path data of Stull, Wyatt, and Plass [19] to develop transmissivity functions for H_2O, CO_2, N_2O, CH_4, and CO for the wavelength range from 1.0 to 5.0 μ. These functions express absorption as a function of two frequency-dependent parameters, $2\pi\alpha_0'/d$ and $S/2\pi\alpha_0'$, and two slant-path parameters, W and $\overline{P}$. Absorption spectra computed by Oppel's method differ from spectra obtained by any other published method which is based upon a closed-form band model in that the spectra have a relatively high resolution (approximately 0.005 μ). The higher resolution resulted from the laboratory data that were used and the method of performing the empirical fit.

A sample of the laboratory data of Burch et al. is shown in figure 38. Two curves are presented for the 2.7-μ H_2O band for two values of absorber concentration, each for a different equivalent broadening pressure. Note that the resolution is such that spectral line structure is observable. Oppel preserved this structure by evaluating the frequency-dependent parameters at each maximum, minimum, and inflection point of the absorption spectra. The procedure employed in performing this evaluation is exactly that which is described in section 2.3. This method is in contrast to that employed by other authors who either invoke a smoothing process that removes most of the spectral detail in the absorption band or use laboratory data that are of relatively low resolution.

3.7.1. CARBON DIOXIDE. Oppel fitted the Elsasser model to the data of Burch, et al. [1] for the 2.7- and 4.3-μ bands of CO_2 to obtain values of $2\pi\alpha_0'S/d^2$ and S/d which are presented in tables 11 and 12, respectively.

The exact Elsasser equation and the strong-line and weak-line approximations are, respectively:

$$A = \sinh\beta \int_0^Y I_0(y) \exp(-y\cosh\beta)\, dy \tag{86}$$

$$A = \operatorname{erf}\left[\frac{1}{2}\frac{(2\pi\alpha_0' S)}{d^2} WP\right]^{1/2} \tag{57}$$

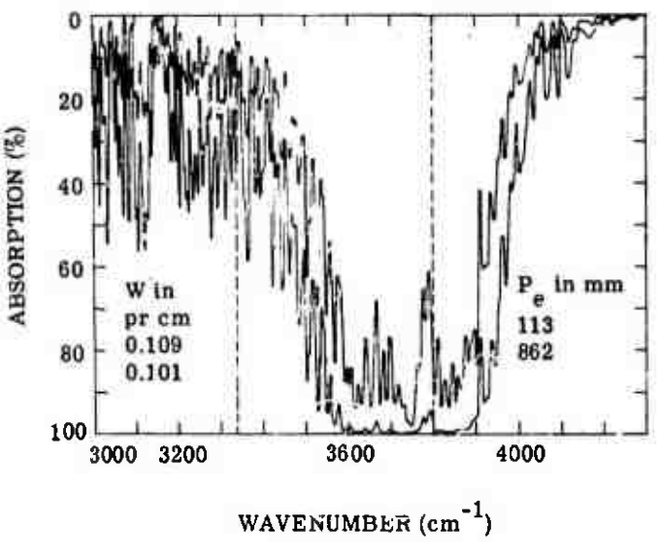

FIGURE 38. ABSORPTION VS. WAVENUMBER FOR 2.7-μ WATER VAPOR BAND

TABLE 11. ABSORPTION CONSTANTS FOR CARBON DIOXIDE FOR THE 2.7-μ BAND

λ (μ)	$2\pi a_0' S/d^2$	S/d
2.6434	0.15 E-8	0.33 E-3
2.6504	0.6 E-7	0.16 E-2
2.6674	0.5 E-4	0.37
2.6724	0.25 E-3	0.50
2.6738	0.315 E-3	0.50
2.6802	0.55 E-3	0.55
2.6831	0.54 E-3	0.88
2.6882	0.28 E-3	0.86
2.6911	0.195 E-3	0.54
2.6940	0.26 E-3	0.38
2.6969	0.325 E-3	0.52
2.7027	0.345 E-3	0.70
2.7086	0.28 E-3	0.74
2.7137	0.135 E-3	0.62
2.7211	0.39 E-4	0.44
2.7322	0.10 E-4	0.15
2.7397	0.15 E-4	0.025
2.7473	0.75 E-4	0.076
2.7548	0.26 E-3	0.36
2.7579	0.30 E-3	0.55
2.7609	0.255 E-3	0.58
2.7663	0.13 E-3	0.53
2.7685	0.81 E-4	0.33
2.7739	0.24 E-3	0.26
2.7778	0.28 E-3	0.42
2.7801	0.27 E-3	0.47
2.7855	0.165 E-3	0.44
2.7917	0.7 E-4	0.29
2.7941	0.56 E-4	0.16
2.8027	0.35 E-4	0.13
2.8129	0.84 E-5	0.07
2.8153	0.58 E-5	0.037
2.8177	0.39 E-5	0.027
2.8241	0.2 E-5	0.017
2.8281	0.165 E-5	0.005
2.8345	0.155 E-5	0.003
2.8433	0.197 E-5	0.0039
2.8514	0.165 E-5	0.0033
2.8555	0.13 E-5	0.0024
2.8620	0.45 E-6	0.001
2.8686	0.97 E-7	0.3 E-4
2.8752	0.24 E-7	
2.8777	0.1 E-7	
2.8810	0.7 E-9	

TABLE 12. ABSORPTION CONSTANTS FOR CARBON DIOXIDE FOR THE 4.3-μ BAND

λ (μ)	$2\pi a_0' S/d^2$	S/d
4.149	0.0	0.0
4.158	2.6 E-10	0.00026
4.167	2.95 E-8	0.0059
4.175	1.92 E-5	0.24
4.184	1.39 E-4	0.87
4.193	5.13 E-4	2.05
4.202	5.14 E-3	15.1
4.211	1.2 E-2	26.15
4.219	2.04 E-2	34.6
4.228	3.34 E-2	41.6
4.237	3.48 E-2	41.5
4.246	3.42 E-2	37.2
4.255	1.2 E-2	12.25
4.264	2.34 E-2	25.5
4.274	2.81 E-2	32.7
4.283	2.53 E-2	31.6
4.292	2.07 E-2	26.5
4.301	2.33 E-2	28.4
4.310	1.07 E-2	12.16
4.319	1.34 E-2	13.9
4.329	8.46 E-3	7.7
4.338	4.58 E-3	3.58
4.348	3.7 E-3	2.72
4.357	1.74 E-3	1.25
4.367	1.34 E-3	0.974
4.376	4.31 E-4	0.322
4.386	5.07 E-4	0.39
4.396	1.03 E-3	0.825
4.405	1.47 E-3	1.224
4.415	9.87 E-4	0.866
4.425	5.67 E-4	0.522
4.435	4.25 E-4	0.34
4.444	1.23 E-4	0.131
4.454	7.1 E-5	0.0825
4.464	4.14 E-5	0.053
4.474	2.34 E-5	0.0304
4.484	9.92 E-6	0.0167
4.494	3.18 E-6	0.00618
4.505	9.6 E-7	0.0024
4.515	0.0	0.0

$$A = 1 - \exp(-S/dW) \tag{88}$$

where $Y = \dfrac{\beta\psi}{\sinh\beta}$

$$\beta = \frac{2\pi\alpha_0'}{d}\mathrm{P}$$

$$\psi = \frac{S}{2\pi\alpha_0'}\frac{W}{P}$$

To compute absorption spectra by Oppel's method for a slant path, simply determine W and $\overline{P}$ by the appropriate equations given in section 2.4 or by the computer program given in appendix I. Substitute these values into the equations. If either of the two approximations to the Elsasser function is used, the values of β and ψ should be compared with table 1 to confirm the valid application of the model selected.

3.7.2. WATER VAPOR. The statistical model with an exponential distribution of line strength was used to describe absorption by H_2O for the spectral region from 1.0 to 5.0 μ. This function was fitted to the data of Howard et al. for the three absorption bands centered at 1.14, 1.4, and 1.88 μ, and the data of Burch et al. for the 2.7- and 3.1-μ bands. High-resolution absorption spectra for H_2O are not available for the 4 to 5 μ region. However, Stull et al. have calculated homogeneous absorption spectra for this spectral region using the quasi-random model. These calculated absorption spectra were used by Oppel to determine the statistical band-model constants. The empirical procedure used to evaluate the frequency-dependent parameters $S/2\pi\alpha_0'$ and S/d for the entire region from 1.0 to 5.0 μ was analogous in every detail to that used for CO_2. The results of the empirical fit are presented in table 13. Absorption for the exact statistical model is given by

$$A = 1 - \exp\left[-\beta\psi/(1 + 2\psi)^{1/2}\right] \tag{89}$$

and the strong-line and weak-line approximations are, respectively,

$$A = 1 - \exp\left[-\left(\frac{1}{2}\beta^2\psi\right)^{1/2}\right] \tag{90}$$

and

$$A = 1 - \exp(-\beta\psi) \tag{91}$$

where β and ψ are defined as for CO_2. In general, neither of the approximations is used to compute absorption since the exact statistical model is given in a convenient closed form. If the exact function is used, it is not necessary to check the limits of β and ψ since the function is defined for all values.

TABLE 13. ABSORPTION COEFFICIENTS FOR WATER VAPOR

λ (μ)	$S/2\pi\alpha'_0$	S/d	λ (μ)	$S/2\pi\alpha'_0$	S/d
1.07875	0.0	0.0	1.13379	4.7 E 5	1.9 E 1
1.07991	5.	7. E-3	1.13507	6.5 E 5	1.9 E 1
1.08108	1. E 1	8.5 E-3	1.13636	2.2 E 6	2.4 E 1
1.08225	1.2 E 1	1.1 E-2	1.13766	6.2 E 6	6.8 E 1
1.08342	1.6 E 1	1.3 E-2	1.13895	2.5 E 7	1.5 E 2
1.08460	2.6 E 1	1.5 E-2	1.14025	7.5 E 7	2.4 E 2
1.08576	4.5 E 1	1.7 E-2	1.14155	2.3 E 8	3.5 E 2
1.08696	7.5 E 1	4. E-2	1.14286	4.3 E 8	4.8 E 2
1.08814	1.5 E 2	5.6 E-2	1.14416	8.5 E 8	6. E 2
1.08932	2.9 E 2	7. E-2	1.14548	1.4 E 9	8.4 E 2
1.09051	4.2 E 2	8.5 E-2	1.14679	2.1 E 9	1.1 E 3
1.09170	6.8 E 2	1.1 E-1	1.14811	2.5 E 9	1.2 E 3
1.09290	1.1 E 3	1.3 E-1	1.14943	2.4 E 9	1.1 E 3
1.09409	1.7 E 3	1.5 E-1	1.15075	2. E 9	9. E 2
1.09529	2.3 E 3	1.7 E-1	1.15207	1.2 E 9	6. E 2
1.09649	2.7 E 3	2. E-1	1.15340	4.5 E 8	3.8 E 2
1.09769	2.9 E 3	2.3 E-1	1.15473	1.3 E 8	2.5 E 2
1.09890	2.8 E 3	2.5 E-1	1.15607	4. E 7	1.8 E 2
1.10011	2.6 E 3	2.6 E-1	1.15741	1.5 E 7	1. E 2
1.10132	2.4 E 3	2.7 E-1	1.15875	4. E 6	6. E 1
1.10254	2.2 E 3	2.9 E-1	1.16009	1.5 E 6	2.9 E 1
1.10375	2.15 E 3	3.1 E-1	1.16144	4.4 E 5	1.2 E 1
1.10497	2.2 E 3	3.5 E-1	1.16279	9.5 E 4	6.5
1.10619	2.3 E 3	3.8 E-1	1.16414	4.5 E 4	4.5
1.10742	2.4 E 3	4.3 E-1	1.16550	2.8 E 4	3.
1.10865	2.7 E 3	4.8 E-1	1.16686	1.9 E 4	2.
1.10988	2.9 E 3	5.5 E-1	1.16822	1.2 E 4	1.4
1.11111	3.3 E 3	6.2 E-1	1.16959	8.8 E 3	1.1
1.11235	3.9 E 3	7.4 E-1	1.17096	6.6 E 3	8.7 E-1
1.11359	4.7 E 3	8.5 E-1	1.17233	5. E 3	6.8 E-1
1.11483	5.7 E 3	9.6 E-1	1.17371	3.7 E 3	5.1 E-1
1.11607	7.2 E 3	1.1	1.17509	2.8	3.8 E-1
1.11732	9.5 E 3	1.4	1.17647	2.1	3.5 E-1
1.11857	1.3 E 4	1.7	1.17786	1.5	3.3 E-1
1.11982	1.8 E 4	2.1	1.17925	1.2	3.1 E-1
1.12108	2.5 E 4	2.7	1.18064	9.5	2.8 E-1
1.12233	3.9 E 4	3.4	1.18203	7.7	2.6 E-1
1.12360	5.1 E 4	5.2	1.18343	6.5	2.4 E-1
1.12486	6.6 E 4	8.5	1.18483	5.2	2.2 E-1
1.12613	8.8 E 4	1.4 E 1	1.18624	4.3	2. E-1
1.12740	1.2 E 5	2.1 E 1	1.18765	3.3	1.8 E-1
1.12867	1.6 E 5	2.9 E 1	1.18906	2.7	1.6 E-1
1.12994	2.1 E 5	2.8 E 1	1.19048	2.1	1.5 E-1
1.13122	2.7 E 5	2.5 E 1	1.19190	1.6	1.3 E-1
1.13250	3.5 E 5	2.1 E 1	1.19332	1.2	1.2 E-1

TABLE 13. ABSORPTION COEFFICIENTS FOR WATER VAPOR (Continued)

λ (μ)	$S/2\pi\alpha'_0$	S/d	λ (μ)	$S/2\pi\alpha'_0$	S/d
1.19474	9.7	1.1 E-1	1.30378	2.0 E 1	1.8 E-1
1.19617	7.5	9.0 E-2	1.30548	2.4 E 1	2.1 E-1
1.19760	5.8	7 5 E-2	1.30719	2.9 E 1	2.3 E-1
1.19760	4.5	6.1 E-2	1.30890	3.5 E 1	2.5 E-1
1.19904	3.5	5.2 E-2	1.31062	4.3 E 1	2.8 E-1
1.20048	2.7	4.4 E-2	1.31234	5.4 E 1	3.1 E-1
1.20192	2.2	4. E-2	1.31408	6.6 E 1	3.5 E-1
1.20337	1.8	3.6 E-2	1.31579	8. E 1	3.8 E-1
1.20627	1.4	3.4 E-2	1.31752	9.5 E 1	4.2 E-1
1.20773	1.15	3.2 E-2	1.31926	1.1 E 2	4.7 E-1
1.20919	9.5	3.0 E-2	1.32100	1.3 E 2	5.2 E-1
1.21065	8.	2.7 E-2	1.32275	1.6 E 2	5.8 E-1
1.21212	6.8	2.4 E-2	1.32450	1.9 E 2	6.4 E-1
1.21359	5.3	1.7 E-2	1.32626	2.3 E 2	7.2 E-1
1.21507	4.6	1.2 E-2	1.32802	2.7 E 2	8.2 E-1
1.21654	3.9	8.0 E-2	1.32979	3.3 E 2	9.3 E-1
1.21803	3.3	4.5 E-3	1.33156	3.9 E 2	1.05
1.21951	2.8	2.6 E-3	1.33333	4.7 E 2	1.2
1.22100	2.3	1.6 E-3	1.33511	5.5 E 2	1.4
1.22249	2.0	1. E-3	1.33690	8.6 E 2	1.7
1.22399	1.0 E-3	1.0 E-5	1.33869	8.3 E 2	1.9
1.22549	1.0 E-3	1.0 E-5	1.34028	1.1 E 3	2.2
1.22699	1.0 E-3	1.0 E-5	1.34288	1.5 E 3	2.8
1.22850	1.0 E-3	1.0 E-5	1.34409	1.9 E 3	3.3
1.26904	1.1	1.8 E-2	1.34590	2.6 E 3	4.1
1.27065	1.15	2. E-2	1.34771	3.5 E 3	5.1
1.27226	1.2	2.3 E-2	1.34953	4.6 E 3	6.3
1.27389	1.3	2.6 E-2	1.35135	7. E 3	8.3
1.27551	1.4	2.9 E-2	1.35318	1. E 4	1. E 1
1.27714	1.5	3.2 E-2	1.35501	1.4 E 4	1.2 E 1
1.27877	1.6	3.5 E-2	1.35685	2.2 E 4	1.5 E 1
1.28041	1.8	4. E-2	1.35870	3.8 E 4	2. E 1
1.28205	2.1	4.5 E-2	1.36054	5.3 E 4	2.5 E 1
1.28370	2.5	5. E-2	1.36240	8.2 E 4	3.1 E 1
1.28535	3.	5.6 E-2	1.36426	1.4 E 5	4.1 E 1
1.28700	3.6	6.2 E-2	1.36612	2.8 E 5	5.4 E 1
1.28866	4.4	7. E-2	1.36799	4.3 E 5	6.6 E 1
1.29032	5.2	8. E-2	1.36986	6.8 E 5	8.3 E 1
1.29199	6.4	9. E-2	1.37174	1.1 E 6	1.0 E 2
1.29366	7.4	1. E-1	1.37363	1.9 E 6	1.2 E 2
1.29534	8.8	1.1 E-1	1.37552	2.9 E 6	1.6 E 2
1.29702	1. E 1	1.2 E-1	1.37741	4.5 E 6	2.5 E 2
1.29870	1.2 E 1	1.4 E-1	1.37931	7. E 6	2.9 E 2
1.30039	1.4 E 1	1.5 E-1	1.38122	1.1 E 7	4.3 E 2
1.30208	1.7 E 1	1.7 E-1	1.38313	1.8 E 7	6.0 E 2

TABLE 13. ABSORPTION COEFFICIENTS FOR WATER VAPOR (Continued)

λ (μ)	$S/2\pi\alpha'_0$	S/d	λ (μ)	$S/2\pi\alpha'_0$	S/d
1.38504	2.1 E 7	7.4 E 2	1.47710	9.9 E 3	3.5
1.38696	2.6 E 7	8.7 E 2	1.47929	8.5 E 3	3.1
1.38889	2.8 E 7	9.5 E 2	1.48148	7.4 E 3	2.8
1.39082	2.8 E 7	9.1 E 2	1.48368	6.5 E 3	2.4
1.39276	2.6 E 7	8.3 E 2	1.48588	5.6 E 3	2.1
1.39470	2.4 E 7	7.2 E 2	1.48810	4.9 E 3	1.9
1.39665	2.2 E 7	6.3 E 2	1.49031	4.3 E 3	1.6
1.39860	1.9 E 7	5.3 E 2	1.49254	3.6 E 3	1.4
1.40056	1.7 E 7	4.2 E 2	1.49477	3.1 E 3	1.2
1.40252	1.4 E 7	3.4 E 2	1.49701	2.6 E 3	1.
1.40449	1.25 E 7	2.8 E 2	1.49925	2.2 E 3	8.8 E-1
1.40647	1.05 E 7	2.4 E 2	1.50150	1.9 E 3	7.9 E-1
1.40845	9. E 6	2.1 E 2	1.50376	1.6 E 3	6.9 E-1
1.41044	7.4 E 6	1.9 E 2	1.50602	1.3 E 3	6. E-1
1.41243	6.3 E 6	1.7 E 2	1.50830	1.1 E 3	5.3 E-1
1.41443	5.3 E 6	1.6 E 2	1.51057	9.5 E 2	4.6 E-1
1.41643	4.5 E 6	1.5 E 2	1.51286	7.9 E 2	4. E-1
1.41844	3.6 E 6	1.4 E 2	1.51515	7.5 E 2	3. E-1
1.42045	3.1 E 6	1.35 E 2	1.51745	7. E 2	2.2 E-1
1.42248	2.6 E 6	1.3 E 2	1.51976	6.6 E 2	1.6 E-1
1.42450	2.2 E 6	1.25 E 2	1.52207	6.2 E 2	1.1 E-1
1.42653	1.8 E 6	1.2 E 2	1.52439	5.9 E 2	8.1 E-2
1.42857	1.5 E 6	1. E 2	1.52672	5.2 E 2	6.2 E-2
1.43062	1.3 E 6	9.4 E 1	1.52905	4.6 E 2	4.8 E-2
1.43266	1.05 E 6	8.6 E 1	1.53139	4.1 E 2	3.8 E-2
1.43472	8.6 E 5	7.8 E 1	1.53374	3.55 E 2	3. E-2
1.43678	7.2 E 5	7. E 1	1.53610	3.3 E 2	2.4 E-2
1.43885	6. E 5	6.2 E 1	1.53846	1.3 E 2	2. E-2
1.44092	4.6 E 5	5.2 E 1	1.54083	5. E 1	1.6 E-2
1.44300	3.9 E 5	4.4 E 1	1.54321	2. E 1	1.4 E-2
1.44509	3.2 E 5	3.5 E 1	1.54560	8.	1.1 E-2
1.44718	2.5 E 5	2.8 E 1	1.54799	1.15 E 1	2.17 E-2
1.44928	1.8 E 5	2.4 E 1	1.55039	1.13 E 1	2.13 E-2
1.45138	1.2 E 5	2. E 1	1.55280	1.01 E 1	1.67 E-2
1.45349	8.7 E 4	1.7 E 1	1.55521	8.19	1.62 E-2
1.45560	6.2 E 4	1.4 E 1	1.55763	7.2	1.65 E-2
1.45773	4.3 E 4	1.2 E 1	1.56006	7.95	1.77 E-2
1.45985	3.6 E 4	9.	1.56250	9.18	1.85 E-2
1.46199	3.1 E 4	8.8	1.56495	9.2	2.13 E-2
1.46413	2.7 E 4	7.8	1.56740	8.89	2.45 E-2
1.46628	2.2 E 4	6.9	1.56986	1.35 E 1	3.46 E-2
1.46843	1.85 E 4	6.1	1.57233	2.35 E 1	3.18 E-2
1.47059	1.59 E 4	5.3	1.57480	1.12 E 1	1.62 E-2
1.47275	1.36 E 4	4.6	1.57729	1.55 E 1	1.98 E-2
1.47493	1.17 E 4	4.	1.57978	5.99	1.57 E-2

TABLE 13. ABSORPTION COEFFICIENTS FOR WATER VAPOR (Continued)

λ (μ)	$S/2\pi\alpha'_0$	S/d	λ (μ)	$S/2\pi\alpha'_0$	S/d
1.58228	9.99	2.72 E-2	1.70358	1.2 E 3	1.9 E-2
1.58479	8.92	2.57 E-2	1.70648	7.8 E 3	2.2 E-2
1.58730	5.25	1.51 E-2	1.70940	8.8 E 3	2.5 E-2
1.58983	5.37	1.42 E-2	1.71233	9.2 E 3	3. E-2
1.59236	7.66	1.66 E-2	1.71527	9.3 E 3	3.5 E-2
1.59490	7.1	1.49 E-2	1.71821	9.2 E 3	4.1 E-2
1.59744	5.75	1.11 E-2	1.72117	9. E 3	4.7 E-2
1.60000	1.35 E 1	2.25 E-2	1.72414	7.2 E 3	5.4 E-2
1.60256	1.33 E 1	2.35 E-2	1.72712	5.8 E 3	6.3 E-2
1.60514	6.29	1.08 E-2	1.73010	4.8 E 3	7.2 E-2
1.60772	4.66	7.5 E-1	1.73310	4. E 3	8.2 E-2
1.61031	6.57	1.08 E-2	1.73611	3.2 E 3	9.5 E-2
1.61290	6.47	9.75 E-1	1.73913	2.6 E 3	1.1 E-1
1.61551	5.28	7.64 E-1	1.74216	2.4 E 3	1.3 E-1
1.61812	4.24	6.18 E-1	1.74520	2. E 3	1.5 E-1
1.62075	4.41	6.44 E-1	1.74825	1.78 E 3	1.7 E-1
1.62338	1.72 E 1	1.88 E-2	1.75131	1.5 E 3	1.9 E-1
1.62602	2.25 E 1	1.92 E-2	1.75439	1.5 E 3	2.2 E-1
1.62866	1.56 E 1	1.2 E-2	1.75747	1.5 E 3	2.5 E-1
1.63132	5.45	5.08 E-1	1.76056	1.5 E 3	2.9 E-1
1.63399	4.41	3.95 E-1	1.76367	1.46 E 3	3.4 E-1
1.63666	3.97	3.89 E-1	1.76678	1.42 E 3	3.7 E-1
1.63934	4.44	4.31 E-1	1.76991	1.36 E 3	4.8 E-1
1.64204	1.84 E 1	1.43 E-2	1.77305	1.35 E 3	5. E-1
1.64474	2.42 E 1	1.41 E-2	1.77620	1.32 E 3	5.8 E-1
1.64745	3.11	2.35 E-1	1.77936	1.3 E 3	6.7 E-1
1.65017	3.67	2.98 E-1	1.78253	1.3 E 3	8. E-1
1.65289	1.29 E 1	1.07 E-2	1.78571	1.35 E 3	9.3 E-1
1.65563	1.82 E 1	1.3 E-2	1.78891	1.45 E 3	1.1
1.65837	2.9 E 1	2.4 E-2	1.79211	1.6 E 3	1.2
1.66113	3.02 E 1	2.13 E-2	1.79533	1.7 E 3	1.4
1.66389	1.11 E 1	6.88 E-1	1.79856	2. E 3	1.7
1.66667	3.	2.53 E-1	1.80180	2.5 E 3	2.1
1.66945	4.19	3.13 E-1	1.80505	3.1 E 3	2.6
1.67224	4.61	3.79 E-1	1.80832	3.8 E 3	3.2
1.67504	7.79	5.48 E-1	1.81159	4.9 E 3	4.2
1.67785	1.24 E 1	8.36 E-1	1.81488	6.1 E 3	5.6
1.68067	1.29 E 1	8.48 E-1	1.81818	9. E 3	7.
1.68350	1.06 E 1	7.87 E-1	1.82149	1.04 E 4	9.
1.68634	8.05	6.44 E-1	1.82482	2.1 E 4	1.2 E 1
1.68919	8.08	6.31 E-1	1.82815	3.3 E 4	1.6 E 1
1.69205	6.74	5.57 E-1	1.83150	4.3 E 4	2.3 E 1
1.69492	1.	1.2 E-1	1.83486	6.4 E 4	3.2 E 1
1.69779	4. E 1	1.4 E-2	1.83824	8.6 E 4	4.7 E 1
1.70068	2.2 E 2	1.6 E-2	1.84162	1.2 E 5	8.6 E 1

TABLE 13. ABSORPTION COEFFICIENTS FOR WATER VAPOR (Continued)

λ (μ)	$S/2\pi\alpha'_0$	S/d	λ (μ)	$S/2\pi\alpha'_0$	S/d
1.84502	1.8 E 5	1.6 E 2	2.01207	5. E 2	3.9 E-1
1.84843	2.5 E 5	2.8 E 2	2.01613	4.2 E 2	3.3 E-1
1.85185	3.3 E 5	2.5 E 2	2.02020	3. E 2	2.8 E-1
1.85529	4.5 E 5	2. E 2	2.02429	2.15 E 2	2.3 E-1
1.85874	6.5 E 5	1.7 E 2	2.02840	1.6 E 2	2.0 E-1
1.86220	8. E 5	1.3 E 2	2.03252	1.15 E 2	1.7 E-1
1.86567	9.2 E 5	1.1 E 2	2.03666	8.5 E 1	1.4 E-1
1.86916	1. E 6	1.2 E 2	2.04082	6.8 E 1	1.2 E-1
1.87266	1.08 E 6	1.4 E 2	2.04499	5.3 E 1	9.8 E-2
1.87617	1.15 E 6	1.8 E 2	2.04918	3.8 E 1	8. E-2
1.87970	1.16 E 6	2.2 E 2	2.05339	2.7 E 1	6.6 E-2
1.88324	1.16 E 6	2.3 E 2	2.05761	1.8 E 1	5.8 E-2
1.88679	1.12 E 6	2. E 2	2.06186	1.25 E 1	5.9 E-2
1.89036	1.05 E 6	1.7 E 2	2.06612	8.6	6.1 E-2
1.89394	9.2 E 5	1.1 E 2	2.07039	6.	6.5 E-2
1.89753	7.5 E 5	8. E 1	2.07469	4.	7. E-2
1.90114	4.9 E 5	7.5 E 1	2.07900	2.8	7.2 E-2
1.90476	3.65 E 5	7.9 E 1	2.083333	1.9	6.6 E-2
1.90840	3.15 E 5	1.1 E 2	2.08768	1.3	5.2 E-2
1.91205	2.7 E 5	1.3 E 2	2.09205	9. E-1	3.7 E-2
1.91571	2.55 E 5	1.5 E 2	2.09644	6.5 E-1	2.6 E-2
1.91939	2.35 E 5	1.65 E 2	2.10084	4.5 E-1	1.7 E-2
1.92308	2.24 E 5	1.75 E 2	2.10526	3.2 E-1	1.08 E-2
1.92676	2.2 E 5	1.75 E 2	2.10970	1.0 E-3	1.0 E-5
1.93050	2.1 E 5	1.9 E 2	2.11416	1.0 E-3	1.0 E-5
1.93424	2. E 5	1.9 E 2	2.11864	1.0 E-3	1.0 E-5
1.93798	1.83 E 5	1.9 E 2	2.12314	1.0 E-3	1.0 E-5
1.94175	1.7 E 5	1.6 E 2	2.12766	5.7 E 1	3.43 E-2
1.94553	1.45 E 5	1.1 E 2	2.13220	1.07 E 1	1.03 E-2
1.94932	1.24 E 5	8. E 1	2.13675	1.47 E 1	1.23 E-2
1.95313	1.02 E 5	5.8 E 1	2.14133	4.49 E 2	1.24 E-1
1.95695	8.6 E 4	4. E 1	2.14592	5.54 E 2	1.59 E-1
1.96078	6.6 E 4	2.8 E 1	2.15054	1.09 E 2	4.33 E-2
1.96464	4.5 E 4	2.1 E 1	2.15517	1.48 E 1	1.24 E-2
1.96850	2.8 E 4	1.2 E 1	2.15983	2.04 E 1	1.58 E-2
1.97239	1.8 E 4	7.5	2.16450	1.36 E 1	1.14 E-2
1.97628	1.07 E 4	5.2	2.16920	4.32 E 4	9.7 E-1
1.98020	6.7 E 3	3.5	2.17391	2.91 E 2	7.42 E-2
1.98413	4. E 3	2.4	2.17865	6.34	6. E-1
1.98807	2.6 E 3	1.6	2.18341	6.55	6.59 E-1
1.99203	1.6 E 3	1.2	2.18818	1.36 E 2	6.2 E-2
1.99601	1.1 E 3	9.5 E-1	2.19298	1.31 E 2	6.96 E-2
2.00000	9.2 E 2	7.5 E-1	2.19780	1.27 E 2	9.07 E-2
2.00401	7.6 E 2	6. E-1	2.20264	1.76 E 2	1.64 E-1
2.00803	6.2 E 2	4.6 E-1	2.20751	2.62 E 2	1.3 E-1

TABLE 13. ABSORPTION COEFFICIENTS FOR WATER VAPOR (Continued)

$\frac{\lambda}{(\mu)}$	$S/2\pi\alpha'_0$	S/d	$\frac{\lambda}{(\mu)}$	$S/2\pi\alpha'_0$	S/d
2.21239	1.67 E 2	1.66 E-1	2.45700	4.39 E 2	6.46 E-1
2.21729	1.51 E 2	1.26 E-1	2.46305	4.85 E 2	7.49 E-1
2.22222	2.64 E 2	1.74 E-1	2.4697	5.11 E 4	4.38
2.22717	3.78 E 2	2.48 E-1	2.4749	2.32 E 4	2.53
2.23214	2.76 E 2	1.98 E-1	2.4802	2.11 E 4	6.65
2.23714	3.06 E 2	2.6 E-1	2.4832	3.92 E 4	5.28
2.24215	6. E 2	4.14 E-1	2.4876	3.14 E 4	8.83
2.24719	5.05 E 2	3.97 E-1	2.4938	2.15 E 4	1. E 1
2.25225	4.15 E 2	3.11 E-1	2.5013	1.67 E 4	9.86
2.25734	4.43 E 2	3.18 E-1	2.5050	5.09 E 4	1.03 E 1
2.26244	2.55 E 2	2.05 E-1	2.5088	3.63 E 4	1.59 E 1
2.26757	1.52 E 2	1.38 E-1	2.5113	3.07 E 4	1.39 E 1
2.27273	1.61 E 2	1.45 E-1	2.5189	2.48 E 4	2.6 E 1
2.27790	1.62 E 2	1.37 E-1	2.5240	1.73 E 5	3.45 E 1
2.28311	1.32 E 2	1.15 E-1	2.5284	9.29 E 4	5.16 E 1
2.28833	1.06 E 2	9.35 E-2	2.5361	1.15 E 5	9.2 E 1
2.29358	8.66 E 1	7.76 E-2	2.5394	1.03 E 5	7.22 E 1
2.29885	8.62 E 1	7.1 E-2	2.5445	1.52 E 5	1.44 E 2
2.30415	9.43 E 1	6.82 E-2	2.5497	5.65 E 5	9.06 E 1
2.30947	6.94 E 1	6.75 E-2	2.5562	2.7 E 5	1.12 E 2
2.31481	6.5 E 1	5.83 E-2	2.5628	6.69 E 6	1.41 E 3
2.32019	6.45 E 1	5.55 E-2	2.5661	8.5 E 5	4.57 E 2
2.32558	6.29 E 1	5.41 E-2	2.5707	1.31 E 5	2.59 E 2
2.33100	6.79 E 1	5.65 E-2	2.5773	1.15 E 5	2.32 E 2
2.33645	6.8 E 1	5.66 E-2	2.5840	1.3 E 6	8.13 E 2
2.34192	8.21 E 1	7.93 E-2	2.5893	7.88 E 5	5.98 E 2
2.34742	7.88 E 1	7.98 E-2	2.5920	1.31 E 6	1.02 E 3
2.35294	8.24 E 1	8.39 E-2	2.5974	1.31 E 5	2.88 E 2
2.35849	8.84 E 1	8.62 E-2	2.6021	2.02 E 5	4.95 E 2
2.36407	8.67 E 1	9.31 E-2	2.6089	1.27 E 5	2.94 E 2
2.36967	9.27 E 1	9.89 E-2	2.6144	1.36 E 5	4.07 E 2
2.37530	9.91 E 1	1.04 E-1	2.6219	1.74 E 5	2.51 E 2
2.38095	9.92 E 1	1.09 E-1	2.6288	6.22 E 4	2.38 E 2
2.38663	1.03 E 2	1.15 E-1	2.6337	4.9 E 4	9.65 E 1
2.39234	1.05 E 2	1.21 E-1	2.6399	5.67 E 4	1.26 E 2
2.39808	1.05 E 2	1.25 E-1	2.6434	7.03 E 4	1.13 E 2
2.40385	5.26 E 1	9.58 E-2	2.6504	7.88 E 4	1.93 E 2
2.40964	9.79 E 1	1.37 E-1	2.6674	1.53 E 5	6.18 E 2
2.41546	1.03 E 2	1.5 E-1	2.6724	1.19 E 5	4.89 E 2
2.42131	9.81 E 1	1.62 E-1	2.6738	1.85 E 5	6.09 E 2
2.42718	1.06 E 2	1.83 E-1	2.6802	8.04 E 4	3.05 E 2
2.43309	1.32 E 2	2.18 E-1	2.6831	8.64 E 4	3.09 E 2
2.43902	1.69 E 2	2.49 E-1	2.6882	7.07 E 4	2.15 E 2
2.44499	1.76 E 2	2.91 E-1	2.6911	7.98 E 4	2.59 E 2
2.45098	2.49 E 2	3.97 E-1	2.6940	8.88 E 4	3.07 E 2

TABLE 13. ABSORPTION COEFFICIENTS FOR WATER VAPOR (Continued)

λ (μ)	$S/2\pi\alpha'_0$	S/d	λ (μ)	$S/2\pi\alpha'_0$	S/d
2.6969	4.34 E 4	1.47 E 2	2.9507	5.43 E 4	1.21 E 1
2.7027	4.83 E 4	1.31 E 2	2.9551	1.72 E 4	1.18 E 1
2.7086	3.05 E 4	2.49 E 2	2.9612	2.47 E 3	2.32
2.7137	1.2 E 5	2.13 E 2	2.9718	1.24 E 4	1.57 E 1
2.7211	3.09 E 5	5.79 E 2	2.9782	2.13 E 4	1.3 E 1
2.7322	7.18 E 4	1.24 E 2	2.9895	6.27 E 3	2.05
2.7397	2.02 E 5	4.95 E 2	2.9940	1.63 E 4	8.18
2.7473	6.15 E 4	1.39 E 2	3.0030	3. E 4	6.85
2.7548	6.89 E 4	2.78 E 2	3.0075	8.37 E 4	8.01
2.7579	1.1 E 5	2.72 E 2	3.0139	1.5 E 4	4.74
2.7609	1.52 E 5	2.86 E 2	3.0211	9.92 E 3	1.12 E 1
2.7663	6.69 E 4	2.94 E 2	3.0248	5.22 E 4	7.72
2.7685	6.64 E 4	2.5 E 2	3.0303	1.49 E 4	8.14
2.7739	6.46 E 4	1.71 E 2	3.0358	8.65 E 3	9.81
2.7778	7.2 E 4	1.9 E 2	3.0395	2.45 E 4	8.43
2.7801	7.63 E 4	1.8 E 2	3.0441	2.39 E 4	1.01 E 1
2.7855	8.46 E 4	2.3 E 2	3.0488	1.77 E 4	1.67 E 1
2.7917	6.27 E 4	1.15 E 2	3.0534	3.21 E 4	7.6
2.7941	4.97 E 4	8.74 E 1	3.0600	1.94 E 4	8.28
2.8027	1.32 E 5	2.55 E 2	3.0675	1.19 E 4	9.68
2.8129	1.15 E 5	1. E 2	3.0722	4.48 E 4	7.19
2.8153	9.17 E 4	1.05 E 2	3.0779	2.19 E 4	1.28 E 1
2.8177	9.23 E 4	1.36 E 2	3.0386	1.05 E 4	7.03
2.8241	1.3 E 5	8.17 E 1	3.0883	7.01 E 3	8.86
2.8281	9.38 E 4	6.12 E 1	3.0941	3.13 E 4	8.63
2.8345	6. E 4	1.07 E 2	3.0989	4.9 E 3	6.25
2.8433	6.24 E 4	3.74 E 1	3.1075	1.66 E 4	9.86
2.8514	5.74 E 4	6. E 1	3.1162	1.15 E 5	6.43
2.8555	6.88 E 4	8.03 E 1	3.1211	1.44 E 4	9.78
2.8620	3.49 E 4	3.87 E 1	3.125	9.55 E 3	8.12
2.8686	5.2 E 4	2.83 E 2	3.1299	2.48 E 3	2.2
2.8752	1.8 E 4	1.5 E 1	3.1348	1.47 E 3	1.42
2.8777	1.6 E 4	1.49 E 1	3.1397	9.38 E 3	7.67
2.8810	1.78 E 4	1.5 E 1	3.1447	7.25 E 3	7.1
2.8860	7.93 E 3	1.54 E 1	3.1496	3.54 E 3	4.28
2.8944	8.93 E 3	5.91	3.1546	8.14 E 2	9.24 E-1
2.9028	5.7 E 4	3.89 E 1	3.1596	2.3 E 2	4.57 E-1
2.9104	1.13 E 4	8.03	3.1646	1.26 E 2	2.7 E-1
2.9146	1.07 E 4	8.73	3.1696	1.02 E 2	2.29 E-1
2.9163	1.55 E 4	8.16	3.1746	3.3 E 2	4.26 E-1
2.9240	2.48 E 4	2.6 E 1	3.1797	1.31 E 3	1.30
2.9308	4.92 E 3	4.14	3.1847	1.28 E 3	1.56
2.9326	9.71 E 3	3.81	3.1898	8.01 E 3	7.34
2.9412	6.61 E 3	7.17	3.1949	1.38 E 4	1.13 E 1
2.9481	3.02 E 4	1.56 E 1	3.2	7.69 E 3	1.1 E 1

TABLE 13. ABSORPTION COEFFICIENTS FOR WATFR VAPOR (Continued)

λ (μ)	$S/2\pi\alpha'_0$	S/d	λ (μ)	$S/2\pi\alpha'_0$	S/d
3.2051	8.07 E 3	1. E 1	3.4542	9.16 E 1	1.72 E-1
3.2103	1.1 E 4	1.29 E 1	3.4602	5.26 E 1	1.13 E-1
3.2154	1. E 4	1.11 E 1	3.4662	8.36 E 1	1.11 E-1
3.2206	1.07 E 4	1.29 E 1	3.4722	1.6 E 2	2.28 E-1
3.2258	7.96 E 3	1.45 E 1	3.4783	5.21 E 1	1.19 E-1
3.2310	6.42 E 3	1.11 E 1	3.4843	3.61 E 1	5.31 E-2
3.2362	5.26 E 2	8.78 E-1	3.4904	4.46 E 1	8.09 E-2
3.2415	8.41 E 3	4.87	3.4965	7.35 E 1	1.13 E-1
3.2468	1.4 E 4	1.02 E 1	3.5026	7.05 E 1	9.14 E-2
3.2520	5.07 E 2	6.47 E-1	3.5088	3.83 E 1	8.84 E-2
3.2573	9.14 E 3	4.35	3.5149	3.52 E 1	8.62 E-2
3.2626	4.61 E 4	1.5 E 1	3.5211	4.77 E 1	1.29 E-1
3.2680	4.67 E 3	3.33	3.5273	5.23 E 1	8.3 E-2
3.2733	4.15 E 2	6.4 E-1	3.5336	5.4 E 1	8.39 E-2
3.2787	1.07 E 3	1.21	3.5398	5.27 E 1	8.38 E-2
3.2840	5.82 E 2	6.47 E-1	3.5461	3.78 E 1	5.25 E-2
3.2895	3.61 E 3	1.94	3.5524	6.22 E 1	1.49 E-1
3.2949	1.59 E 4	1.48 E 1	3.5587	4.83 E 1	7.63 E-2
3.3003	8.88 E 3	8.47	3.5651	2.31 E 1	4.39 E-2
3.3058	4.64 E 3	5.16	3.5714	5.31 E 1	1.55 E-1
3.3113	4.09 E 3	3.83	3.5778	7.1 E 1	1.3 E-1
3.3167	3.86 E 3	2.01	3.5842	7.83 E 1	1.14 E-1
3.223	1.56 E 3	1.37	3.5907	1.27 E 2	1.9 E-1
3.3278	9.1 E 1	1.71 E-1	3.5971	3.7 E 1	3.28 E-2
3.3333	6.1 E 1	1.09 E-1	3.6036	4.6 E 1	4.26 E-2
3.3389	5.05 E 2	4.56 E-1	3.6101	4.67 E 1	7.68 E-2
3.3445	2.78 E 3	1.87	3.6166	2.62 E 1	3.83 E-2
3.3500	1.67 E 2	2.88 E-1	3.6232	4.36 E 1	3.47 E-2
3.3557	5 05 E 2	5.69 E-1	3.6298	5.41 E 1	5.92 E-2
3.3613	9.43 E 3	5.3	3.6364	4.06 E 1	4.99 E-2
3.367	1.15 E 3	1.12	3.6430	2.83 E 1	3.82 E-2
3.3727	1.09 E 3	1.13	3.6496	3.14 E 1	5.97 E-2
2.3784	1.31 E 2	2.02 E-1	3.6563	3.65 E 1	4.7 E-2
3.3841	1.22 E 3	8.97 E-1	3.6630	6.29 E 1	5.57 E-2
3.3898	2.22 E 3	1.79	3.6697	2.02 E 2	3.78 E-1
3.3956	2.15 E 3	1.73	3.6765	1.07 E 2	3.92 E-1
3.4014	1.64 E 2	2.48 E-1	3.6832	4.18 E 1	1.42 E-1
3.4072	1.03 E 2	1.68 E-1	3.69	2.24 E 1	8.36 E-2
3.4130	1.05 E 3	8.31 E-1	3.6969	1.73 E 1	5.33 E-2
3.4188	8.84 E 1	7.17 E-1	3.7037	2.59 E 1	3.54 E-2
3.4247	2.d E 2	3.32 E-1	3.7106	4.03 E 1	5.58 E-2
3.4305	1.33 E 2	2.03 E-1	3.7175	3.11 E 1	3.53 E-2
3.4364	1.98 E 2	3.06 E-1	3.7244	3.74 E 1	2.32 E-2
3.4423	5.51 E 2	5.29 E-1	3.7314	5.99 E 1	6.8 E-2
3.4483	1.59 E 2	2.09 E-1	3.7383	4.26 E 1	5.1 E-2

TABLE 13. ABSORPTION COEFFICIENTS FOR WATER VAPOR (Continued)

λ (μ)	$S/2\pi\alpha'_0$	S/d	λ (μ)	$S/2\pi\alpha'_0$	S/d
3.7453	1.23 E 2	5.89 E-2	4.089	3.91 E 1	2.2 E-2
3.7523	5.76 E 1	6.22 E-2	4.098	3.88 E 1	2.81 E-2
3.7594	4.92 E 1	5.88 E-2	4.107	7.32 E 1	4.97 E-2
3.7665	3.89 E 1	2.32 E-2	4.115	1.86 E 2	9.7 E-2
3.7736	4.39 E 1	4.42 E-2	4.124	3.87 E 1	2.49 E-2
3.7807	5.25 E 1	7.12 E-2	4.132	4.16 E 1	2.34 E-2
3.7879	5.42 E 1	2.71 E-2	4.141	4.77 E 1	3.19 E-2
3.7951	2.65 E 1	2.29 E-2	4.149	3.87 E 1	2.74 E-2
3.8023	4.74 E 1	5.94 E-2	4.158	3.77 E 1	2.38 E-2
3.8095	4.13 E 1	4.12 E-2	4.167	4.81 E 1	2.56 E-2
3.8168	2.76 E 1	2.19 E-2	4.175	5.82 E 1	3.55 E-2
3.8241	3.41 E 1	3.48 E-2	4.184	6.11 E 1	4.99 E-2
3.8314	3.55 E 1	4.78 E-2	4.193	3.91 E 1	2.75 E-2
3.8388	2.97 E 1	2.03 E-2	4.202	3.57 E 1	2.8 E-2
3.8462	2.98 E 1	2.07 E-2	4.211	4.05 E 1	2.53 E-2
3.8536	3. E 1	3.79 E-2	4.219	6.97 E 1	5.36 E-2
3.861	2.92 E 1	2.9 E-2	4.228	2.07 E 2	1.17 E-1
3.8685	3. E 1	1.94 E-2	4.237	3.7 E 1	3.43 E-2
3.876	3.28 E 1	2.38 E-2	4.246	3.86 E 1	3.36 E-2
3.8835	2.62 E 1	3.18 E-2	4.255	3.36 E 1	2.98 E-2
3.8911	3.35 E 1	2.4 E-2	4.264	3.49 E 1	3.19 E-2
3.8986	4.07 E 1	1.94 E-2	4.274	4.37 E 1	4.5 E-2
3.9063	2.83 E 1	2.22 E-2	4.283	6.33 E 1	5.22 E-2
3.9139	2.45 E 1	2.27 E-2	4.292	3.74 E 1	4.22 E-2
3.9216	3.51 E 1	2.7 E-2	4.301	4.03 E 1	4.02 E-2
3.9293	5.5 E 1	1.99 E-2	4.310	4.42 E 1	4.07 E-2
3.937	2.77 E 1	2.12 E-2	4.319	4.34 E 1	4.32 E-2
3.9448	3.18 E 1	2.01 E-2	4.329	3.21 E 1	3.46 E-2
3.9526	5.29 E 1	2.23 E-2	4.338	4.65 E 1	5.46 E-2
3.9604	3.4 E 1	1.96 E-2	4.348	6.02 E 1	5.86 E-2
3.9683	3.42 E 1	2.12 E-2	4.357	6.17 E 1	6.86 E-2
3.9761	3.87 E 1	1.94 E-2	4.367	3.55 E 1	4.5 E-2
3.9841	5.75 E 1	2.34 E-2	4.376	4.6 E 1	5.59 E-2
3.9920	3.87 E 1	2.18 E-2	4.386	7.55 E 1	8.2 E-2
4.	3.93 E 1	2.44 E-2	4.396	5.73 E 1	6.84 E-2
4.008	4.2 E 1	2.11 E-2	4.405	6.28 E 1	7.62 E-2
4.016	4.12 E 1	2. E-2	4.415	4.62 E 1	4.26 E-2
4.024	4.16 E 1	2.09 E-2	4.425	6.99 E 1	7.47 E-2
4.032	6.32 E 1	3.4 E-2	4.435	8.3 E 1	9.94 E-2
4.04	4.68 E 1	2.57 E-2	4.444	9.09 E 1	1.18 E-1
4.049	4.19 E 1	2.15 E-2	4.454	5.28 E 1	6.32 E-2
4.057	4.09 E 1	2.26 E-2	4.464	7.87 E 1	9.36 E-2
4.065	4. E 1	2.2 E-2	4.474	2.12 E 2	2.49 E-1
4.073	7.81 E 1	4.97 E-2	4.484	2.34 E 2	2.87 E-1
4.082	5.28 E 1	3.28 E-2	4.494	1.25 E 2	1.49 E-1

TABLE 13. ABSORPTION COEFFICIENTS FOR WATER VAPOR (Continued)

λ (μ)	$S/2\pi\alpha'_0$	S/d	λ (μ)	$S/2\pi\alpha'_0$	S/d
4.505	4.61 E 1	5.97 E-2	4.773	1.93 E 3	2.02
4.515	2.09 E 2	2.14 E-1	4.785	6.76 E 3	7.08
4.525	4.59 E 2	7.31 E-1	4.796	6.42 E 2	1.08
4.535	5.96 E 2	6.87 E-1	4.808	5.93 E 2	7.69 E-1
4.545	1.15 E 2	1.48 E-1	4.819	1.34 E 3	1.33
4.556	1.1 E 2	1.16 E-1	4.831	7.02 E 2	1.16
4.566	3.44 E 2	2.9 E-1	4.843	4.39 E 4	2.62 E 1
4.576	6.5 E 2	7.31 E-1	4.854	1.35 E 4	7.99
4.567	2. E 2	1.86 E-1	4.866	6.61 E 1	2.22 E-1
4.598	1.15 E 2	1.16 E-1	4.878	2.97 E 2	4.7 E-1
4.608	2.35 E 2	2.57 E-1	4.889	2.07 E 4	1.02 E 1
4.618	6.74 E 2	7.78 E-1	4.902	1.6 E 4	1.31 E 1
4.629	1.37 E 3	1.36	4.914	6.27 E 2	1.22
4.640	8.19 E 2	1.1	4.926	6.22 E 2	8.91 E-1
4.651	5.04 E 2	6.96 E-1	4.938	2.78 E 3	3.38
4.662	7.28 E 2	1.09	4.950	4.64 E 4	2.29 E 1
4.673	2.17 E 3	2.45	4.963	4.11 E 4	2.5 E 1
4.684	8.68 E 3	4.63	4.975	3.02 E 3	4.34
4.695	1.57 E 2	2.44 E-1	4.986	9.81 E 2	1.32
4.706	8.72 E 2	9.88 E-1	5.	2.02 E 3	2.55
4.717	4.19 E 2	5.92 E-1			
4.728	2.63 E 3	2.17			
4.739	8.01 E 2	1.17			
4.751	1.6 E 2	4.86 E-1			
4.762	5.17 E 2	6.38 E-1			

3.7.3. MINOR CONSTITUENTS (N_2O, CH_4, and CO). Oppel made empirical fits to the data of Burch [1] to develop transmissivity functions for N_2O, CH_4, and CO. The procedures involved in performing the empirical fits and calculating absorption are the same as used for H_2O and CO_2. The resulting frequency-dependent parameters are given in tables 14, 15, and 16.

For N_2O, absorption is given by the Elsasser model (eqs. 86-88) and the parameters are given for the spectral region from 4.367 to 4.739 μ.

For CH_4 and CO, absorption is defined by the statistical model (eqs. 89-91) and the parameters are defined from 3.0248 to 4.158 μ for CH_4 and from 4.405 to 5.0 μ for CO.

The foregoing methods for computing atmospheric slant-path absorption allows for the determination of spectra of extremely high resolution compared to the other methods discussed in this section. This primarily caused by the fact that Oppel's empirical fits were based on the most recent laboratory data and the empirical procedures were such that a smoothing process was not used and therefore the spectral character, observable in the laboratory data, was retained.

3.8. METHOD OF W. R. BRADFORD

Bradford [55] made an empirical fit of the Elsasser band-model equations to the laboratory data of Bradford, McCormick, and Selby [56] for the 4.3-μ CO_2 absorption band. Since the method employed by Bradford to determine the frequency-dependent parameters is analogous to that described in section 2.3 it will not be discussed in this section. The band-model equations and frequency-dependent parameters are exactly those used by Oppel; hence, absorption is given by

$$A = \sinh \beta \int_0^Y I_0(Y)(-Y \cosh \beta)\, dY \tag{92}$$

or the strong- or weak-line approximations, respectively,

$$A = \operatorname{erf}\left[\frac{1}{2}\frac{2\pi\alpha_0' S}{d^2} WP\right]^{1/2} \tag{93}$$

$$A = 1 - \exp(-S/dW) \tag{94}$$

The frequency-dependent parameters $2\pi\alpha_0/d$ and $S/2\pi\alpha_0$ are given in table 17 for the wavelength range from 4.184 to 4.454 μ with entries every 5 cm^{-1}. The resolution is on the order of 20 cm^{-1}. It is emphasized that the parameters $2\pi\alpha_0/d$ and $S/2\pi\alpha_0$ listed in the table are not

TABLE 14. ABSORPTION COEFFICIENTS FOR NITROUS OXIDE FOR THE 4.3-μ BAND

λ (μ)	S/d	$2\pi\alpha_0'$S/d
4.367	0.0	0.0
4.376	0.0495	2.48 E-6
4.386	0.123	8.62 E-6
4.396	0.390	4.75 E-5
4.405	0.726	
4.415	1.18	2.0 E-4
4.425	1.98	3.96 E-4
4.435	26.5	1.11 E-2
4.444	47.0	3.1 E-2
4.454	41.4	3.68 E-2
4.464	30.0	3.3 E-2
4.474	26.9	3.63 E-2
4.484	19.4	2.96 E-2
4.494	15.2	2.49 E-2
4.505	20.1	2.86 E-2
4.515	20.9	2.7 E-2
4.525	28.3	1.87 E-2
4.535	30.7	3.44 E-2
4.545	13.1	1.97 E-2
4.556	7.95	1.34 E-2
4.566	4.96	9.72 E-3
4.576	3.51	9.34 E-3
4.587	1.29	4.53 E-3
4.598	0.825	4.13 E-3
4.608	0.341	2.25 E-3
4.618	0.245	1.7 E-3
4.629	0.175	1.15 E-3
4.640	9.94 E-2	5.62 E-4
4.651	5.15 E-2	2.41 E-4
4.662	3.48 E-2	1.38 E-4
4.673	2.54 E-2	8.38 E-5
4.684	1.8 -2	4.21 E-5
4.695	8.6 E-3	2.42 E-5
4.706	3.3 E-3	2.48 E-5
4.717	2.2 E-3	1.08 E-5
4.728	5.7 E-3	1.48 E-5
4.739	0.0	0.0

TABLE 15. ABSORPTION COEFFICIENTS FOR METHANE

λ (μ)	$S/2\pi\alpha'_0$	S/d	λ (μ)	$S/2\pi\alpha'_0$	S/d	λ (μ)	$S/2\pi\alpha'_0$	S/d
3.0248	1. E-1	0.	3.2103	2.9 E 3	6.85 E-1	3.4014	6.8 E 2	3.4 E-1
3.0303	3. E-1	2. E-3	3.2154	2.98 E 3	7.2 E-1	3.4072	5.2 E 2	3. E-1
3.0358	5. E-1	4. E-3	3.2206	2.98 E 3	7.38 E-1	3.4130	3.1 E 2	1.7 E-1
3.0395	5. E-1	5. E-3	3.2258	2.89 E 3	7.5 E-1	3.4188	1.47 E 2	1.05 E-2
3.0441	1.	6. E-3	3.2310	2.78 E 3	7.59 E-1	3.4247	2.5 E 1	8.66 E-2
3.0488	5.	7. E-3	3.2362	2.78 E 3	7.68 E-1	3.4305	2. E 1	8.12 E-2
3.0534	1. E 1	8. E-3	3.2415	3.24 E 3	7.75 E-1	3.4364	1.8 E 1	7.63 E-2
3.0600	4. E 1	1. E-2	3.2468	3.6 E 3	7.8 E-1	3.4423	1.5 E 1	7.07 E-2
3.0675	7. E 1	1. E-2	3.2520	3.92 E 3	7.8 E-1	3.4483	1.3 E 1	6.52 E-2
3.0722	1.1 E 2	1.2 E-2	3.2573	3.26 E 3	7.55 E-1	3.4542	1.05 E 1	6.01 E-2
3.0779	1.3 E 2	1.3 E-2	3.2626	2.6 E 3	6.75 E-1	3.4802	9.	5.35 E-2
3.0836	1.5 E 2	1.4 E-2	3.2680	2.22 E 3	5.5 E-1	3.4662	7.3	4.25 E-2
3.0883	2. E 2	1.5 E-2	3.2733	1.8 E 3	4.4 E-1	3.4722	5.8	3.3 E-2
3.0941	2.5 E 2	1.5 E-2	3.2787	1.36 E 3	4.15 E-1	3.4783	4.85	3.59 E-2
3.0989	3.2 E 2	1.5 E-2	3.2840	7. E 2	4.05 E-1	3.4843	4.2	2.24 E-2
3.1075	3.7 E 2	1.6 E-2	3.2895	2.5 E 2	4.07 E-1	3.4904	3.75	2.06 E-2
3.1162	4. E 2	1.7 E-2	3.2949	4. E 2	5.75 E-1	3.4965	3.4	2. E-2
3.1211	3.7 E 2	1.8 E-2	3.3003	7. E 2	7.5 E-1	3.5026	3.3	2.02 E-2
3.125	3.2 E 2	2. E-2	3.3058	1.01 E 3	9.55 E-1	3.5088	3.5	2.16 E-2
3.1299	2.7 E 2	2.1 E-2	3.3113	7. E 2	9. E-1	3.5149	3.8	2.35 E-2
3.1348	2. E 2	2.3 E-2	3.3167	4.2 E 2	5. E-1	3.5211	4.3	2.56 E-2
3.1397	1. E 2	2.5 E-2	3.3223	2.2 E 2	3.25 E-1	3.5273	5.75	2.63 E-2
3.1447	5. E 1	2.6 E-2	3.3278	1. E 2	2.3 E-1	3.5336	6.9	2.65 E-2
3.1496	2. E 1	2.8 E-2	3.3333	4. E 2	3.25 E-1	3.5398	6.9	2.66 E-2
3.1546	2. E 1	3.4 E-2	3.3389	8.15 E 2	3.8 E-1	3.5461	6.45	2.63 E-2
3.1596	4. E 1	4.8 E-2	3.3445	6.8 E 2	4.01 E-1	3.5524	6.	2.6 E-2
3.1646	7. E 1	6.7 E-2	3.3500	8.35 E 2	4.1 E-1	3.5587	5.5	2.52 E-2
3.1696	1.25 E 2	9.1 E-2	3.3557	7.7 E 2	4.1 E-1	3.5651	5.15	2.36 E-2
3.1746	1.8 E 2	1.32 E-1	3.3613	7.15 E 2	4.05 E-1	3.5714	4.8	2.17 E-2
3.1797	1. E 3	2.5 E-1	3.367	6.5 E 2	4. E-1	3.5778	4.5	2. E-2
3.1847	1.75 E 3	3.45 E-1	3.3727	5.8 E 2	3.92 E-1	3.5842	4.25	1.83 E-2
3.1898	2.2 E 3	4.36 E-1	3.3784	5.4 E 2	3.83 E-1	3.5907	4.1	1.7 E-2
3.1949	2.45 E 3	5.27 E-1	3.3841	5.7 E 2	3.75 E-1	3.5971	4.18	1.57 E-2
3.2	2.64 E 3	5.9 E-1	3.3898	6.1 E 2	3.65 E-1	3.8036	4.35	1.49 E-2
3.2051	2.8 E 3	6.45 E-1	3.3956	8.65 E 2	3.55 E-1	3.6101	4.6	1.4 E-2

TABLE 15. ABSORPTION COEFFICIENTS FOR METHANE (Continued)

λ (μ)	$S/2\pi\alpha'_0$	S/d	λ (μ)	$S/2\pi\alpha'_0$	S/d	λ (μ)	$S/2\pi\alpha'_0$	S/d
3.6166	4.75	1.31 E-2	3.7879	3.6	5.55 E-3	3.9761	9.9 E-1	2.6 E-3
3.6232	4.8	1.18 E-2	3.7951	3.75	5.07 E-3	3.9841	9.4 E-1	2.53 E-3
3.6298	4.83	1.15 E-2	3.8023	3.55	4.93 E-3	3.9920	9. E-1	2.53 E-3
3.6364	4.8	1.09 E-2	3.8095	2.75	5.2 E-3	4.	8.5 E-1	2.56 E-3
2.6430	4.55	1.05 E-2	3.8168	2.34	5.55 E-3	4.008	8.1 E-1	2.68 E-3
3.6496	4.15	1. E-2	3.8241	1.80	5.98 E-3	4.016	7.7 E-1	2.77 E-3
3.6563	3.75	9.5 E-3	3.8314	1.77	5.85 E-3	4.024	7.3 E-1	2.55 E-3
3.6630	3.5	9. E-3	3.8388	1.74	5.45 E-3	4.032	6.8 E-1	2.17 E-3
3.6697	3.38	8.8 E-3	3.8462	1.89	5.01 E-3	4.04	8.4 E-1	2.23 E-3
3.6765	3.43	8.7 E-3	3.8536	1.65	4.62 E-3	4.049	6. E-1	2.35 E-3
3.6832	3.55	8.7 E-3	3.861	1.6	4.57 E-3	4.057	5.5 E-1	2.5 E-3
3.69	3.67	9. E-3	3.8685	1.56	4.75 E-3	4.065	5. E-1	2.53 E-3
3.6969	3.8	9.2 E-3	3.876	1.52	4.88 E-3	4.073	4.6 E-1	2.3 E-3
3.7037	3.8	8.88 E-3	3.8835	1.48	4.75 E-3	4.082	4.2 E-1	2.05 E-3
3.7106	3.75	8.45 E-3	3.8911	1.44	4.5 E-3	4.089	3.8 E-1	1.9 E-3
3.7175	3.7	8. E-3	3.8986	1.4	4.27 E-3	4.098	3.5 E-1	1.65 E-3
3.7244	3.45	7.45 E-3	3.9083	1.35	4. E-3	4.107	3. E-1	1.45 E-3
3.7314	3.25	6.85 E-3	3.9139	1.32	3.75 E-3	4.115	2.5 E-1	1.25 E-3
3.7383	2.85	6.75 E-3	3.9216	1.28	3.56 E-3	4.124	2. E-1	1. E-3
3.7453	2.7	6.86 E-3	3.9293	1.24	3.37 E-3	4.132	1.7 E-1	7.5 E-4
3.7523	2.55	6.99 E-3	3.937	1.2	3.2 E-3	4.141	1.5 E-1	5.5 E-4
3.7594	2.4	7.1 E-3	3.9448	1.15	3.05 E-3	4.149	1. E-1	3.5 E-4
3.7665	2.65	6.95 E-3	3.9526	1.1	2.92 E-3	4.158	5. E-2	1.5 E-4
3.7736	3.1	6.6 E-3	3.9604	1.06	2.8 E-3			
3.7807	3.4	6.07 E-3	3.9683	1.03	2.7 E-3			

TABLE 16. ABSORPTION COEFFICIENT FOR CARBON MONOXIDE

$\frac{\lambda}{(\mu)}$	$S/2\pi\alpha'_0$	S/d	$\frac{\lambda}{(\mu)}$	$S/2\pi\alpha'_0$	S/d
4.405	1. E 1	1. E-2	4.717	1.01 E 4	2.45
4.415	2. E 1	2. E-2	4.728	1.07 E 4	2.53
4.425	4. E 1	4. E-2	4.739	1.05 E 4	2.4
4.435	6. E 1	6. E-2	4.751	1. E 4	2.2
4.444	8. E 1	9. E-2	4.762	9.35 E 3	2.
4.454	1. E 2	1.2 E-1	4.773	8. E 3	1.66
4.464	1.2 E 2	1.6 E-1	4.785	6.5 E 3	1.37
4.474	1.4 E 2	2.2 E-1	4.796	5.1 E 3	1.12
4.484	2. E 2	2.7 E-1	4.808	4. E 3	8.8 E-1
4.494	3.6 E 2	3.3 E-1	4.819	2.9 E 3	7.1 E-1
4.505	8. E 2	4. E-1	4.831	2.3 E 3	5.3 E-1
4.515	2.1 E 3	5.5 E-1	4.843	1.6 E 3	3.7 E-1
4.525	4.8 E 3	7.3 E-1	4.854	1.3 E 3	2.7 E-1
4.535	6.4 E 3	1.1	4.866	8.4 E 2	2.2 E-1
4.545	8.4 E 3	1.5	4.878	5.7 E 2	1.6 E-1
4.556	9.5 E 3	2.1	4.889	3.3 E 2	1.1 E-1
4.566	1.05 E 4	2.63	4.902	2. E 2	7. E-2
4.576	1.15 E 4	3.	4.914	1.62 E 2	5. E-2
4.587	1.26 E 4	3.26	4.926	1.49 E 2	4.5 E-2
4.598	1.36 E 4	3.4	4.938	1.38 E 2	4. E-2
4.608	1.4 E 4	3.45	4.950	1.3 E 2	3.5 E-2
4.618	1.3 E 4	3.36	4.963	1.23 E 2	3. E-2
4.629	1.07 E 4	3.03	4.975	1.17 E 2	3. E-2
4.640	8.3 E 3	2.26	4.986	1.12 E 2	2.5 E-2
4.651	5.8 E 3	1.53	5.	1.09 E 2	2. E-2
4.662	4.3 E 3	9.7 E-1			
4.673	3.6 E 3	1.25			
4.684	4.8 E 3	1.52			
4.695	6.35 E 3	1.63			
4.706	8.30 E 3	2.14			

TABLE 17. BAND PARAMETERS FOR CARBON DIOXIDE FOR THE 4.3-μ BAND

$\frac{\lambda}{(\mu)}$	$\nu/(cm^{-1})$	$2\pi a_0/d$	$S/2\pi a_0$	$2\pi a_0' S/d^2$
4.184	2390	1.380	0.072	1.804 E-4
4.193	2385	0.560	1.750	7.221 E-4
4.202	2380	0.580	8.700	3.851 E-3
4.211	2375	0.610	24.0	1.175 E-2
4.219	2370	0.880	31.0	3.159 E-2
4.228	2365	1.140	29.5	5.045 E-2
4.237	2360	1.180	28.5	5.222 E-2
4.246	2355	1.220	21.0	4.113 E-2
4.255	2350	1.280	10.5	2.263 E-2
4.264	2345	1.200	19.3	3.657 E-2
4.274	2340	1.080	24.0	3.683 E-2
4.283	2335	1.030	24.0	3.350 E-2
4.292	2330	0.920	22.5	2.508 E-2
4.301	2325	1.110	15.3	2.436 E-2
4.310	2320	0.960	12.7	1.540 E-2
4.319	2315	1.000	7.30	9.605 E-3
4.329	2310	1.000	5.00	6.579 E-3
4.338	2305	1.100	2.65	4.220 E-3
4.348	2300	1.020	1.98	2.710 E-3
4.357	2295	1.100	1.18	1.879 E-3
4.367	2290	0.980	0.70	8.846 E-4
4.376	2285	0.990	0.38	4.900 E-4
4.386	2280	0.630	0.73	3.812 E-4
4.396	2275	0.420	1.45	3.366 E-4
4.405	2270	0.380	1.55	2.945 E-4
4.415	2265	0.330	1.70	2.436 E-4
4.425	2260	0.365	1.05	1.840 E-4
4.435	2255	0.520	0.48	1.710 E-4
4.444	2250	0.700	0.265	1.710 E-4
4.454	2245	0.770	0.112	8.737 E-5

values per unit pressure; hence, the prime (') has been deleted from the half-width term, α_0. To obtain the necessary parameters for equation 92 simply divide by sea-level pressure P_0.

For the spectral region from 4.184 to 4.454 μ, the methods of Oppel and Bradford are basically the same. The same equations were used and the parameters are defined for exactly the same wavelengths. The values are slightly different for the two authors, however, which undoubtedly resulted from the fact that different collections of laboratory data were used in performing the empirical fits.

3.9. METHOD OF A. E. S. GREEN, C. S. LINDENMEYER, AND M. GRIGGS

A. E. S. Green, C. S. Lindenmeyer, and M. Griggs have pursued the problem of developing methods for calculating atmospheric molecular absorption. The results of their efforts are published in three reports [57-59].

Basically their work consisted of empirically fitting the strong-line approximation to the statistical model to laboratory homogeneous absorption spectra in order to obtain transmissivity functions which define the spectral absorption for the atmospheric gases, H_2O, CO_2, O_3, N_2O, CO, and CH_4. The transmissivity functions are given as functions of the equivalent sea-level path, W^*, and two wavelength-dependent parameters W_e and η. Specifically,

$$T = \exp - \left(\frac{W^*}{W_e}\right)^{\eta} \tag{95}$$

where W_e is the quantity of absorber at 740 mm Hg and 300°K corresponding to a transmission of $T = e^{-1}$. This function defines the transmission for all six absorbing species.

The method employed by Green et al. [57] to determine the frequency-dependent parameters W_e and η was as follows. Consider a sample of laboratory data taken from the work of Burch shown in Figure 39. Each curve represents the absorption as a function of wavelength for a homogeneous path at 300°K for some absorber concentration W and some equivalent pressure P_e. Each value of W is reduced to an absorber concentration at standard pressure W^* by the expression

$$W^* = W\frac{P_e}{P_0}$$

For each wavelength throughout the interval the curves define several values of transmission $T_1, T_2, \ldots, T_n$, each corresponding to a value of W^*. These transmission data were plotted using graph paper in which the ordinate was ℓn (-ℓn T) and the abscissa was ℓn W^*. The re-

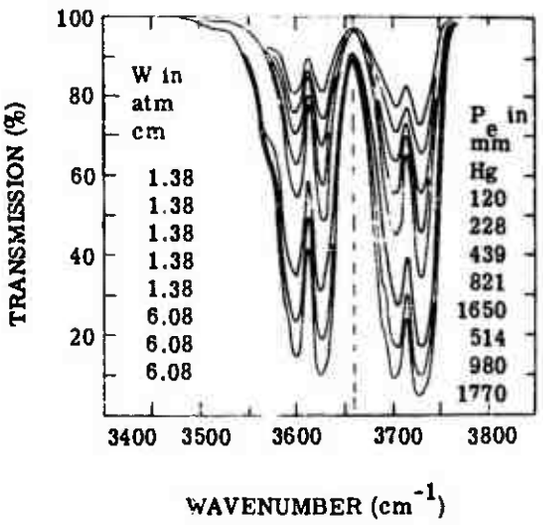

FIGURE 39. TRANSMISSION VS. WAVENUMBER FOR 2.7-μ CARBON DIOXIDE BAND

sulting data points define a straight line whose slope is η and abscissa intercept is W_e. Five such curves are shown in figure 40. The case illustrated is for the 2.7-μ CO_2 band. Each line defines W_e and η for one wavelength. This process was repeated at approximately every 0.01 μ throughout the absorption band to obtain a plot of W_e versus wavelength.

This procedure was repeated for each absorption band and each absorbing gas for the wavelength region from 1.0 to 10.0 μ. The values of W_e and η at 740 mm Hg and 300°K are given in figure 41. The values of W_e for the same pressure and temperature are also given in table 18. Table 19 is a listing of the laboratory data which were used for the various gases and absorption bands to determine the values of W_e and η.

To apply the method of Green et al. [57], one need simply determine, for a given slant path, the value of W^* for each absorbing gas as outlined in section 2.4.3. The values of transmission can then be computed for each gas using equation 95 and the values of W_e and η. The final value of transmission for a given wavelength would then be the product of the transmission of each of the absorbing gases.

Noting figure 41, one may observe that the curves of W_e versus wavelength are presented on a very compressed scale, limiting the accuracy with which one can determine the value of wavelength which corresponds to a given value of W_e. The data given in table 18 were compiled from these curves; hence the above inaccuracies are inherent in these data also.

In an effort to increase the accuracy of the original work of Green et al. [57], J. A. Rowe [60] of the Aerospace Corporation replotted the original data of W_e versus wavelength on a highly expanded scale. Some adjustments in the W_e values were made based on other sources of absorption spectra than those given in table 19. The exact sources of data used by Rowe and the specific reasons for modifying the results of the initial empirical fit made by Green et al. are not known at the present time. Rowe's modifications of Greens original work will be given in an Aerospace report which is to be published in the near future.

3.10. METHOD OF R. O. CARPENTER

R. O. Carpenter [61] developed a method for calculating the emission from CO_2 at elevated temperature for the 4.3-μ absorption band. His method is based on the Elsasser band model, but the frequency-dependent parameters were calculated from theory rather than being determined from laboratory data using empirical procedures. Even though Carpenter's method was developed for predicting high-temperature CO_2 emission, it is directly applicable to atmospheric slant-path problems.

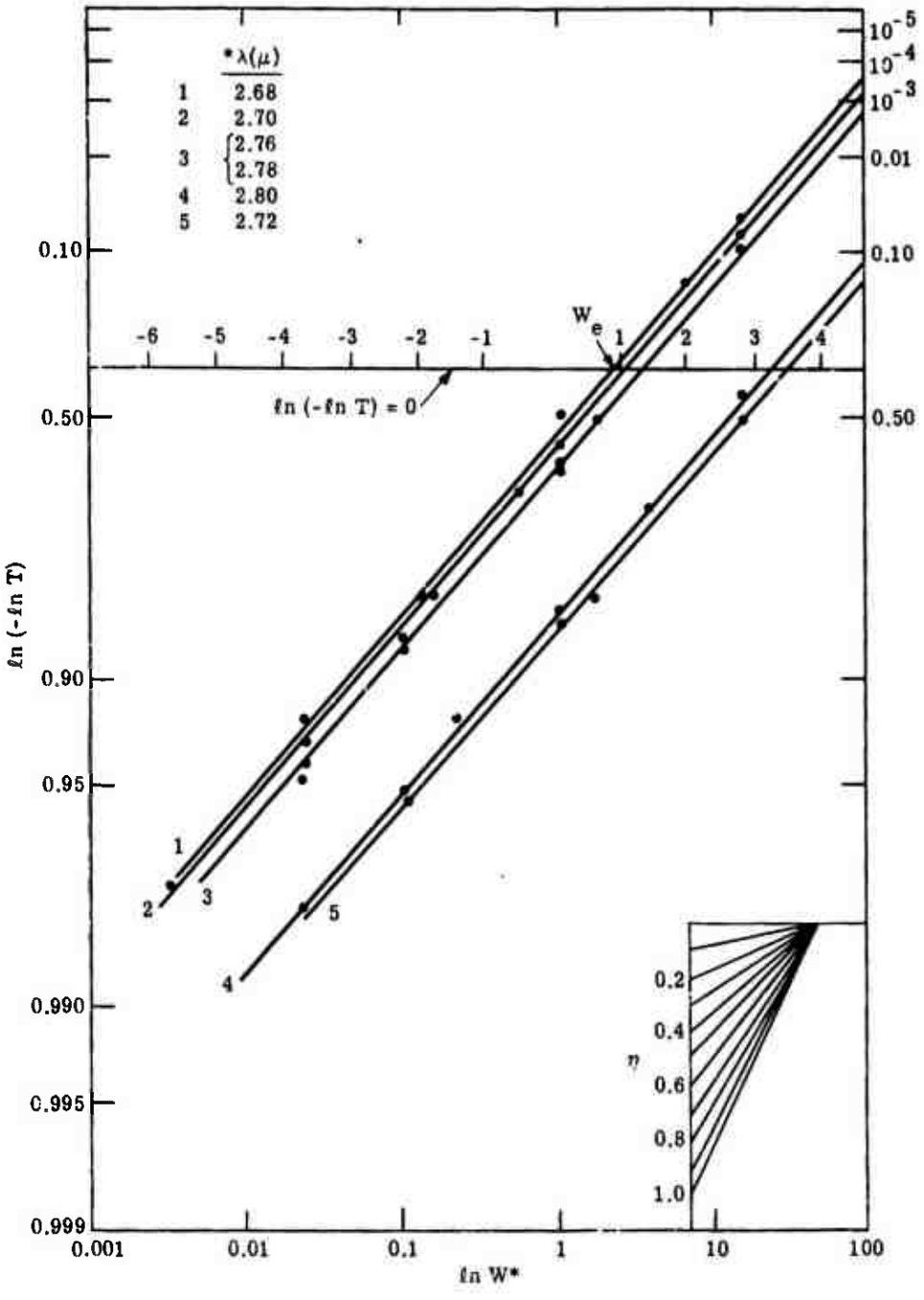

FIGURE 40. PROCEDURE FOR DETERMINING W_e AND η. The case illustrated is for the 2.7-μ carbon dioxide band.

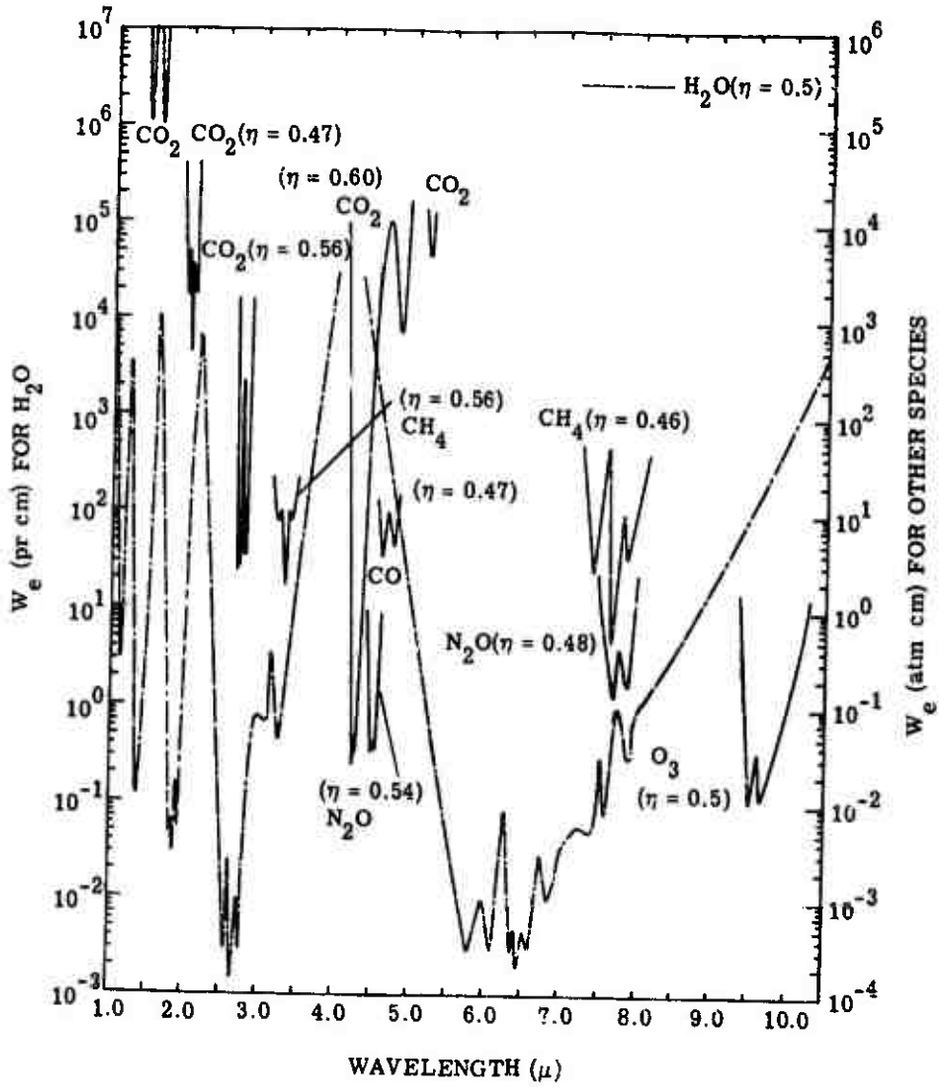

FIGURE 41. VALUES OF W_e AT 740 MM AND 300°K FOR ATMOSPHERIC-ABSORBING SPECIES

TABLE 18. VALUES OF W_e

λ (μ)	H_2O	CO_2	λ (μ)	H_2O	CO_2
1.03	7,600		1.92	0.1	10^{10}
1.05	1,500		1.94	0.4	20,000
1.075	130		1.95	0.86	3,500
1.1	14		1.96	1.9	1,700
1.13	3		1.98	7.2	10,000
1.15	5.8		2.00	18	1,100
1.18	30		2.95	35	450
1.2	120		2.03	69	1,500
1.23	3,500		2.04	100	10,000
1.25	390		2.06	210	1,700
1.28	21		2.10	1,000	29,000
1.30	4.4		2.15	4,800	
1.35	0.17		2.167	6,500	
1.37	0.12		2.20	2,500	
1.38	0.14		2.30	65	
1.40	0.23	10^6	2.40	4.15	
1.42	0.4	1.5×10^5	2.50	0.19	
1.43	0.56	1.1×10^5	2.59	0.003	
1.44	0.8	1.6×10^5	2.63	0.02	
1.46	1.95	4.7×10^5	2.66	0.0037	1,600
1.475	4.0	10^8	2.675	0.0015	3.2
1.50	14.0		2.68	0.0016	2.5
1.55	190		2.69	0.0022	5.4
1.555		10^6	2.70	0.003	2.8
1.58	1,650	1.2×10^5	2.72	0.0058	40
1.595	5,000	9.6×10^4	2.735	0.0095	220
1.61	10,000	1.5×10^5	2.74	0.01	120
1.65	1,250	10^6	2.76	0.005	3.6
1.70	360		2.77	0.0032	12
1.75	10		2.775	0.003	7
1.80	0.65		2.80	0.027	25
1.82	0.14		2.84	0.052	950
1.835	0.044		2.90	0.26	
1.88	0.08		2.93	0.52	
1.87	0.03		2.96	0.74	
1.882	0.15		3.00	0.80	
1.91	0.056		3.06	0.62	
			3.10	0.78	

TABLE 18. VALUES OF W_e (Continued)

λ (μ)	H_2O	CO_2	CO	N_2O	CH_4	O_3
3.18	3.8				22	
3.2	0.6				8	
3.22	0.48				8	
3.26	0.48				10	
3.32	1.4				1.7	
3.37	2.7				10	
3.38	3.1				8	
3.42	5.5				10	
3.47	11				20	
3.5	18					
3.7	5,000					
3.975	30,000					
4.1		10,000				
4.2		0.6				
4.235		0.026				
4.255		0.054				
4.275		0.036				
4.3	27,000	0.12				
4.35	16,500	1.8				
4.4	8,800	200		1		
4.47	3,900	600		0.035		
4.485	3,050	1,300		0.0425		
4.52	2,200	1,900	20	0.037		
4.60	1,050	3,300	35	0.96		
4.85	540	10,400	8			
4.75	200	2,500	4.3			
4.82	84	740	13.4			
4.85	62	1,200	20			
4.92	27	1,700				
5.00	11					
5.13	3	14,000				
5.17	2	4,500				
5.23	0.92	1,300				
5.45	0.058					
5.5	0.084					
5.725	0.0088					
5.8	0.0115					
5.875	0.0033					
6.025	0.01					
8.1	0.0034					
6.3	0.085					
6.375	0.003					

TABLE 18. VALUES OF W_e (Continued)

$\frac{\lambda}{(\mu)}$	H_2O	CO_2	CO	N_2O	CH_4	O_3
6.425	0.005					
6.45	0.002					
6.525	0.0046					
6.575	0.0025					
8.60	0.0033					
8.625	0.0025					
6.75	0.03					
6.775	0.0058					
6.62	0.02					
6.85	0.005					
6.93	0.08					
6.975	0.023					
7.025	0.042					
7.125	0.01					
7.15	0.08					
7.18	0.021					
7.2	0.08				66	
7.25	0.046				55	
7.3	0.08				22	
7.35	0.047				8	
7.4	0.3				3	
7.42	0.115				2.5	
7.45	0.044				4.6	
7.50	0.076			4.6	10.6	
7.55	0.325			0.42	26	
7.60	0.080			0.3	47	
7.63	0.23			0.21	0.3	
7.675	1.0			0.13	0.55	
7.775	1.0			0.4	5.4	
7.8	0.4			0.31	10	
7.85	0.98			0.19	3.8	
7.875	0.58			0.17	4.3	
7.95	0.25			0.58	8	
8.00	0.5			2.7	12.5	
8.025	1.0			6.3	16	
8.15	1.7				48	
8.175	1.85				57	
8.3	2.8					
8.6	7.6					
8.9	19					

TABLE 18. VALUES OF W_e (Continued)

λ (μ)	H_2O	CO_2	CO	N_2O	CH_4	O_3
9.2	48					
9.34	74					1.5
9.4	86					0.062
9.49	115					0.011
9.55	140					0.022
9.61	170					0.035
9.65	200					0.0125
9.7	240					0.015
9.9	470					0.042
10.0	660					0.098
10.22	1,600					2.7
10.5	5,500					

TABLE 19. LABORATORY DATA USED TO DETERMINE VALUES OF W_e AND η

Molecule	Band (μ)	Reference	η
N_2O	4.4-4.6	Burch et al. [1]	0.54
N_2O	7.5-8.0	Burch et al.	0.48
CH_4	3.15-3.45	Burch et al.	0.56
CH_4	7.25-8.15	Burch et al.	0.46
CO	4.5-4.85	Burch et al.	0.47
CO_2	4.1-4.65	Burch et al.	0.5
CO_2	2.66-2.84	Burch et al.	0.56
CO_2	1.93-2.09	Howard et al. [30]	0.5
CO_2	1.55-1.65	Howard et al.	0.5
CO_2	1.4-1.47	Howard et al.	0.5
H_2O	1.03-1.24	Howard et al.	0.5
H_2O	1.24-1.61	Howard et al.	0.5
H_2O	1.61-2.16	Howard et al. and Burch et al.	0.53
H_2O	2.16-3.90	Howard et al.	0.54
H_2O	4.40-10.0	Howard et al. and Burch et al.	0.5
O_3	9.3-10.2	Walshaw [34]	0.5

Recall that the transmission averaged over one period of a regular Elsasser band under conditions of strong-line absorption is given by

$$\bar{\tau} = 1 - \operatorname{erf}\left(\frac{\pi\alpha S}{d^2}W\right)^{1/2} \tag{96}$$

The most common procedure followed at this point was to empirically fit this function to laboratory data to evaluate the frequency-dependent parameter $\pi\alpha S/d^2$. Carpenter chose to evaluate this quantity from theoretical considerations for homogeneous paths at 280°K and 740 mm Hg. Therefore, the W in equation 96 becomes W^* and the half-width becomes α_0.

For homogeneous paths at standard conditions the half-width, line spacing, and integrated intensity do not vary from point to point along the path. Further, for a regular band the half-width and line spacing are independent of frequency. Basically, Carpenter found it necessary only to determine the variation of the integrated intensity from period to period throughout the band. This was accomplished by using both theory and experimental results. With all parameters specified, Carpenter calculated the transmission for several homogeneous paths. His results are shown in figure 42. Each curve represents the transmission for a given absorber concentration where 1 gm/cm^2 equals 509 atm cm of CO_2. Since these curves were calculated from equation 96 after first determining the spectral coefficient $\pi\alpha_0 S/d^2$, each of the curves should define the same generalized absorption coefficient which could be used to calculate the absorption for any value of W^*. This is not the case, however, and the reasons for this inconsistency between curves is not known. For example, at 2273 cm^{-1} we have

$$T_1 = 0.13 \text{ for } W^* = 5.09$$

$$T_2 = 0.54 \text{ for } W^* = 0.509$$

$$T_3 = 0.39 \text{ for } W^* = 0.0509$$

Applying these values to equation 96, we have $\left(\pi\alpha_0 S/d^2\right)_1 = 0.229$, $\left(\pi\alpha_0 S/d^2\right)_2 = 0.216$, and $\left(\pi\alpha_0 S/d^2\right)_3 = 0.190$, which is a spread in the data of approximately 20%. Because of the inconsistency in the data, no single curve should be used to specify the absorption coefficients. In order that the results obtained by Carpenter's method could be compared with other authors, a set of coefficients was determined for 21 discrete wavelengths by making a best fit to the data in a least-squares sense. The results of this effort are given in table 20. These coefficients in conjunction with the function $\bar{\tau} = 1 - \operatorname{erf}\{[C(\eta)W^*]^{1/2}\}$ define a method for computing absorption for the 4.3-μ CO_2 band.

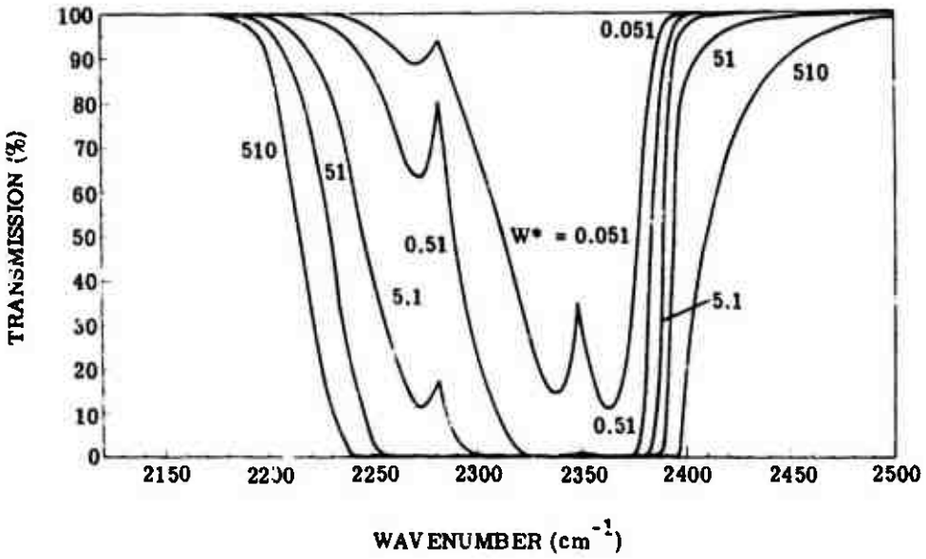

FIGURE 42. TRANSMISSION VS. WAVENUMBER FOR 4.3-μ CARBON DIOXIDE BAND AT 280°K

TABLE 20. ABSORPTION COEFFICIENTS FOR CARBON DIOXIDE

λ (μ)	Absorption Coefficient C(η)
4.167	0.159 E-2
4.184	0.631 E-2
4.202	0.527
4.219	15.108
4.228	21.820
4.237	25.036
4.246	15.890
4.255	10.738
4.264	14.153
4.283	18.813
4.301	13.487
4.320	5.239
4.348	2.268
4.367	0.648
4.386	0.102
4.405	0.159
4.425	0.908 E-1
4.444	0.175 E-1
4.464	0.123 E-1
4.484	0.498 E-2
4.505	0.235 E-2

3.11. METHOD OF V. R. STULL, P. J. WYATT, AND G. N. PLASS

Stull, Wyatt, and Plass used the quasi-random model to calculate the spectral transmission of H_2O and CO_2. Spectral transmission of these two gases was calculated for a large number of homogeneous paths and the results are presented in the form of extensive tables. The total work of these authors is published in two volumes [19, 62] which include a detailed description of the quasi-random model, the methods used in calculating the spectral transmission based on this model, and tabulated transmission data.

Basically, the method employed is that which is described in section 2.2.6. Equations 34 and 35 were used assuming only five intensity decades for each subinterval, D_k. Also, calculations were made for both the Lorentz line shape and the Benedict line shape. To remove the artificial effects introduced by dividing the frequency interval into subintervals of width D_k, the interval was subdivided twice, each subdivision being called a mesh. The final transmission spectrum was then the average of the results obtained from the two meshes.

In using the quasi-random model, the only parameter that was calculated from theory was that of line intensities, which were subsequently grouped into intensity decades; these decades in turn defined a value for the average decade line intensity, $\bar{S}_i$. Wyatt, Stull, and Plass further defined $\bar{S}_i$ by normalizing their results against the laboratory data of Howard Burch, and Williams [1, 30]. The normalization was carried out in the following manner. The values of $\bar{S}_i$ were calculated for each decade and all intervals. Transmission data were then calculated based on these values of $\bar{S}_i$. Calculated integrated absorptions were compared with the laboratory data for large frequency intervals (>400 cm^{-1}) and the values of $\bar{S}_i$ were adjusted accordingly. This process was repeated until a set of $\bar{S}_i$ values was obtained that yielded a best fit of the calculated data with the laboratory data in a least-squares sense. The entire process was carried out for two mesh sizes (20 cm^{-1} and 5 cm^{-1}) and a two-dimensional generalization of the least-squares method was used to obtain a final set of $\bar{S}_i$ values.

It is obvious from the above discussion that the initial selection of the $\bar{S}_i$ values is immaterial since the empirical process will always converge.

Table 21 summarizes the various homogeneous paths for which transmission data are tabulated. It is noted that for each gas there are six entries in the table. The first is the wavelength interval over which the computations were performed. The second gives the range of W values, the third gives the pressure range, and the fourth gives the temperature range. The last two give, respectively, the frequency spacing between entries and the resolution. Since there are 15 different W values, 7 pressures, and 3 temperatures, each line in this table, for either gas, encompasses transmission spectra for 315 paths.

TABLE 21. HOMOGENEOUS PATHS FOR WHICH TRANSMISSION DATA ARE TABULATED

Line Shape	Gas	Wavelength Range (cm^{-1})	W Range (pr cm)	Pressure Range (atm)	Temperature (^{o}K)	Entries (cm^{-1})	Resolution (cm^{-1})
Lorentz	H_2O	1000-3400	0.001-50	0.01-1.0	200-300	2.5	5.0
Lorentz		1000-10,000	0.001-50	0.01-1.0	200-300	10	20
Lorentz		1000-10,000	0.001-50	0.01-1.0	200-300	25	50
Lorentz		1000-10,000	0.001-50	0.01-1.0	200-300	50	100
Benedict	CO_2	507.5-9250.	0.2-10,000	0.01-1.0	200-300	2.5	5
Lorentz		507.5-9255.	0.2-10,000	1.0	300	2.5	5
Benedict		520.0-9999.	0.2-10,000	0.01-1.0	200-300	10	20
Benedict		550.0-9975.	0.2-10,000	0.01-1.0	200-300	25	50
Benedict		600.0-9950.	0.2-10,000	0.01-1.0	200-300	50	100

Such an extensive set of data not only gives transmission spectra for numerous homogeneous paths but can easily be used to determine the absorption for any homogeneous path. If the values of W, $\overline{P}$, and T for a given path are all bounded by the values shown in table 21, then the transmission can be determined by simple interpolation procedures. Also, these data can be used in place of measured spectra to specify the band parameters for the Elsasser or statistical model. This was done by Oppel who fitted the Elsasser model to these data for the spectral region from 4.0 to 5.0 μ. This procedure allows for the calculation of transmission spectra for slant paths that are not bounded by the range of values in the tables.

The interpolation procedure to be used is that suggested by the authors — simply a logarithmic interpolation between nonzero values of the absorption. The absorption is expressed in the form

$$A = 1 - \tau = e^{-f(P,T,W)} \tag{97}$$

where f is usually a complicated function of pressure P, temperature T, and absorber concentration W. At points where one or both of the tabular values of transmission τ is equal to unity, linear interpolation on τ provides more than sufficient accuracy. Otherwise it is far more accurate to interpolate f(P, T, W). Since only three significant figures are given in the tables, in general, a first-order interpolation provides sufficient accuracy. From equation 97 one has

$$f(P, T, W) = \ln A$$

When the absorptance at constant P is plotted against W on a log-log graph, the resulting curve has only a small curvature and displays long linear sections. Similar remarks apply to an absorptance curve at constant W plotted against P. For these reasons, the most accurate interpolation is obtained by taking equal logarithmic intervals for P and W so that

$$\Delta f = \frac{\partial f}{\partial x}\Delta x + \frac{\partial f}{\partial T}\Delta T + \frac{\partial f}{\partial y}\Delta y$$

where $x = \ln P$ and $y = \ln W$. Thus, $f(P + \Delta P, T + \Delta T + W + \Delta W) = f(P, T, W) + \Delta f$ and

$$\tau(P + \Delta P, T + \Delta T, W + \Delta W) = 1 - A(P + \Delta P, T + \Delta T, W + \Delta W) = 1 - \exp[-(f + \Delta f)]$$

The following example illustrates the method described above.

Given: P = 1 atm, T = 300°K

at W = 2.0, τ = 0.648, A = 0.352

at W = 5.0, τ = 0.425, A = 0.575

P = 0.5 atm, T = 300°K

at W = 2.0, τ = 0.715, A = 0.285

at W = 5.0, τ = 0.545, A = 0.455

Find: $\tau(P, W)$ at $W = 3.2$, $P = 0.75$, $T = 300^{\circ}K$

Procedure: $A(1, 2.0) = 0.352$; $f = 1.0441$

$A(1, 5.0) = 0.575$; $f = 0.5534$

$A(0.5, 2.0) = 0.285$; $f = 1.2553$

$A(0.5, 5.0) = 0.455$; $f = 0.7875$

$\ell n\ (2.0) = 0.6931$; $\ell n\ (1.0) = 0.0000$

$\ell n\ (3.2) = 1.1631$; $\ell n\ (0.75) = -0.2877$

$\ell n\ (5.0) = 1.6094$; $\ell n\ (0.5) = -0.6931$

Hence: $$\Delta f = \frac{\partial f}{\partial(\ell n\ W)}\Delta(\ell n\ W) + \frac{\partial f}{\partial(\ell n\ P)}\Delta(\ell n\ P)$$

$$= \frac{0.5534 - 1.0441}{1.6094 - 0.6931}(1.1631 - 0.6931) + \frac{1.2553 - 1.0441}{-0.6931 + 0.0000}(-0.2877)$$

$$= -0.2517 + 0.0877 = -0.1640$$

Therefore: $f(0.75, 3.2) = f(1, 2.0) + \Delta f = 1.0441 - 0.1640 = 0.8801$

$$\tau(0.75, 3.2) = 1 - e^{-0.8801} = 0.585$$

In order to calculate transmission for atmospheric slant paths, the equivalent path parameters $\overline{P}$ and W^* are first determined by the methods used in section 2.3. The equivalent temperature may be assumed to be the average temperature without introducing a significant error. Once the equivalent homogeneous-path parameters are determined, the spectral transmission can be calculated according to the interpolation procedure.

Plass [63] used this method to calculate the spectral transmission over slant paths from initial altitudes of 15, 25, 30, and 50 km to the outer limit of the atmosphere. Results are presented in the form of tables for paths from the vertical to the horizontal in 5° steps. Values are given for CO_2 from 500 to 10,000 cm^{-1} and for H_2O from 1000 to 10,000 cm^{-1} for both a "dry" stratosphere and a "wet" stratosphere.

Plass assumed that CO_2 was uniformly mixed throughout the atmosphere at 0.033% by volume. H_2O distributions were based on the work of Gutnick [64, 65]. For the "dry" stratosphere H_2O was assumed to be constant at 0.045 gm/km air. For the "wet" stratosphere the values used are given in table 22.

The use of the quasi-random model to describe the spectral-line structure of atmospheric gases is most rigorous and undoubtedly results in a more accurate representation of the line structure than does any other band model. However, it is not possible to express the transmissivity functions generated through the use of this model in a closed form. It is therefore a difficult and laborious task to apply them to arbitrary atmospheric slant paths. For this reason

TABLE 22. MIXING RATIO FOR "WET" STRATOSPHERE MODEL

Altitude (km)	Mixing Ratio (gm H_2O per kg air)
15	0.0090
16	0.0095
17	0.0105
18	0.012
19	0.015
20	0.018
21	0.022
22	0.027
23	0.033
24	0.040
25	0.048
26	0.058
27	0.069
28	0.087
29	0.11
30	0.13
31	0.16
32	0.18
33 and above	0.20

it is felt that the most useful aspect of the work of Wyatt, Stull, and Plass is not the methods they employed, but rather their extensive results.*

3.12. METHOD OF A. THOMSON AND M. DOWNING

Thomson and Downing were involved in a program that required knowledge of the transmission of the atmosphere from 2.0 to 5.0 μ for atmospheric paths that extended from the surface of the earth to the limit of the atmosphere. To determine such transmission spectra they used the transmissivity functions developed by Howard, Burch, and Williams for H_2O for the 2.7-μ and 3.2-μ absorption bands and the results of Carpenter for the 4.3-μ CO_2 band. Their only original contribution consisted of determining a method for calculating absorption caused by CO_2 for the 2.7-μ band. This work was based on the results of Thomson [66]. Their complete work is presented in reference 67. Since the works of Howard and Carpenter have been previously discussed, only the results of their work related to CO_2 absorption at 2.7 μ will be discussed here.

The transmission for the 2.7-μ CO_2 band was calculated directly from the strong-line approximation to the Elsasser band model. Since Thomson and Downing developed their method for sea-level paths only, the transmission is given by

$$A = \operatorname{erf}\left[\frac{\pi\alpha_0 S(\nu) W^*}{d^2}\right]^{1/2} \tag{98}$$

Thomson et al. derived an approximate expression for the mean or "smeared" integrated intensity of a linear molecule which is given as

$$S(\nu) = S_0 \frac{T_0}{T} \frac{|\nu - \nu_0|}{(\Delta\nu)^2} e^{-(\nu-\nu_0)^2/(\Delta\nu)^2}$$

where S_0 is the total-band intensity and $\Delta\nu = 2\sqrt{BkT/hc}$, in which k = Boltzmann's constant, h = Planck's constant, and c = velocity of light. B is the rotational constant and has the value of 0.39 cm^{-1} [68].

The 2.7-μ CO_2 band consists of two adjacent bands; as reported by Thomson and Downing, one is centered at 3716 cm^{-1} and has a value for S_0 at 298°K of 42.3 cm^{-2}-atm^{-1}; the other band is centered at 3609 cm^{-1} and has a value for S_0 at 298°K of 23.6 cm^{-2}-atm^{-1}. The values

*Unfortunately, the tables could not be included in this document because of their considerable length. However, copies are obtainable from the Defense Documentation Center in Washington. (Note the AD numbers on ref. 19, 62, and 63.)

for α_0 and d were determined to be 0.064 cm^{-1} and 1.56 cm^{-1}, respectively. With all of the parameters specified, the transmission is easily calculated for any equivalent path W^*. The results of a sample calculation are shown in figure 43, which is the transmission to the top of the atmosphere for vertical paths extending from six different altitudes for the band centered at 3716 cm^{-1}. It is interesting to note the peak in transmission at the band center, approximately 3610 cm^{-1}. Even for large quantities of absorber these peaks reach 100% transmission. If the absorption of CO_2 were measured at infinite resolution such peaks would indeed be observable; however, for a resolution consistent with the Elsasser model (i.e., the averaging interval is equal to d = 1.56 cm^{-1} for this calculation), such peaks would be smoothed and a value of 100% transmission would not be observable. Therefore, it appears that the results obtained by this method are not in agreement with the initial assumption of a regular Elsasser band model. The peaks are very narrow, however, and from the standpoint of total-band absorption their method yields results that are comparable with other methods and experimental field measurements.

3.13. METHOD OF T. ELDER AND J. STRONG

Elder and Strong [69] derived a useful, simple method for predicting the average total absorption — the average being taken over broad spectral intervals — caused by H_2O for homogeneous paths. The spectral regions of interest to Elder and Strong were the so-called infrared "windows."

In figure 44 a low-resolution curve is presented of transmission versus wavenumber for the spectral region from 0.7 to 14.0 μ. It is noted that there are eight regions of low absorption. Each of the low-absorption regions is called an atmospheric window and is spectrally defined in the figure. The boundaries are indicated by the dotted lines in the centers of the absorption bands.

Note that the window transmissions are not unity as they would be if the optical path were evacuated. This is primarily a result of continuous attenuation. Elder and Strong developed empirical functions, based primarily on open-air field measurements, which specify the average window transmission resulting from molecular absorption for each of the window regions shown in figure 44. They assumed that the average window transmission for each of the eight windows could be represented to a first approximation by the expression

$$T = -k \log W^* + t_0 \tag{99}$$

where k and t_0 are empirical constants and W^* is the equivalent sea-level concentration of H_2O. Thus, when measured values of T and W^* are plotted for any window on semi-log graph paper, the experimental points should fall on a straight line with slope -k and with an intercept t_0.

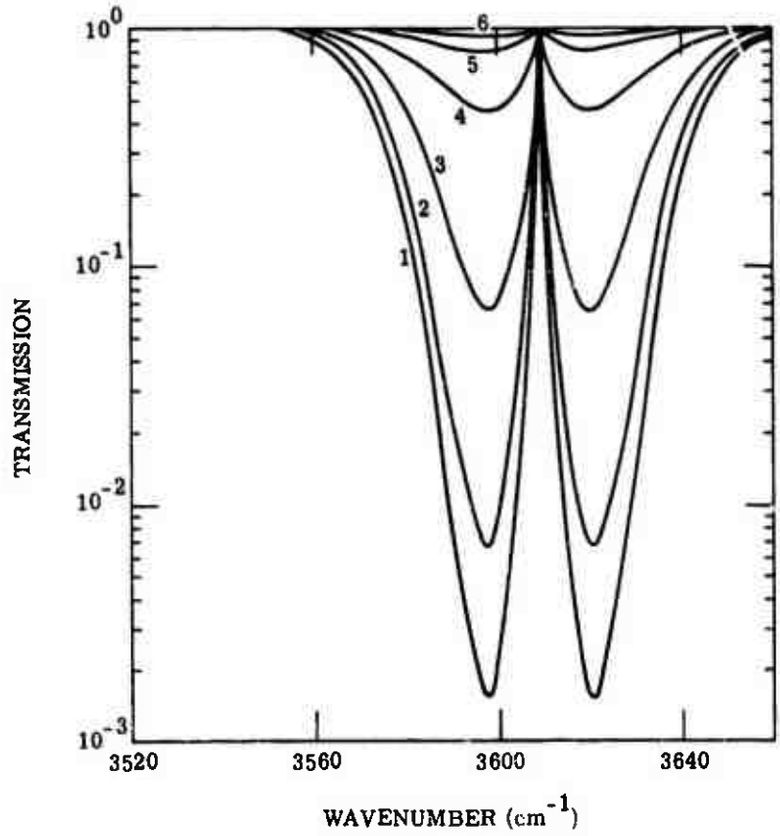

FIGURE 43. TRANSMISSION TO TOP OF ATMOSPHERE FROM INDICATED ALTITUDES AS A FUNCTION OF WAVENUMBER FOR 3716-CM^{-1} CARBON DIOXIDE BAND. Altitudes: curve 1, 15,000 ft; curve 2, 20,000 ft; curve 3, 30,000 ft; curve 4, 50,000 ft; curve 5, 75,000 ft; curve 6, 100,000 ft.

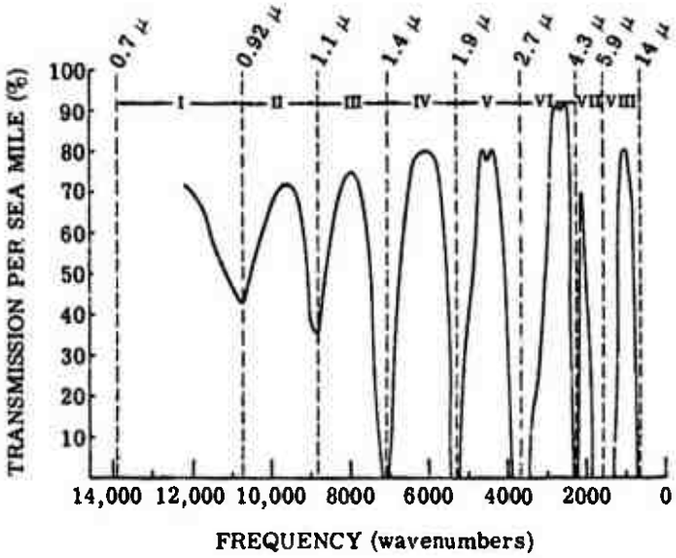

FIGURE 44. ABSOLUTE INFRARED TRANSMISSION OF THE ATMOSPHERE. Adapted from reference 97.

Figure 45 contains graphs of T vs. log W^* for windows I to VII. Window VIII was not treated since this procedure required adjacent windows to determine the envelope spectrum which was used to determine the amount of continuous attenuation. The data used in the curves are summarized in table 23. The circled dots on figures 45d, 45e, 45f, and 45g were not obtained from observed spectra, as were the other points, but were calculated indirectly from observations reported in references 84-87.

The empirical constants associated with the solid straight lines on the graphs are given in table 24. The average straight lines of these seven graphs show the validity of equation 99, while the points show the agreement of the observed data.

In figures 45d, 45e, and 45f, a dashed curve is drawn. This curve represents the transmission as predicted for no-haze conditions from the published tables of Yates [88] (also see ref. 89). It can be seen that in the region of the Howard/Ohio State data, the fit with the straight line is good, but the extrapolations to long paths do not always agree with other observations, nor with the straight line.

The work of Elder and Strong is represented completely by equation 99 and the coefficients given in table 23. This empirically derived expression provides a very useful and simple method for computing values of window transmission but should be used with some reservations. First, this work is based on data that were measured earlier than 1950. Therefore, the results are somewhat dated and no attempt has been made to verify the empirical constants with more recent measurements. However, their method is the only one available for predicting values of window transmission without first computing spectral absorption.

Secondly, their method should not be applied to paths containing concentrations greater than those shown in figure 45a-45f. In general, this value is approximately 2 atm cm H_2O and therefore limits the method to relatively short paths.

3.14. SUMMARY

In this section methods for computing absorption for homogeneous paths based on assumed models of the band structure were presented. A summary of this information is given in table 25. For each researcher or research group, the gases treated, band models assumed, wavelength range over which the method is applicable, and the experimental data used to determine the frequency-dependent parameters are stated. All methods presented yield values of spectral absorption with the exception of that of Elder and Strong. Their method yields values of average absorption for only the window regions. Of the methods which can be used to compute spectral absorption, the method of Stull, Wyatt, and Plass is the only one which does not give the transmissivity function in closed form. This is because they used the quasi-random model.

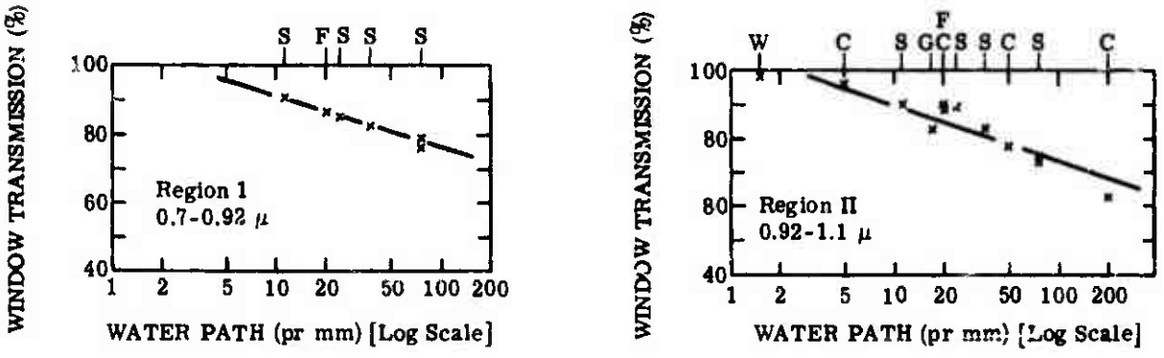

(a) Window I

(b) Window II

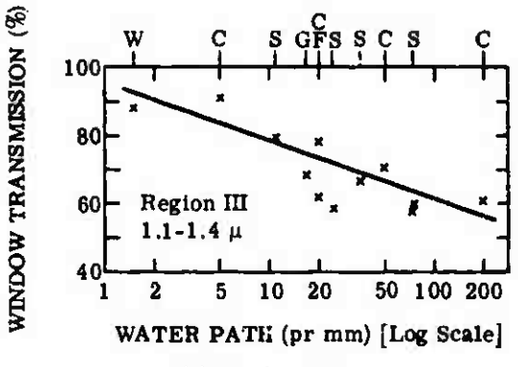

(c) Window III

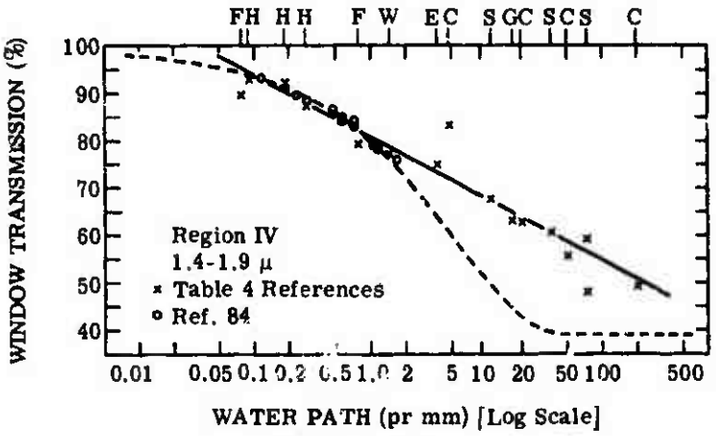

(d) Window IV

FIGURE 45. WINDOW TRANSMISSION. Letters are identified with sources in table 23.

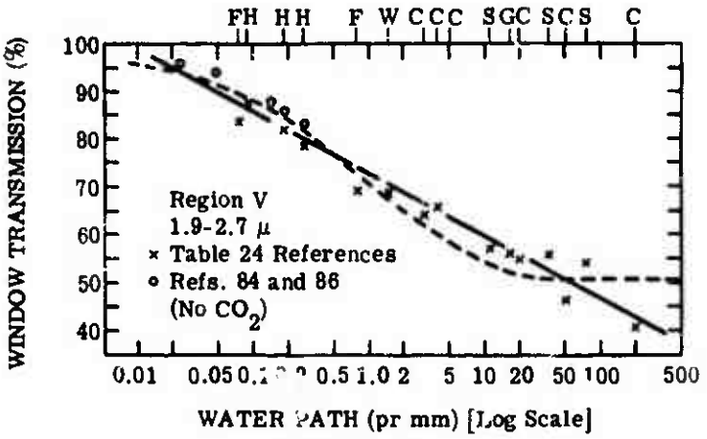

(e) Window V

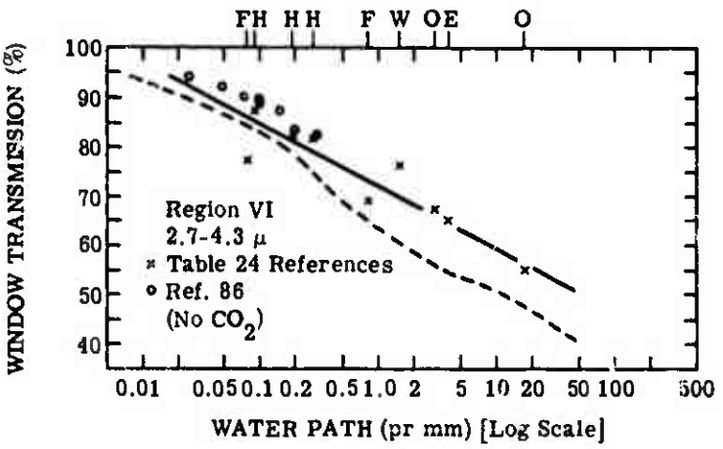

(f) Window VI

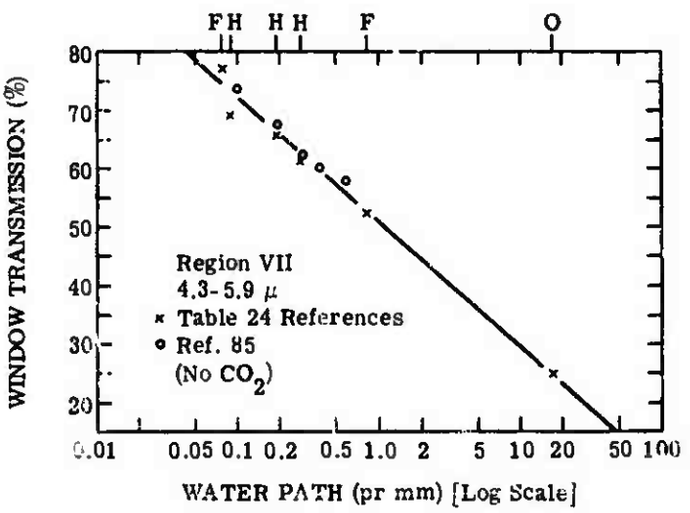

(g) Window VII

FIGURE 45. WINDOW TRANSMISSION. Letters are identified with sources in table 23. (Continued)

TABLE 23. WINDOW TRANSMISSION (percent)

Source	Code*	Water Path (pr mm)	I	II	III	IV	V	VI	VII
Fowle [70-75]	F	0.08	--	--	--	89.9	83.5	77.1	77.5
Howard [76]	H	0.09	--	--	--	93.0	87.0	87.5	69.7
Howard [76]	H	0.19	--	--	--	92.0	82.0	82.2	86.2
Howard [76]	H	0.28	--	--	--	88.0	78.4	81.5	81.2
Fowle [70-75]	F	0.82	--	--	--	79.6	68.9	69.0	52.4
Hettner [77]	W	1.5	--	98.5	88.6	77.0	88.5	76.2	--
Elliott et al. [78-79]	E	3.05	--	--	--	--	63.5	67.5	--
Elliott et al. [78-79]	E	3.9	--	--	--	75.0	65.4	65.3	--
Fischer [80]	C	5.0	--	98.6	91.8	83.3	71.1	--	--
Strong [81]	S	11.0	91.0	90.0	79.0	68.0	57.0	--	--
Gebbie [82-83]	G	17	--	82.6	68.0	63.4	55.8	55.6	25.0
Fischer [80]	C	20	--	88.8	78.4	63.2	54.8	--	--
Fowle [70-75]	F	20	86.0	89.0	62.0	--	--	--	--
Strong [47]	S	24	85.0	89.0	58.0	--	--	--	--
Strong [81]	S	36	82.0	83.0	67.0	61.0	55.0	--	--
Fischer [80]	C	50	--	77.5	70.0	55.5	46.4	--	--
Strong [81]	S	75	79.0	73.5	58.0	47.0	54.0	--	--
Strong [81]	S	75	75.0	75.0	59.0	59.0	54.0	--	--
Fischer [80]	C	200	--	62.8	60.1	49.4	40.6	--	--

*Reference designation on figure 45.

TABLE 24. EMPIRICAL CONSTANTS FROM FIGURE 45
$T = -k \log W + t_0$

T is window transmission in percent
W is water path precipitable millimeters

Window	Region (μ)	k	t_0	T = 100% if W is less than (mm)
I	0.70 to 0.92	15.1	106.3	0.26
II	0.92 to 1.1	16.5	106.3	0.24
III	1.1 to 1.4	17.1	96.3	0.058
IV	1.4 to 1.9	13.1	81.0	0.036
V	1.9 to 2.7	13.1	72.5	0.008
VI	2.7 to 4.3	12.5	72.3	0.006
VII	4.3 to 5.9	21.2	51.2	0.005
VIII	5.9 to 14	(not treated)		

Example: for window VI and 0.03 precipitable millimeters of water,
$T = -12.5 (\log 0.03) + 72.3 = -12.5 (8.477 - 10) + 72.3$
$= -12.5 (-1.523) + 72.3 = +19.0 + 72.3$
$= 91.3\%$.

TABLE 25. SUMMARY OF BAND-MODEL METHODS FOR COMPUTING ATMOSPHERIC ABSORPTION

Author	Gas	Band Model	Wavelength Range (μ)	Experimental Data
Bradford	CO_2	Elsasser	4.184-4.454	Bradford, McCormack, and Selby
Thomson and Downing	CO_2	Elsasser	4.0-4.5	Theoretical
Elsasser	CO_2	Empirical	11.77-18.2	Cloud; Howard et al.
	H_2O	Statistical	4.39-250	Palmer; Howard, et al.
	O_3	Empirical	8.85-16.4	Summerfield, Walshaw
Oppel	CO_2	Elsasser	2.64-2.88 4.15-4.52	Burch et al.
	H_2O	Statistical	1.08-4.0 4.0-5.0	Burch et al.; Howard et al. Stull, Wyatt, and Plass
	N_2O	Elsasser	4.36-4.74	Burch et al.
	CH_4	Statistical	3.02-4.16	Burch et al.
	CO	Statistical	4.4-5.0	Burch et al.
Altshuler	CO_2	Empirical	1.0-15.0	Howard et al.
	H_2O	Statistical	1.0-9.0	Howard et al.
			9.1-20.0	Taylor and Yates
			20-40	Palmer et al.
			40-250	Stanevich
	O_3	Elsasser	4.4-16.5	Strong
	N_2O	Elsasser	3.8-18.0	Shaw
Zachor	CO_2	(a) Elsasser	1.0-5.3	Howard et al.
		(b) Two overlapping Elsasser bands	1.0-5.3	
	O_3	Elsasser	9.3-10.2	Walshaw et al.
Howard, Burch, and Williams	H_2O	Statistical	1.0-10.6	Howard et al.
Carpenter	CO_2	Elsasser	4.167-4.51	Theoretical

TABLE 25. SUMMARY OF BAND-MODEL METHODS FOR COMPUTING ATMOSPHERIC ABSORPTION (Continued)

Author	Gas	Band Model	Wavelength Range (μ)	Experimental Data
Lindquist	H_2O	Statistical	1.-9.2	Howard et al.
Green and Griggs	CO_2	Statistical	1.0-10.0	Howard et al. Burch et al.
	H_2O	Statistical	1.0-10.0	Howard et al. Burch et al.
	O_3	Statistical	9.3-10.2	Walshaw et al.
	N_2O	Statistical	4.4-4.6 7.5-8.0	Burch et al.
	CH_4	Statistical	3.15-3.45 7.25-8.15	Burch et al.
	CO	Statistical	4.15-4.85	Burch et al.
Stull, Wyatt, and Plass	CO_2	Quasi-random	1.0-20.0	Theoretical*
	H_2O	Quasi-random	1.0-20.0	Theoretical*
Elder and Strong	H_2O	Empirical	0.7-5.9**	See appropriate section

*The results of Stull, Wyatt, and Plass were normalized against the laboratory data of Howard et al. for each absorption band.

**The results of Elder and Strong give average window transmission for seven windows in the wavelength range.

Since there are many different methods available for computing absorption for a given gas and for a given spectral interval (for the 4.3-μ CO_2 band there are seven methods available), the infrared researcher must select the best method to use for a given application considering the trade-offs between accuracy, resolution, and amount of computational labor. The resolution obtainable from any given method and the amount of computational labor involved have been made quite clear in the previous discussions. However, the accuracy with which a given method can predict atmospheric absorption is yet to be established.

There are basically two approaches one can use to determine the accuracy with which a method based on a band model can predict spectral absorption. The first of these is to compute spectral absorption by the direct integration of the general transmissivity function as outlined in section 2.1 for broad ranges of absorber concentration and pressure. These results are then compared with the results obtained by each of the methods listed in table 25. Such comparisons would be indicative but not necessarily conclusive for several reasons. The rigorous calculation requires a priori knowledge of such band parameters as line strength, line half-width, and line location which are determined from both theory and experimental measurement. Also, the number of spectral lines that must be taken into account increases as the quantity of absorber increases. Therefore, even the direct integration calculation includes assumptions and approximations which, in the final analysis, should be verified with experimental field measurements. Unfortunately, even if the rigorous calculation could yield results that approximate the true absorption spectra for an atmospheric slant path better than any other technique, the state of the art is such that it could not be applied to all spectral regions. This results from the fact that the band parameters are fairly accurately known for only a small portion of the spectrum. For the spectral regions for which the rigorous calculation has been performed, comparisons are made with band-model methods. These are presented and discussed in section 5.

The second approach is to simply compare the results obtained from the band-model methods with experimental field measurements. It is felt that such comparisons yield the most conclusive results if the slant-path field measurements are made under such conditions that the quantity of absorber in the path can accurately be determined. Comparisons of this type are also presented and discussed in section 5.

It is emphasized that the motivation behind the development of the band-model methods was to generate methods for computing slant-path absorption which yield good first-order approximation to the true absorption spectra, while at the same time requiring a minimal amount of computation. As will be shown in section 5, many of the methods have achieved this goal for a large portion of the infrared spectrum.

4
DISTRIBUTION OF ATMOSPHERIC MOLECULAR ABSORBING GASES

4.1. INTRODUCTION

In section 2 it was stated that the atmosphere contains six different gases that attenuate tnfrared radiation by a process known as molecular absorption. Those gases are CO_2, H_2O, O_3, N_2O, CH_4, and CO. In order to determine the amount of radiation absorbed oy a particular absorbing species as the radiation traverses an atmospheric slant path it is necessary to reduce the siant-path absorber concentration to an equivaient concentration for a homogeneous path. To perform this reduction it is first necessary to determine the pressure, temperature, and density of each absorbing gas at each point aiong the siant path. Hence it is necessary to have a priori knowledge of the distribution of prcssure, temperature, and density as a function of aititude. The distribution of pressure and temperature is not a controversial subject and for purposes of atmospheric absorption caiculations the values pubiished in the U. S. Standard Atmosphere 1962 are adequate. The distribution of density for the various gases, however, has been subject to considerable research. This section discusses the present state of knowledge pertaining to these density distributions.

Recali that the density of a given absorber is given by

$$\rho_{gas} = \rho_{air} M_{gas}$$

where ρ_{air} is the density of air and M_{gas} is the mixing ratio of the gas expressed as percent by volume (equivaient to mole fraction). The mixing ratios of CO_2, O_3, CH_4, CO, and N_2O are normally expressed in these units. However, the mixing ratio for H_2O is normally expressed as percent by weight, grams of H_2O per kilogram of air being the standard unit.

4.2. CARBON DIOXIDE

Carbon dioxidc is a strong absorber of infrared radiation in three rather broad spectral regions centered at approximateiy 2.7, 4.3, and 15 μ. CO_2 data are of specific importance to two main groups of scientists; meteorologists and systems engineers. The former, who are concerned with radiative transfer, have special interest in the 15-μ CO_2 band and require highiy accurate mixing ratio data. The latter find aii three CO_2 bands of importance, and unlike the meteorologist, the systems engineer does not need painstakingly accurate data. The vast majority of the work done in this area is pointed toward satisfying systems requirements, which is also the goal of this report. The following study is presented in this iight.

All researchers are in general agreement that CO_2 is uniformly mixed throughout the atmosphere for altitudes up to 50 km. Since data are extremely sparse for greater altitudes, specific conclusions cannot be made. However, air density is minute for altitudes greater than 50 km, and, for purposes of atmospheric absorption, it may be considered negligible.

The available information reporting values of CO_2 content have been reviewed and the results are presented in table 26. Note that all authors are in close agreement. The average deviation is less than 2% and the percent difference between the maximum and minimum value is only 5%. These values are averages of a great many measurements made at many different locations. The most extensive measurement program was that of Keeling [91] which consisted of continuous measurements from 1957 to 1961 at Hawaii, Antartica, and California for altitudes to 5 km. His results indicated that the CO_2 concentration shows monthly variations of approximately 2 ppm, having a maximum value in April and a minimum in December. He also indicated that the average yearly increase in CO_2 is approximately 1.0 ppm. In addition, Callendar [96] and Bray [95] separately have shown evidence that the CO_2 concentration has increased in the last 50 years. Callendar reported an average yearly increase of approximately 0.7 ppm, attributing the increase to industrial activity and the clearing, draining, and burning of vegetation. Presented in table 27 are some comparisons Bray made to demonstrate the CO_2 increase over the last 100 years.

It is emphasized that the data in table 27 are averages of a large number of measurements and that various isolated measurements show large deviations from the accepted average value. For example, concentrations less than 150 ppm have been recorded in polar areas while data taken near Africa have shown concentrations as high as 700 ppm. Also, most observations indicate that the CO_2 content is higher near industrial or urban areas than in rural areas. In general, the measurements indicate that the CO_2 content is higher at night than during the day. Although little work has been performed at high altitudes, Glueckauff [93] has reported values between 50 and 70 ppm less than the norm for stratospheric balloon flights over England.

On the basis of the data presented in table 26 and the fact that Bray's value is based upon an extensive literature survey, one could reasonably choose a value of 320 ppm for atmospheric-absorption calculations. This value was used for all calculations presented in this report.

4.3. NITROUS OXIDE

Nitrous oxide was first recognized as a permanent constituent of the atmosphere by Adel [97] in 1939, and since that time a number of other authors have measured the N_2O concentration. Data of Goldberg and Muller [98] and Goody and Walshaw [99] support the assumption that the

TABLE 26. CONCENTRATION OF CARBON DIOXIDE

Source	CO_2 Content (ppm)
Handbook of Geophysics [90]	314
Keeling [91]	314
Callendar [92]	320
Glueckauff [93]	330
Fonselious [94]	321-329
Bray [95]	320
Average	321 ± 5

TABLE 27. ATMOSPHERIC CARBON DIOXIDE FOR 1857—1906 AND 1907—1956, VARIOUS CATEGORIES

Category	Mean (1857—1906)	Mean (1907—1956)
Unweighted Values		
Yearly, all values	321	350
Yearly, non-urban	312	332
Summer, non-urban	305	314
April, non-urban	311	318
August, non-urban	295	315
Weighted Values		
Yearly, all values*	313	337
Yearly, non-urban*	309	326
Summer, non-urban*	299	315
April, non-urban	316	317
August, non-urban	299	317
Yearly, non-urban**	293	319
Summer, non-urban**	293	315

*Weighted by opinions in literature and by maximum-minimum variability in relation to mean.

**Weighted by maximum-minimum variability only.

fractional concentration is uniform with altitude. The former authors indicate that N_2O is uniformly mixed to an altitude of 15 km, while Goody and Walshaw show uniform distribution to 10 km and suggest a good probability of uniformity to 40 km.

Presented in table 28 is a summary of the available data on the N_2O concentration, a value which is not well agreed upon. One possible reason for the diversity was reported by Groth and Schierholz [105]. Using laboratory data, they suggest that aerobic bacterial decomposition of nitrogen compounds is a major source of N_2O, which might imply that its concentration is dependent upon geographic location and seasonal variation. Bates and Witherspoon [106] also suggest that these photochemical reactions are the major sources of N_2O in the atmosphere.

For all calculations performed in this report, a value of 0.28 ppm for N_2O concentration was used. The choice was based on the fact that this value was predominant in the most recent measurements.

4.4. CARBON MONOXIDE AND METHANE

Carbon monoxide and methane are the two remaining gases that are, except for localized conditions, uniformly mixed as a function of altitude. These gases are relatively weak absorbers and exist in the atmosphere at concentrations which are relatively low compared to that of CO_2.

The abundance of CO has been investigated to a much greater extent than that of CH_4. A summary of the CO data is presented in table 29. Note that there is considerable variation in the data, with Shaw [110] giving the lowest value of 0.075 ppm and Bowman [104] reporting the highest value of 1.1 ppm. The remaining data have an average value of approximately 0.12 ppm. The reason for these differences is undoubtedly a result of the different methods of measurement. For example, Shaw's values were determined from solar spectra observed from a ground level station. Therefore, the CO concentration represents a mean value for a slant path extending to the limit of the atmosphere. The possibility of an increased concentration caused by the industrial activity would have little effect on such a path. Bowman's data, in contrast, were determined from air samples taken at ground level stations in or near the city, and are therefore biased data. The remaining data were determined from solar spectra or from air samples far removed from industry or urban areas. If we neglect Bowman's data it appears that a good representative average mixing ratio for CO is 0.12 ppm. This value was used for all calculations in this report.

The available data on CH_4 is very sparse. Bowman [104] reports a value of 2.4 ppm based on an experimental procedure the same as that used for CO. Goldberg [115] reports a value of

TABLE 28. CONCENTRATION OF NITROUS OXIDE

Author	Date	Location	Content (ppm)
Adel [97]	1941	Arizona	0.38
Shaw, Sutherland, and Wormell [49]	1948	England	1.25
McMath and Goldberg [100]	1949	Michigan	0.5
Slobod and Krogh [101]	1950	Texas	0.5
Birkeland, Burch, and Shaw [102]	1957	Chesapeake Bay	0.43
Birkeland [103]	1957	Ohio	0.28
Bowman [104]	1959	Ohio	0.28
U. S. Standard Atmosphere	1962		0.5

TABLE 29. CONCENTRATION OF CARBON MONOXIDE

Location	Observers	Mean Concentration (ppm)	Range (ppm)
Columbus, Ohio	Migeotte [107]	0.125*	---
Columbus, Ohio	Bowman [104]	1.1	0.4-2.2
Columbus, Ohio	Shaw and Howard [108-110]	0.125**	0.075-0.25
Columbus, Ohio	Shaw [111]	0.075**	0.05-0.125
Ottawa, Canada	Locke and Herzberg [112]	0.1625	0.09-0.18
Jungfraujoch, Switzerland	Benesch, Migeotte, and Neven [113]	0.075**	0.025-0.11
Flagstaff, Arizona	Adel [114]	0.125*	---

*Concentration determined from published spectra.

**Concentration reduced to sea level assuming uniform vertical distribution.

1.1 ppm. Since the available data are so meager, it is fortunate that CH_4 is a minor contributor to slant-path absorption.

4.5. OZONE

Ozone is formed primarily in the mesosphere by photochemical dissociation of oxygen as a result of ultraviolet radiation from the sun. Its distribution is variable with altitude, showing maximum concentration between 15 and 30 km. Presented in figure 46 is a typical vertical profile of ozone distribution [116]. The units of O_3 concentration are atmospheric centimeters (at STP) per kilometer of air. To convert these units to parts per million, two steps are required. First, convert the values on the abscissa to partial pressure of O_3 in micromillibars. This conversion is given by $P_{O_3} = 10\frac{T}{T_0} \times P_0 \times$ atm cm/km, where T is the temperature at the given altitude. The O_3 concentration in parts per million for any given altitude is then given by the ratio of the O_3 partial pressure to air pressure at that altitude, or ppm = P_{O_3}/P_{air}, where P_{O_3} is in micromillibars and P_{air} is in millibars.

It is noted that the O_3 concentration is approximately 0.004 atm cm/km at sea level, which would cause negligible absorption even for very long paths. It increases to a maximum of approximately 0.02 atm cm/km at 23 km and then gradually decreases with increasing altitude. It is emphasized that, since this is only a typical profile, the concentration for a specific season or a given geographical location can vary markedly from that shown.

The O_3 mixing-ratio profile appears to have a significant seasonal and latitudinal variation, as is seen in figures 47 and 48 [90]. Note that the shape of the profile changes under different conditions. In figure 47 there appears to be a yearly cyclic change in the distribution. Starting in the colder months, the peak concentration increases to a maximum in August. There also appears to be a tendency for the peak to rise in altitude as it grows in magnitude. Figure 48 seems to indicate that the profile "flattens out" with increasing latitude at the same time at which the peak concentration becomes less. These changes in the profile, however, do not become a critical concern unless a specific application calls for a long, near-horizontal path between 15 and 30 km. In this case, use of different profiles could give significant differences and it is recommended that under these circumstances a profile should be used that had been obtained under very similar temporal, seasonal, and latitudinal conditions as the path in question.

Figures 49 and 50 show the average distribution of total O_3 (for a vertical path through the atmosphere) over the northern hemisphere for the maximum and minimum seasons [117]. Total O_3 in equatorial regions averages about 0.24 atm cm and varies only slightly with season. The amount increases to the north reaching annual averages in excess of 0.4 atm cm. North of the

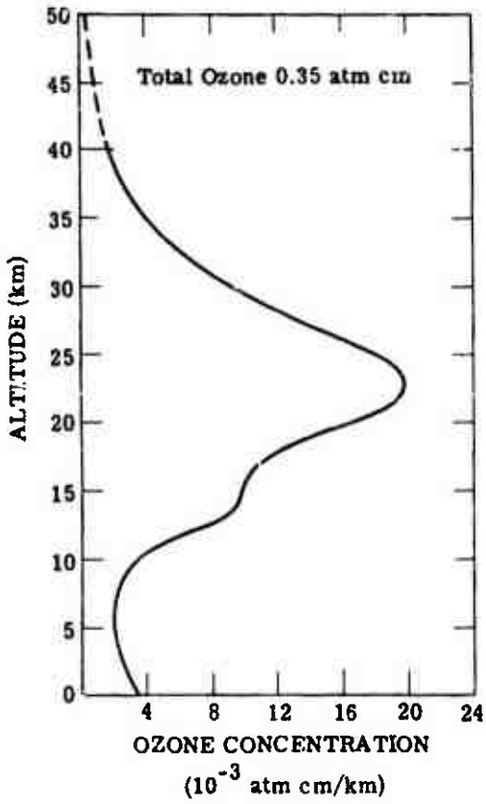

FIGURE 46. REPRESENTATIVE OZONE CONCENTRATION PROFILE. Solid curve developed from ozonesonde network data, dashed curve from chemical-equilibrium theory [116].

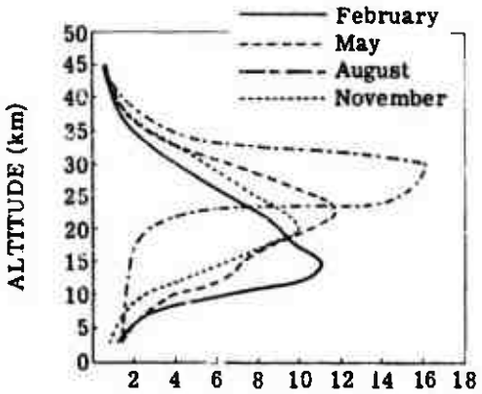

FIGURE 47. SEASONAL VARIATION OF OZONE CONCENTRATION AT FLAGSTAFF [90]

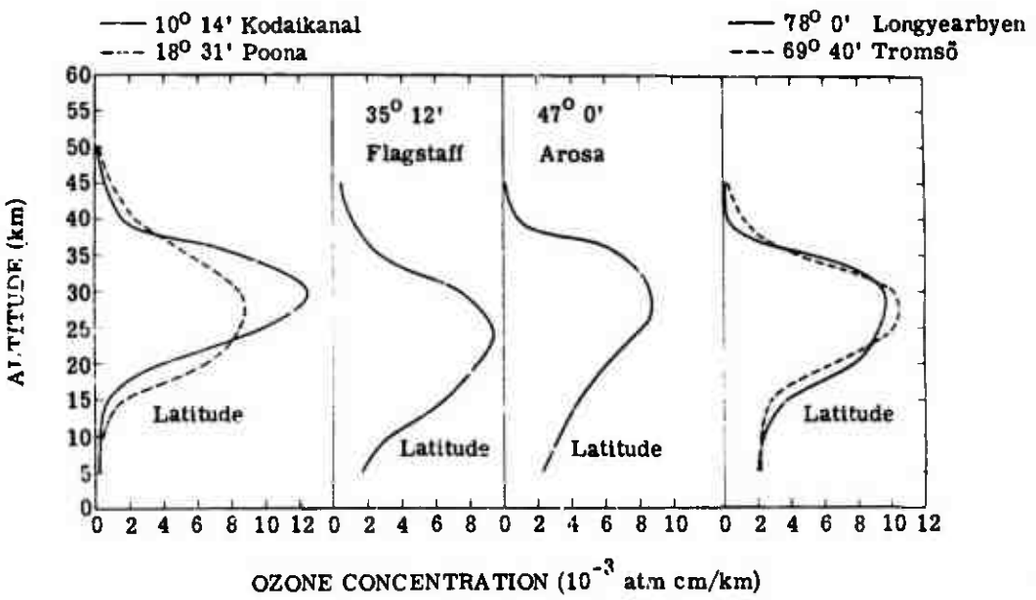

FIGURE 48. LATITUDINAL VARIATION OF OZONE CONCENTRATION [90]

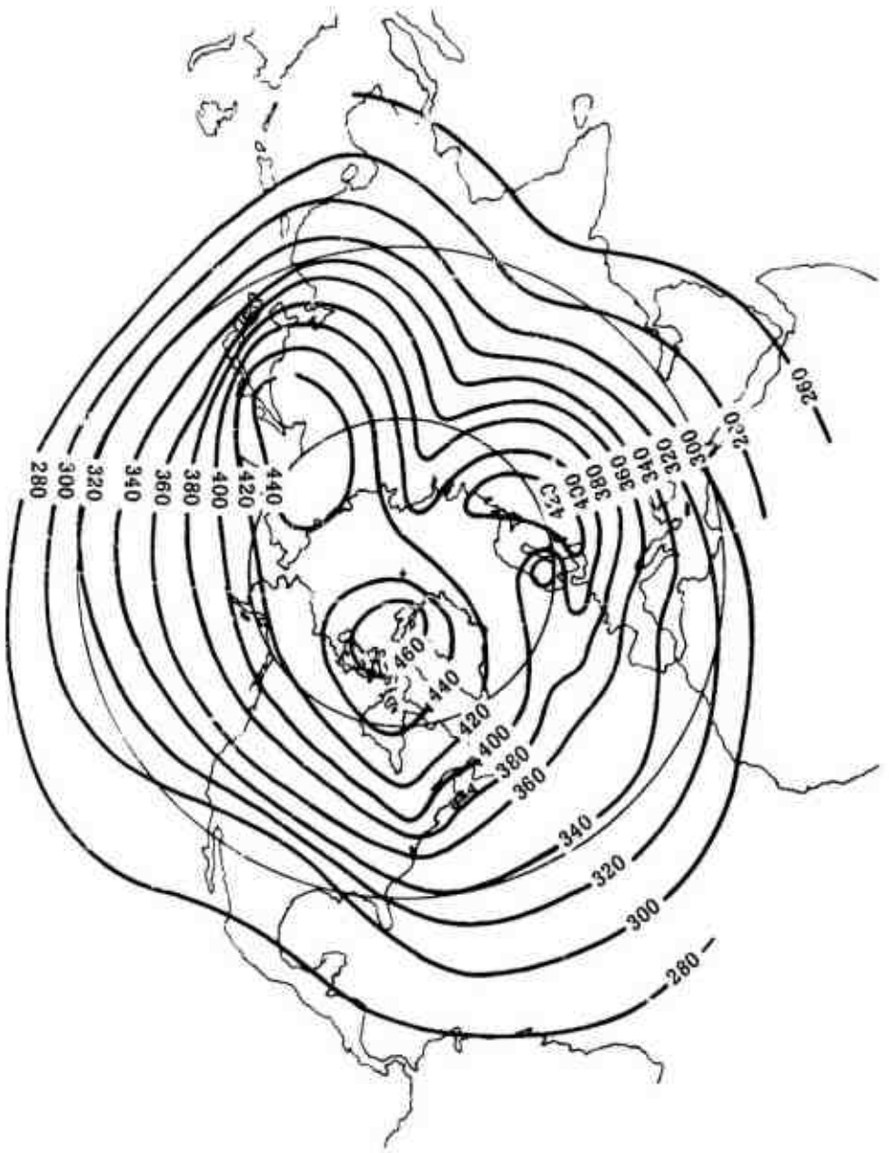

FIGURE 49. AVERAGE DISTRIBUTION OF TOTAL OZONE OVER THE NORTHERN HEMISPHERE IN THE SPRING

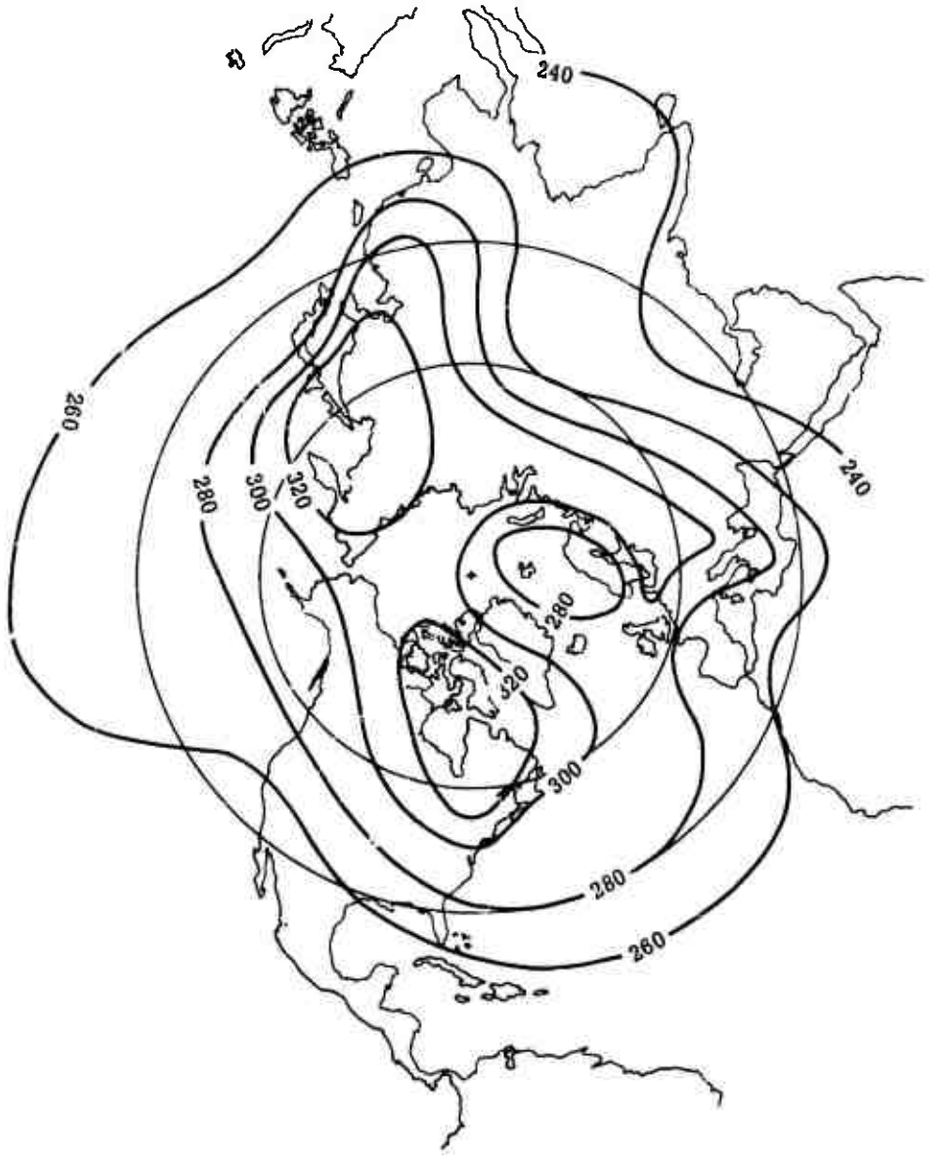

FIGURE 50. AVERAGE DISTRIBUTION OF TOTAL OZONE OVER THE NORTHERN HEMISPHERE IN THE FALL

tropical zone, the variation with season is approximately sinusoidal with a distinct maximum in early spring and a distinct minimum in the fall. The general features of the O_3 distribution conform roughly to the features of the mean circulatory pattern of the lower atmosphere. Larger amounts of O_3 are associated with regions of low pressure and warm temperature above the tropopause.

It can be seen that the typical profile in figure 46 can be adapted for different latitudes by simply shifting the curve right or left so that the area under the curve (with respect to the altitude axis) equals the total vertical O_3 content. To illustrate the procedure, let us assume that one wanted to correct the profile in figure 46 to one which contains 0.42 atm cm of O_3. The curve must now be shifted to the right to include an additional area of 0.07 atm cm. The new curve is presented in figure 51. This method of choosing an O_3 profile will yield results which are reasonably accurate with respect to all the variable conditions.

If a more precise O_3 profile is required it is desirable to consult an extensive measurement program so that a curve more closely aligned with the particular application could be obtained. One such publication of O_3 profiles is the result of an experimental program initiated by the Air Force Cambridge Research Laboratories [118]. A network of eleven ozonesonde stations was established in North America, ranging in location from the Canal Zone in the south to Thule, Greenland, in the north, which produced hundreds of high-resolution observations of vertical O_3 distributions. The reports from this group include O_3 data for both the winter and summer months. Also included are average O_3 distribution for overlapping bimonthly periods.

4.6. WATER VAPOR

Water vapor is the most variable constituent in the atmosphere and compared to other atmospheric gases is probably the most difficult to measure at low temperatures and concentrations. Because of these difficulties and the inaccuracies of the early measurements, the only data that are considered in this review are those from a few of the most recent measurements.

Since air cannot remain in a supersaturate state, the maximum moisture content is temperature dependent. Combining this effect with the effect of evaporation, the previous environment or past history of a given air mass affects the H_2O concentration of that air mass. However, no tenable theory of atmospheric circulation has been able to explain how the history of the air mass determines its H_2O content. As a consequence of the temperature and evaporation effects, the H_2O concentration has a great temporal and spatial variation; and the task of determining a correct H_2O profile for a given season, geographic location, and for a given day therefore

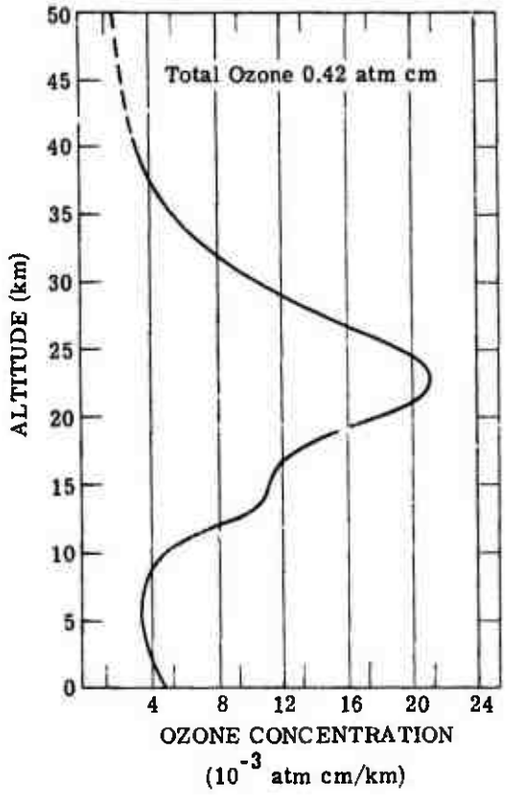

FIGURE 51. SHIFTING OF PROFILE III-1 TO CONTAIN TOTAL OZONE OF 0.42 ATM CM

becomes arduous indeed. The most desirable method would be to take on-the-spot measurements, thereby determining the "exact" profile for that location. This procedure has been done by some researchers, notably Kowall of Lockheed [119], but for the most part this type of measurement would be impractical if not impossible. If the on-the-spot profile is not feasible, a reasonable H_2O profile to use is that which has been taken under approximately the same conditions and for a location consistent with a particular application. Another possibility would be to use an "average" profile (one averaged for all parameters of interest) and to rely upon the fact that the mean error is tolerable.

Available humidity data can be classified conveniently into two altitude ranges: sea level to about 7 km and from that point to 31 km. In this study the average elevation of annual mid-latitude tropopause has been taken as 11 km, in accordance with the standard atmosphere; elevations above 11 km will be referred to as stratospheric and those below 11 km will be referred to as tropspheric.

Up to 7 km where the conventional radiosonde humioity element often functions, a veritable wealth of data exists. Summaries of radiosonde ascents are published as a part of the official publication of various weather services. A reasonably good world-wide sample of data is also published by the U. S. Weather Bureau as part of the CLIMAT reports (Monthly Climatic Data for the World). Low-level humidity data are so plentiful that world-wide maps have appeared for the mid-seasonal months giving the amount of precipitable water from the surface to approximately 5 km [120]. It is important to note, however, that these maps give average H_2O content; they by no means specify the profiles with accuracy on any given day. Even the most casual observer is aware of the day-to-day fluctuations in near-ground-level humidity, but even hour-by-hour changes occur which affect the profile considerably. Shown in figure 52 are low-altitude measurements made by Kowall [119] which indicate deviations of as much as an order of magnitude of H_2O content. Needless to say, no H_2O profile other than an instantaneous on-the-spot one will yield exact compliance with the conditions of a measurement. However, as is seen in figure 52, there are profiles available which give a reasonably close approximation to the average condition and which can be used with reasonable accuracy when direct measurement is not feasible.

Moisture data are scarce above 7 km compared to those at the lower levels. With two exceptions, all stratospheric moisture measurements have been taken unsystematically by individuals and/or organizations interested in the field. These ascents were made sporadically whenever the time, location, funds, etc., were available. Less than 50 such stratospheric ascents have succeeded, and only about 10 have reached or exceeded 31 km. Table 30 lists the

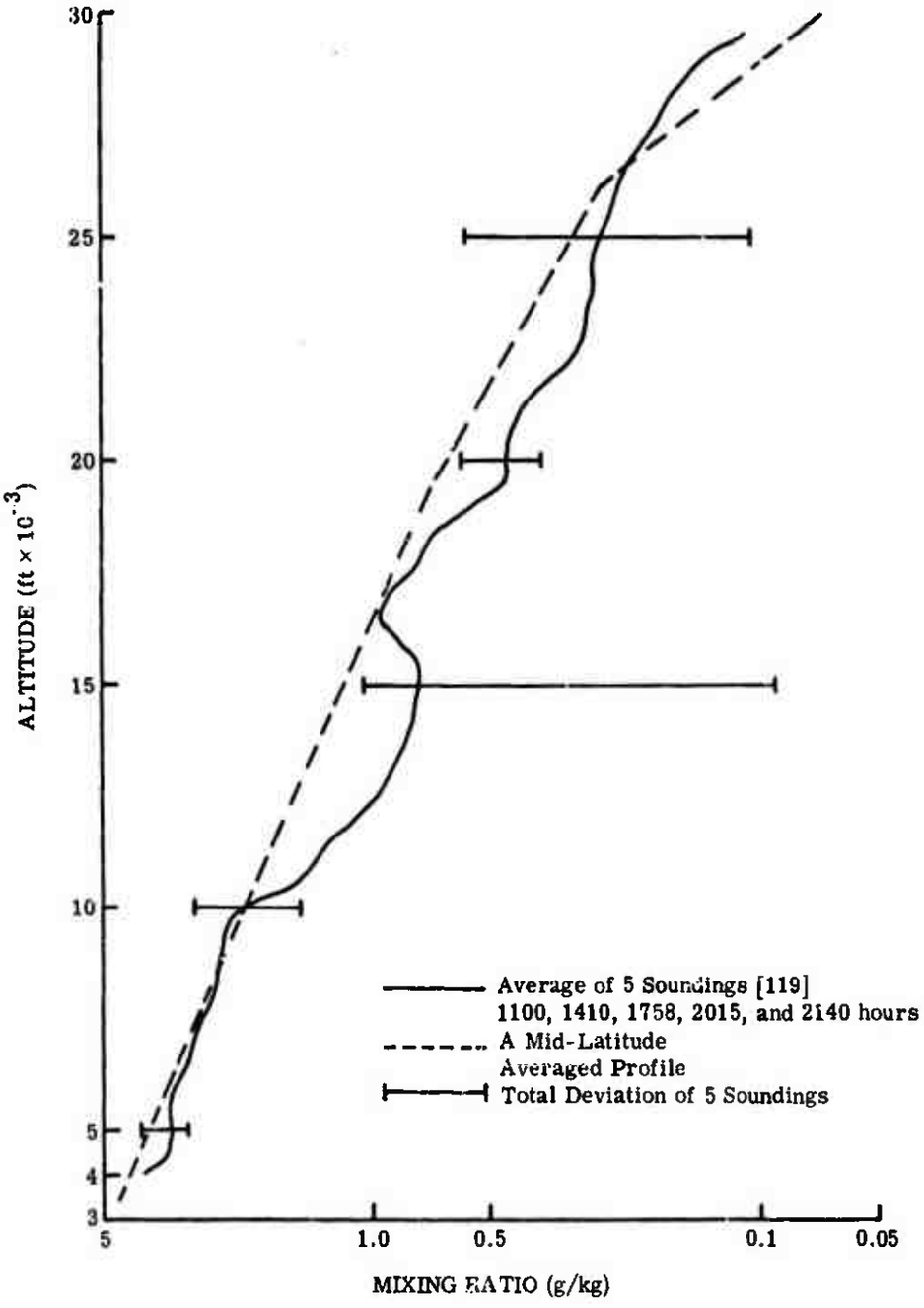

FIGURE 52. VARIATION OF ATMOSPHERIC WATER VAPOR WITH ALTITUDE.
26 October 1964.

TABLE 30. INSTRUMENTS, INVESTIGATORS, AND ORGANIZATIONS RESPONSIBLE FOR NONSYSTEMATIC STRATOSPHERIC HUMIDITY MEASUREMENTS

Instrument	Reference	Organization
Automatic frostpoint hygrometer	Barrett, Herndon, and Carter, 1950 [121]	University of Chicago
Vapor trap	Barclay et al., 1960 [122] Brown et al., 1961 [123]	United Kingdom Atomic Energy Authority (UKAEA)
Automatic frostpoint hygrometer	Brown and Pybus, 1960 [124]	USA Ballistic Research Laboratories (BRL)
Automatic frostpoint hygrometer	Mastenbrook and Dinger, 1960, 1961 [125, 126]	USN Research Laboratory (NRL) and (CBA)
Infrared spectrometer and automatic frost-point hygrometer	Murcray, Murcray, Williams, 1961 [127]	University of Denver
Infrared spectrometer "Sunseeker"	Murcray, Murcray, Williams, 1964 [128]	University of Denver
Molecular sieve	Steinberg and Rohrbough, 1961 [129]	General Mills, Inc.

instruments, principal investigators, and organizations maktng these nonsystematic stratospheric ascents yielding discrete moisture data at given altitudes.

Two sets of more or less systematic probes of stratospheric humidity conditions have been made. The British Meteorological Research Flights (MRF) used manually operated frost-point hygrometers; maximum altitudes reached by the aircraft were about 15 km. Most ascents were over southern England [130], but some were as far away as northern Norway [131] and Kenya [132]. Nearly 400 ascents over southern England, well distributed throughout the year, reached or exceeded 9 km. The Japanese Meteorological Agency (JMA) utilized balloon-borne automatic frostpoint hygrometers at Sappora, Tateno, Hachejoshima, and Kagoshima [133]. On several occasions two ascents were made in one day; on some days soundings were made at two or more stations simultaneously. About 100 ascents reached 9 km; 2 ascents reached 31 km.

Presented in figure 53 are the profiles determined by the authors cited in table 31. Also shown in this figure are the average profiles given by the aforementioned groups who have taken systematic measurements.

The Barrett mean is a nonrigorous average of the original Barrett data derived at The University of Michigan in order to present these data in comparison with the other profiles. Figure 54 shows the original Barrett data. The other mean profiles (i.e., the JMA mean and the NRL mean) were taken from published works. The profiles in figure 53 show a decrease in mixing ratio with altitude to a minimum value several kilometers above the tropopause, the exact altitude differing from researcher to researcher. Above this point the mixing ratio increases to at least 32 km, the highest altitude to which analysis could be extended. Above 32 km most researchers merely use a constant mixing ratio, a method which yields adequate results. The points of greatest disagreement are: (1) the altitude at which the minimum occurs and (2) the magnitude of the mixing ratio at this mintmum. Researchers have reported altitudes of 12 to 18 km for this knee in the curve, with values of between 2×10^{-3} g/kg and 2×10^{-2} g/kg for the mixing ratio of the minimum point. As yet no noncontroversial theory has been advanced to explain the physical mechanism involved, so that no definitive statement can be given to indicate which values to use. Let us simply say that the most recent data [128] indicate the knee at about 16.5 km with a mixing ratio of 2×10^{-3} g/kg.

Since the mixing-ratio data are necessary prerequisites for the calculation of the amount of H_2O in a particular atmospheric path, many authors have found it advantageous to obtain simple functional approximations to a mixing-ratio profile. Figure 55 presents the approximation obtained by Zachor [27]. It can be seen that Zachor, for each profile under consideration,

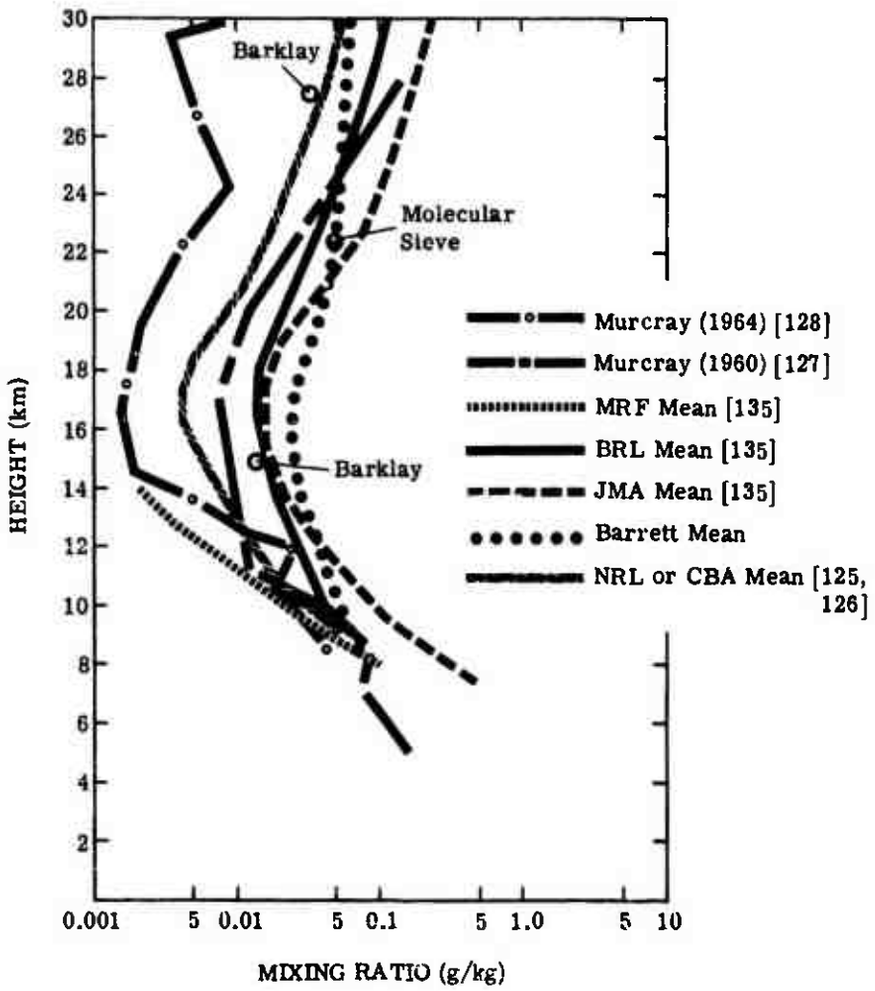

FIGURE 53. WATER VAPOR MIXING-RATIO PROFILES

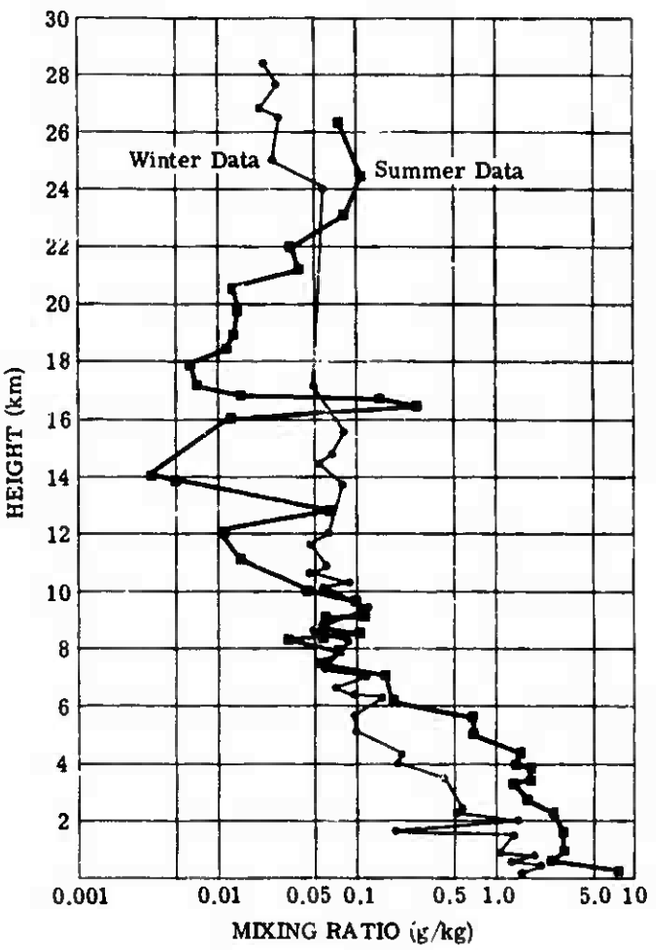

FIGURE 54. SUMMER AND WINTER MIXING RATIOS OF BARRETT [121]

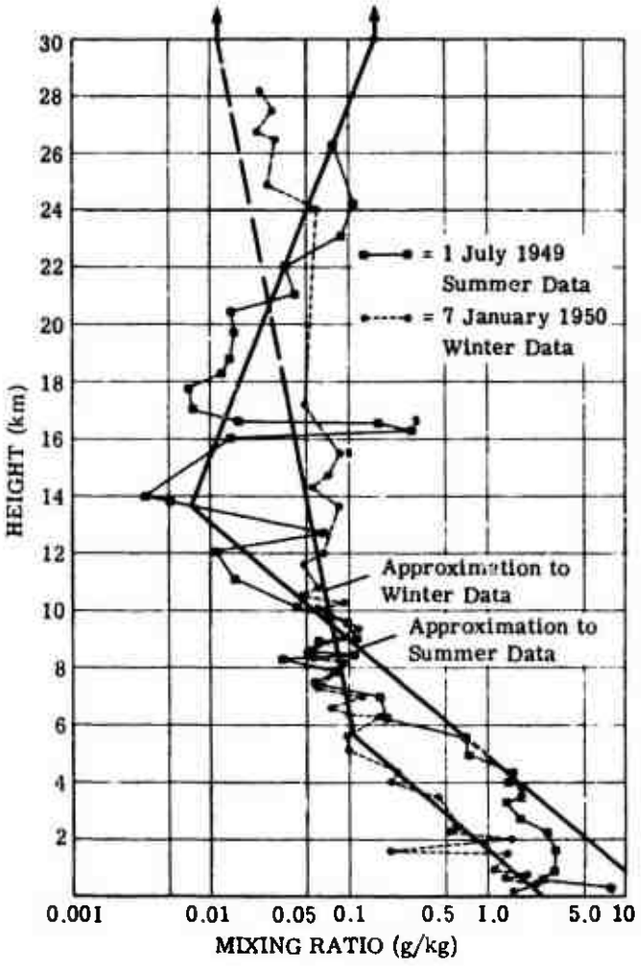

FIGURE 55. ZACHOR'S SUMMER AND WINTER MIXING-RATIO APPROXIMATIONS [27]

used two straight lines to approximate the data of Barrett. Since the data are on a log scale the work became merely a fitting of exponential curves to Barrett's results.

Oppel [134], with his IRMA (Infrared Model Atmospheres) computer subroutine, has provided other convenient models for the H_2O distribution. He derived tropical dry, Arctic dry, and temperate wet approximate H_2O profiles. The basic data Oppel approximated were Gutnick's work for the mid-latitude profile [135] and Mastenbrook's [125] study for the tropical profile. As there have been no Arctic stratospheric measurements, the Arctic model was contrived by specifying the relative humidity at 60% in the troposphere and using a constant mixing ratio of approximately 0.0055 g/kg above the tropopause. Most researchers agree that these are good assumptions. The profiles attained in this fashion are presented in figure 56. It can be seen that Oppel's work cannot be applied to a system where a high degree of accuracy is needed, as his IRMA profiles do not nearly conform to measured data from the altitude of minimum mixing ratio upward. However, because of their simplicity and because they yield somewhat reasonable results, they are very useful in giving thumbnail approximations that may be needed in less critical system applications.

Lindquist [136] at The University of Michigan has also generated an approximate profile, based on the 2.7-μ spectroscopic measurements made by CARDE (Canadian Armament Research Defense Establishment). Lindquist, using wavelength intervals where there is only H_2O absorption, calculated an approximate H_2O profile from the measured transmission values. His results are shown in figure 57. Since the CARDE data were obtained completely over Florida, this profile is characteristic of that particular geographical location. As with Oppel's work, Lindquist predicts a constant mixing ratio at high altitudes which is not in agreement with most researchers.

Gutnick, selecting what he considered to be the most reliable data, has attempted to define an average profile under mid-latitude conditions (fig. 58). Gutnick strove to make his average profile (1) representative of all months or seasons, (2) representative of the climatic types comprising the selected area, (3) based on an unbiased sample, i.e., the selected sample must represent average conditions and not some unusual year or years, (4) physically consistent with known information, e.g., at any altitude, the mean dewpoint cannot be warmer than the mean temperature.

For study of the tropopause, measurements made in Fuknaka (by JMA) and in Washington, D. C. (by CBA), were used in the averaging. In the stratosphere the following data were used for the averaging at 9-, 11-, 14-, 17-, 20-, 26-, 29-, and 31 km levels.

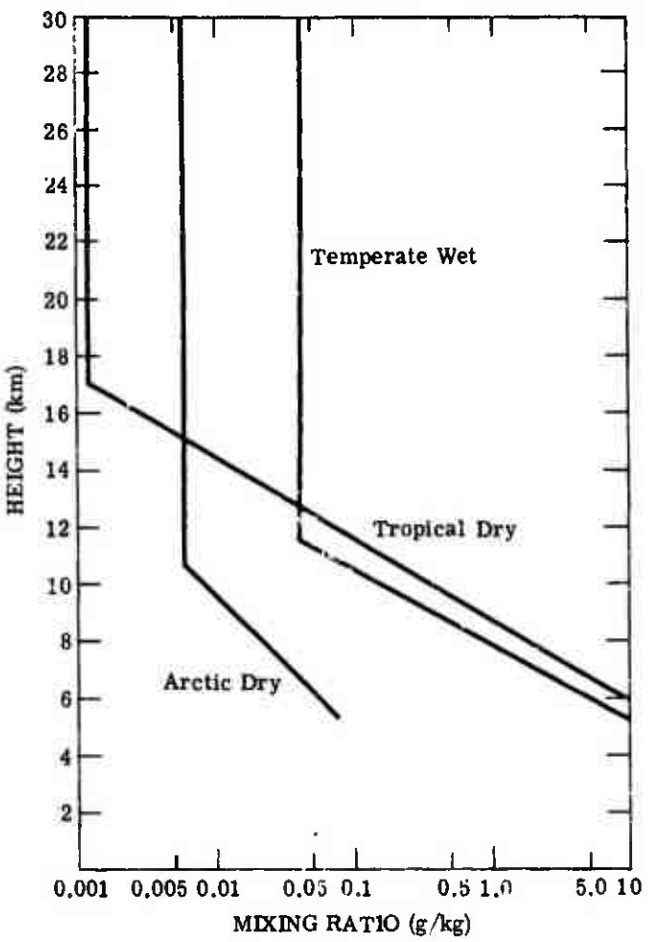

FIGURE 56. IRMA APPROXIMATE WATER VAPOR PROFILES [134]

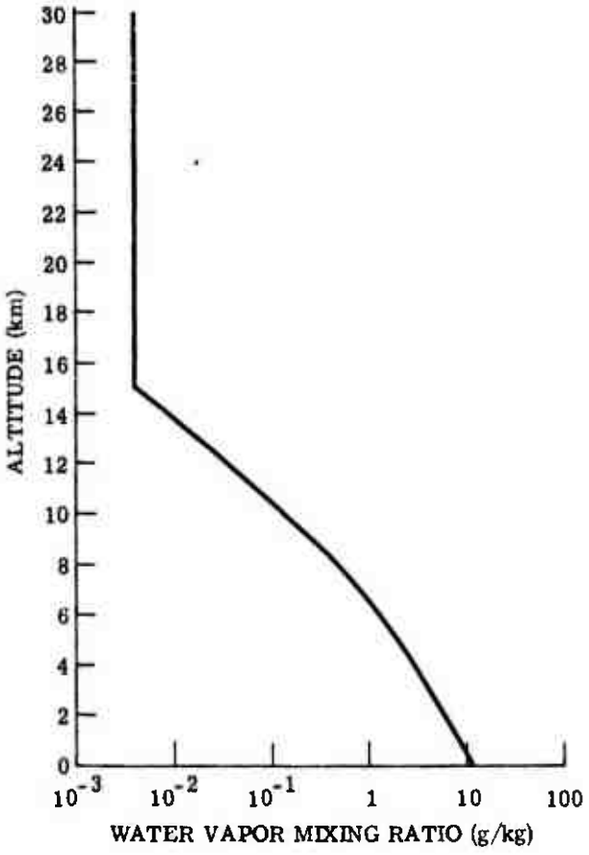

FIGURE 57. AVERAGE WATER VAPOR PROFILE OVER FLORIDA. Current best estimate, obtained from CARDE solar spectra [136].

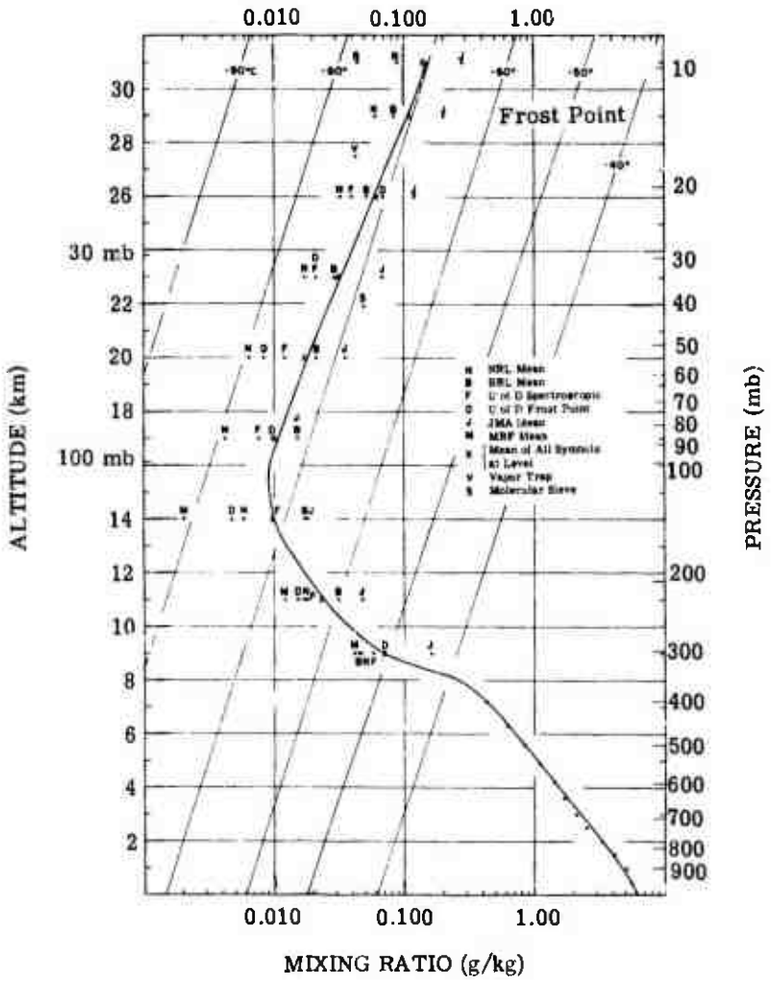

FIGURE 58. GUTNICK'S AVERAGE WATER VAPOR PROFILE [135]

(1) Three NRL profiles of 8 February 1960, 8 April 1960, and 27 June 1960 were selected [126]. All were taken at the NRL Chesapeake Bay Annex (CBA) some 40 miles southeast of Washington, D. C.

(2) Two Ballistic Research Laboratory (BRL) ascents, on 3 April 1960 at Aberdeen, Maryland (unpublished), and 29 April 1960 at Ft. Monmouth, N. J. [137], were selected by Brown and Pybus [124] from their extensive series of nonsystematic moisture ascents, from the Arctic to the Antarctic.

(3) Two University of Denver ascents were chosen: an infrared spectrometer flight on 18 April 1960 and a hygrometric ascent on 1 March 1961, both at Holloman Air Force Base, Alamogordo, N. M. [127].

(4) The UKAEA nitrogen-cooled vapor trap was flown over southern England seven times in the spring or summer of 1958, 1959, and 1960 [123]. Samples were taken at elevations ranging from 24.4 to 30.2 km (mean height 27.5 km).

(5) The General Mills molecular sieve ascent of 15 March 1961 was used, that in which two units were flown at San Angelo, Tex.

(6) JMA data which were carefully screened and therefore very reliable.

(7) The large number of MRF ascents. (The high scientific caliber of the personnel taking the observations and the carefully tested instrumentation made their inclusion a virtual necessity.)

All stratospheric moisture ascents used in the averaging are presented in figure 58. The final average curve was plotted giving equal weight to each of the mixing-ratio values. Note that all the data lie within an order of magnitude of the mean curve.

The mixing-ratio profile shows an almost logarithmic decrease with height from the surface to about 7 km, then a very steep moisture gradient to 9 km. From 9 km the mixing ratio decreases less rapidly to 14 km, then is almost constant to 17 km, reaching its minimum value in this layer. From 17 to 31 km the mixing ratio increases logarithmically with height. Figure 59 shows a surprising comparison between Gutnick's average curve and Zachor's approximation to Barrett's summer profile.

In order to obtain a feeling for the deviation of atmospheric transmission with the change of H_2O profiles, a comparison was made between the transmission spectra from 1 to 10 μ for two paths using two extreme profiles. The profiles were picked by encompassing all the points in figure 58. The results are given in figure 60; the two profiles are designated as HI and LO.

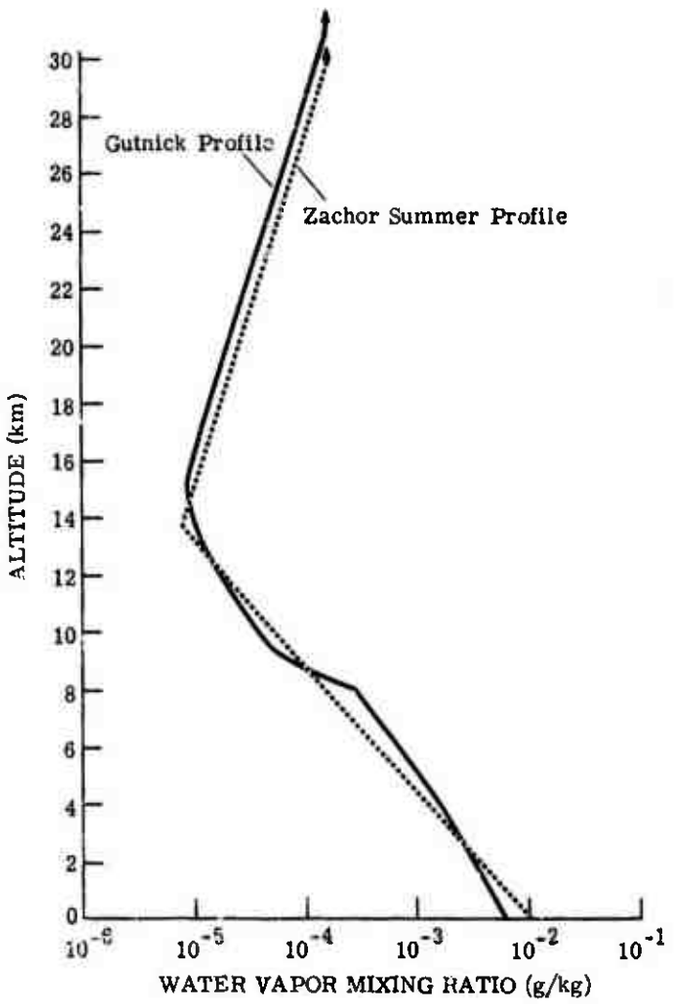

FIGURE 59. COMPARISON OF GUTNICK'S AVERAGE PROFILE TO ZACHOR'S APPROXIMATION OF BARRETT'S DATA

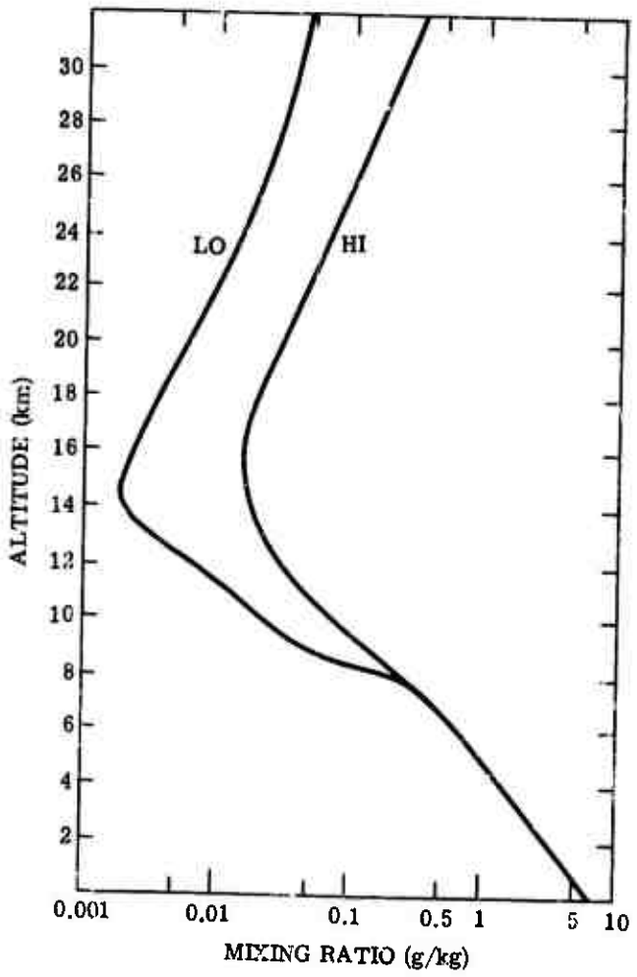

FIGURE 60. MIXING-RATIO PROFILES BOUNDING THE DATA SHOWN IN FIGURE 58

The paths chosen for consideration were (1) a vertical path straight through the atmosphere (0 to 100 km), and (2) a horizontal path at 15.5 km whose range extends approximately 19 km. The second path was chosen to show the maximum deviation of transmission, as it lies at the altitude of approximately the largest spread between profiles HI and LO.

Altshuler's method of computing the transmission was used and therefore it was required to calculate the value of W^* for only two profiles for each path. The results of the investigation proved to be rather enlightening. For the long vertical path W^* was calculated to be 1.392 precipitable cm for HI and 1.387 precipitable cm for LO. With this very small deviation in the W^* values the expected results of small deviation in the transmission was obtained. In fact, the maximum deviation at any point was between 1% and 2% transmission.

When the horizontal path was computed, values of W^* were found to be 6.928×10^{-4} precipitable cm for HI and 9.325×10^{-5} precipitable cm for LO. The transmission was calculated and plotted for each of the two profiles, with the comparison obtained shown in figure 61. As can be seen in the figure, the maximum difference between the curves is about 18%. This large difference, however, only manifests itself in the center of the very strong H_2O absorbing bands at 2.7 μ and 6.3 μ. Otherwise, the two curves seem to compare very well.

It can be inferred by these comparisons that for nearly vertical paths of any range, the transmission is not critically dependent on the H_2O profile selected. However, when long slant paths at large zenith angles or nearly horizontal paths are under consideration, more care must be taken in the selection of a profile; especially, if data are required near the strongly absorbing 2.7- and 6.3-μ bands.

SUMMARY

Since the H_2O distribution has a significant temporal and spatial variation, choosing a published H_2O profile to use for a particular application is a nonexact process. For high-altitude paths, above 20 km, Gutnick's profile or Zachor's summer profile probably will yield the best results. At above 20 km their profiles are very representative of the decrease in concentration of water vapor with increasing altitude. For altitudes of between 10 and 20 km, near the bend in the profile, the most recent measurements [128, 138] indicate the use of a profile whose minimum concentration is approximately 2×10^{-3} g/kg. Murcray's 1964 profile and the MRF data then would be the best to use. As for low-altitude paths, below 10 km, almost any profile can be used, yielding as good results as can be expected.

The moisture profiles presented herein undoubtedly will yield better data as the state of the art advances. This is especially desirable as there is still a question as to the exactness

of the stratospheric data. However, despite the limitations, it appears that the present knowledge of the H_2O distribution will be sufficient until the expected revisions appear.

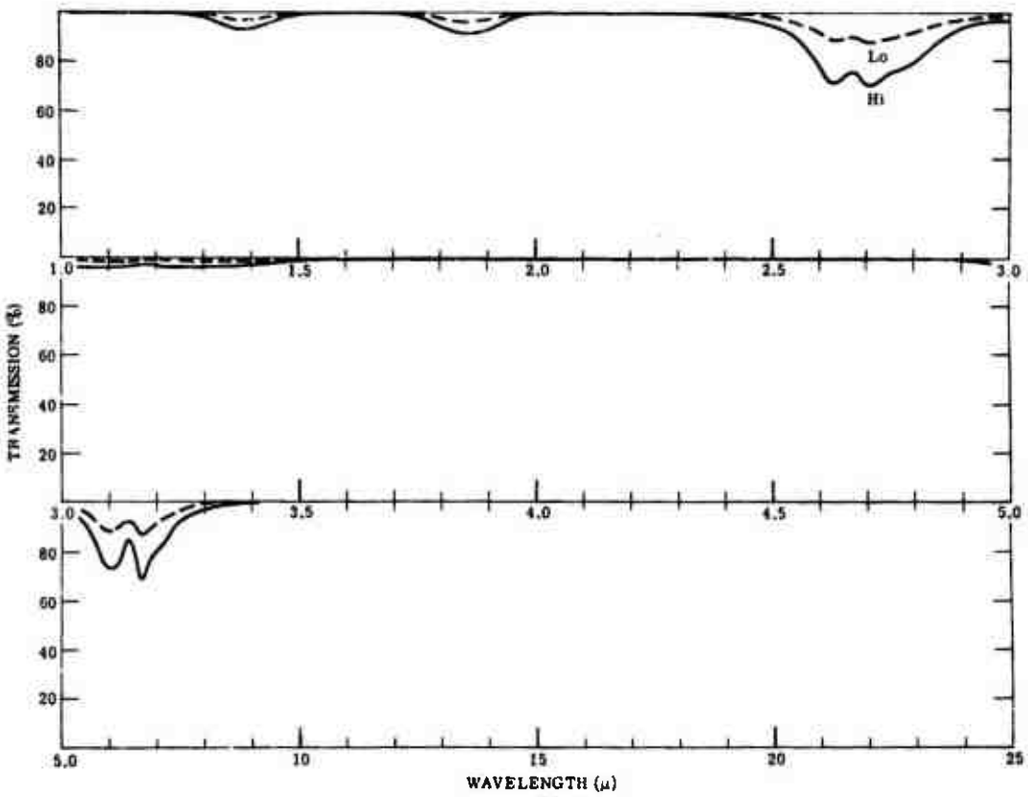

FIGURE 61. COMPARISON OF SPECTRA FOR HORIZONTAL PATH 19 KM LONG AT 15.5-KM ALTITUDE. Each spectrum was computed for the respective profile shown in figure 60.

5
SUMMARY OF OPEN-AIR FIELD MEASUREMENTS OF ABSORPTION SPECTRA

As was mentioned in section 3.14, perhaps the best approach to evaluating the quality of methods for computing atmospheric absorption based on band models is a direct comparison of computed atmospheric attenuation spectra with spectra obtained from open-air measurements. In an attempt to facilitate such comparisons in this report, a bibliography was assembled which represents a reasonably complete listing of the measurements that have been made which were reduced to absolute values of absorption versus wavelength. Table 31 presents a summary of the measurements included in this bibliography. Such pertinent information as path description, spectral region considered, resolution, and instrumentation is included in order to give the researcher a basis for selecting open-air data to be used for comparison with spectra computed by any of the methods presented in section 3.

TABLE 31. SUMMARY OF OPEN-AIR FIELD MEASUREMENTS OF ABSORPTION SPECTRA

Researcher	Path Data	Spectral Region	Resolution	Instrumentation	Comments
Taylor and Yates [42, 139]	3 horizontal sea level paths. Ranges: 0.3, 5.5, and 16.25 km. 1 slant path 27.7 km in range from 9.3 to 11.1 kft in altitude	0.5-15 μ for 0.3-km path 0.5-25 μ	$\lambda/\Delta\lambda \approx 300$ with the 0.3-km path at 1-2 cm^{-1}	Unmodulated source, Perkin-Elmer monochromator with LiF prism 0.5 to 5.5 μ, Perkin-Elmer 12-c spectrometer with NaCl prism 5-16 μ	(1) Path parameters obtainable from reference. (2) Scattering was present.
Gebbie et al. [82, 33]	2 horizontal paths approximately 100 ft above sea level. Ranges: 2264 and 4476 yd	1-14 μ	≤0.02 LiF ≤0.1 NaCl	Chopped source, single autocollimating spectrometer. Prism: 1-5.5 LiF 5.5-14 NaCl	(1) Path parameters obtainable from reference. (2) Fair quantity of scattering was present.
Cumming et al. [140]	126 solar spectra. Taken from 0.12 to 13.7 km. Zeniths: 6°-91.3°	3500-4000 cm^{-1} 8 with spectra 3000-4000 cm^{-1}	0.76 to 2 cm^{-1}	Sun seeker airborne Perkin-Elmer 99-G double monochromator with grating	(1) Path parameters obtainable from reference. (2) Paths presented are from 10.7, 12.2, and 13.7 km in altitude. Not all spectra are presented in reference.
Farmer et al. [141]	4 horizontal paths at 5.2 km altitude. Ranges: 0.777, 1.486, 1.909, and 6.4 km	3.5-5.5 μ	0.001 to 0.01 μ	Grating spectrometer with an f/6 input	Path parameters obtainable in reference.
Berlinquette and Tate [142]	3 horizontal paths at 6 m above sea level. Ranges: 0.27, 0.87, and 1.2 km	0.8-5.9 μ	$\lambda/\Delta\lambda$ variable from 100-1100	Chopped source with Perkin-Elmer 12-c spectrometer	(1) Path parameters obtainable in reference. (2) Since it took 2.5 hr to scan the wavelength spectrum, the data are functions of variable H_2O concentration.

TABLE 31. SUMMARY OF OPEN-AIR FIELD MEASUREMENTS OF ABSORPTION SPECTRA (Continued)

Researcher	Path Data	Spectral Region	Resolution	Instrumentation	Comments
Markle [143]	Solar spectra taken from 10-14 km. Zeniths: 48°-89°	2.3-? μ	~0.03 μ	Airborne sun seeker, Perkin-Elmer 103 monochromator with LiF prism	
Murcray et al. [144, 145]	13 slant paths, from ground to altitudes 1.2 to 22.8 km. Zeniths: $1.75 \leq \sec\theta \leq 2.81$	2800-5100 cm^{-1}	10 cm^{-1}	Balloon-borne, single-pass Littrow spectrometer with LiF prism	In reference 145, measurements were also indicated in 6.3-μ region; however, they were not published.
Murcray et al. [146, 147]	Solar spectra taken from 8.4-30.9 km	1400-2600 cm^{-1}		Balloon-borne Ebert grating spectrometer	Only a small number of spectra taken were published.
Murcray et al. [148]	138 solar spectra taken from 0-31 km. Zeniths: $1.37 \leq \sec\theta \leq 3.04$	2.4-3.0 μ	0.5-0.7 μ	Balloon-borne Czerny Turner grating spectrometer	
Elliott et al. [78]	2 horizontal paths. Ranges: 1000 and 2000 yd	1-5 μ	0.035-3 μ	Single NaCl prism monochromator	Path parameters obtainable in text.
Kyle et al. [148]	30 solar spectra taken from altitudes 10.7 - 32.5 km. Zeniths: $14.65 \leq \theta \leq 44.72$	2240-2400 cm^{-1}	0.5 to 0.7 cm^{-1}	Double-pass Czerny Turner grating spectrometer with a sun seeker	

6
SUMMARY OF LABORATORY MEASUREMENTS OF HOMOGENEOUS-PATH SPECTRA

As was mentioned in section 2.3, deriving a method for the computation of atmospheric absorption spectra entails empirically fitting a band-model function to a collection of homogeneous absorption spectra. Table 32 presents the results of researchers who have published the main body of competent laboratory measurements of absorption spectra, including the information necessary to facilitate choosing the best data for a given application.

The purpose of the table is twofold. First, it is intended for those who wish to perform their own empirical fits of existing band-model functions to laboratory data, or to empirically fit newly derived transmissivity functions. Second, it is intended for those who wish to see whether or not a particular method based on a band model is consistent with the slant paths under consideration (i.e., to ensure that the slant-path absorber concentrations are bounded by the laboratory data). In choosing a particular set of data one is referred to the suggestions in section 2.3, with emphasis on one particular point. To obtain best results, the ranges of absorber concentration and equivalent pressure specified for the laboratory data should encompass the intended range of W and P for which the researcher intends to calculate atmospheric transmission.

It can be observed from table 32 that only three authors, Howard, Burch, and Walshaw, present data of sufficient range of W and P that they can be used in a fitting procedure. In fact, for a great many applications, even their data are of questionable utility. For instance, a slant path at a zenith angle of 60° extending through the entire atmosphere contains approximately 30 pr cm H_2O reduced to STP. In the table, however, it is seen that no researcher has carried out measurements with samples of H_2O in excess of about 4 pr cm. Therefore, to predict absorption for such a path by a band-model method based on these laboratory data would require extrapolation of the data, which in general yields poor results. It would be desirable to obtain further laboratory measurements, particularly those measurements containing a large amount of absorber, for a broad range of equivalent broadening pressures. However, because the present state of the art is inadequate in this area, the researcher must content himself with the available data until further measurements are performed.

There is one final recommendation for those who wish to use the data cited in this section for performing empirical fits. Although the referenced works present curves that can be used directly, it is suggested that an attempt be made to secure better representations of the data by directly contacting the people involved in taking the laboratory measurements.

TABLE 32. SUMMARY OF LABORATORY MEASUREMENTS OF HOMOGENEOUS-PATH ABSORPTION SPECTRA

Gas	Band (μ)	Observed Interval	Range of Pressures* (mm Hg)	Range of Absorber, W**	No. of Curves	Resolution† (approx.)	Researchers
CO_2	1.6 & 1.4	8000-7200	75-760	540-8100	13	0.12	Howard et al. [30]
	2.0	4500-5400	10-760	108-8630	32	0.9 μ	Howard et al.
	2.7	3300-4100	1-755	11-1619	67	0.07 μ	Howard et al.
	2.7	3450-3850	14.2-2065	0.164-24.4	32	10-15 cm^{-1}	Burch et al. [1]
	4.3	2200-2450	3.8-2115	0.0108-22.8	53	5-10 cm^{-1}	Burch et al.
	4.3 & 4.8	2000-2500	1-735	9-1570	43	0.1 μ	Howard et al.
	4.3	2250-2450	38-780	1.0-300	10	10 cm^{-1}	Bradford [56]
	5.2	1800-2000	10-735	104-1570	9	0.1 μ	Howard et al.
	9.398 & 10.41	900-1100	103-3800	48-11,200	25	5-10 cm^{-1}	Burch et al.
		720-875	103-3800	305-11,200	14	5-10 cm^{-1}	Burch et al.
	15	500-900	20-745	1-863	37	0.5 μ	Howard et al.
		495-875	0.26-3190	0.0118-2470	30	5-10 cm^{-1}	Burch et al.
H_2O	1.1	8250-9500	9.8-740	0.03-1.93	41	0.13 μ	Howard et al.
	1.38	6500-8000	3-740	0.026-3.85	62	0.12 μ	Howard et al.
	1.875	4000-8000	3-740	0.028-3.85	62	0.1 μ	Howard et al.
	1.875	4950-5800	27.5-872	0.0033-0.101	14	20 cm^{-1}	Burch et al.
	2.7 & 3.2	2800-4400	2-750	0.017-2.1	114	0.07 μ	Howard et al.
	2.7	3000-4300	27.5-882	0.0033-0.101	5	20 cm^{-1}	Burch et al.
	6.3	1000-2200	2.5-742	0.021-1.49	80	0.4 μ	Howard et al.
	6.3	1200-2200	14.0-805	0.0041	15	8 cm^{-1}	Burch et al.
H_2O		200-500	0.78-600	0.0041-0.143		5-10 cm^{-1}	Palmer [43]
O_3	9.6	1000-2560	11.2-744	0.00278-1.968		7 cm^{-1}	Walshaw [34]
CO	4.866	2000-2250	1-3210	0.00096-22.2	147	25 cm^{-1}	Burch et al.
	2.347	4100-4400	54-756	36.6-1140	26	15-20 cm^{-1}	Burch et al.
CH_4	3.311	2700-3200	2-3085	0.015-188	88	25 cm^{-1}	Burch et al.
	6.452 & 7.657	1100-1800	3.8-3050	0.026-188	86	10 cm^{-1}	Burch et al.
N_2O	4.0	2400-2650	22.4-746	0.38-18.6	8	20 cm^{-1}	Burch et al.
	4.5	2100-2300	1.0-3120	0.00016-76.4	177	25 cm^{-1}	Burch et al.
	4.5	2100-2300	99.8-849	0.01-2.3	65		Abels [150]
	7.78 & 8.57	1100-1400	3.2-3035	1.37-46.7	11	10 cm^{-1}	Burch et al.
	14.45 & 18.98	500-800	4.5-851	1.89-359	7	6 cm^{-1}	Burch et al.

* Pressure designated is generally the equivalent pressure.
** W is expressed in precipitable centimeters for H_2O and in atmospheric centimeters for the other gases.
† Resolution specified is ordinarily center-band resolution and is used only to give an approximate designation.

7
COMPARISON OF ATMOSPHERIC MOLECULAR ABSORPTION SPECTRA

In this section, molecular absorption spectra computed by each of the methods presented in section 3, except that of Elder and Strong, are compared with slant-path field measurements of absorption and with absorption spectra calculated by the rigorous method. Absorption spectra were also computed by each of the band-model methods for five atmospheric paths common to many infrared applications; these data were plotted on a common graph. The comparisons presented are indicative of both the degree of "spread" in the data and the accuracy with which "computed spectra"* can approximate the true absorption spectra for an atmospheric path.

7.1. COMPARISON OF COMPUTED SPECTRA WITH SPECTRA MEASURED BY TAYLOR AND YATES

Figures 62 and 63 are comparisons of measured and computed spectra for a 1000-ft, horizontal, sea-level path. The measured data were recorded by Taylor and Yates [42] using a Model 83 Perkin-Elmer monochromator with a lithium fluoride prism for the region from 1.0 to 5.5 μ and a Model 12-C spectrometer with a sodium chloride prism for the region from 5 to 16 μ. The average resolution of the measured data, $\lambda/\Delta\lambda$, is about 300.

For this path only CO_2 and H_2O contribute significantly to absorption. Nitrous oxide absorption is observable at approximately 4.5 μ but is only a minor contributor. The concentration of H_2O was determined by Taylor and Yates from average values of temperature, pressure, and relative humidity measured along the path. The atmospheric centimeters of CO_2 and N_2O were calculated assuming mixing ratios of 320 and 0.28 ppm, respectively. The effective broadening pressure for all gases was taken to be 760 mm Hg. Using the path parameters noted on figures 62 and 63, we calculated the absorption spectra by each of the methods of section 3; the results are superposed on the Taylor and Yates spectra. Nitrous oxide absorption was computed only by the methods of Oppel, Green and Griggs, and Altshuler since the other researchers did not develop transmissivity functions for this gas.

A cursory examination of figures 62 and 63 shows that the comparison is better in some spectral regions than in others, but in general the spread in the data is rather large. The best general agreement of the various spectra is displayed in the spectral region from 2.5 to 3.0 μ and the greatest divergence is noted from 4.5 to 5.0 μ.

*The term "computed spectra" refers to spectra computed by the methods of section 3 and is not to be confused with the rigorous calculation.

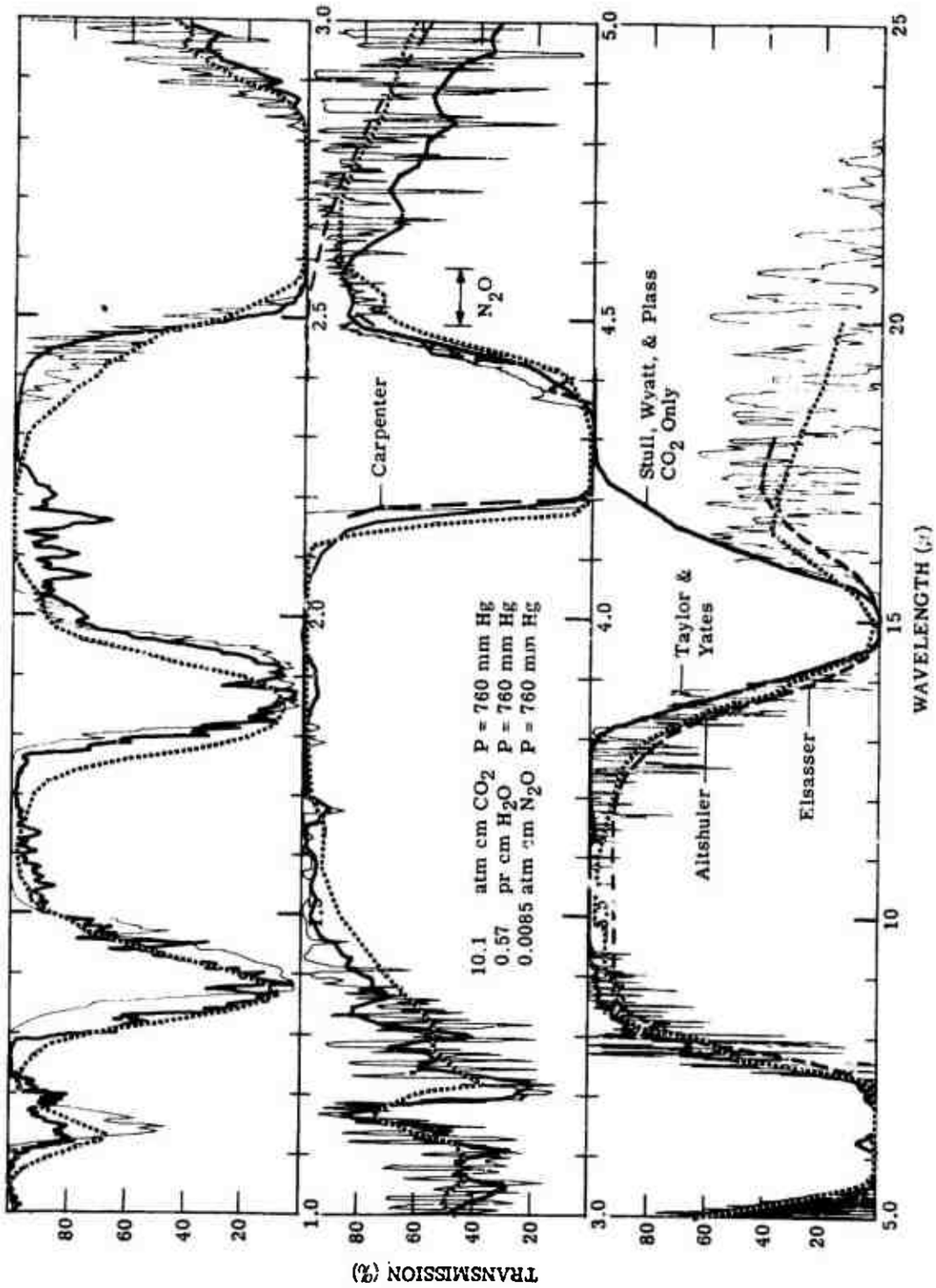

FIGURE 62. COMPARISON OF MEASURED SPECTRA OF TAYLOR AND YATES WITH COMPUTED SPECTRA OF ALTSHULER; ELSASSER; STULL, WYATT, AND PLASS; AND CARPENTER

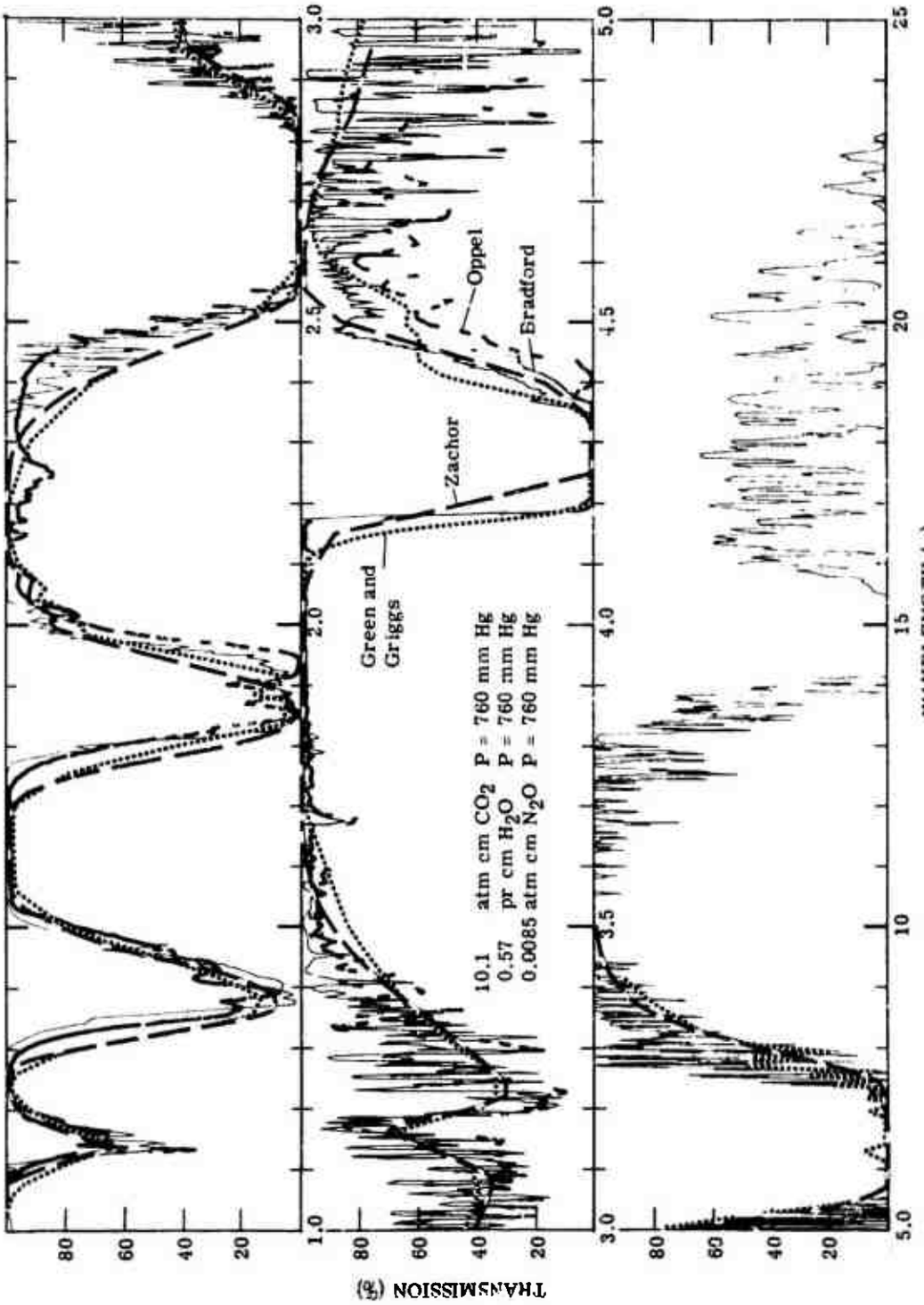

FIGURE 63. COMPARISON OF MEASURED SPECTRA OF TAYLOR AND YATES WITH COMPUTED SPECTRA OF BRADFORD; GREEN AND GRIGGS, OPPEL; AND ZACHOR

Unfortunately, no single method yields results that compare with the measured data for the entire spectral interval displayed; however, each method compares well for certain intervals. For example, the results of Oppel are in extremely close agreement with the data of Taylor and Yates from 2.5 μ to the center of the 4.3-μ band but are in relatively poor agreement from 4.4 μ to 5.0 μ. Oppel's data agree reasonably well for each of the three short-wavelength H_2O bands but indicate H_2O absorption centered at 2.5 μ that is not present in the measured data or other computational methods. Stull et al. show H_2O absorption at slightly shorter wavelengths (approximately 2.1 μ) that is stronger and has a different spectral character. Stull's results for this region also are not in agreement with other sources of data. The reasons for these differences are not known at the present time.

After careful examination of the figures, similar general observations can be made concerning any one of the many methods. A critical analysis of the reasons for a particularly good agreement or a poor agreement for a given method is difficult to perform because of the many variables involved in its development. However, a general disagreement between measured and computed spectra can in some instances be attributed to the laboratory data used in the development of the computational method selected. In certain cases the disagreement can be attributed specifically to the laboratory data. For example, for the three H_2O bands centered at 1.14, 1.38, and 1.88 μ, respectively, there is noted a spectral shift between the measured data and the spectra computed by the methods of Altshuler, Zachor, and Green and Griggs. The spectra of these researchers are consistent with the laboratory data used to specify the spectral absorption coefficients—each used the data of Howard et al.—therefore, the disagreement is attributed to differences in two sets of measured data, that obtained by Howard and that obtained by Taylor and Yates. Most researchers are in general agreement that the spectra of Taylor and Yates are spectrally correct for all three H_2O bands, and Oppel has shifted his results an appropriate amount to achieve a better spectral agreement for these bands.

The comparison presented in figures 62 and 63 indicates that through a proper choice of computational methods for each of the respective absorption bands a single spectrum could be computed which is in very good agreement with the measured data of Taylor and Yates.

The spectra previously discussed demonstrate, to a limited extent, the type of comparison obtainable for each of the absorption bands throughout that portion of the infrared spectrum of interest to the infrared researcher. (The only band that was not represented is the 9.6-μ O_3 band since O_3 does not exist in sufficient quantity at sea level to cause an observable amount of absorption for a 1000-ft path.) It would indeed be enlightening if extensive comparisons

could be made between measured and computed spectra for the entire spectral interval for a variety of absorber concentrations and equivalent pressures. Unfortunately, measured data of such extent do not exist to facilitate such comparisons. The experimentalists have confined their extensive field-measurement programs almost exclusively to the measurement of spectra for only the central portion of the 2.7-μ and 4.3-μ bands. Therefore, comparison between computed and measured spectra of reasonable extent could be made only for these spectral regions. Future measurement programs will hopefully be concerned with the other bands and the window regions.

7.2. COMPARISON OF COMPUTED SPECTRA WITH THE RIGOROUS CALCULATION FOR THE 2.7-μ H_2O BAND

To emphasize the appearance of H_2O computed spectra for the 2.7-μ band under conditions of high resolution, comparisons of spectra calculated by the rigorous method were made with computed spectra for two homogeneous paths which contained H_2O as the only absorber. The spectral region for which the comparisons were made extends from 2.5 μ to approximately 2.86 μ.

Gates et al. [7] calculated the H_2O absorption spectra at infinite resolution by summing the contribution to absorption of approximately 4500 lines. These spectra were then degraded to a lower resolution by scanning the spectra with a triangular slit function which is given by $S(\nu) = a - |\nu - \nu_1|$ where $a = 1.0\ cm^{-1}$ is one-half the spectral slit width. Spectra were computed by each of the band-model of section 3 methods and superposed on the Gates data. The results are presented in figures 64 through 75. The absorber concentration used in calculating the spectra presented in figures 64-69 is approximately that amount of H_2O which would exist in a sea-level path 1 m long with the relative humidity equal to 50%. For the same atmospheric conditions, the equivalent path length for the spectra presented in figures 70-75 would be 10 m long. To further aid the comparison of the two sources of data, the Gates spectra were smoothed to a resolution approximately equal to the resolution of each respective computed curve.

After a cursory examination of the data presented in these figures it becomes obvious that the spectra computed by the band-model methods are of very low resolution when one notes the extremely fine structure inherent in H_2O molecular absorption. The resolution of the band-model spectra ranges from approximately 40 cm^{-1} for the methods of Altshuler, Howard et al., Green and Griggs, and Lindquist, to approximately 10 cm^{-1} for Oppel's method. Theoretically, the resolution of band-model methods for H_2O is limited to a spectral interval which contains a sufficient number of lines to cause the infinite product of the statistical model to converge

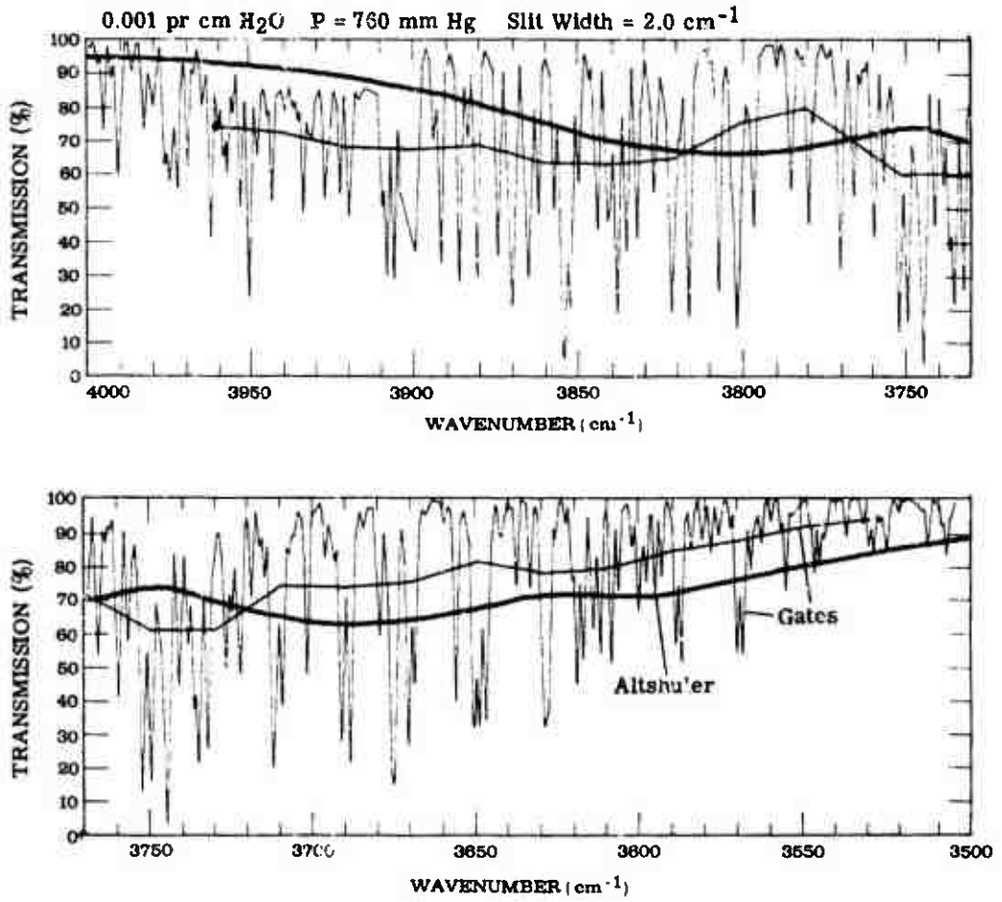

FIGURE 64. COMPARISON OF CALCULATED (RIGOROUS) SPECTRA OF GATES WITH COMPUTED SPECTRA OF ALTSHULER. Resolution of smoothed Gates curve is 40 cm^{-1}.

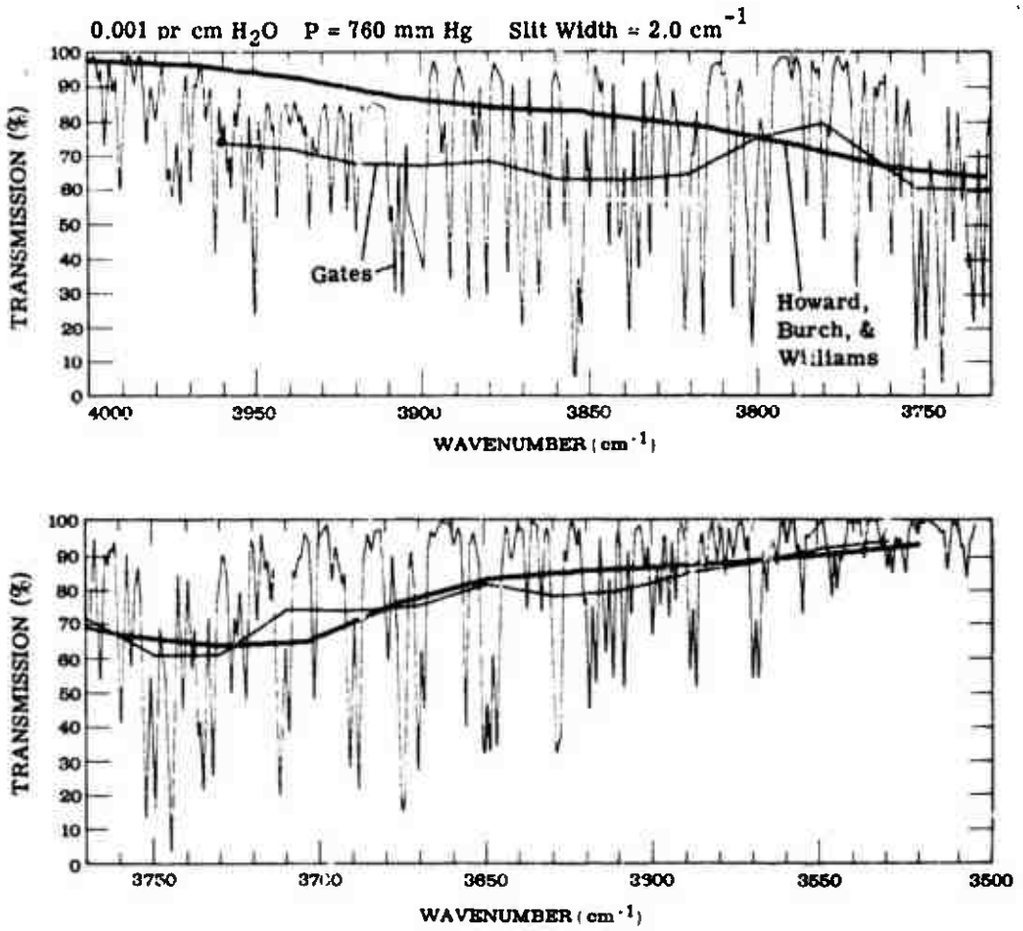

FIGURE 65. COMPARISON OF CALCULATED (RIGOROUS) SPECTRA OF GATES WITH COMPUTED SPECTRA OF HOWARD, BURCH, AND WILLIAMS. Resolution of smoothed Gates curve is 40 cm^{-1}.

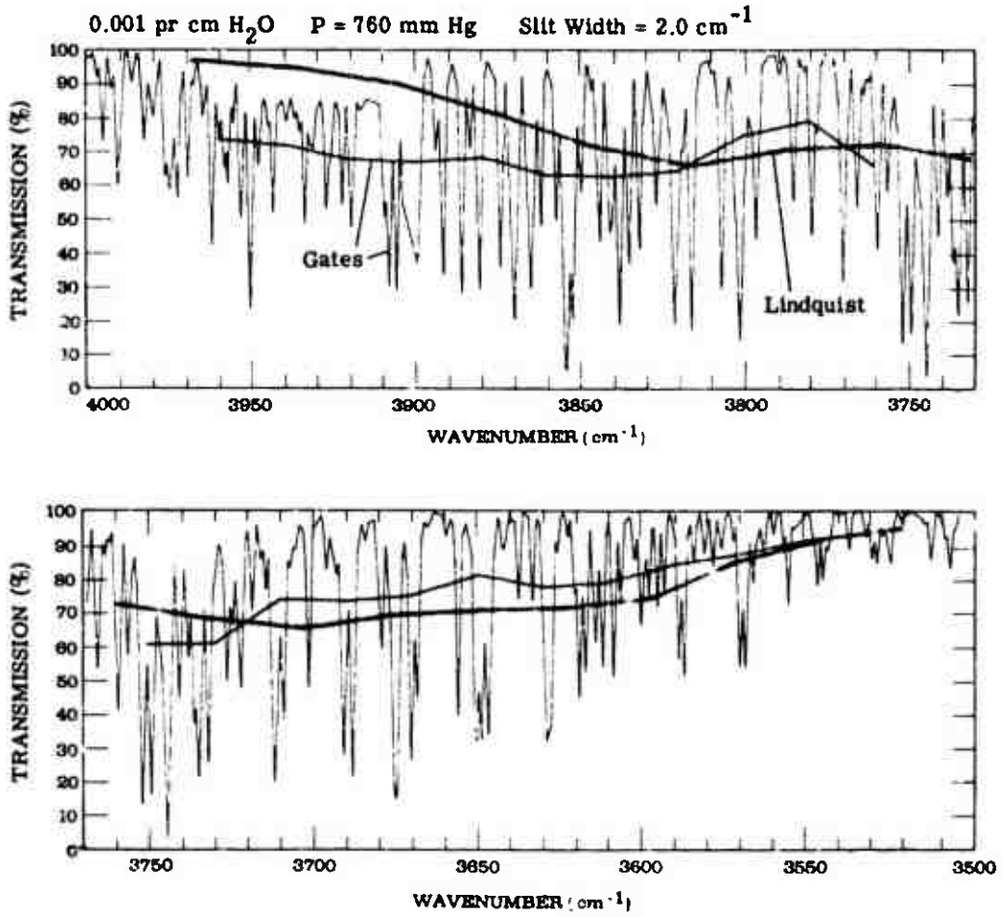

FIGURE 66. COMPARISON OF CALCULATED (RIGOROUS) SPECTRA OF GATES WITH COMPUTED SPECTRA OF LINDQUIST. Resolution of smoothed Gates curve is 40 cm^{-1}.

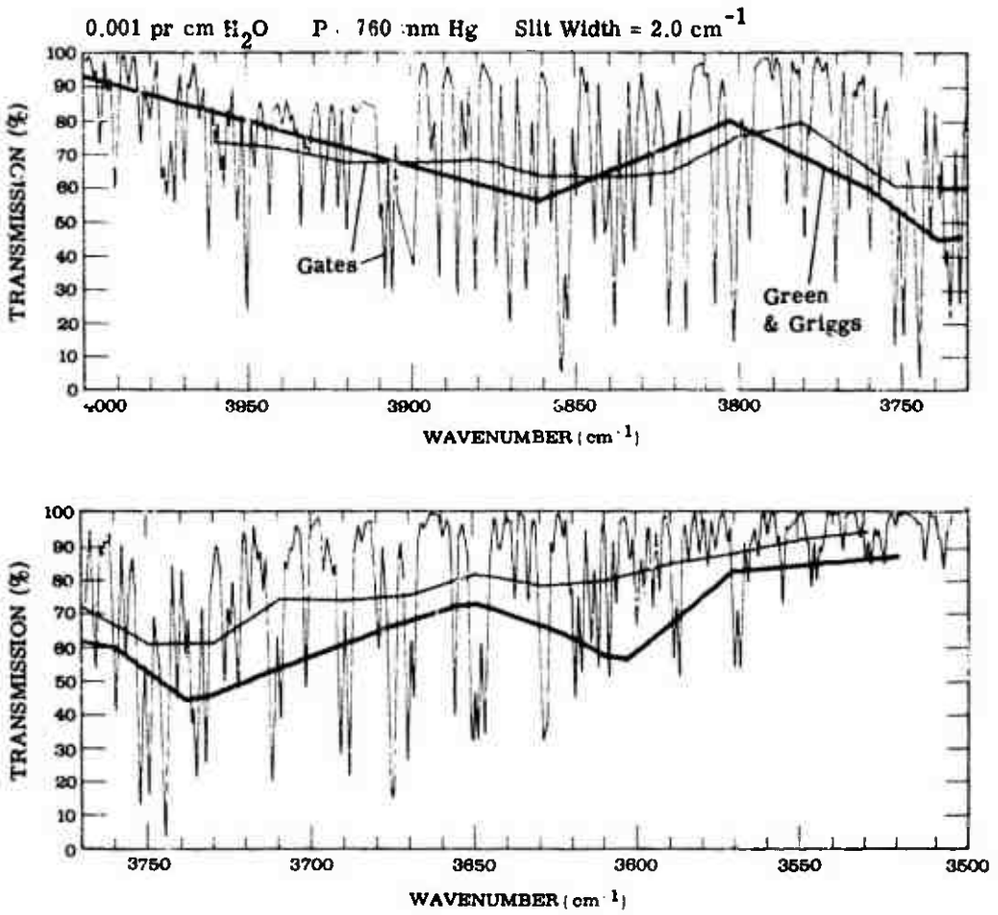

FIGURE 67. COMPARISON OF CALCULATED (RIGOROUS) SPECTRA OF GATES WITH COMPUTED SPECTRA OF GREEN AND GRIGGS. Resolution of smoothed Gates is 40 cm^{-1}.

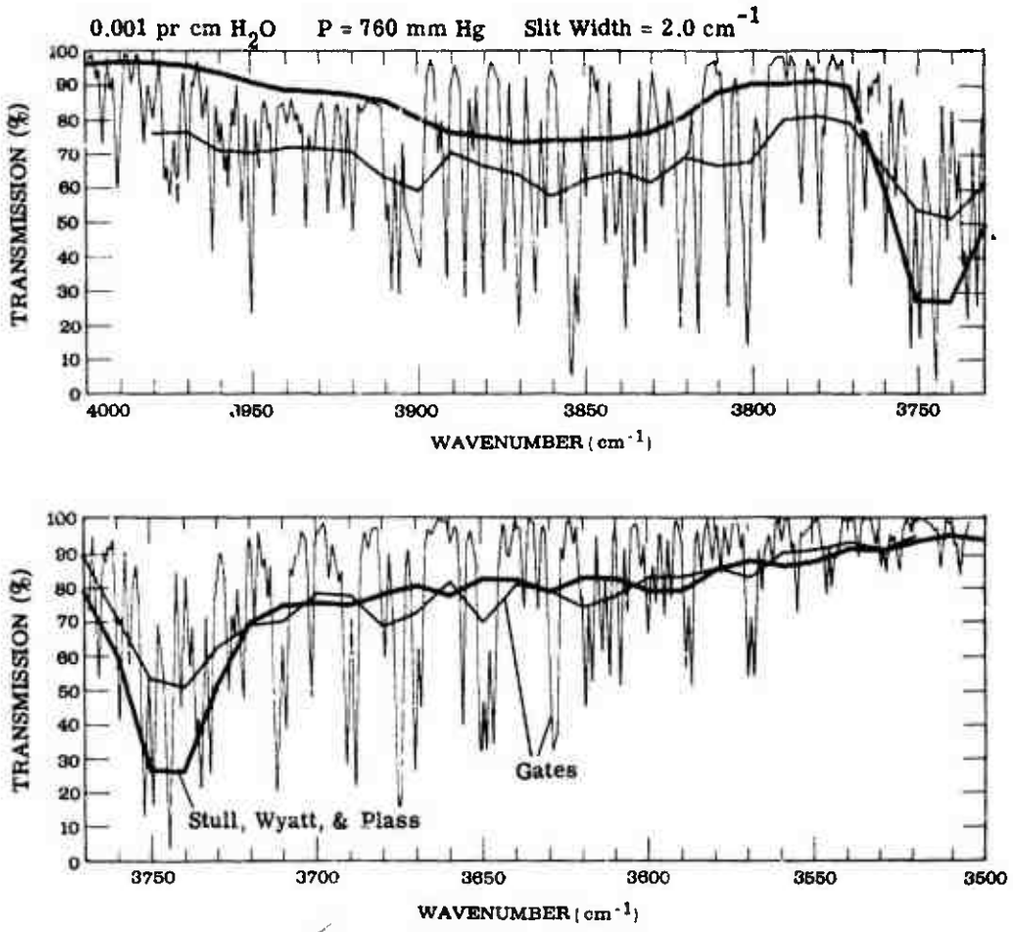

FIGURE 68. COMPARISON OF CALCULATED (RIGOROUS) SPECTRA OF GATES WITH COMPUTED SPECTRA OF STULL, WYATT, AND PLASS. Resolution of smoothed Gates curves is 20 cm^{-1}.

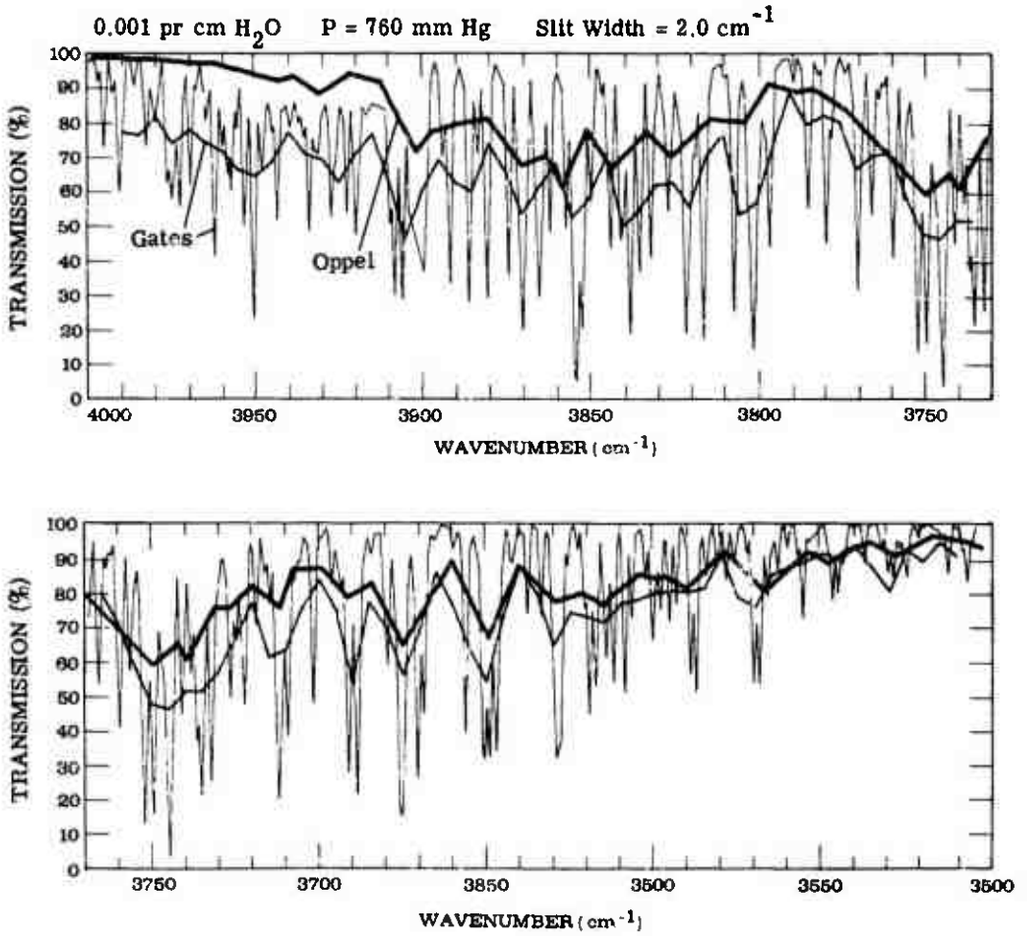

FIGURE 69. COMPARISON OF CALCULATED (RIGOROUS) SPECTRA OF GATES WITH COMPUTED SPECTRA OF OPPEL. Resolution of smoothed Gates curve is 10 cm^{-1}.

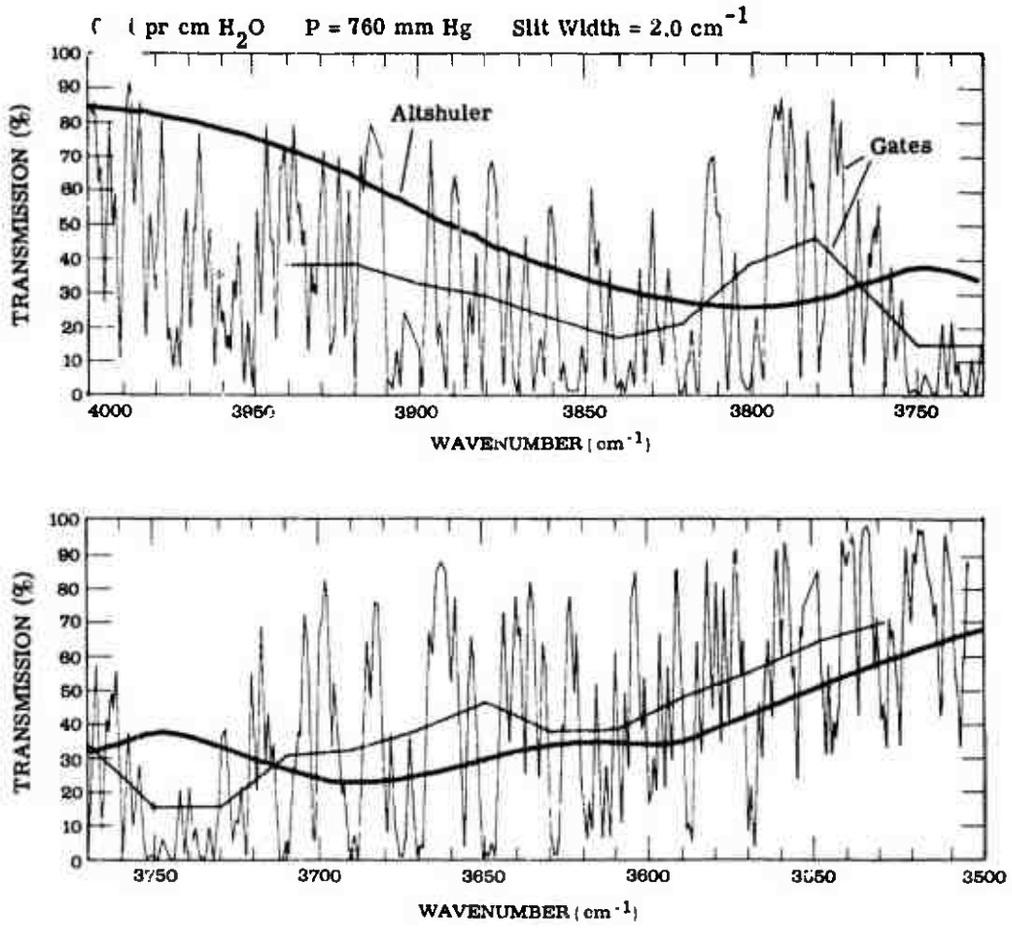

FIGURE 70. COMPARISON OF CALCULATED (RIGOROUS) SPECTRA OF GATES WITH COMPUTED SPECTRA OF ALTSHULER. Resolution of smoothed Gates curve is 40 cm^{-1}.

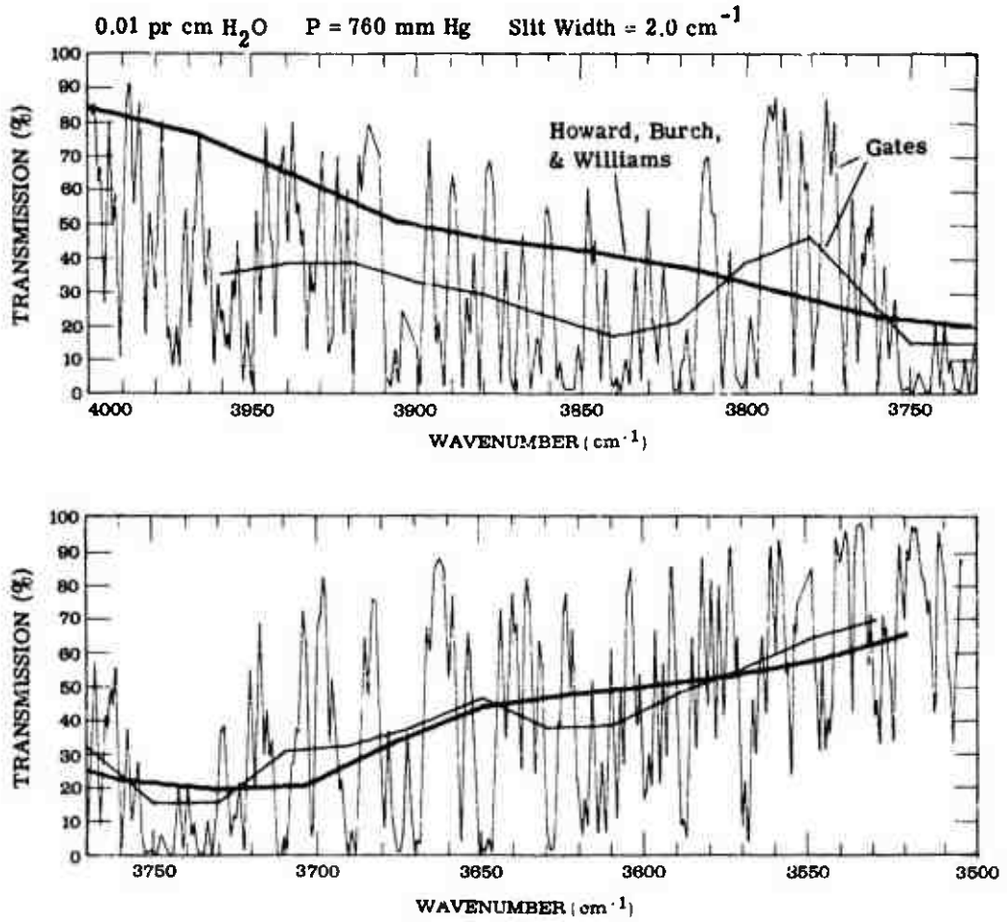

FIGURE 71. COMPARISON OF CALCULATED (RIGOROUS) SPECTRA OF GATES WITH COMPUTED SPECTRA OF HOWARD, BURCH, AND WILLIAMS. Resolution of the smoothed Gates curve is 40 cm^{-1}.

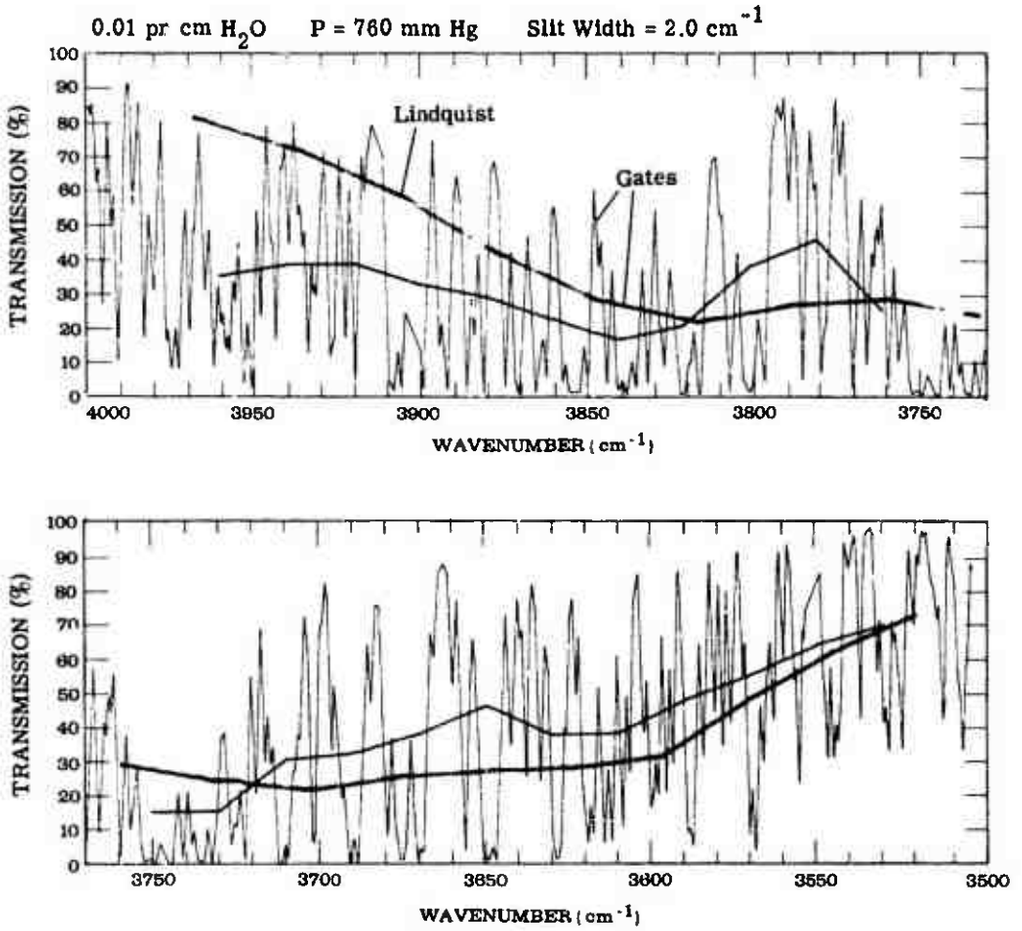

FIGURE 72. COMPARISON OF CALCULATED (RIGOROUS) SPECTRA OF GATES WITH COMPUTED SPECTRA OF LINDQUIST. Resolution of the smoothed Gates curve is 40 cm^{-1}.

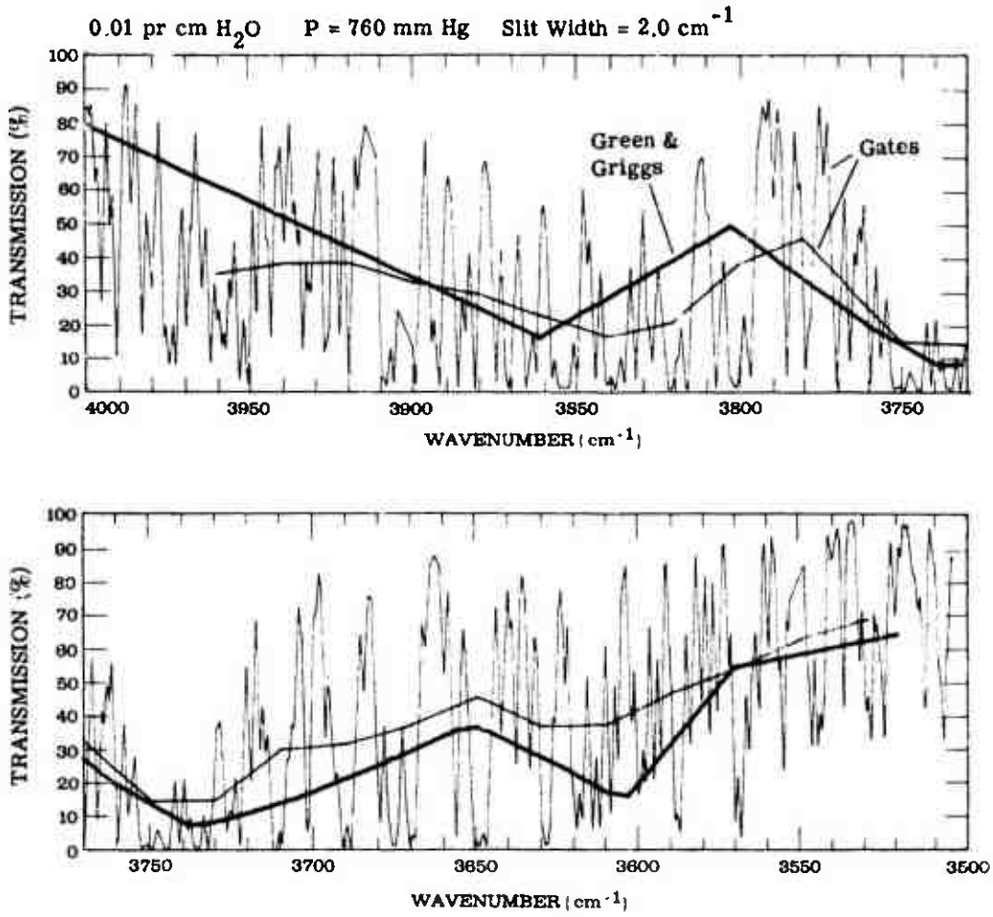

FIGURE 73. COMPARISON OF CALCULATED (RIGOROUS) SPECTRA OF GATES WITH COMPUTED SPECTRA OF GREEN AND GRIGGS. Resolution of the smoothed Gates curve is 40 cm^{-1}.

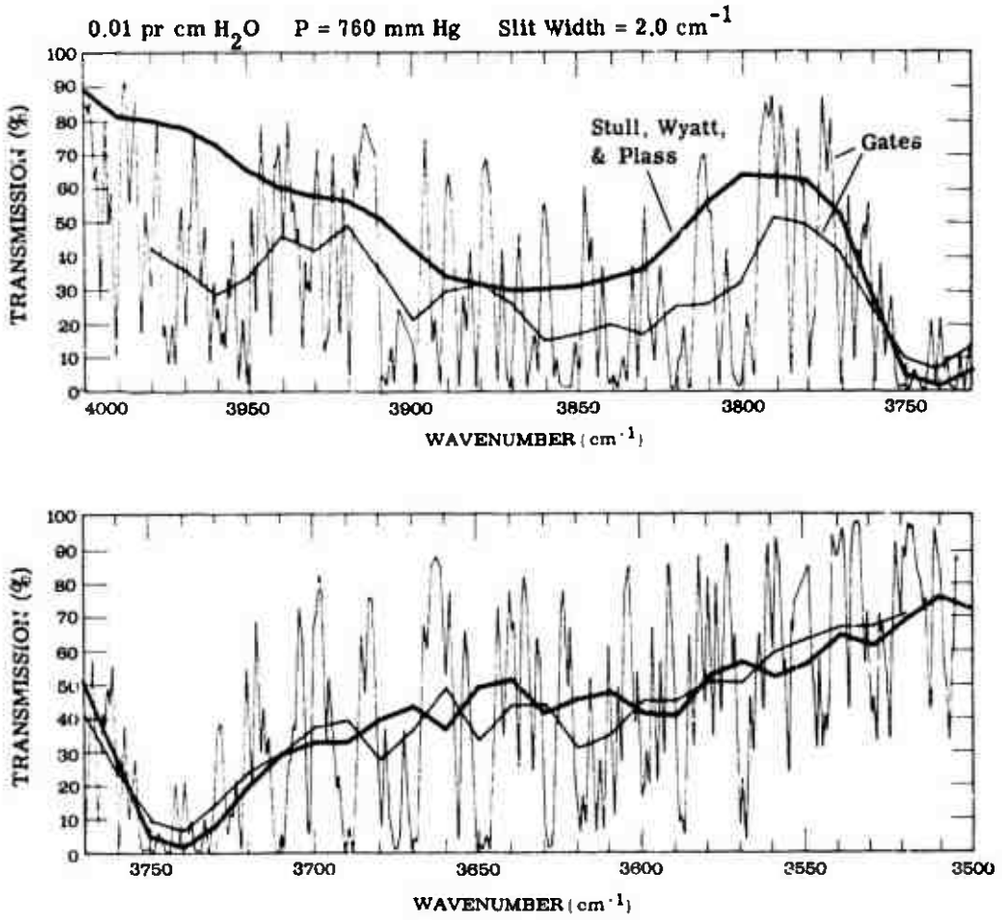

FIGURE 74. COMPARISON OF CALCULATED (RIGOROUS) SPECTRA OF GATES WITH COMPUTED SPECTRA OF STULL, WYATT, AND PLASS. Resolution of smoothed Gates curve is 20 cm^{-1}.

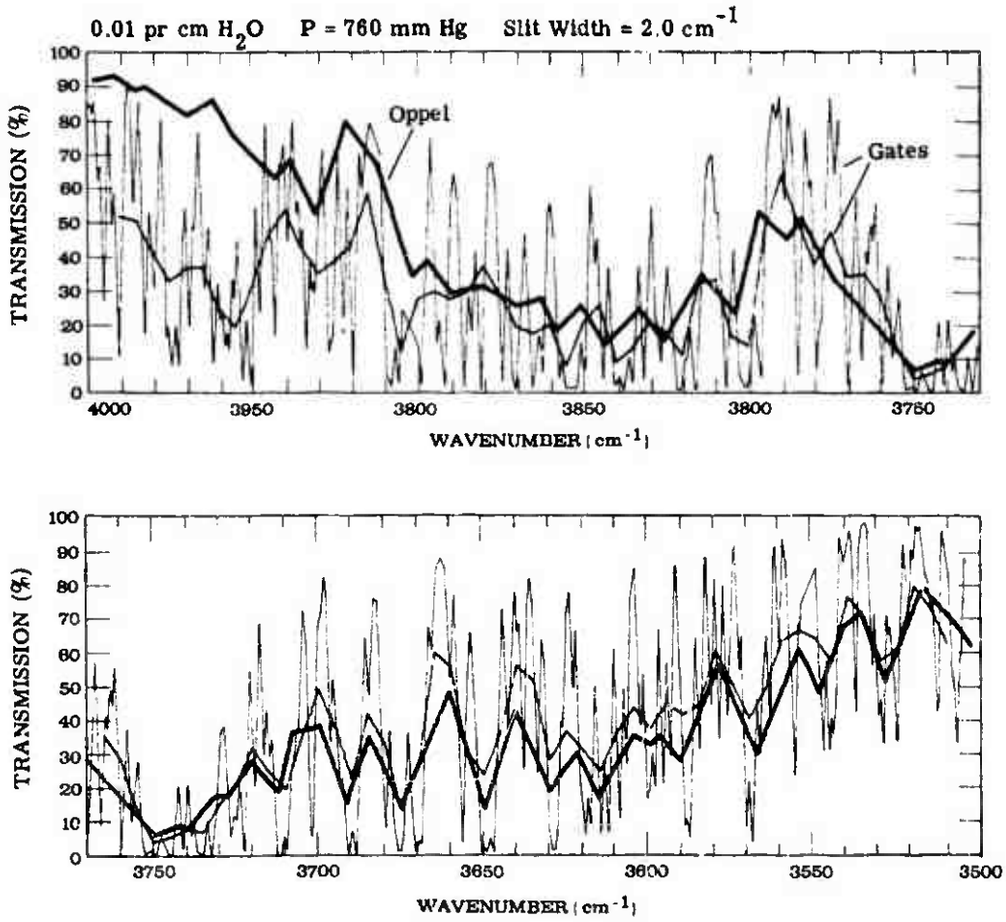

FIGURE 75. COMPARISON OF CALCULATED (RIGOROUS) SPECTRA OF GATES WITH COMPUTED SPECTRA OF OPPEL. Resolution of smoothed Gates curve is 10 cm^{-1}.

to an exponential (see sec. 2.2.4). For n = 50, where n is the number of lines in a given spectral interval, the exponential approximates the infinite product to an error ≤ 0.01. For the 2.7-μ H_2O band a spectral interval of approximately 5 cm^{-1} would be required to include 50 lines, so the maximum resolution obtainable for this spectral region has nearly been achieved by Oppel. In general, it is not practical to attempt to achieve the maximum resolution obtainable from the statistical model since the computational labor required in performing the empirical fit becomes excessive and the laboratory data must have a nearly precise spectral calibration. It is suggested that if extremely high resolution spectra are required, the exact calculation should be used rather than a band-model method.

Note in the figures that, for each curve, as the spectral interval of comparison becomes larger the comparison between the average values of transmissions improves. To demonstrate the comparison for the entire spectral region presented, each curve was integrated from 4000 to 3500 cm^{-1} and the values of $\bar{\tau}$ and $\int A\,d\nu$ were determined. The results are presented in tables 33 and 34. Note that the maximum difference between the Gates data and computed data is less than 18%.

One factor that contributes largely to this difference is that the computed spectra are consistently higher than the Gates data for the spectral region from 4000 to approximately 3800 cm^{-1}. This difference results from the laboratory data used to determine the absorption coefficients used in the band-model methods. That is, the computed spectra are consistent with the laboratory data for this spectral region. Hence, the differences between the Gates data and the computed spectra result from a difference between the laboratory data and the Gates spectra, and is therefore not characteristic of the band model. This difference suggests that even though spectra obtained by the rigorous method are of very high resolution and supposedly highly accurate, such results should not be accepted as correct until they are supported by experimental data.

Unfortunately, an experimental measurement for this amount of H_2O is not available, so it is not possible to determine the corrections of any single spectrum. However, the spread in the data is sufficiently small to indicate that the probable error between any of the given values and the true values would be tolerable for most broadband systems applications.

7.3. COMPARISON OF COMPUTED SPECTRA WITH SLANT-PATH FIELD MEASUREMENTS FOR THE 2.7-μ BAND

The Canadian Armament Research and Defense Establishment (CARDE) [140] recorded many infrared solar spectra for the 2.7-μ H_2O and CO_2 bands at many different elevation angles

TABLE 33. VALUES OF AVERAGE TRANSMISSION AND TOTAL-BAND ABSORPTION FOR THE SPECTRA PRESENTED IN FIGURES 64-69. Integrations were taken from 2.5 to 2.8571 μ.

Author	$\bar{\tau}$	$\int A d\nu$
Altshuler	0.760	119.8
Howard, Burch, and Williams	0.826	87.1
Lindquist	0.796	102.1
Green and Griggs	0.702	149.2
Stull, Wyatt, and Plass	0.803	98.4
Oppel	0.831	84.5
Average	0.786	106.9
Gates	0.765	117.5

TABLE 34. VALUES OF AVERAGE TRANSMISSION AND TOTAL-BAND ABSORPTION FOR THE SPECTRA PRESENTED IN FIGURES 70-75. Integrations were taken from 2.5 to 2.8571 μ.

Author	$\bar{\tau}$	$\int A d\nu$
Altshuler	0.436	281.9
Howard, Burch, and Williams	0.464	267.9
Lindquist	0.431	284.7
Green and Griggs	0.378	310.8
Stull, Wyatt, and Plass	0.473	263.3
Oppel	0.415	292.6
Average	0.433	283.5
Gates	0.397	301.5

with electro-optical equipment installed in an RCAF CF-100 Mark 4 jet aircraft. Almost all measurements were made in the region of Cape Kennedy, Florida, at altitudes of 10.7, 12.2, and 13.7 km. These data were reduced to absolute values of slant-path transmission from the aircraft to the top of the atmosphere. Three representative spectra were selected from the CARDE data and each is compared to spectra computed by the methods of section 3.

Before the computations could be performed it was necessary to determine for each path the effective broadening pressure and absorber concentrations for the two absorbing gases, H_2O and CO_2. These slant-path parameters were calculated with the program described in appendix I using the following input data:

(1) Pressures and temperature profiles were taken from the U. S. Standard Atmosphere 1962 since the exact pressure and temperature distributions existing at the time of the measurement are not known.

(2) Carbon dioxide was assumed to be uniformly mixed at 320 ppm. Because of the uniformity in the CO_2 measurements described in section 4.2, this approximation is felt to be quite valid.

(3) The amount of water vapor in each of the paths was taken from the work of Lindquist [136]. He determined the amount of water vapor in each of the CARDE paths by comparing the CARDE spectra with infinitely resolved water vapor spectra in the 3847- to 3860-cm^{-1} region (where no CO_2 absorption exists). The water vapor spectra were calculated by the rigorous method employing a direct slant-path pressure integration. For the rigorous calculation, Lindquist used the line positions and line parameters of Gates et al. [7].

The slant-path parameters calculated by the computer program described in appendix I using the above meteorological data are presented on each of the figures in conjunction with the altitude, zenith angle, and resolution of the CARDE data. These slant-path parameters were used to compute the absorption spectra by each of the methods discussed in section 3 which are applicable to the 2.7-μ band, and the results of these computations are presented in figures 76 through 90. As for the Gates data, the CARDE data were smoothed to a resolution comparable to the resolution of the computed spectra.

In general, the comparison of computed and measured spectra is surprisingly close. The methods of Aitshuler and Zachor yield spectra that display the greatest divergence from the measured data, and the methods of Stull et al., Green and Griggs, and Oppel show the best agreement. Oppel's spectra for all large paths show remarkable agreement considering the procedures involved. All authors, however, are in general disagreement with the CARDE data

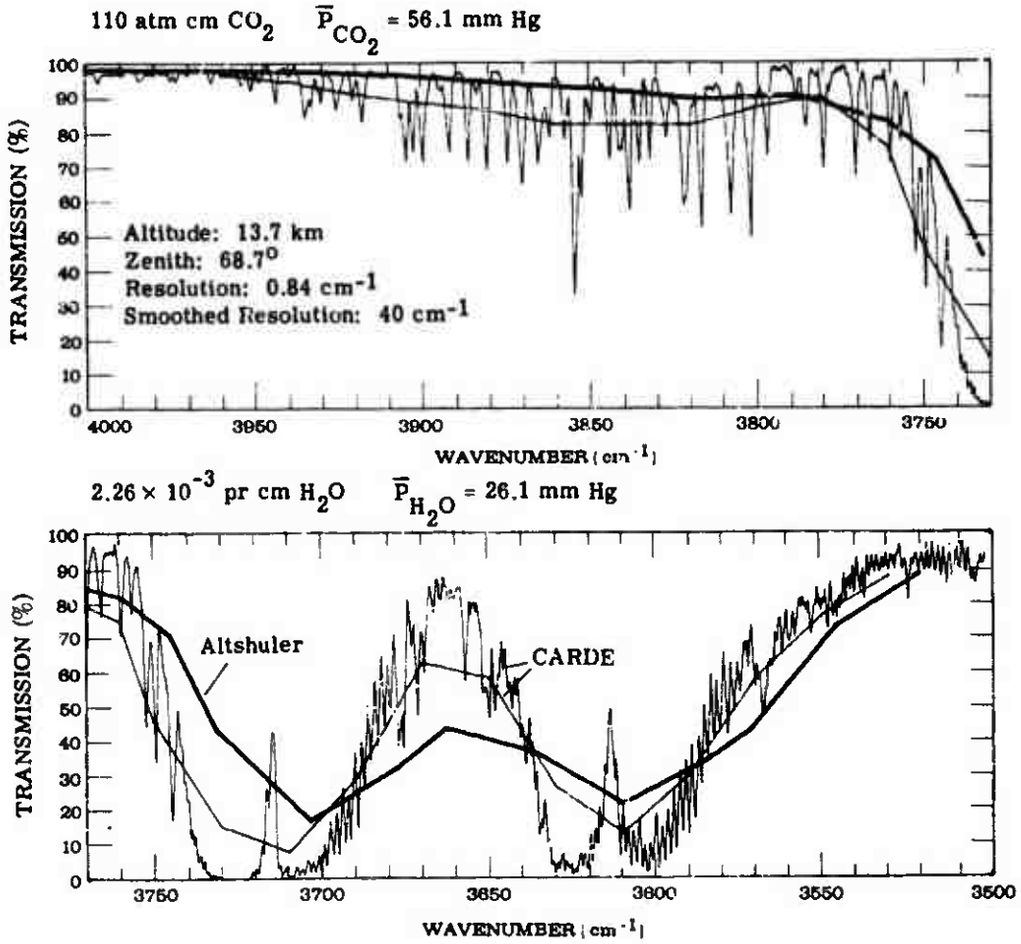

FIGURE 76. COMPARISON OF CARDE SOLAR SPECTRA WITH COMPUTED SPECTRA OF ALTSHULER

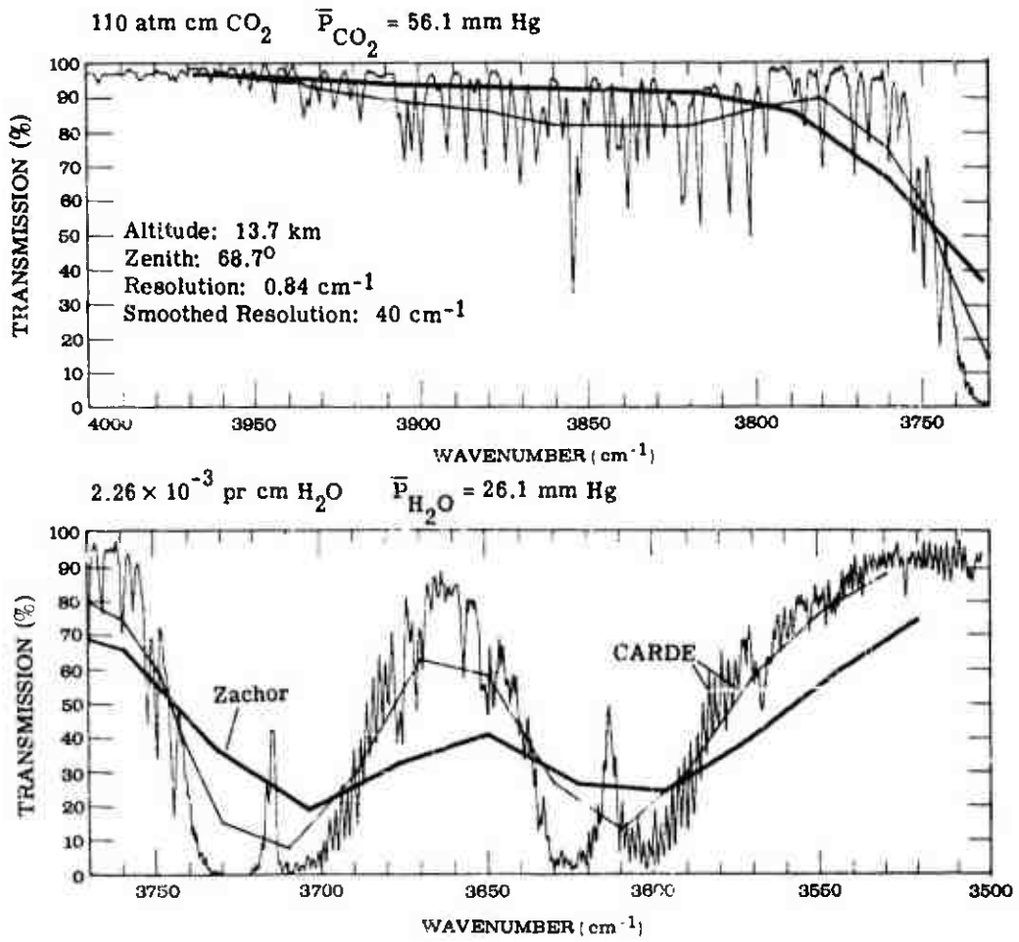

FIGURE 77. COMPARISON OF CARDE SOLAR SPECTRA WITH COMPUTED SPECTRA OF ZACHOR

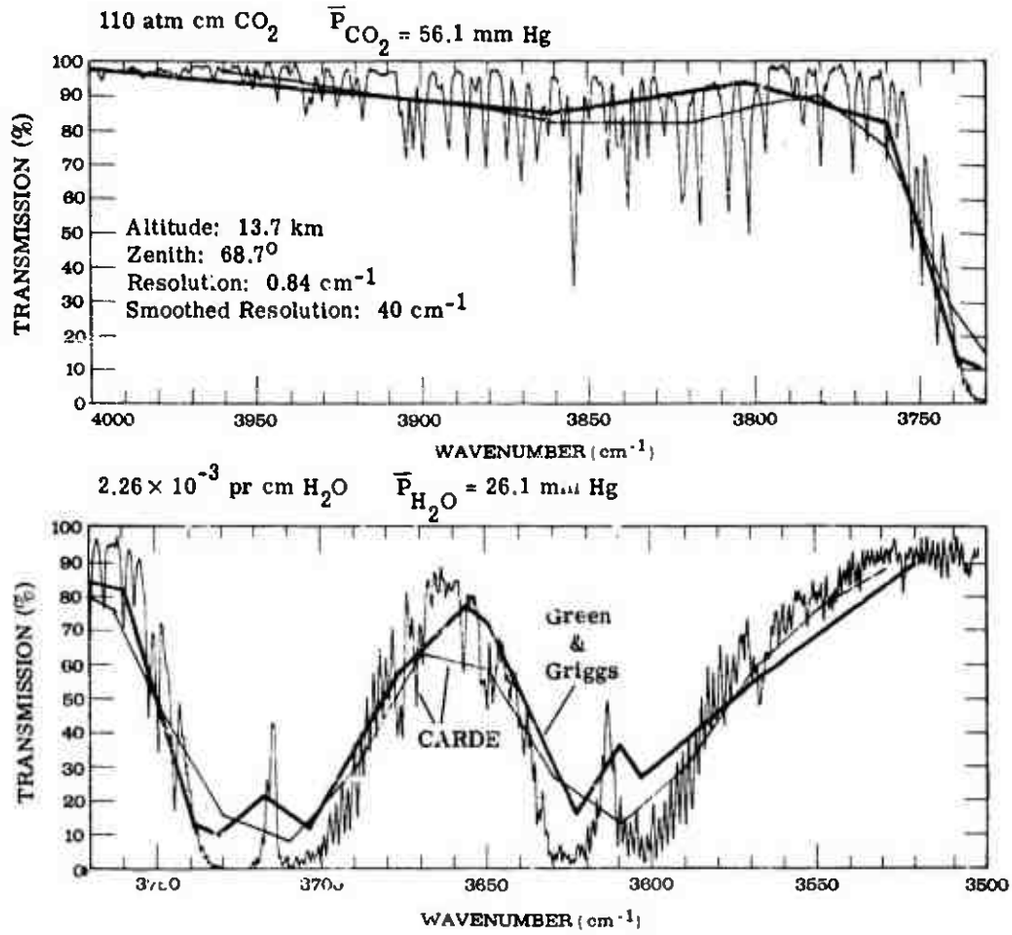

FIGURE 78. COMPARISON OF CARDE SOLAR SPECTRA WITH COMPUTED SPECTRA OF GREEN AND GRIGGS

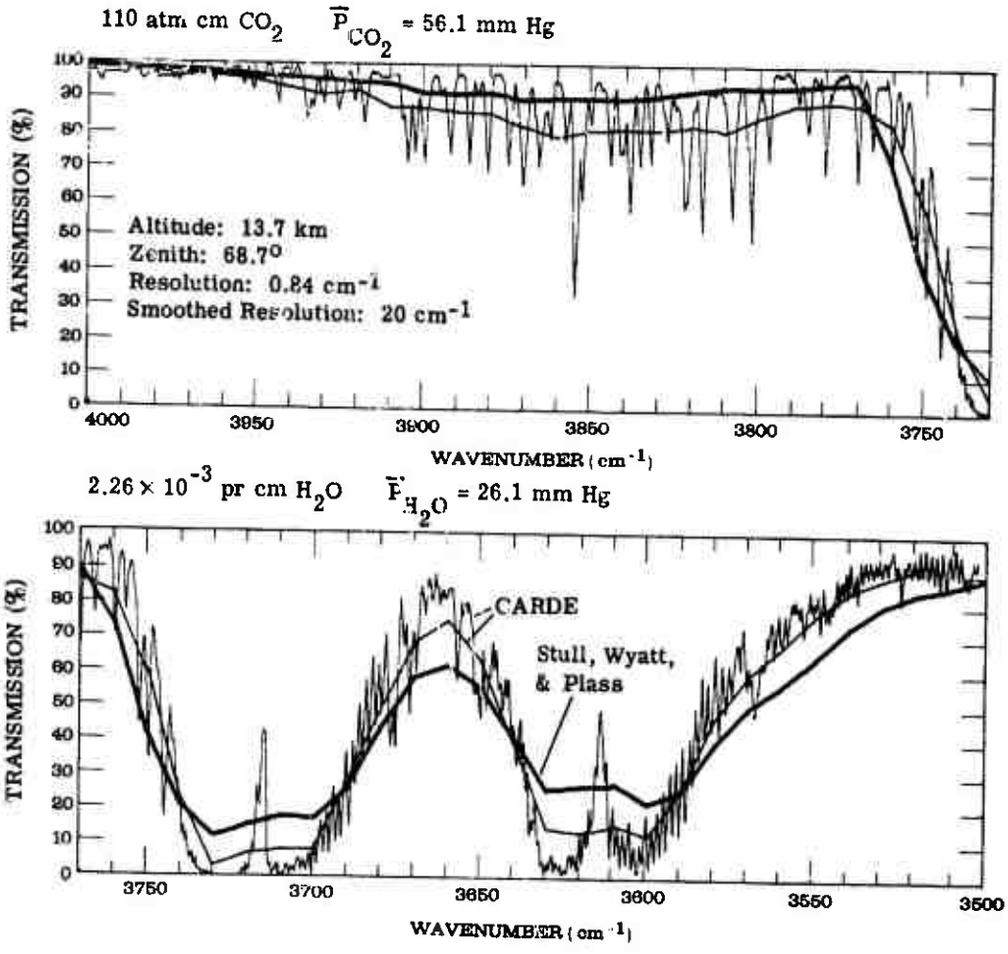

FIGURE 79. COMPARISON OF CARDE SOLAR SPECTRA WITH COMPUTED SPECTRA OF STULL, WYATT, and PLASS

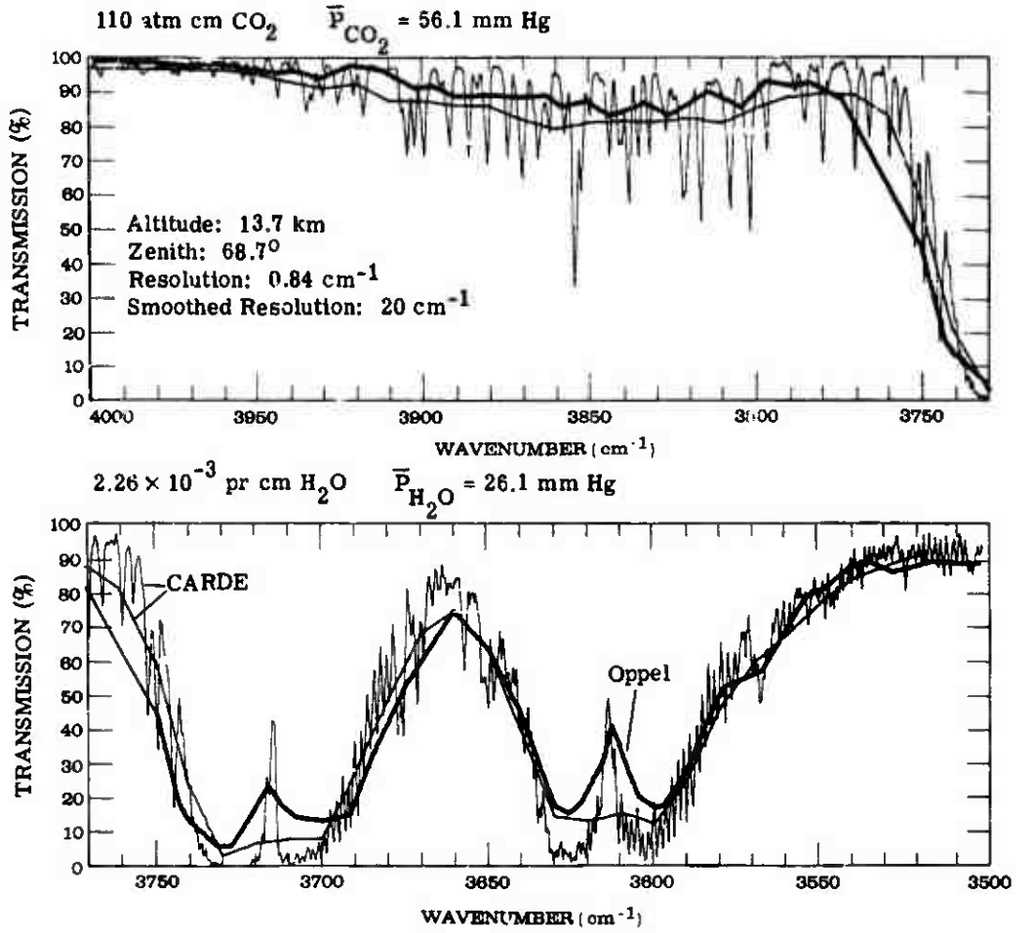

FIGURE 80. COMPARISON OF CARDE SOLAR SPECTRA WITH COMPUTED SPECTRA OF OPPEL

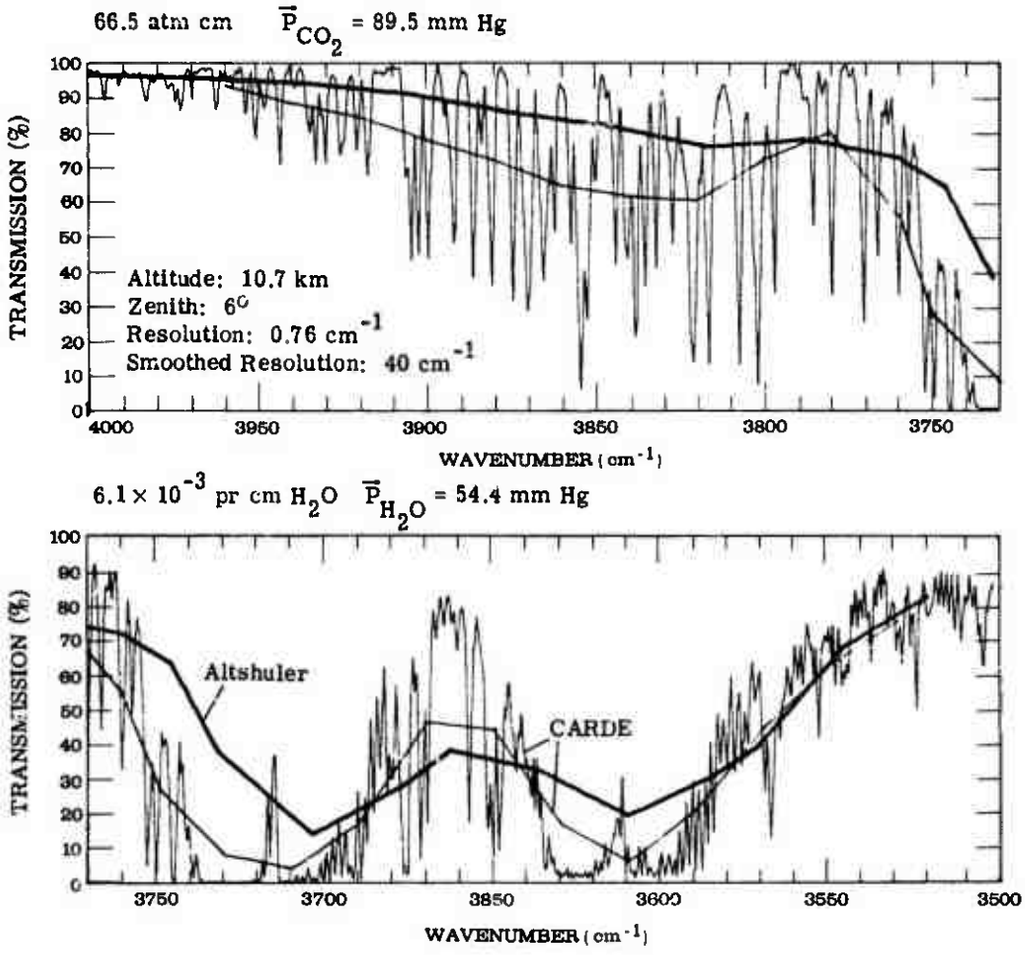

FIGURE 81. COMPARISON OF CARDE SOLAR SPECTRA WITH COMPUTED SPECTRA OF ALTSHULER

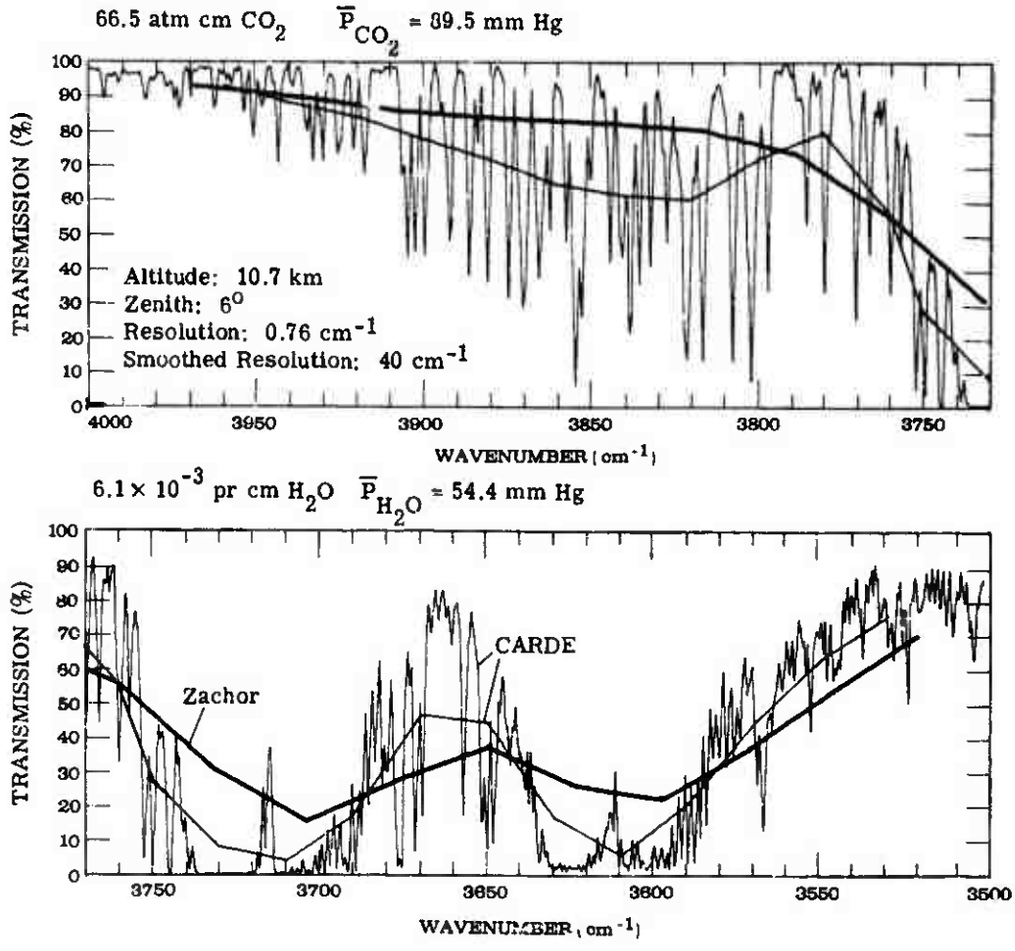

FIGURE 82. COMPARISON OF CARDE SOLAR SPECTRA WITH COMPUTED SPECTRA OF ZACHOR

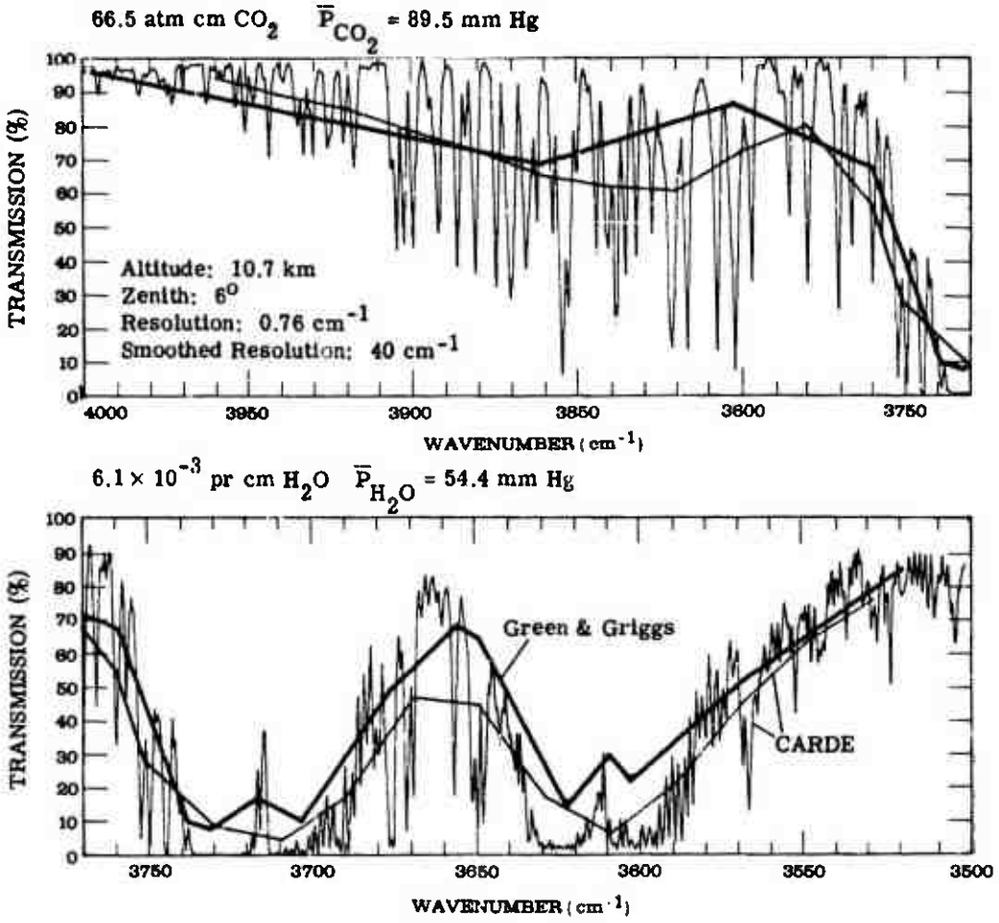

FIGURE 83. COMPARISON OF CARDE SOLAR SPECTRA WITH COMPUTED SPECTRA OF GREEN AND GRIGGS

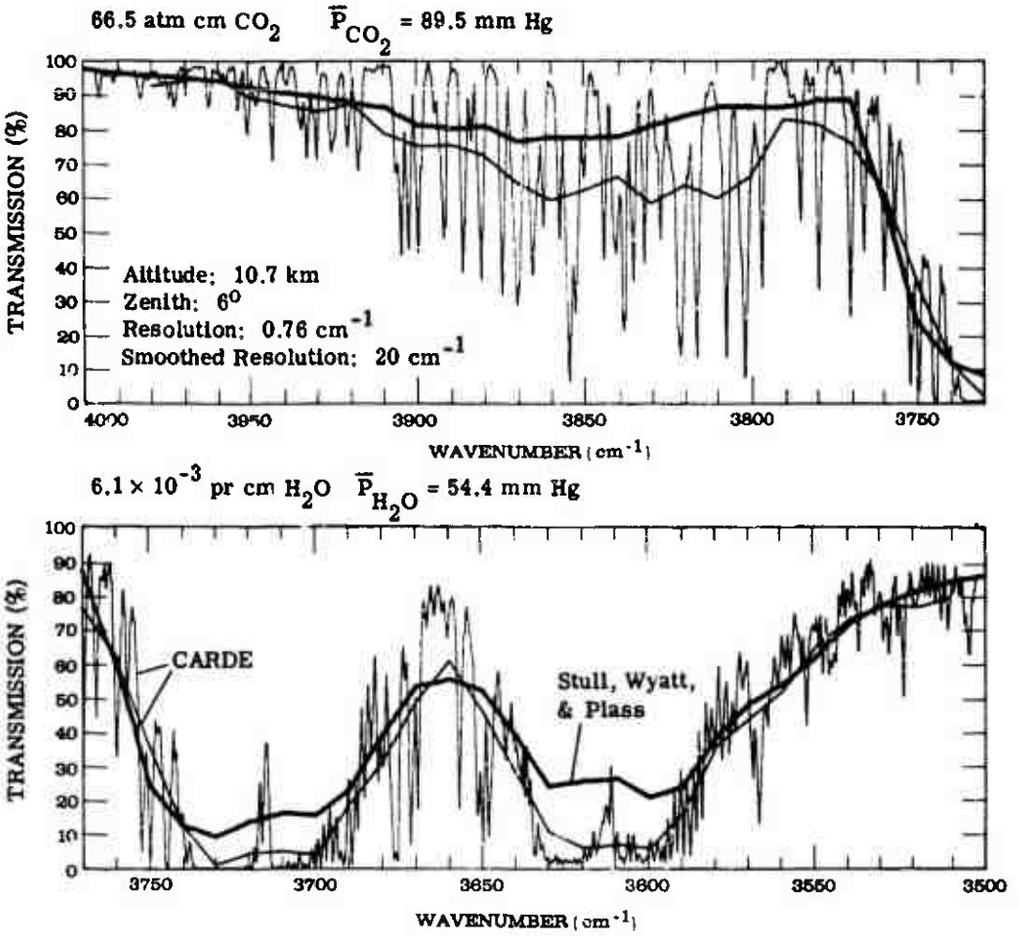

FIGURE 84. COMPARISON OF CARDE SOLAR SPECTRA WITH COMPUTED SPECTRA OF STULL, WYATT, AND PLASS

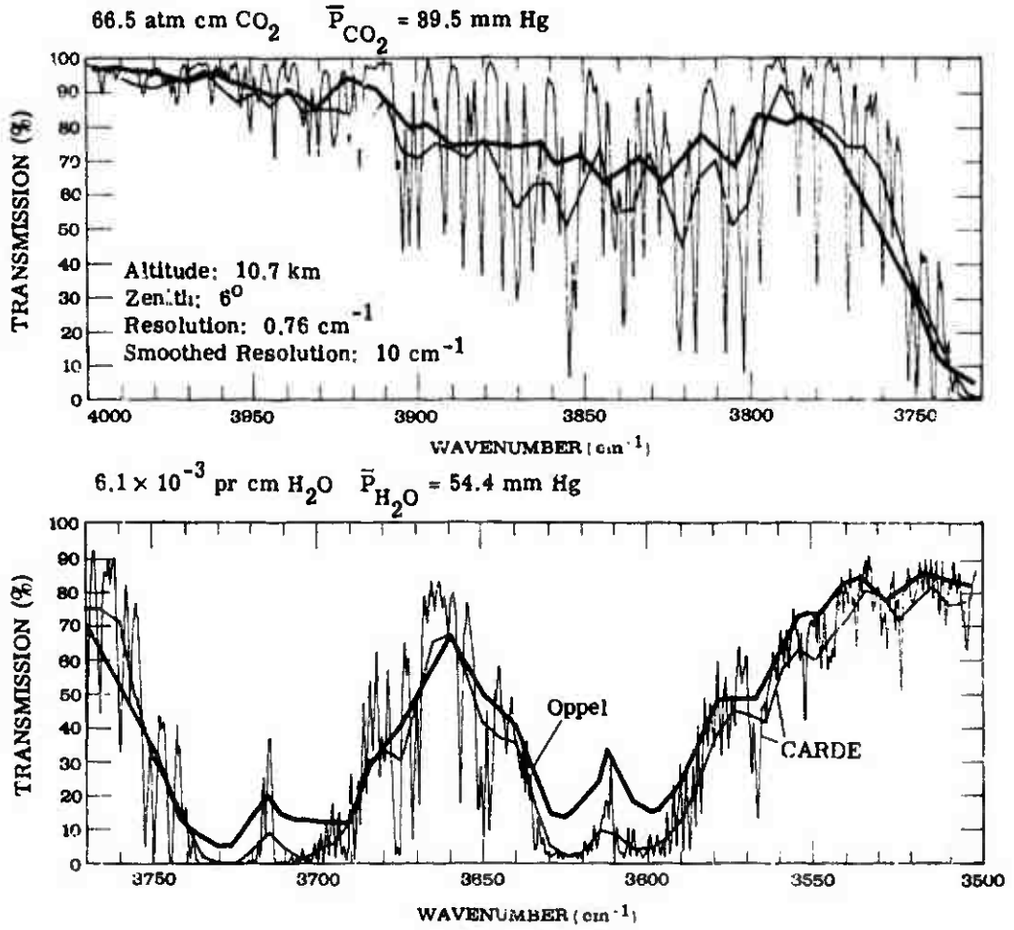

FIGURE 85. COMPARISON OF CARDE SOLAR SPECTRA WITH COMPUTED SPECTRA OF OPPEL

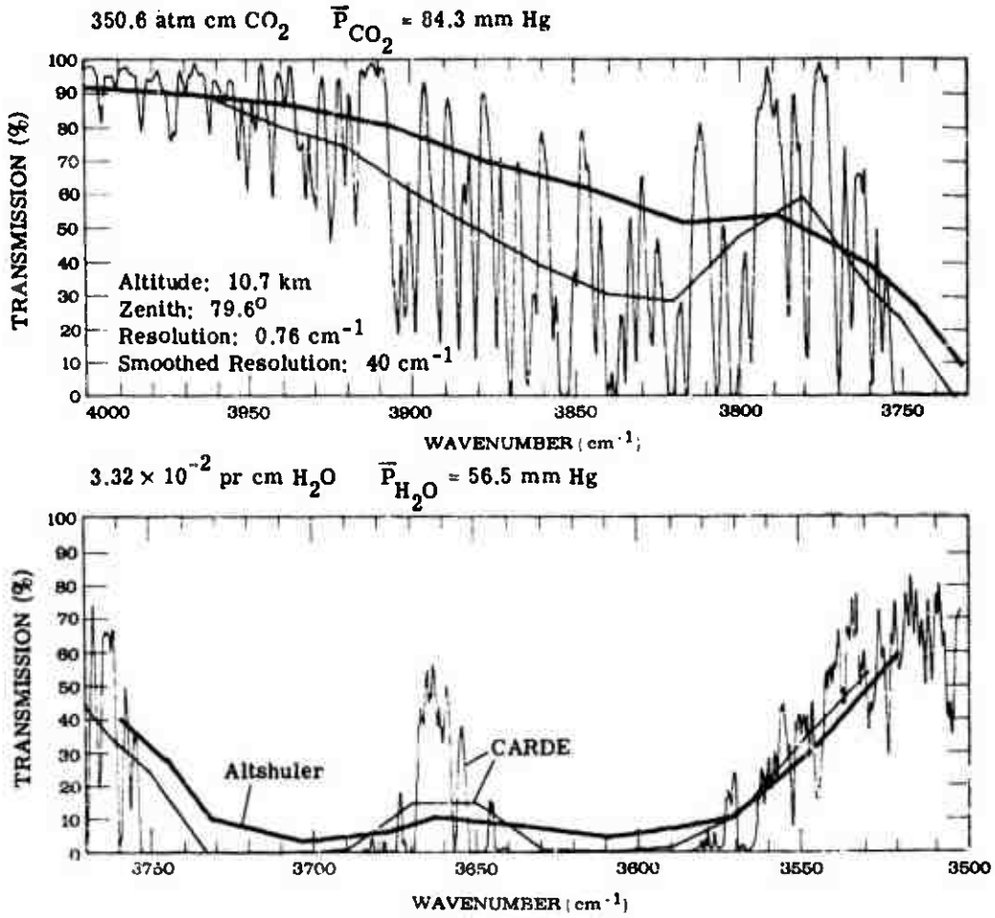

FIGURE 86. COMPARISON OF CARDE SOLAR SPECTRA WITH COMPUTED SPECTRA OF ALTSHULER

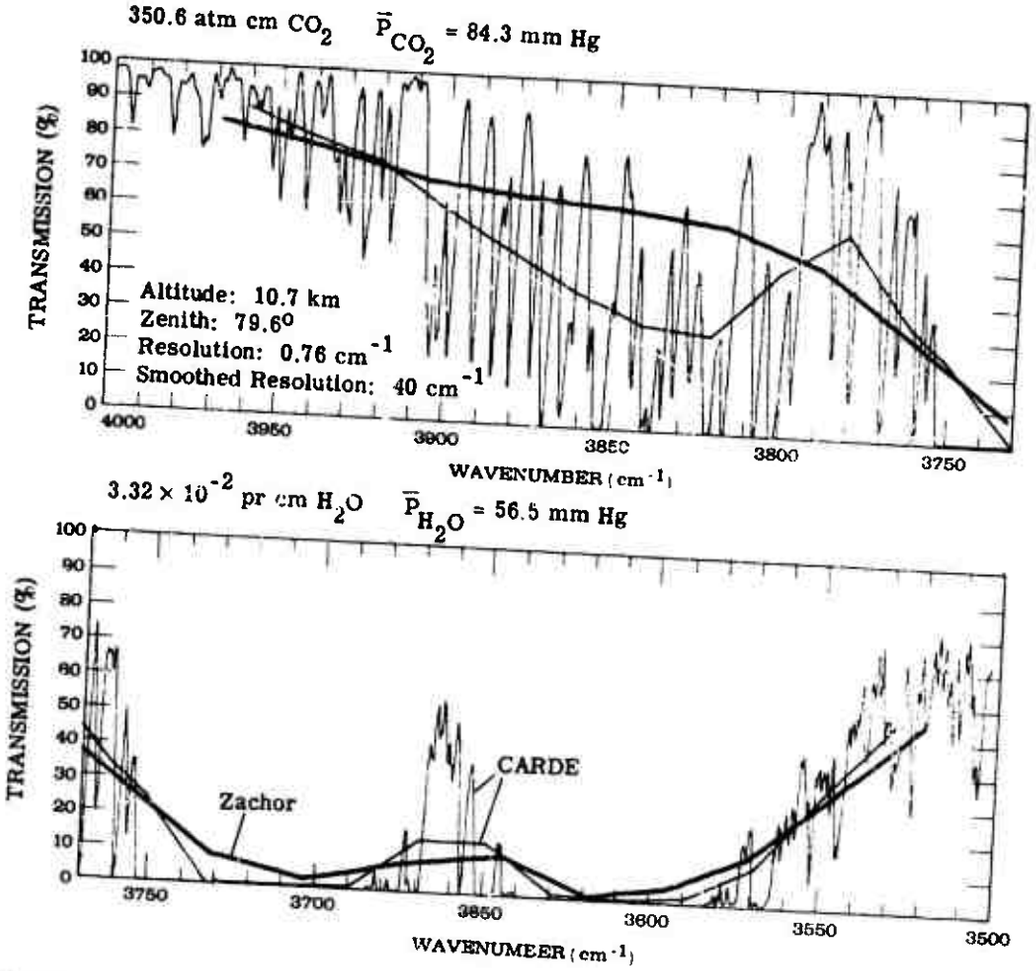

FIGURE 87. COMPARISON OF CARDE SOLAR SPECTRA WITH COMPUTED SPECTRA OF ZACHOR

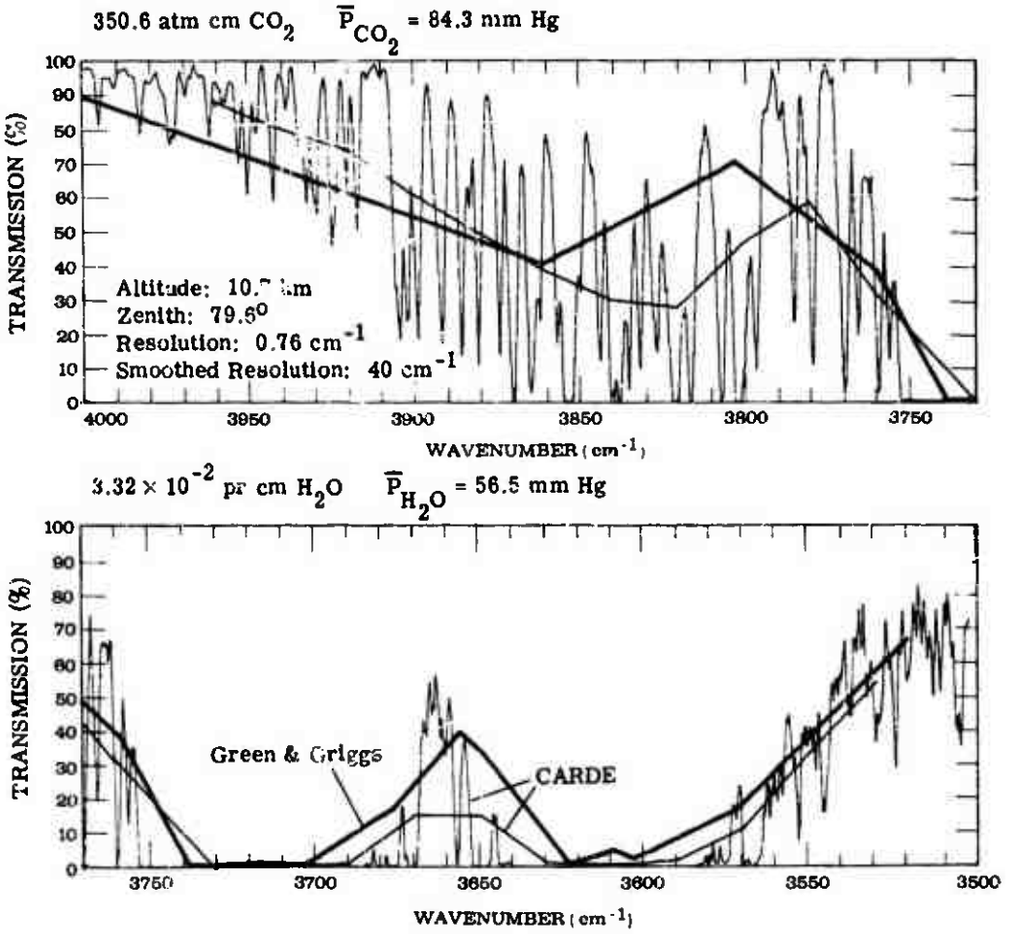

FIGURE 88. COMPARISON OF CARDE SOLAR SPECTRA WITH COMPUTED SPECTRA OF GREEN AND GRIGGS

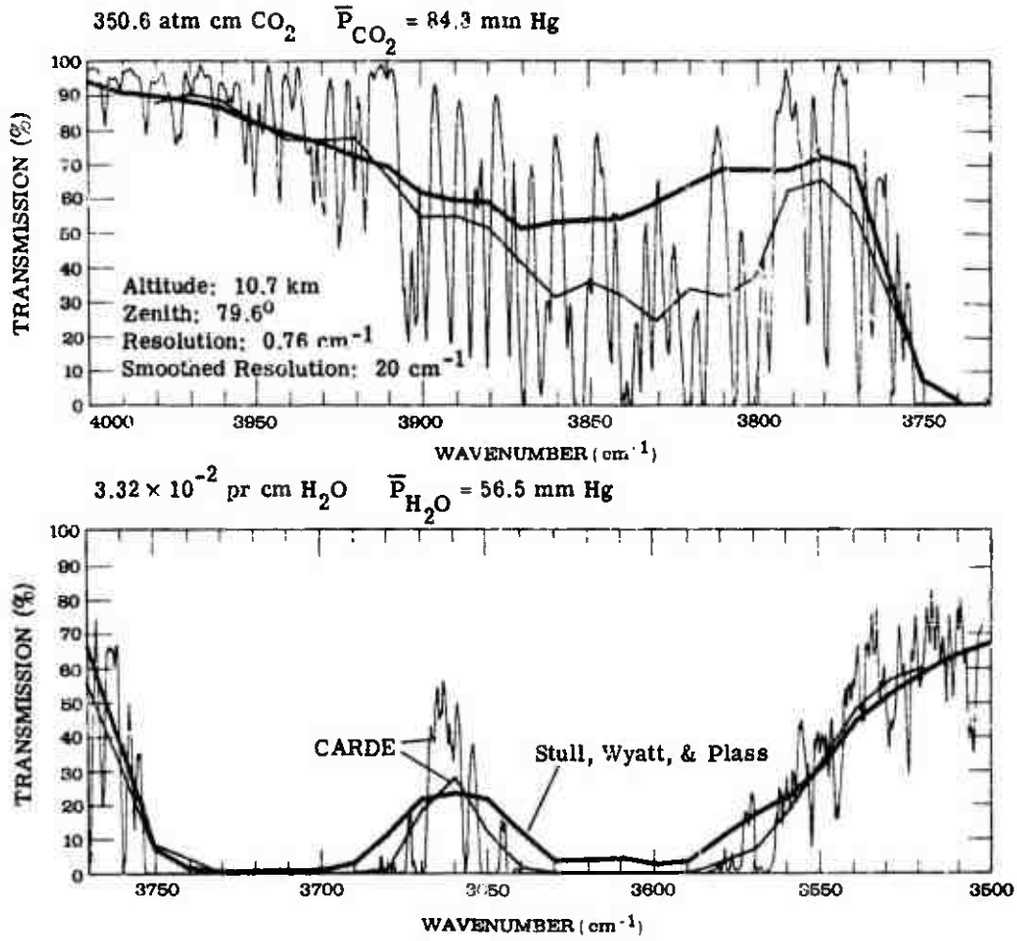

FIGURE 89. COMPARISON OF CARDE SOLAR SPECTRA WITH COMPUTED SPECTRA OF STULL, WYATT, AND PLASS

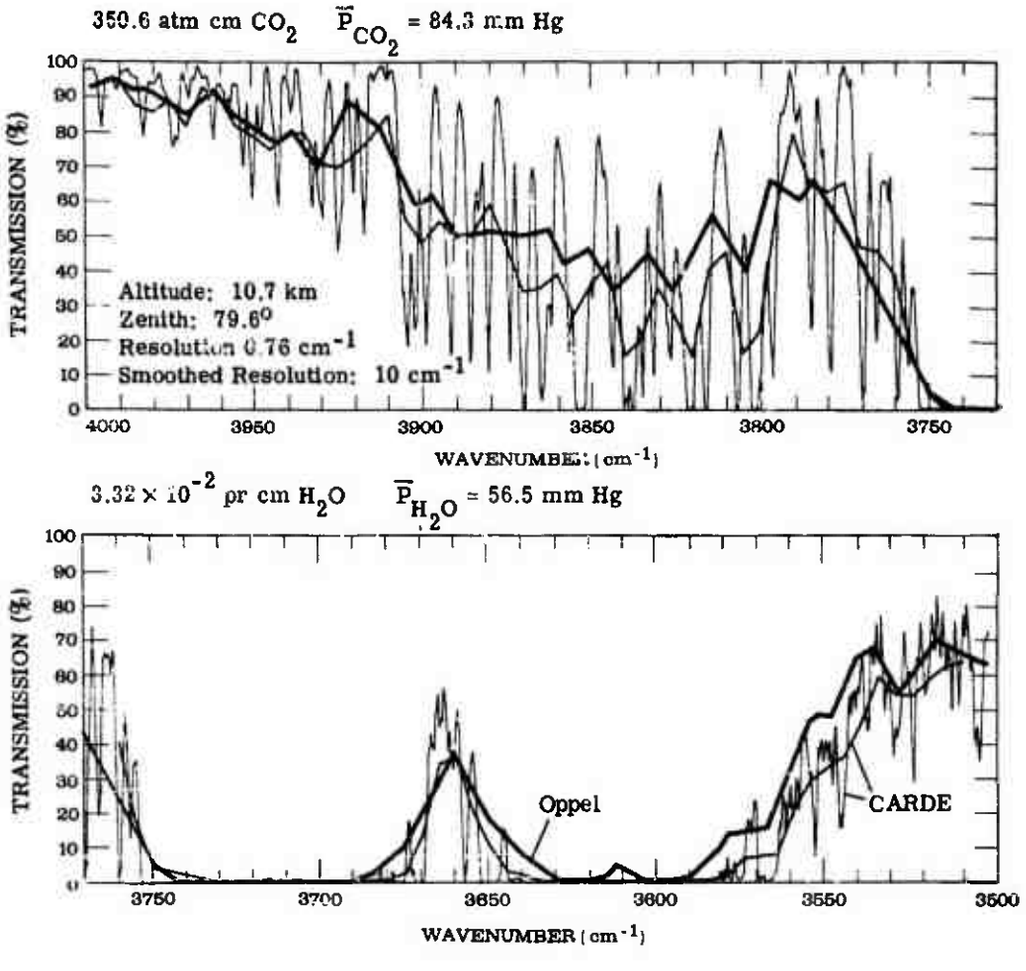

FIGURE 90. COMPARISON OF CARDE SOLAR SPECTRA WITH COMPUTED SPECTRA OF OPPEL

for the spectra region from 3900 to 3800 cm^{-1}. The computed data are high on the average by approximately 10 percentage points in transmission. Oppel's spectra show better agreement for this spectral region than do any of the other data. Since general disagreement for broad spectral intervals is usually related to the laboratory data, indications are that the data of Burch et al. [1] are in closest agreement to the CARDE data.

To further compare the computed and measured data, average transmission and integrated absorption values were determined for each curve. The results are presented in tables 35, 36, and 37. The path containing the least amount of absorber represented in figures 76-80 shows the best comparison with the CARDE data. The values of Oppel and Stull et al. compare almost exactly. As the quantity of absorber increases, the comparison is slightly poorer, as noted for the paths shown in figures 81-90. However, in all cases, the difference is no greater than 8 percentage points and in general is much less. For most applications, such results would be more than adequate.

7.4. COMPARISON OF COMPUTED SPECTRA WITH SLANT-PATH FIELD MEASUREMENTS FOR THE 4.3-μ BAND

The next series of comparisons is indicative of the degree of accuracy with which the band-model methods can predict absorption for the 4.3-μ CO_2 absorption band for high-altitude slant paths.

Kyle et al. [149] made a series of high-altitude, balloon-borne solar-spectra measurements for the 4.3-μ CO_2 band which were reduced to absolute values of transmission. Three spectra were selected from Kyle's work, representing slant paths extending from 30, 25.6, and 15.2 km, respectively, to the limit of the atmosphere. These three paths were selected to facilitate comparisons for levels of absorption that extend from that which is relatively weak to that which is relatively strong.

To compare these spectra with spectra calculated by the band-model methods, it was first necessary to determine the equivalent path parameters for each of the Kyle paths. These parameters were computed with the computer program previously described, using the same input data that were used for the determination of the equivalent parameters for the CARDE paths. Water vapor data were not required for this computation since H_2O does not absorb in the 4.3-μ band. The altitude, zenith, CO_2 absorber concentration, and equivalent pressure are noted on each figure.

The first of these comparisons (fig. 91) demonstrates the comparison between measured and computed spectra for an extremely high altitude slant path. It is noted that the results of

TABLE 35. VALUES OF AVERAGE TRANSMISSION AND TOTAL-BAND ABSORPTION FOR THE SPECTRA PRESENTED IN FIGURES 78-80. Integrations were taken from 2.5 to 2.8571 μ.

Author	$\bar{\tau}$	$\int A d\nu$
Altshuler	0.683	158.6
Zachor	0.654	172.9
Green and Griggs	0.681	159.7
Stull, Wyatt, and Plass	0.663	167.1
Oppel	0.669	165.3
Average	0.671	184.7
CARDE	0.668	166.0

TABLE 38. VALUES OF AVERAGE TRANSMISSION AND TOTAL-BAND ABSORPTION FOR THE SPECTRA PRESENTED IN FIGURES 81-85. Integrations were taken from 2.5 to 2.8571 μ.

Author	$\bar{\tau}$	$\int A d\nu$
Altshuler	0.826	188.9
Zachor	0.598	201.9
Green and Griggs	0.608	197.1
Stull, Wyatt, and Plass	0.613	193.3
Oppel	0.595	202.3
Average	0.607	196.3
CARDE	0.557	221.5

TABLE 37. VALUES OF AVERAGE TRANSMISSION AND TOTAL-BAND ABSORPTION FOR THE SPECTRA PRESENTED IN FIGURES 86-90. Integrations were taken from 2.5 to 2.8571 μ.

Author	$\bar{\tau}$	$\int A d\nu$
Altshuler	0.415	292.5
Zachor	0.400	300.1
Green and Griggs	0.400	300.1
Stull, Wyatt, and Plass	0.414	293.1
Oppel	0.392	303.1
Average	0.404	297.8
CARDE	0.368	315.8

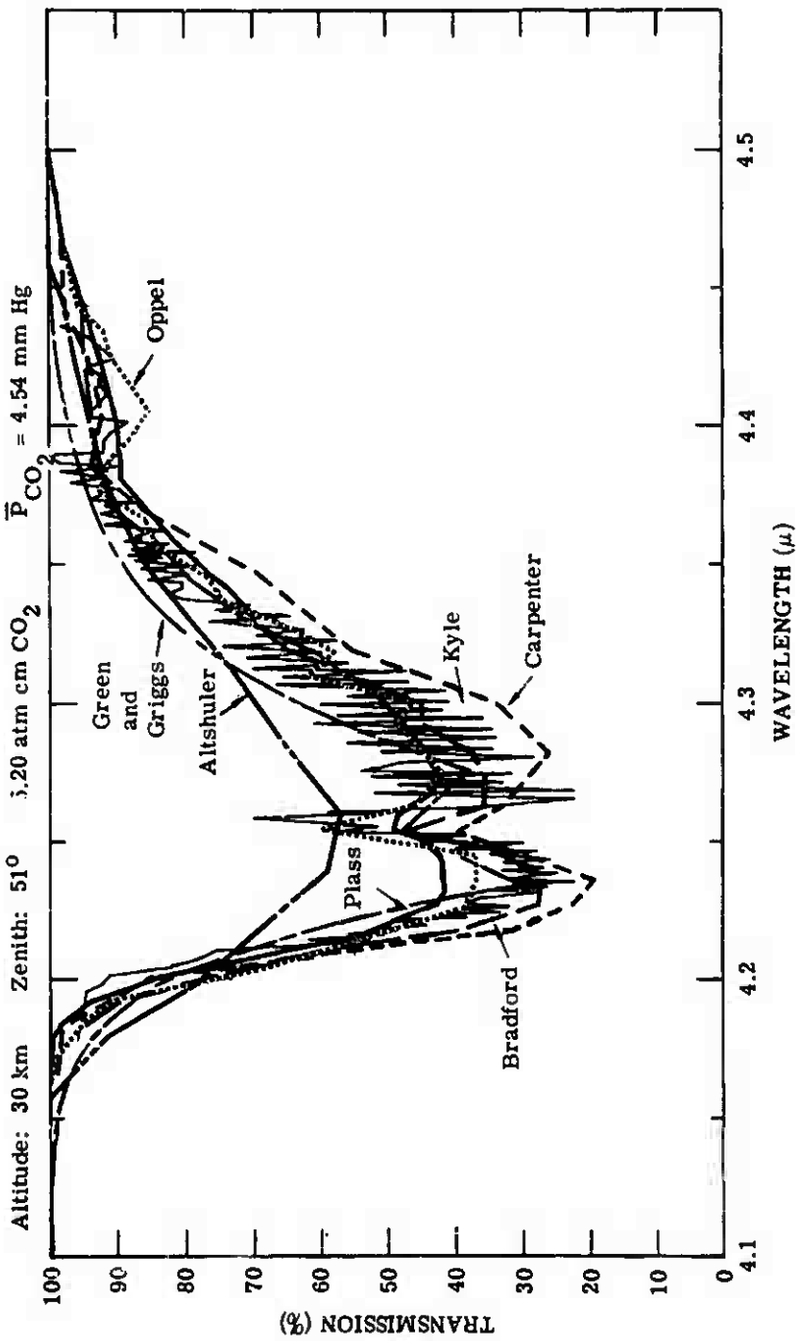

FIGURE 91. COMPARISON OF SOLAR SPECTRA OF KYLE WITH COMPUTED SPECTRA OF BRADFORD; PLASS; CARPENTER; OPPEL; ALTSHULER; AND GREEN AND GRIGGS

Altshuler compare rather poorly with the Kyle data, possibly because the laboratory data of Howard et al. used by Altshuler to determine the absorption coefficient did not include paths containing quantities of absorber as small as those contained in this particular path. Therefore, the results of Altshuler are extrapolations of the laboratory data rather than interpolations, a condition which should be avoided.

The remaining five methods all compare reasonably well, showing a maximum difference in the center of the band of approximately 20 percentage points in transmission. The spectra of Carpenter show the greatest amount of absorption and Bradford's spectra show the closest agreement. Each of the spectra was integrated to determine values of average transmission, and it is noted from the data presented in table 38 that all of the integrated values compare to the Kyle data within 7 percentage points, the methods of Bradford, Oppel, and Plass compare almost exactly.

The next comparison (fig. 92) has an absorption level approximately 25% higher than that displayed in figure 91. Altshuler's spectra are high by an amount approximately equal to that shown in the previous comparison. The spectra of Bradford, Oppel, Plass, and Carpenter show a slightly better agreement in the central portion of the band, but their integrated values (note table 39) compare as those shown in table 38. The spectrum of Green and Griggs does not compare as well as that shown previously, the integrated value being less than the measured data by approximately 10%, as compared to a difference of less than 4% for the spectrum shown in figure 91.

Figure 93 emphasizes the comparison of the Kyle and computed spectra in the wings of the band, the absorber concentration being sufficient to cause total absorption in the center of the band. The spectrum of Carpenter is the only one which compares well for the short-wavelength edge of the Kyle spectrum. For the long-wavelength edge of the band, the spectrum of Plass compares best. The integrated values of absorption given in table 40 demonstrate, as for the two previous comparisons, that the methods of Bradford, Oppel, Plass, and Carpenter yield values of average transmission that compare extremely well to the Kyle values, and the values computed by the method of Green and Griggs are consistently high. It is interesting to note that Altshuler's results were high for the two previous comparisons, but are low by approximately 20% for the high-absorption path.

In section 3 it was shown that Altshuler used a transmissivity function for the 4.3-μ CO_2 band that was empirically derived and that Green and Griggs employed the statistical model, whereas the methods of the other four authors were based on the Elsasser model. Since the line structure of CO_2 is assumed to be more regular than random, the Elsasser model reportedly

TABLE 38. VALUES OF AVERAGE TRANSMISSION AND TOTAL-BAND ABSORPTION FOR THE SPECTRA PRESENTED IN FIGURE 91. Integrations were taken from 4.1 to 4.5 μ.

Author	$\bar{\tau}$	$\int A\,d\nu$
Altshuler	0.856	31.3
Green and Griggs	0.830	36.8
Bradford	0.780	48.4
Oppel	0.791	46.0
Plass	0.796	44.9
Carpenter	0.748	55.4
Average	0.800	43.8
Murcray	0.793	45.6

TABLE 39. VALUES OF AVERAGE TRANSMISSION AND TOTAL-BAND ABSORPTION FOR THE SPECTRA PRESENTED IN FIGURE 92. Integrations were taken from 4.1 to 4.5 μ.

Author	$\bar{\tau}$	$\int A\,d\nu$
Altshuler	0.698	65.4
Green and Griggs	0.714	62.2
Bradford	0.647	77.7
Oppel	0.646	77.9
Plass	0.631	81.2
Carpenter	0.619	83.8
Average	0.654	74.7
Murcray	0.643	78.5

TABLE 40. VALUES OF AVERAGE TRANSMISSION AND TOTAL-BAND ABSORPTION FOR THE SPECTRA PRESENTED IN FIGURE 93. Integrations were taken from 4.1 to 4.5 μ.

Author	$\bar{\tau}$	$\int A\,d\nu$
Altshuler	0.302	151.2
Green and Griggs	0.405	132.0
Bradford	0.360	140.9
Oppel	0.341	145.0
Plass	0.339	145.4
Carpenter	0.377	137.1
Average	0.354	140.2
Murcray	0.367	137.4

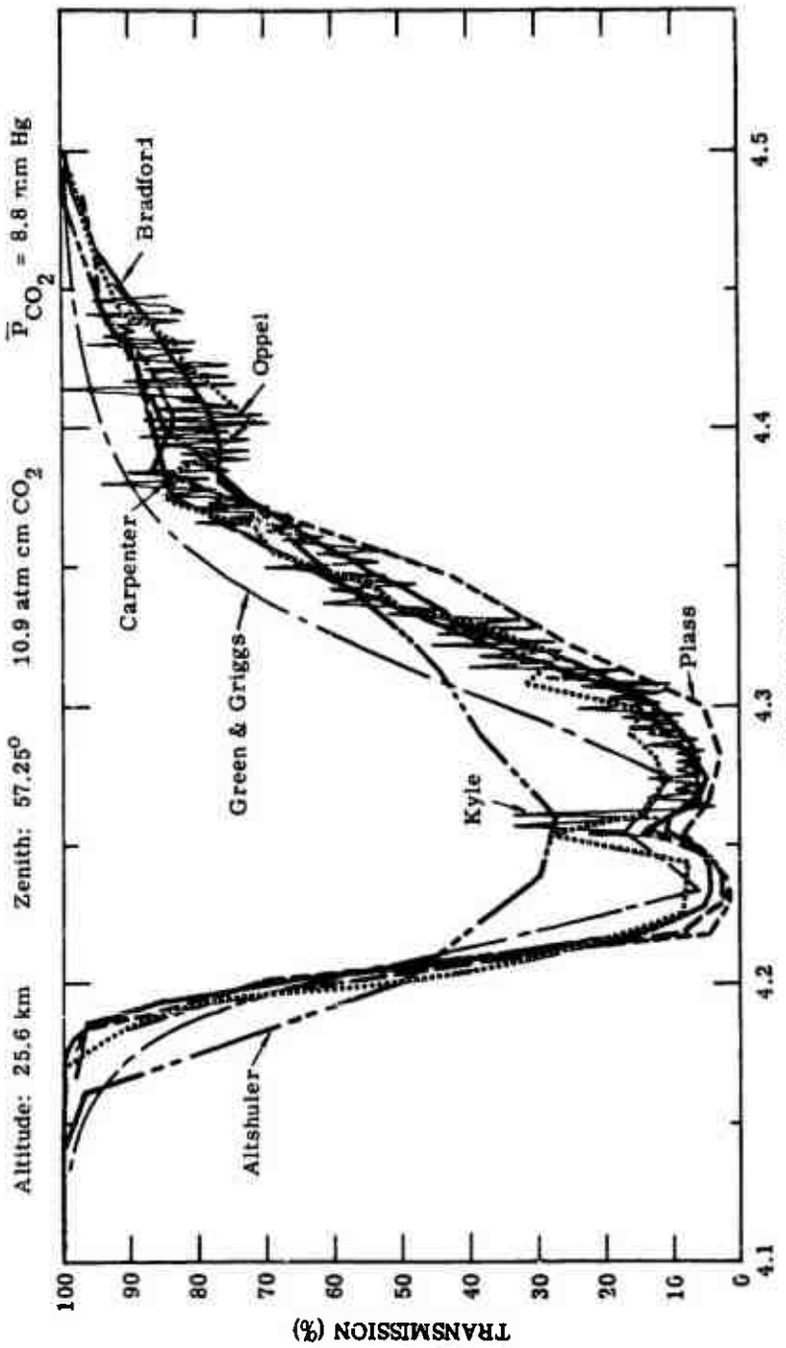

FIGURE 92. COMPARISON OF SOLAR SPECTRA OF KYLE WITH COMPUTED SPECTRA OF BRADFORD; PLASS; CARPENTER; OPPEL; GREEN AND GRIGGS; AND ALTSHULER

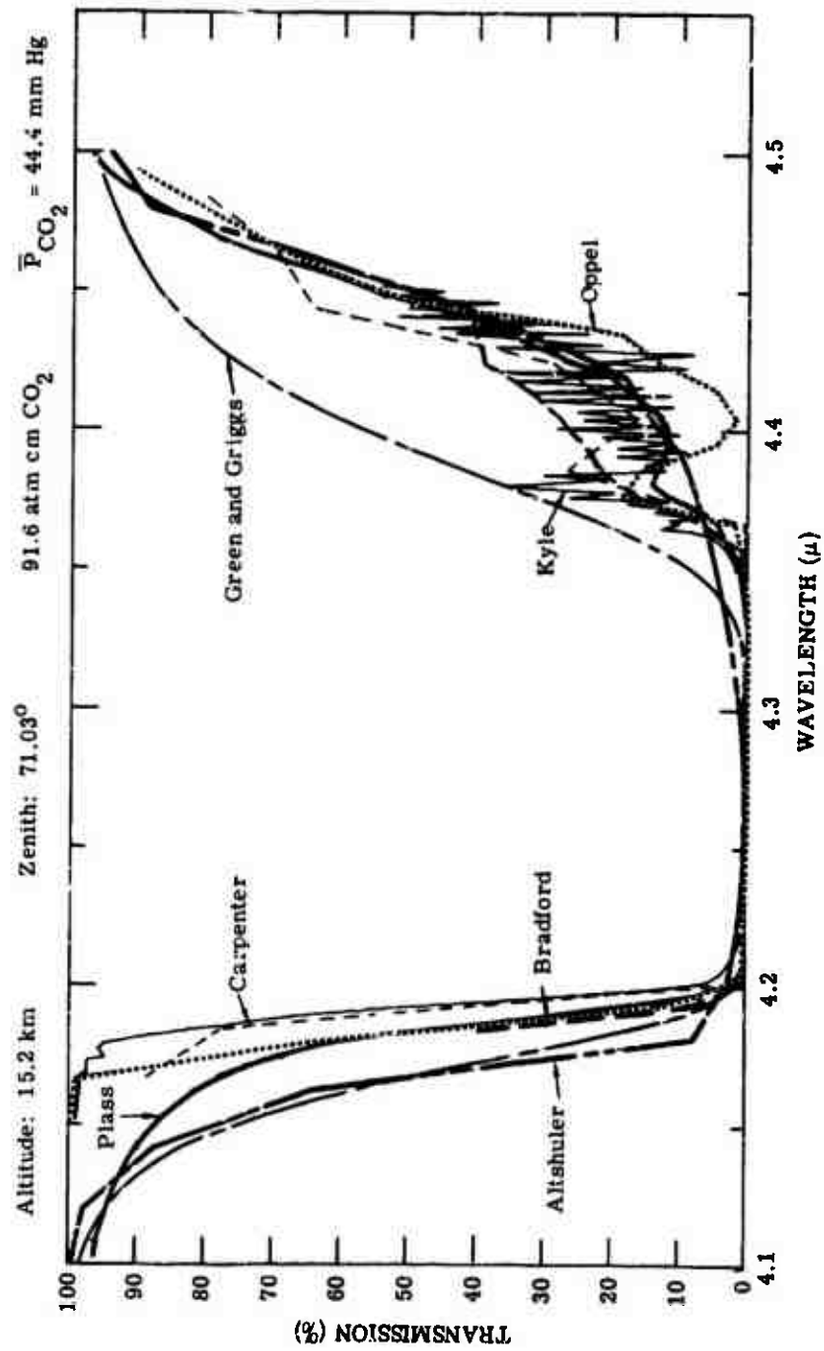

FIGURE 93. COMPARISON OF SOLAR SPECTRA OF KYLE WITH COMPUTED SPECTRA OF PLASS; CARPENTER; BRADFORD; OPPEL; GREEN AND GRIGGS; AND ALTSHULER

describes the line structure more accurately than does the statistical model. The spectra presented in figures 91, 92, and 93 seem to support this statement. Hence, the divergence of the results of Green and Griggs and Altshuler from the Kyle data can possibly be attributed to the model selection.

7.5. COMPARISON OF COMPUTED SPECTRA WITH THE RIGOROUS CALCULATION FOR THE 15-μ BAND

The next absorption band that was selected for comparison was the 15-μ CO_2 band. Unfortunately, experimental field measurements for atmospheric slant paths do not exist for this spectral region; therefore, comparison could be made only among the various calculated spectra.

Drayson [5], using the rigorous method, calculated the spectral transmission from 500 to 859 cm^{-1} at infinite resolution, then averaged his results over various wavenumber intervals. The spectra presented here were averaged over 5-cm^{-1} intervals. His calculations were made for slant paths that extend from a point outside the earth's atmosphere down to 34 different pressure levels, ranging from 0.3 mb (0.0223 mm Hg) to 1013.25 mb (760 mm Hg), for six zenith angles, 0^o, 15^o, 30^o, 45^o, 60^o, and 75^o. Drayson integrated the exact transmissivity function directly with respect to pressure—eliminating the need for the Curtis-Godson approximation—assuming a Lorentz pressure-broadened line shape for high pressures and a mixed Doppler-Lorentz line shape for pressures lower than 100 mb (7.51 mm Hg). The temperature and pressure profiles given in the U. S. Stardard Atmosphere 1962 were assumed throughout, and the mixing ratio of CO_2 was considered by Drayson to be constant at 314 ppm.

Four paths were selected from Drayson's work and his results are compared with spectra computed by the methods of Altshuler, Elsasser, and Plass, which are presented in figures 94-97. The spectra of Altshuler and Elsasser were computed using the equivalent path parameters noted on each curve and the model atmosphere used by Drayson. The spectra of Plass were taken directly from his published tables [63], which were based on the work of Stull et al. [62]. Plass used values of pressure and temperature taken from the ARDC 1959 model atmosphere and a CO_2 mixing ratio of 330 ppm compared to 314 ppm used by Drayson. However, the differences in the model atmospheres used by the two researchers has a small effect on the final transmission values.

The first two of the four comparisons (figs. 94 and 95) are for slant paths extending from 15 km to the limit of the atmosphere at zenith angles of 75^o and 0^o, respectively. The amounts of CO_2 given on the figures are the equivalent amounts of CO_2 for sea-level paths (W^*), which explains the values of equivalent pressure. The high-resolution spectra indicate that there

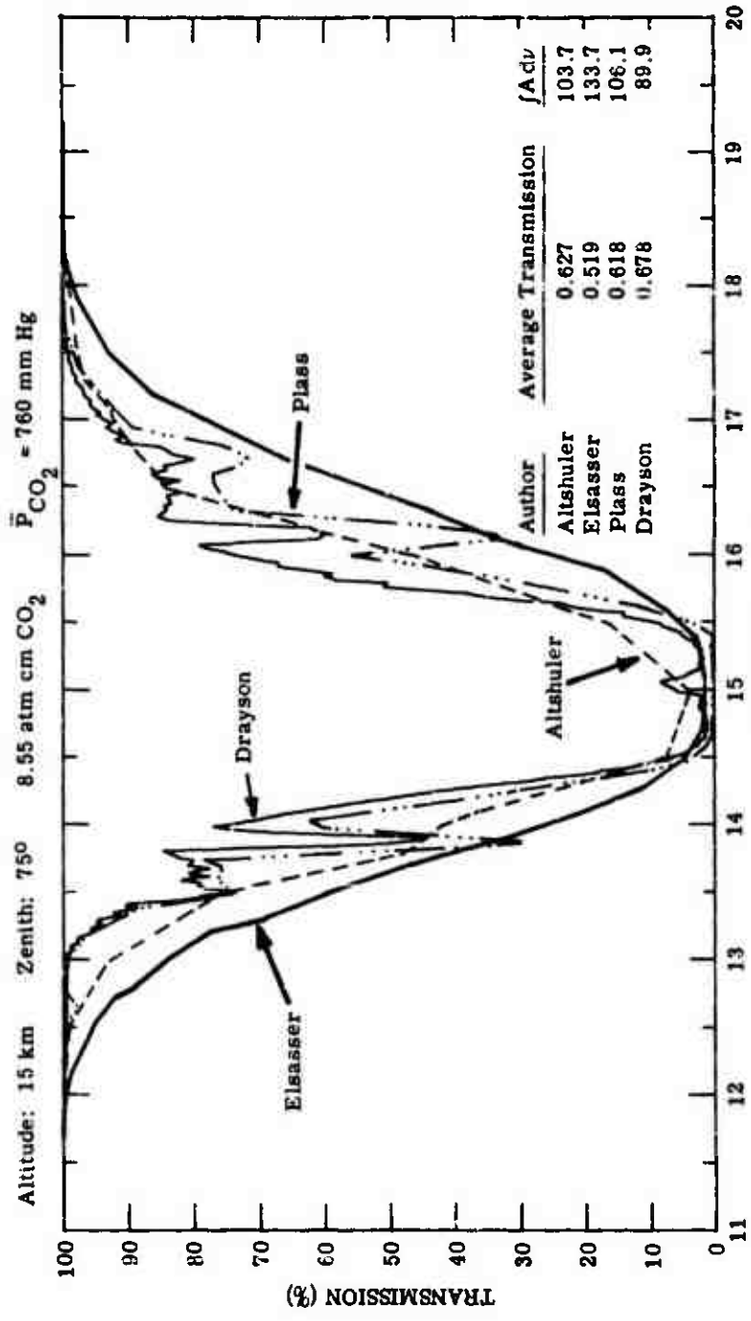

FIGURE 94. COMPARISON OF CALCULATED (RIGOROUS) SPECTRA OF DRAYSON WITH COMPUTED SPECTRA OF ELSASSER, ALTSHULER AND PLASS

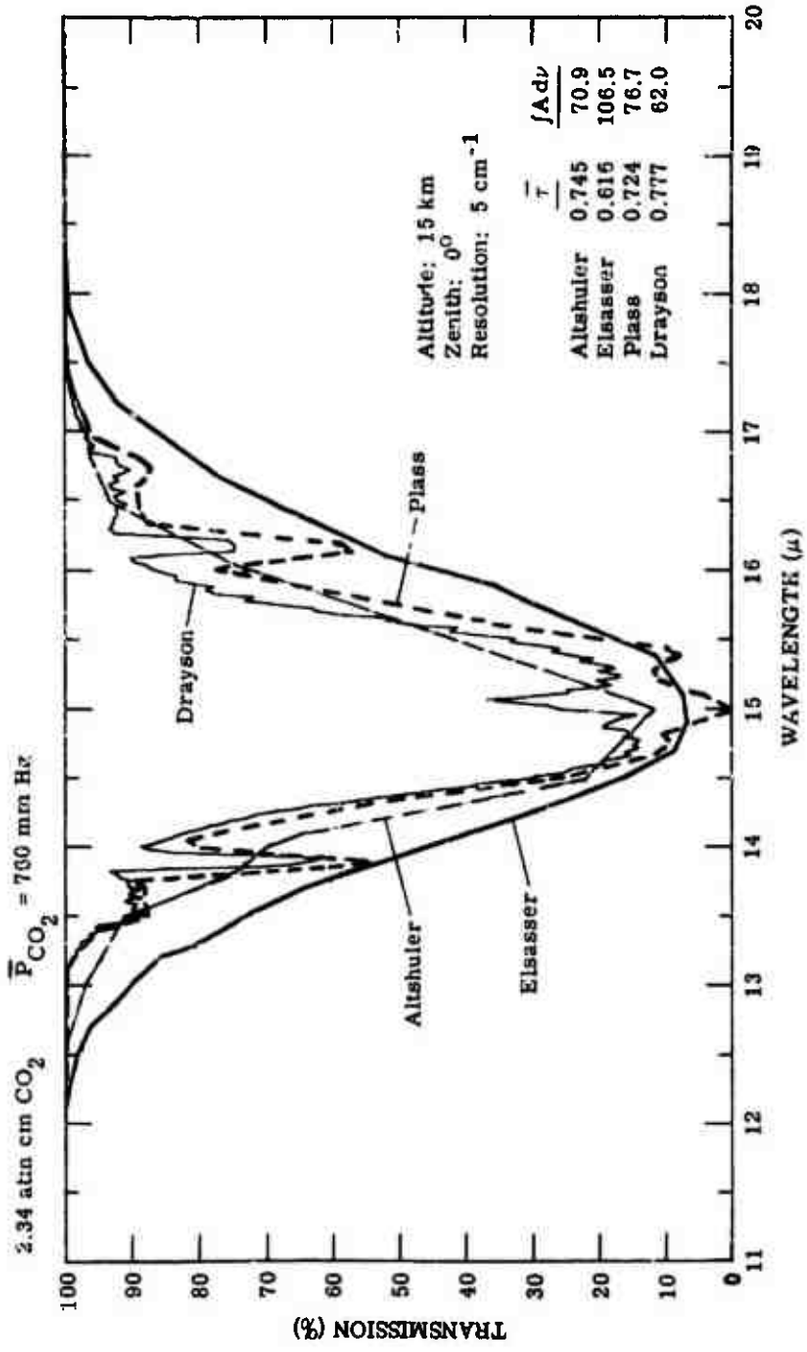

FIGURE 95. COMPARISON OF CALCULATED (RIGOROUS) SPECTRA OF DRAYSON WITH COMPUTED SPECTRA OF ELSASSER, ALTSHULER, AND PLASS

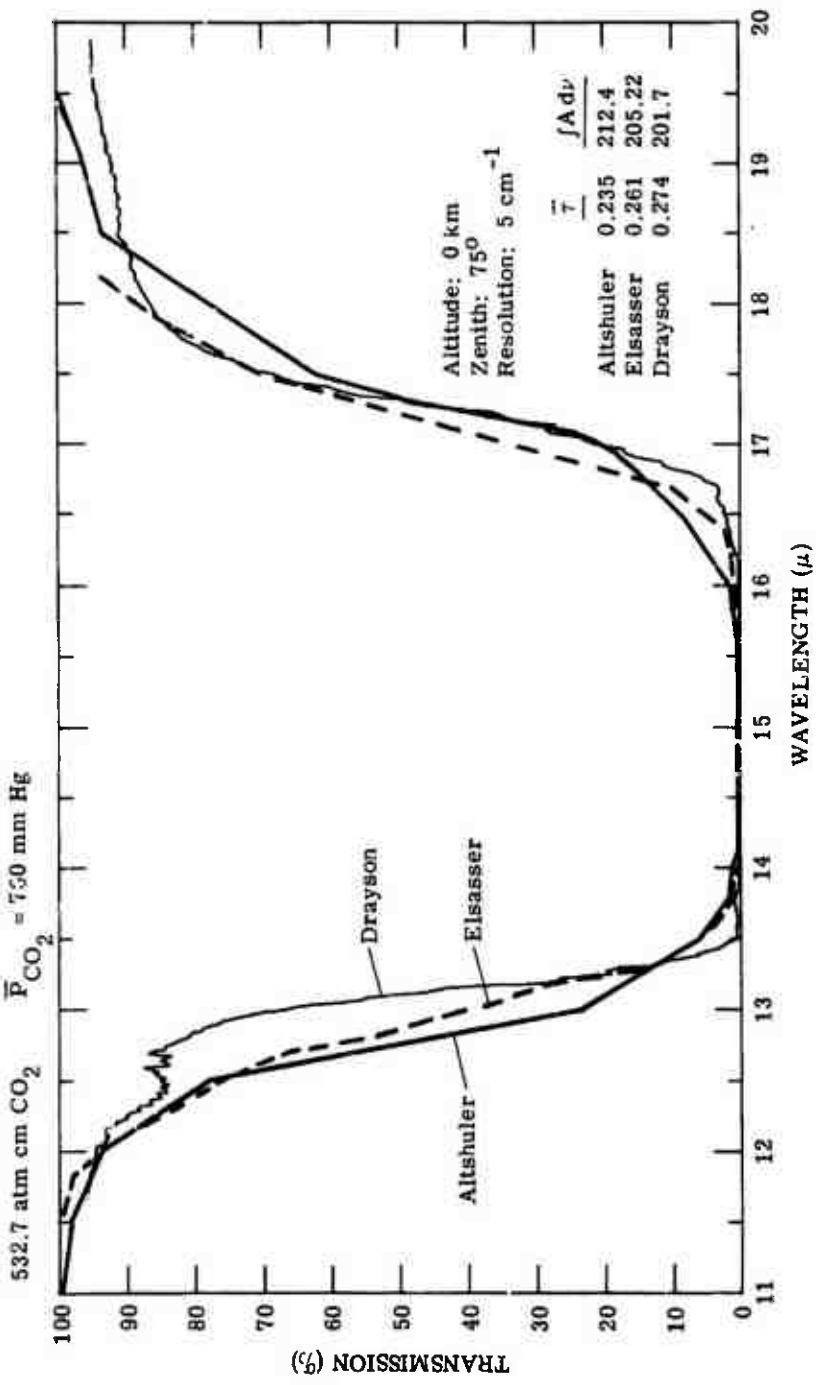

FIGURE 96. COMPARISON OF CALCULATED (RIGOROUS) SPECTRA OF DRAYSON WITH COMPUTED SPECTRA OF ALTSHULER AND ELSASSER

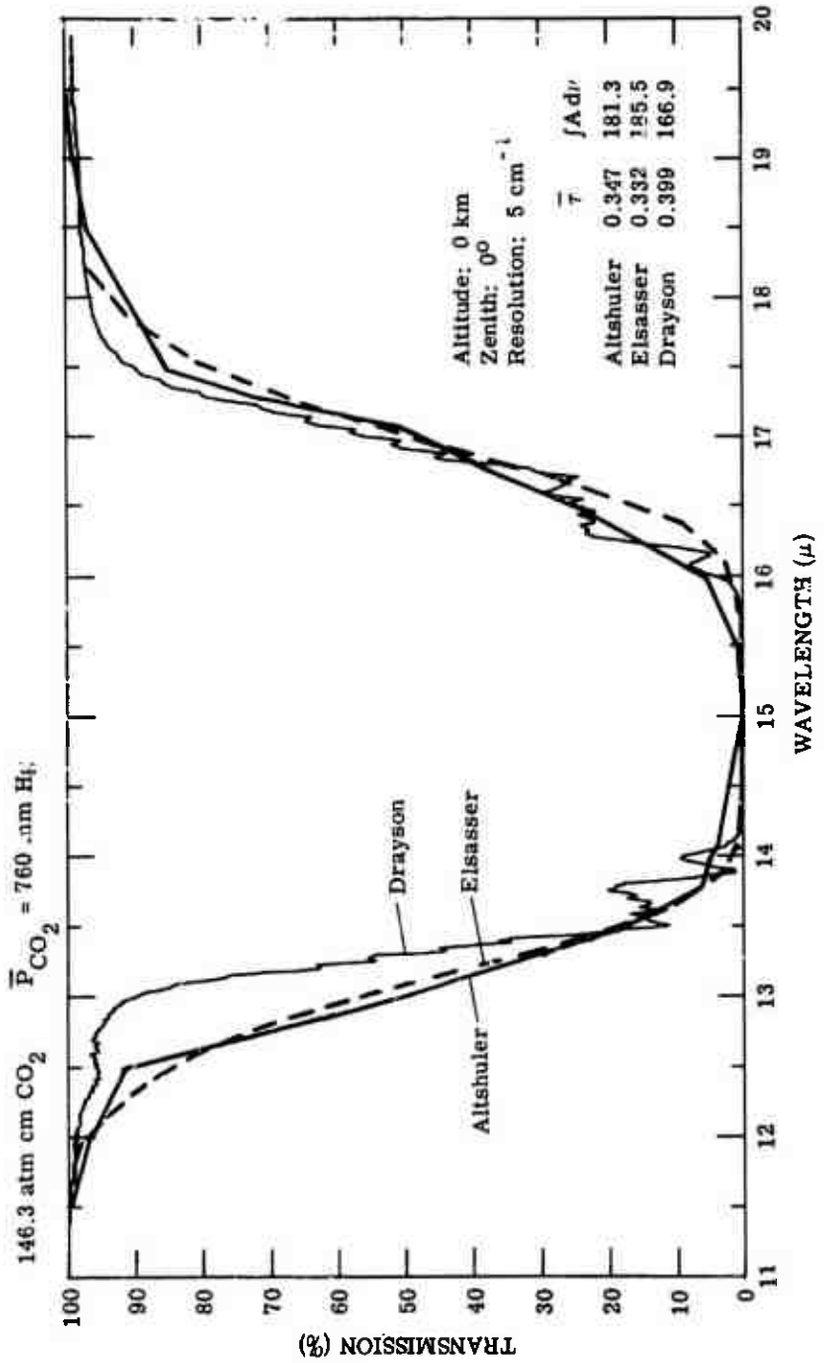

FIGURE 97. COMPARISON OF CALCULATED (RIGOROUS) SPECTRA OF DRAYSON WITH COMPUTED SPECTRA OF ALTSHULER AND ELSASSER

are four distinct regions of relatively high absorption. These are the main P branch and the three main Q branches. As the quantity of absorber and the effective broadening pressure changes, the contribution to absorption of the spectral lines whose centers lie within these main branches varies such that the relative spectral character of the 15-μ CO_2 band changes markedly. It is for this reason that the use of a band model for this band is unsatisfactory if highly accurate results are required. This is borne out particularly by figure 95. Plass's spectrum shows a maximum absorption between the main P and Q branches while the rigorous calculation shows a definite minimum. Also, it is noted that the spectra based on band models show a level of absorption that is consistently higher than the spectra calculated by Drayson. Elsasser gives an average band transmission that is approximately 18 percentage points lower than the Drayson value. The values of Altshuler and Plass compare somewhat better.

The last two comparisons (figs. 96 and 97) were made for slant paths that extend through the entire earth's atmosphere to demonstrate the comparison under conditions of high absorption. Plass did not include low-altitude paths in his tables, so his results could not be compared. For these paths the comparisons between computed spectra and the rigorous calculation are considerably better because the greatest contribution to absorption occurs at low altitudes where the pressures are relatively high. For this band, because of the nature of the spectral line absorption, the Elsasser model and the Curtis-Godson equivalent pressure become better approximations as the pressure and absorber concentration increase.

It is impossible to state conclusively that any one spectrum is more correct than some other spectrum; however, because of the apparent inadequacies in the band-model approach, the spectra of Drayson are more probably correct. Indeed, a series of slant-path field measurements for this spectral region would be enlightening.

7.6. GENERAL COMPARISON OF COMPUTED SPECTRA

All of the figures presented thus far present comparisons of computed spectra with either experimental field measurements or with spectra obtained using the rigorous calculation. The next series of curves include only spectra computed by the methods of section 3 for five slant paths common to a variety of infrared applications. For each path, the three parameters W*, W, and $\overline{P}$ were computed for each gas, using the model atmosphere described in sections 7.1 and 7.3 for temperature, pressure, and CO_2 and N_2O mixing ratios. The mixing ratio used for H_2O was the IRMA wet-temperate model [134]. The mixing ratio used for O_3 was a shifted Elterman profile (see sec. 4.5) that yields 0.44 atm cm O_3 for a vertical path through the entire atmosphere. Using these path parameters, spectra were computed from 1 to 20 μ by each

author's method, except those of Elder and Strong, Bradford, Carpenter, Lindquist, and Howard et al. These were not considered because each method is applicable only to a single absorbing gas. The results of the spectral computations are presented in figures 98 through 102. The path parameters W^*, W, and $\overline{P}$ for each gas are presented on each figure in conjunction with the geometry of the slant path.

The spectra presented in these five figures were included for two reasons: (1) to demonstrate the general nature of absorption for each of the given slant-path geometries, and (2) to indicate the spread in the data for each of the H_2O bands, the N_2O band at 4.5 μ, and the O_3 band centered at approximately 9.6 μ. The 2.7-, 4.3-, and 15-μ bands were previously analyzed, so they are not discussed in this section.

Unfortunately, there is not an experimental spectrum available for any of the slant paths considered in these comparisons; therefore, the correctness of any given spectrum or collection of spectra can be neither substantiated nor refuted. It is felt, however, that the spread in the H_2O, N_2O, and O_3 absorption spectra and variation of this spread in the data as a function of absorber concentration are particularly enlightening.

It is noted in figures 98 through 102 that three of the slant paths begin at the surface of the earth and the remaining two have a minimum altitude of 10.7 km. The most contrasting results observable from these two distinct classes of slant paths is that H_2O shows a relatively small amount of absorption for all bands except the 6.3-μ band, which remains almost opaque at the band center for the path of figure 102. Furthermore, the difference in H_2O absorption between the paths of figures 98 and 99 is quite small, indicating that H_2O does not absorb strongly for altitudes higher than approximately 10,000 ft except for the 6.3-μ band or for slant paths at large zenith angles. Spectra computed by each of the methods presented in these figures for slant paths extending from the limit of the atmosphere down to some 50 different altitudes for a variety of zenith angles would be required to give a reasonably complete description of H_2O absorption. Since our objective was only to indicate the type of comparison obtainable, such extensive computations were considered unnecessary.

The H_2O sea-level equivalent concentrations for the paths presented in figures 98 through 102 are, respectively, 4.46, 3.09, 27.2, 4.82×10^{-3}, and 4.77×10^{-2} pr cm. Comparing each of these values with the data presented in table 32 shows that all but two of these concentrations are bounded by the laboratory data. Therefore, the H_2O spectra presented in figures 98 through 100 represent extrapolations of the laboratory data. As was mentioned earlier, such conditions should be avoided to increase the probability of reliable results. However, absorption spectra for these high H_2O concentrations were included to emphasize the fact that the spread in the

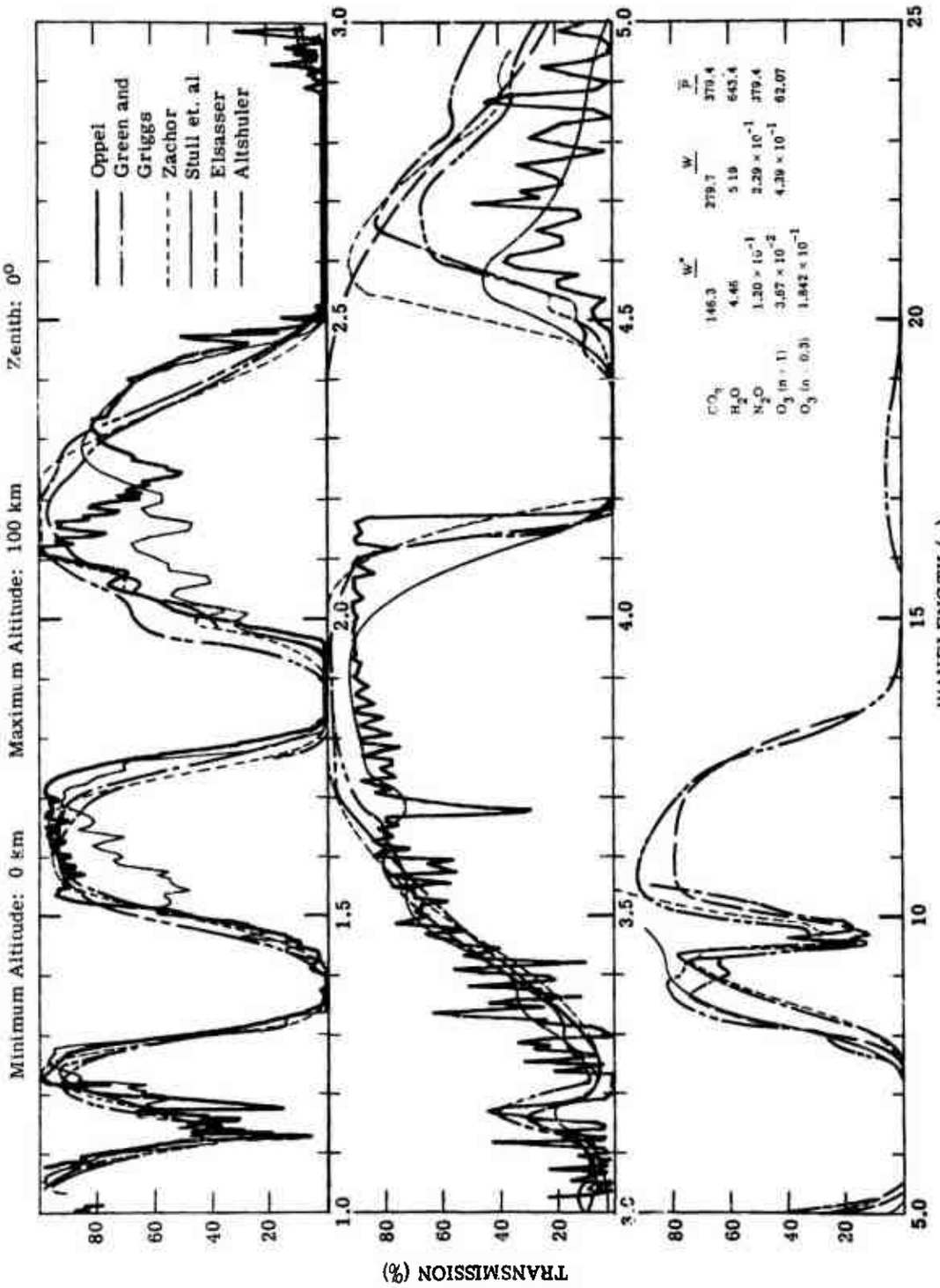

FIGURE 98. COMPARISON OF COMPUTED SPECTRA FOR HIGH-ALTITUDE RECONNAISSANCE PATH

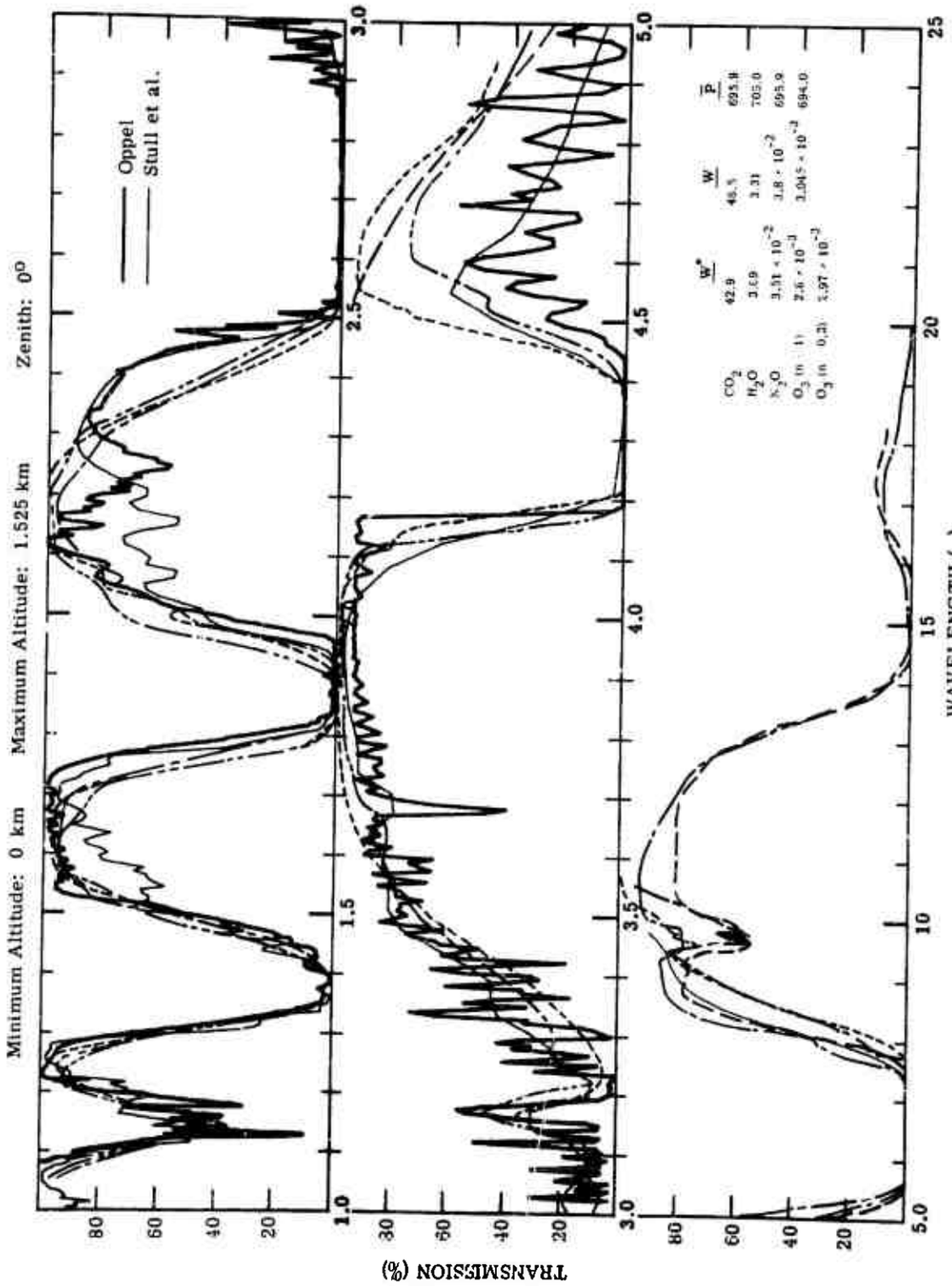

FIGURE 99. COMPARISON OF COMPUTED SPECTRA FOR LOW-ALTITUDE RECONNAISSANCE PATH

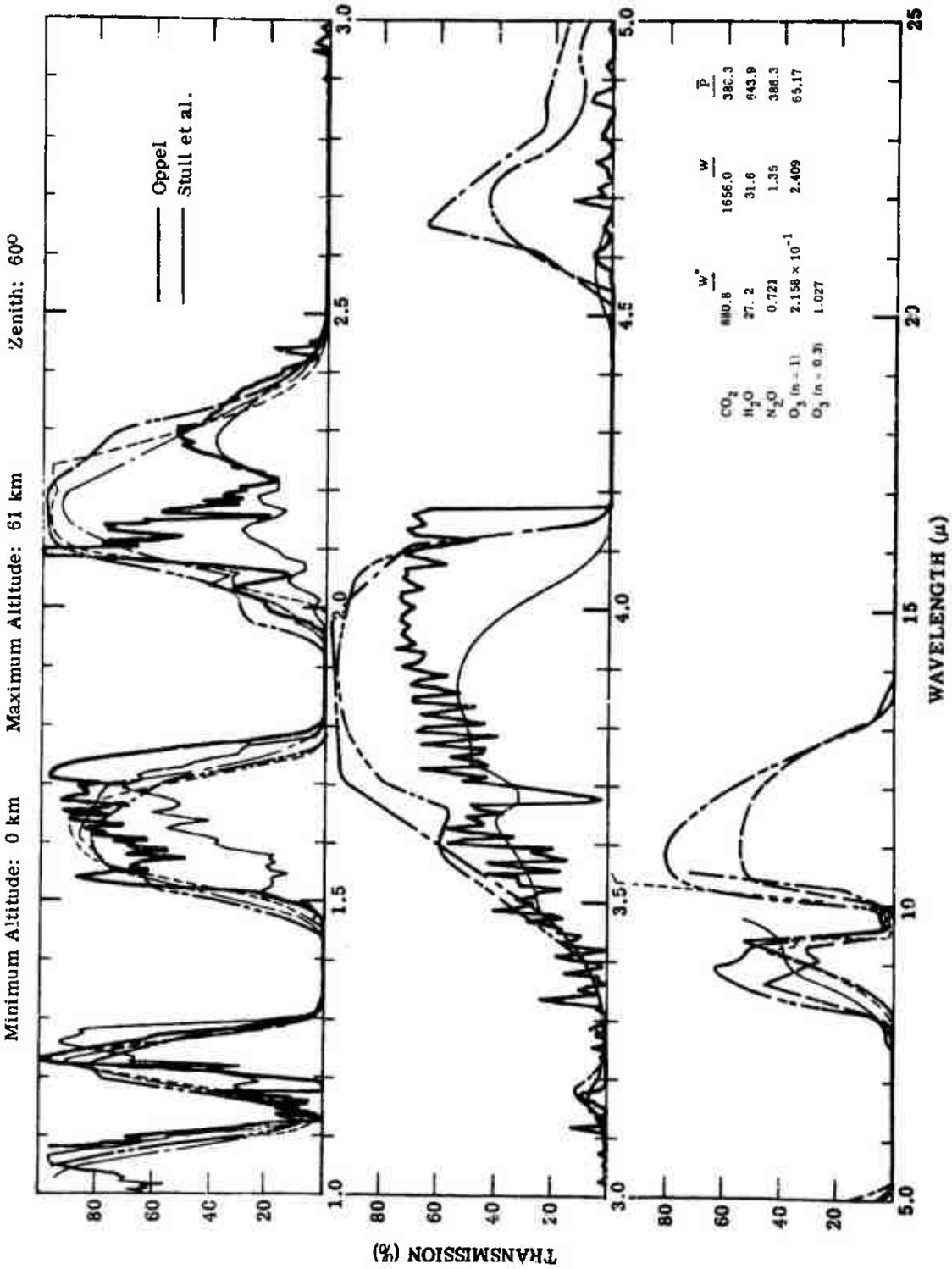

FIGURE 100. COMPARISON OF COMPUTED SPECTRA FOR RE-ENTRY VEHICLE TRACKING PATH (GROUND-BASED)

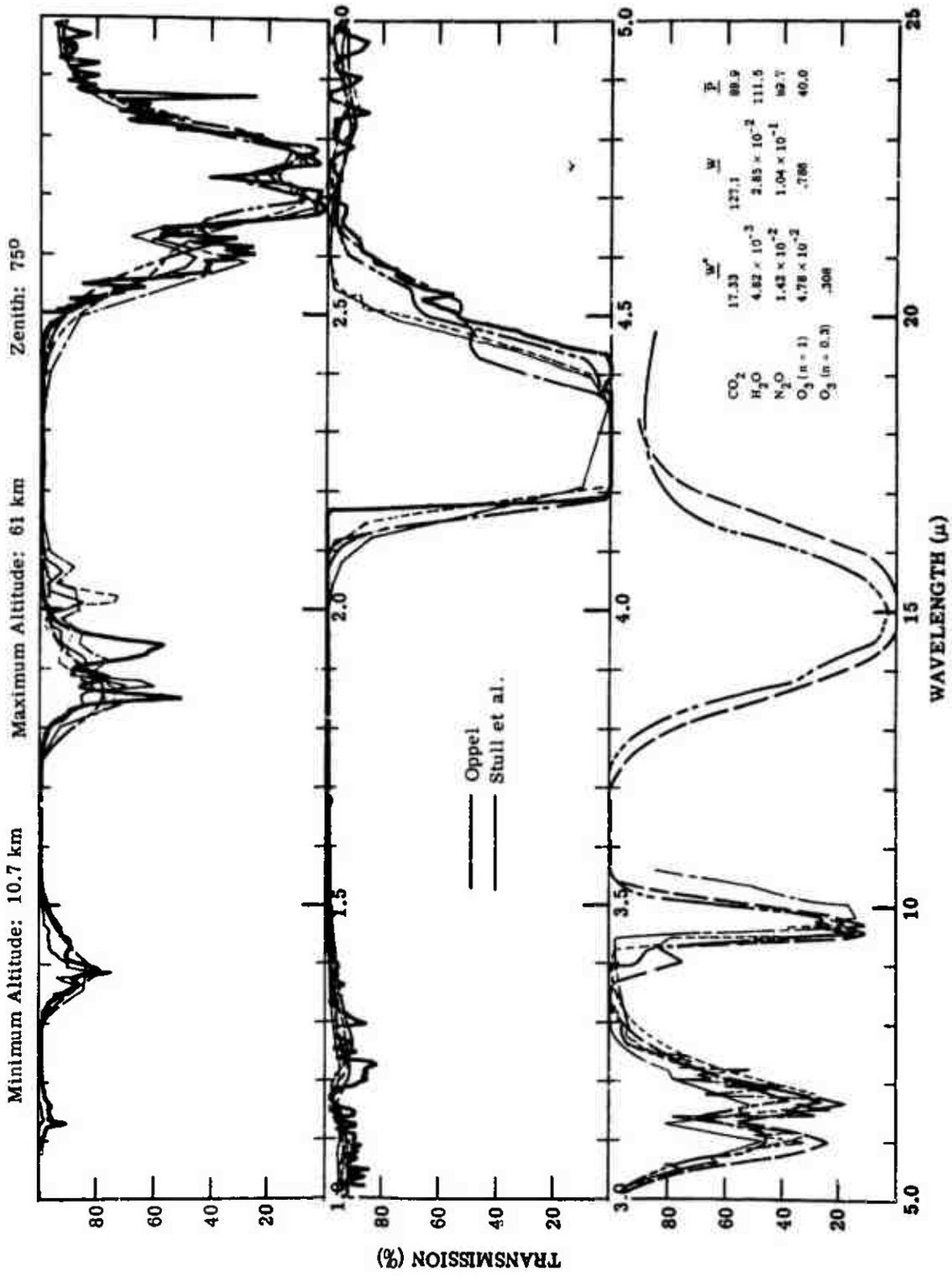

FIGURE 101. COMPARISON OF COMPUTED SPECTRA FOR RE-ENTRY VEHICLE TRACKING PATH (AIRBORNE PLATFORM)

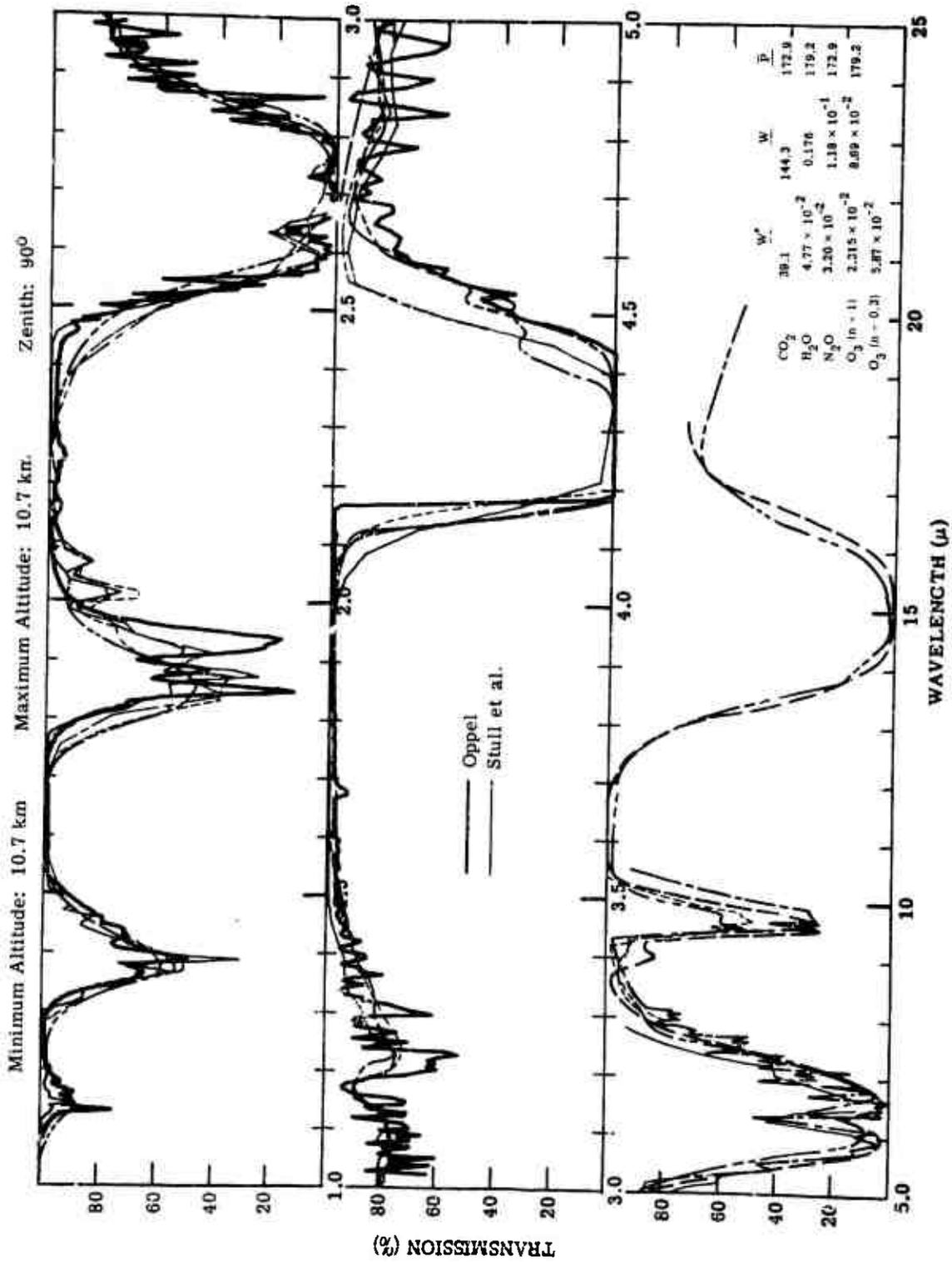

FIGURE 102. COMPARISON OF COMPUTED SPECTRA FOR AIR-TO-AIR PATH

data becomes large as the H_2O concentration increases beyond concentrations that are bounded by the laboratory data. In figures 98 through 102, it is noted that the largest spread in the data exists for the path containing 27.2 pr cm of H_2O. Particularly note the close comparison between the spectra of Zachor, Altshuler, and Green and Griggs and how these data differ from the results of Oppel and Stull et al. The close comparison among these researchers undoubtedly results from the fact that each used the laboratory data of Howard et al. to specify the spectral absorption coefficients. Also, each used the same form of the Goody model in the development of the transmissivity functions presented in section 3. Oppel used the same model as Zachor, Altshuler, and Green and Griggs, but used a different collection of laboratory data. Stull et al., in contrast to the other authors, employed the quasi-random model and used the data of Howard et al. only to normalize the equivalent line intensities.

The H_2O spectra presented and the above discussion seem to indicate that the present state of the art of methods for calculating H_2O spectral absorption are rather poor, particularly for high H_2O concentrations. An enhancement of the present state of the art would require laboratory data at sufficiently high concentrations to bound the H_2O concentrations which exist for long low-altitude paths and atmospheric field measurements to provide a basis for comparison. Until the advent of such data, it is recommended that these methods be applied only to those paths which yield concentrations that are bounded by the laboratory data used to define the absorption coefficient. Under these conditions the spectra presented indicate a spread in the data that is relatively small.

A final point, mentioned in section 7.1, is the apparent spectral shift between the spectra computed by the methods of Zachor, Altshuler, and Green and Griggs and the spectra determined by the methods of Oppel and Stull et al. for the H_2O bands centered at 1.14, 1.38, and 1.88 μ. Other experimental sources indicated that the data of Howard et al. contained errors in spectral calibration, and based on this fact it is recommended that the absorption coefficients determined by Zachor, Altshuler, and Green and Griggs be shifted spectrally to agree with the spectra of Oppel, if their methods are to be employed.

Note in figures 98 through 102 that there are significant differences in the spectra for the spectral region from 4.4 to 4.6 μ. Absorption in this spectral region is caused by the wings of the 4.3 CO_2 band and the 6.3 H_2O band, and the N_2O band which is centered at approximately 4.5 μ with N_2O giving the longest contribution to absorption. Only three researchers developed methods for computing N_2O absorption: Oppel, Green and Griggs, and Altshuler. Therefore, the spectra of Stull et al., Zachor, and Eisasser do not include the effects of this gas. The spectra that include N_2O absorption demonstrate a spread in the data as large as

20 percentage points in transmission at 4.5 μ with no two spectra being in close agreement. The reasons for these differences are difficult to assess, and until field measurements of absorption which can be used as a basis for comparison are made, the tools for evaluating the methods for predicting N_2O absorption are not available.

Figures 98-102 demonstrate that O_3 is a significant absorber at 9.6 μ, particularly if the slant path passes through that region of the atmosphere at which the O_3 concentration is a maximum (see sec. 4.5). The four methods for computing O_3 absorption yield results that are significantly different, the spread in the data becoming greater as the equivalent sea-level path concentration decreases. The spectra for the path containing the least amount of O_3 is shown in figure 99. For this case, the difference between the method which yields the greatest amount of absorption (i.e., Green and Griggs) and the method which yields the least (i.e., Altshuler) is approximately 30 percentage points in transmission. These differences are attributed to a variety of inputs: Zachor, Elsasser, and Altshuler used the Elsasser model; Green and Griggs used the statistical model. Zachor and Green and Griggs used Walshaw's data, Altshuler used three different sources of data, and Elsasser used Summerfield's data originally and later modified his results based on an analysis of Walshaw's data. Elsasser and Green and Griggs used a linear pressure correction on half-width and Zachor and Altshuler used pressure corrections that were highly nonlinear (see sec. 3). Such diversified approaches to the problem and the fact that experimental field measurements of O_3 absorption are not available make it impossible to determine whether one set of results is more correct than another. Obviously, further research is needed for this spectral region.

Considering the spectra presented in figures 98 to 102 in toto, the state of the art does not appear to be particularly good, especially in the wings of the bands, and hence in the window regions, for absorber concentration of sufficient magnitude to cause some absorption in the window regions (note figs. 98 and 100). As the slant-path parameters W and $\overline{P}$ are decreased to values that are bounded by the laboratory data (under these conditions attenuation in the window regions is small), the spread in the computed data becomes small enough to ensure some measure of reliability in aosorption values for the spectral region from 1.0 to approximately 4.4 μ; but there is still a significant spread in the data for the spectral region from 4.4 μ through the 15-μ CO_2 band. These differences are in general caused by the fact that the various authors used different collections of laboratory data and varied methods of fitting the band models to the laboratory data.

It appears, therefore, that in order to improve the methods for computing absorption for the wings of the H_2O bands, the N_2O band, the 9.6-μ O_3 band, and the 15-μ CO_2 band more

research is required, particularly the measurement of homogeneous absorption spectra to update and close the gap in the presently available spectra and open-air field measurements of absorption which can be used as a basis for comparison. Until the advent of such research, the infrared researcher must be content with the present state of the art, realizing that the greatest reliability is achieved for values of W and $\overline{P}$ which are bounded by the laboratory data.

8
SUMMARY AND CONCLUSIONS

Two general methods for computing the absorption spectra for an atmospheric slant path have been discussed: the "rigorous" method and the method which is based on a model of the band structure. The rigorous method involves summing the contribution to absorption of each spectral line and hence is a somewhat exact evaluation of the general transmissivity function for spectral absorption. This direct integration has been performed by Drayson [5] and by Gates et al. [7] for the 15-μ CO_2 band and the 2.7-μ H_2O band, respectively. The rigorous method is desirable since any resolution is attainable and for slant-path calculations of absorption the Curtis-Godson approximation is not required. The method has limited spectral application, however, since all of the band parameters for CO_2 and H_2O are known accurately for only certain wavelength intervals. Also, the evaluation of the general function requires extensive computational labor and is therefore considered impractical for many infrared applications.

The second method, that which is based on assuming a model of the band structure, has been used by many researchers, resulting in methods for computing slant-path spectral absorption for every atmospheric absorbing gas for the wavelength region from 1.0 μ through the long-wavelength rotational H_2O band. The reason for using band models was to develop methods which involve a minimum amount of computation and yet yield good first-order approximations to the true spectra. The methods of twelve authors have been presented and discussed, and spectra computed by each author's method were compared with spectra determined from open-air field measurements, spectra calculated by the rigorous method, and spectra computed by other band-model methods. The most indicative of these comparisons is that of "computed" spectra with slant-path open-air field measurements. Unfortunately, such comparisons were limited to the 2.7- and 4.3-μ bands, since these are the only spectral regions for which measurements were made of slant paths under such conditions that the absorber concentrations could be determined with reasonable accuracy.

After a careful examination of the comparative spectra presented in section 7 and the data summarized in tables 31 and 32, the following general observations were made concerning the methods based on band models.

(1) The 1.14-, 1.38-, 1.88-, 3.2-, and 6.3-μ H_2O Bands

All methods, except Oppel's, were based on laboratory homogeneous spectra that were measured prior to 1955 and have a maximum H_2O concentration of less than 4.0 pr cm. The

data of Howard et al. are apparently shifted to shorter wavelengths for the 1.14-, 1.38-, and 1.88-μ H_2O bands, which is inherent in the methods of Altshuler, Zachor, and Green and Griggs. The only existing comparative open-air field measurements are for homogeneous paths, and therefore the W and $\overline{P}$ approximations could not be evaluated. The comparisons presented for each of the five spectral regions (note figs. 98 and 100) indicate large differences in absorption in the wings of the bands and the window regions for absorber concentrations that are not bounded by the laboratory data. For concentrations which are bounded by the laboratory data the comparisons are greatly improved.

(2) 2.7- and 4.3-μ Bands

For each of these spectral regions extensive laboratory homogeneous-path spectra exist for broad ranges of W and P at relatively high resolution. Reliable slant-path open-air field measurements of absorption are available for the central portion of the 2.7-μ band and for the entire 4.3-μ band. The comparisons (note figs. 76-93) indicate that band-model methods are capable of yielding good first-order approximations to measured data when the spectra are averaged over spectral intervals on the order of 0.04 μ or larger. At significantly higher resolution, the band-model spectra in general display values which differ significantly from measured data. These comparisons further indicate that the equivalent sea-level path and Curtis-Godson approximations can be used effectively.

(3) 4.5-μ N_2O Band

N_2O absorption is the spectral region from 4.4- to 4.6-μ is immersed in the wings of the two adjacent bands of CO_2 and H_2O, which makes it difficult to evaluate the state of the art of methods for predicting absorption due to this gas. However, the differences in the spectra noted in figures 98 through 102 indicate that the state of the art is relatively poor. There exist many homogeneous-path spectra (note table 32) for this gas, but only three researchers have developed computational methods. Since the results of each of these three researchers are in disagreement, more computational methods and open-air measurements of absorption spectra will be required before the state of the art can be improved.

(4) 9.6-μ O_3 Band

For this absorption band the available laboratory homogeneous-path data are extremely meager. The most recent and only relatively extensive measurements have been made by Walshaw [34]; these were used by Zachor and Green and Griggs. The methods of Elsasser and Altshuler were based on data that were less extensive and much older. Open-air field measurements of O_3 absorption for paths for which the O_3 concentration is known do not exist. Therefore, comparisons between computed and measured spectra could not he made. The

intercomparison of computed spectra for this spectral region (note figs. 98-102) displays results which are significantly different; the greatest amount of divergence is noted for those paths which contain the least amount of O_3. The uncertainties in O_3 self-broadening, which resulted in slightly different treatment by the four researchers, is one factor which contributed largely to this difference.

(5) 15-μ CO_2 Band

The 15-μ CO_2 band has not been considered by most researchers; consequently, only three methods for computing absorption spectra are available. Two of these methods employ the Elsasser model and one the quasi-random model. Open-air slant-path field measurements do not exist for this spectral region, so comparisons were made between computed spectra and spectra calculated by the rigorous method. In general, band-model methods tend to overpredict absorption compared to that calculated by the rigorous method, with the spectra of Stull et al. which are based on the quasi-random model, being in closest agreement.

These general observations conclusively indicate that the state of the art of methods for computing atmospheric absorption is far from saturated. Indications are that the concept of band models and such concepts as the "equivalent sea-level path" and the Curtis-Godson approximation are theoretically sound, and when coupled with reliable laboratory homogeneous-path spectra and sound empirical procedures, computational methods can be developed which yield results that are comparable to measured data. However, inconsistencies are observable when the band-model methods are used to compute absorption for absorber concentrations that are not bounded by the laboratory data. Therefore, to enhance the present state of the art of band-model methods, it is suggested that research should be continued with emphasis on the following four areas:

(1) Obtain high-resolution laboratory data for all absorbers and all absorption bands for ranges of concentration and pressure sufficiently broad to bound the slant-path parameters encountered in practice. This would not be a comprehensive program, but one which would close the gaps in present laboratory data. Such data would thus provide a basis for developing a consistent set of band-model methods for computing absorption which would not require extrapolations.

(2) Investigate the various methods used for empirically fitting band models to laboratory data and extend such methods, if necessary, to develop a standard method for use by all researchers.

(3) Determine the band parameters for all absorption bands for the major absorbing constituents and eventually for all absorbers. This would allow for the general application of the rigorous method to any band.

(4) Obtain atmospheric slant-path, high-resolution spectra under such conditions that the quantity of each absorber in the path could be determined. Such data would provide a true test of the degree of correctness of both the exact method and the methods based on band models.

The author feels that the results of the above program should be controlled by a single agency and utilized so that a general program for computing atmospheric transmission could be compiled and made available for general dissemination.

A computer program is being written which utilizes what we consider to be the optimum band-model method for each spectral band, selected from the twelve methods presented in this report. This program, coupled with the slant-path program described in appendix I, will then provide for computing slant-path transmission spectra which are consistent with the present state of the art. The program is being written so that it can be easily modified as the state of the art advances. It will be published as an addendum to this report.

Appendix I
COMPUTER PROGRAM FOR CALCULATING W, W*, AND $\overline{P}$

The three parameters W*, W, and $\overline{P}$ are defined by the following relationships:

$$W^* = \int_0^X \frac{P(x)}{P_0}\left(\frac{T_0}{T(x)}\right)^n \rho(x)\,dx \tag{100}$$

$$W = \int_0^X \rho(x)\,dx \tag{101}$$

$$\overline{P} = \frac{\int_0^X P(x)\rho(x)\,dx}{\int_0^X \rho(x)\,dx} \tag{102}$$

where x = distance along path in meters

P = pressure

T = temperature

ρ = partial density of absorbing gas

Expressing equations 100-102 in terms of pressure, temperature, and mixing ratio, we have

$$W^* = \int_0^X M(x)\left(\frac{P(x)}{P_0}\right)^2\left(\frac{T_0}{T(x)}\right)^{n+1} dx \tag{103}$$

$$W = \int_0^X M(x)\left(\frac{P(x)}{P_0}\right)\left(\frac{T_0}{T(x)}\right) dx \tag{104}$$

$$\overline{P} = \frac{\int_0^X M(x)\left(\frac{P(x)}{P_0}\right)^2\left(\frac{T_0}{T(x)}\right) dx}{\int_0^X M(x)\left(\frac{P(x)}{P_0}\right)\left(\frac{T_0}{T(x)}\right) dx} \tag{105}$$

where M(x) is the mixing ratio of a given absorber expressed in moles of gas per mole of air. Equations 103-105 are then used directly to compute the values of the three parameters for all

gases for which the mixing ratio is given in parts per million (ppm) $\times 10^{-4}$. CO_2, O_3, N_2O, CO, and CH_4 will be in these units. W^* and W as determined by equations 103 and 104 will be in atmospheric centimeters.

To compute the values of the three parameters for water vapor, the mixing ratio in grams of H_2O per kilogram of air is multiplied by the factor 1.225×10^{-4}. Equations 103-105 will then yield the proper values, with W^* and W expressed in precipitable centimeters.

It is noted that the integral

$$I(a, b) = \int_0^X M(x)\left(\frac{P}{P_0}\right)^a\left(\frac{T_0}{T}\right)^b dx \qquad (106)$$

is common to equations 103, 104, and 105. Therefore, each of the parameters may be determined by simply computing equation 106 for different values of a and b. Or,

$$W^* = I(2, n + 1)$$

$$W = I(1, 1)$$

$$\overline{P} = P_0 \frac{I(2, 1)}{I(1, 1)}$$

A computer program has been written in FORTRAN for The University of Michigan IBM 7090 to evaluate I(a, b) for any slant path for which the mixing ratio, temperature, and pressure profiles are known as functions of altitude Z. In the following discussion it is assumed, therefore, that the parameter M(Z) is specified for each absorbing gas and P(Z) and T(Z) are given.

The first step in evaluating I(a, b) is to determine the refracted path through the atmosphere. Consider a spherical earth surrounded by a spherical atmosphere. It is assumed for this calculation that the atmosphere exists in spherical shells, each shell being homogeneous. Under this assumption the refractive index will be constant throughout a given shell, changing abruptly as one passes from one shell to the next. The slant path is defined by the lowest point in the path Z_1, the highest point in the path Z_2, and the angle subtended by Z_1 and Z_2 at the earth's center (see fig. 103).

The first approximation to the true path is the straight line joining Z_1 and Z_2 (see fig. 104). The angle Φ is divided into N equal angular increments $\Delta\phi_1, \Delta\phi_2, \ldots, \Delta\phi_N$, where N is determined from the equation

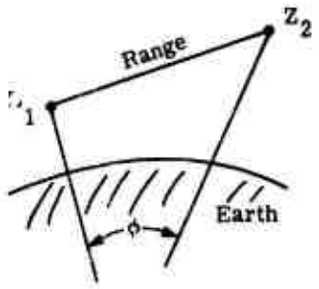

FIGURE 103. PARAMETERS DEFINING GEOMETRY OF SLANT PATH

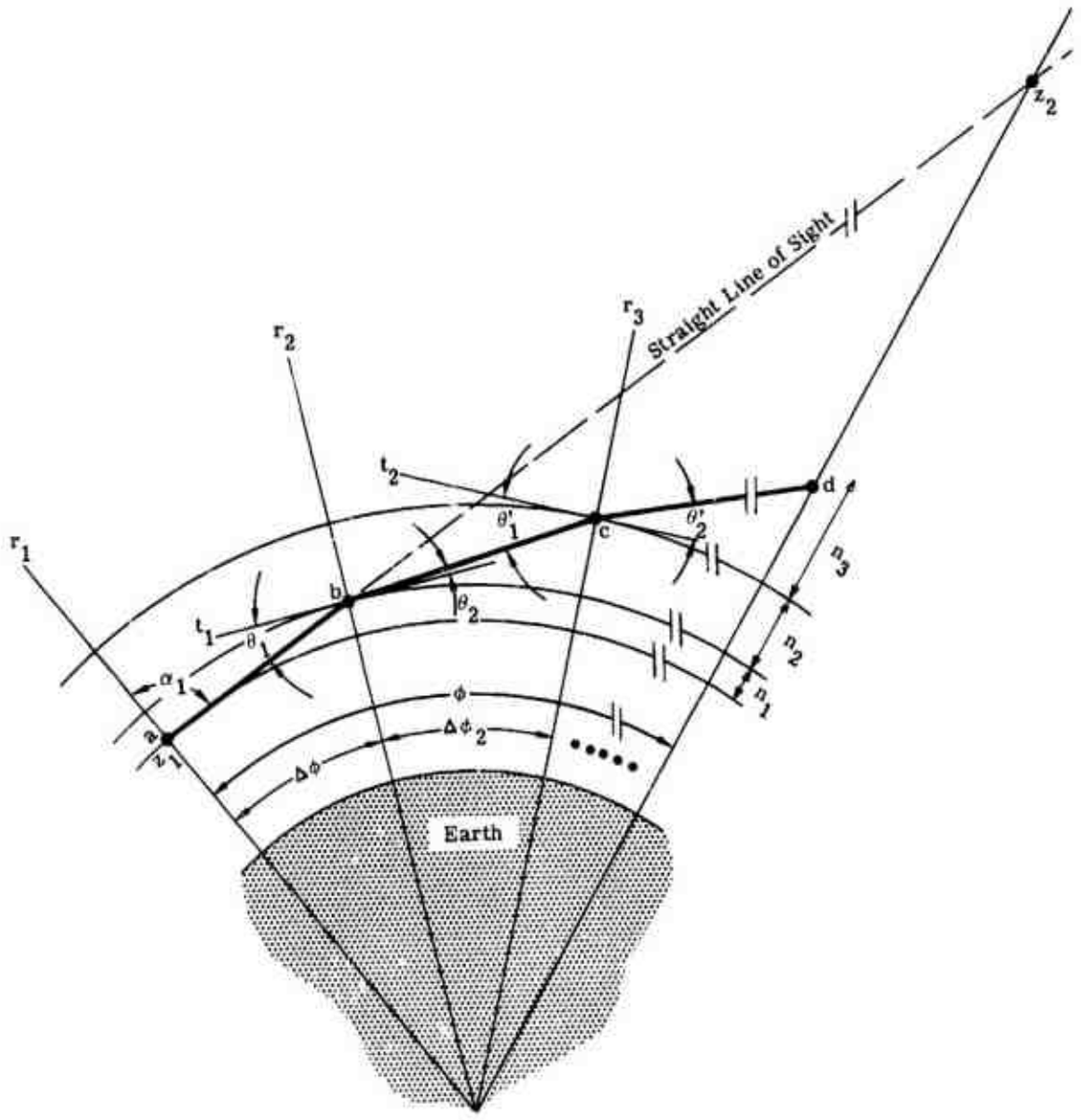

FIGURE 104. SCHEMATIC DIAGRAM OF ATMOSPHERIC REFRACTED PATH

$$N = \max \left\{ \frac{Z_2 - Z_1}{200} ; \frac{\text{range}}{2000} \right\}$$

where Z_1, Z_2 and range are expressed in meters. This method of incrementing the path insured that a point would be calculated at least every 200 m altitude. α_1 is defined as the angle between the line of sight and the radial line r_1. Point b is the point where the line of sight intersects the second radial line r_2. If a tangent line t_1 is drawn through b which is normal to r_2, it is obvious that the angle θ_2 will be given by

$$\theta_2 = \arcsin \left[\frac{n_2}{n_1} \left(\frac{R_e + Z_2}{R_e + Z_1} \right) \sin \theta_1 \right] \tag{107}$$

when n_1 and n_2 are the refractive indexes of the lower shell and upper shell, respectively, and R_e is the radius of the earth.

To determine the refractive index of any given shell the results of Edlen [151] and Penndorf [152] are used. Edlen derived an empirical formula for the refractive index of air near the earth's surface:

$$n_s = 1 + 10^{-8} \left(6432.8 + \frac{294910}{146 - \frac{1}{\lambda^2}} + \frac{25540}{41 - \frac{1}{\lambda^2}} \right)$$

where n_s = refractive index of air at $288^{\circ}K$ and 760 mm Hg

λ = wavelength in microns

The refractive index is also a function of temperature and pressure which is given by Penndorf's relationship

$$n(Z) = 1 + (n_s - 1) \left(\frac{1 + T_s/T_i}{1 + T(Z)/T_i} \right) \frac{P(Z)}{P(s)}$$

where $T_s = 288^{\circ}K$

P_s = 760 mm Hg

T_i = ice temperature

$P(Z)$ = ambient pressure

$T(Z)$ = ambient temperature

As was stated previously, the refractive index of a given shell is assumed to be constant throughout the shell. Also, for purposes of this calculation it is assumed that the value of n_i for the ith shell is the value calculated for the lowest altitude of the shell.

The angle θ_2 in equation 107 defines a new line of sight which intersects the radial line r_3 at point C. A tangent line t_2 is drawn normal to r_3. Then the refracted angle θ_2' is given by Snell's law as before. This procedure is continued until the path intersects the radial line passing through Z_2 at point d. The altitude difference between Z_2 and d is used to increase the angle α. The entire procedure is then repeated until the point d converges to Z_2 within less than 10 m. When the final refracted path is calculated, a range-altitude table is compiled where the range is measured from the lowest point in the path. This table, in conjunction with M(Z), P(Z), and T(Z), therefore specifies M(x), P(x), and T(x). I(a, b) is then evaluated using Simpson's rule to perform the integration over x. By simply changing the values of a and b, each of the path parameters W, W^*, and $\overline{P}$ can be calculated. The program has the flexibility of evaluating I(a, b) simultaneously for as many as four absorbing gases.

A listing of the complete program is presented below. The main program, all subroutines, definition of symbols, and a step-by-step procedure for inputing the data are included.

The main program uses four subroutines:

(1) ATMO. This subroutine calculates the refracted path through the atmosphere between the source and the receiver. The method used is that which was described previously. The input data required are pressure, temperature, and wavelength. To be completely rigorous a new path should be calculated for each wavelength for which transmission values are desired. However, the refractive index of the atmosphere is a slow-varying function of wavelength, so only one path is calculated. The wavelength used is the mean value of the wavelength being considered for a transmission calculation.

(2) UGRAND. The subroutine UGRAND is a function which calculates the integrand of I(a, b) where $I(a,b) = \int_0^X M(x)\left(\frac{P}{P_0}\right)^a\left(\frac{T_0}{T}\right)^b dx$. The input to the function is the value of x at which a value of I(a, b) is desired. The function uses The University of Michigan subroutine TAB to interpolate for a value of Z (altitude) to correspond to the desired x (range). The same routine is called upon for values to be selected from T (temperature) table, P (pressure) table, and M (mixing ratio) table. The integrand is evaluated and returned to the integration routine (SIMPSN).

(3) SIMPSN. This routine integrates a single function and the absolute value of the function by Simpson's rule, the maximum number of intervals being set by the user. The integration process is repeated until either the values of both integrals converge to the true values, the

tolerance being set by the user. or until the Integration has been performed using the maximum number of Intervals. The calling sequences for SIMPSN are:

CALL SETSMP (ALWERR, XMAX, DEBUG)

and

CALL SIMPSN (FUNCTN, XCOWLM, UPPLIM. XINTGL, AINTGL)

The first CALL of SIMPSN should be preceded by a call of SETSMP. ALWERR is the tolerance and is defined as the ratio of the computed error to the value of the integral.

XMAX Is the maximum number (floated) of equally spaced points which the routine will use in attempting to satisfy the tolerance. This number will be used by the routine as set by the user if the number Is even and in the range 6 to 32766. If XMAX Is odd and in that range, it will be treated as if It had been XMAX + 1. If XMAX is greater than 32766, It will be treated as if it had been 32766, and if It is less than 6 it will be treated as if it had been 600.

DEBUG Is a switch which is set to a nonzero value if the user desires to have the Simpson routine printout intermediate information.

FUNCTN is the address of the function which is to compute values of the integrand.

XLOWLM is the floated value of the lower limit of integration.

UPPLIM is the floated value of the upper limit of integration.

XINTGL is the value of the integral obtained.

AINTGL is the value of the integral of the absolute value obtained.

ERROR Is the estimated value of the error obtained.

AERROR is the estimated value of the error of the integral of the absolute value obtained.

(4) SCAN. The subroutine SCAN is used to find the location of some number X in a linearly ordered table. The arguments are:

UN the value whose location is being sought
J if J = 0 the table is considered one dimensional if J = 1 the table Is dimensioned (4, 1)
XLOW the table entry which is closest to, but less than, UN
HIGH the table entry which is closest to, but greater than, UN
KN the Index location of HIGH in TAB
LBH the number of values in TAB

NO if NO = 0, normal exit

if NO = 1, the UN was not found to be within the limits of TAB (1) - TAB (LBH)

if UN is equal to a value in the table, XLOW equals that value, HIGH is set to zero and KN to the index of XLOW.

A detailed procedure for inputing the data to the path program is given below which is preceded by a list of input data symbols:

TMN = Name of temperature table

T = Temperature (^{O}K)

PRS = Name of pressure table

P = Pressure (mm Hg)

NG = Number of gases

XM = Name of gas

AN = a coefficient of I(a, b)

AM = b coefficient of I(a, b)

XMR = Mixing ratio

FE = Mean latitude of path (degrees)

C = Highest altitude of path (meters)

D = Lowest altitude of path (meters)

PHI = Angle subtended by C and D at earth's center (radians)

IDB = Debugging switch

Input Data Format

Temperature Table

Card 1	Column	1-3 The name of the table
All remaining cards		4-63 Contain 5-12 column fields in floating point. The first represents the temperature at the earth's surface, with a total of 261 values.*

Pressure Table — Same as temperature

Mixing-Ratio Data

Card 1	Column	1 The number of gases being used ≦ 4
		Fixed point.
		The following cards through and including mixing ratio are to be repeated for each gas in order of assigned number (1-4)

*The following tables must have 261 values: temperature, pressure, and mixing ratio. Entries 1 through 200 are every 200 m; 201 through 261 are every 1000 m.

Card 2	Column	1-3	Name of gas 1 Right adjusted.
		4-8	a coefficient corresponding to gas 1 ln I (a, b). Floatlng point.
		9-13	b coefficient corresponding to gas 1 ln I (a, b). Floating point.
All remaining cards		4-63	Mixing ratio table for gas 1. 12 Column flelds, floating point, 261 values as for T and P tables. For CO_2, O_3, N_2O, CO, and CH_4 values should be ppm $\times 10^{-4}$. For H_2O values should be $1.225 \times 10^{-4} \times$ g/kg.

The above, starting at card 2, is repeated for each gas used.

Wavelength Data

Card 1	Column	1-4	The value of wavelength for which these calculations are to be made. Floating point.

Path Data (to be repeated for each path)

Card 1	Column	1-4	"Data" indlcating foilowing data as path information.
Card 2		1-12	Latltude (in degrees)
		13-24	Highest path altitude (in meters) measured from earth's surface.
Data in columns 1-48 are in floating point. Data switch in flxed point.		25-36	Lowest altitude (in meters) measured from earth's surface.
		37-48	Angle subtended at earth's center (ln radians).
		50	Data switch right adjusted. If zero, data conslst of reduced optical path for each gas. If 1, it will include the maximum value of the range. A value of 2 will include information from the path calculation.

A complete listing of the main program and all subroutines is presented below. Except for minor modifications for different executive systems, the program can be used directly on any computer capable of handling the FORTRAN language.

MAIN PROGRAM

```
      COMMON ZO,ZR,ZS,PH1,NG,XLAM,NF,JG,RS,AN,AM,Z,ZZ.ZZZ,T,XMR,P,R,IDB,
     1C,D
      DIMENSION R(501),ZZ(501),Z(261),T(261),P(261),XMR(4,261),AN(6),AM(16)
     ZZZ(501),U(4),XM(4)
 1000 FORMAT (4E12.7,12)
 1001 FORMAT (E20.8)
 1002 FORMAT (A3,5E12.7/(3X,5E12.7))
 1004 FORMAT (I1)
 1005 FORMAT (A3,2E5.3/(3X,5E12.7))
 1006 FORMAT (1H1,40X,34HSPECTRAL RADIANCE AND TRANSMISSION)
 1008 FORMAT (1H0,50X,17HTABLES BEING USED//51X,8HPRESSURE,5X,A3/51X,11H
     1TEMPERATURE,2X,A3/(51X,3HGAS10X,A3))
 1013 FORMAT (A6)
 1015 FORMAT (1H-57X4HPATH//42x8HLATITUDET75,E15.6/42x17HRECEIVER ALTITU
     1DET75,E15.6/42x15HSOURCE ALTITUDET75,E15.6/42x15HANGLE SUBTENDEDT7
     25,E15.6/42x24HEMISSIVITY AT THE SOURCET75,E15.6)
F     UGRAND
    4 READ 1002, TNM,(T(K), K=1,261)
      READ 1002, (PRS, (P(K),K=1,261))
      READ INPUT TAPE 7, 1004, NG
      DC 1 J = 1,NG
    1 READ INPUT TAPE 7, 1005, (XM(J),AN(J),AM(J),(XMR(J,K),K=1,261))
      READ INPUT TAPE 7, 1001, XLAM
C                              'DATA' IN COLUMNS 1-4 IMPLIES A NEW PATH
C                              IS TO BE CALCULATED WITH GEOMETRY AND WAVE
C                              LENGTHS FOLLOWING
C
      WRITE OUTPUT TAPE 6,1006
      WRITE OUTPUT TAPE 6,1008, PRS,TNM,(XM(J),J=1,NG)
  100 READ INPUT TAPE 7, 1013, DATA
      IF(DATA - 6HDATA) 4,2,4
    2 READ INPUT TAPE 7,1000, FE,C,D,PH1,IDB
   23 ZO = 19.61330/(3.085462E-6 + 2.27E-7*COS(FE) - 2.E-12*COS(4.*FE))
      ZR = C+ZO
      ZS = D+ZO
      WRITE OUTPUT TAPE 6, 1015,FE,C,D,PH1
      EXT = 0.0
      Z(1)=EXT
      DO 5 J=2,201,1
      EXT=EXT+200.0
    5 Z(J) = EXT
      DO 6 J=202,261,1
      EXT= EXT+1000.
    6 Z(J) = EXT
```

```
C
C                                   CALCULATE PATH
      7   CALL ATMO
          NF = NF
          RS=R(NF)
          DO 9 J =1,NF,1
      9   ZZ(J) =ZZZ(J)-ZO
          NP = RS/200.
          XP = NP
          IF (500. - XP) 10,11,11
     11   IF (XP - 10.) 13,12,12
     13   XP = 10.
          GO TO 12
     10   XP = 500.
     12   XMAX = XP*6.
C                                              R                    N       M
C                                 EVALUATE U  (R) = INTG(M(NG)*(P/PO)  (TO/T)  DR)
C                                           NG      O
C                                 AT 'NP' POINTS FOR EACH GAS
C
    203   CALL SETSMP(1.E-15,XMAX,0.)
          DO 204 I=1,NG,1
          JG = 1
          CALL SIMPSN (UGRAND,R(1),R(NF),UNIT,ABS)
    204   U(I) = UNIT
          IF(IDB) 205,206,205
    205   WRITE OUTPUT TAPE 6, 3002, R(NF),JG,(I,U(I), I=1,NG)
   3002   FORMAT (8HORANGE E14.7,14H INTEGRATION I3,6H GAS I1,8H VALUE E
         114.7,(/45×I1,8×E14.7))
    206   WRITE OUTPUT TAPE 5, 2000, NG,(XM(K),U(K),K=1,NG)
   2000   FORMAT (I1,4(A3,E16.6))
          WRITE OUTPUT TAPE 6, 2001, NG,(XM(K),U(K),K=1,NG)
   2001   FORMAT (1H0.I1,15X,4(A3,E16.8,CX))
          GO TO 100
          END
```

SUBROUTINE UGRAND

```
      FUNCTION UGRAND(X)
      COMMON ZO,ZR,ZS,PH1,EPS,NG,XLAM,NF,JG,RS,CUT,NMN,II,BEX,FAC,DELR,
     1  B,C,D,E,AN,AM,Z,ZZ,ZZZ,T,XMR,P,R,AMD,VK,UK,TAU,FTAU,TAUR,RIN,IDB
      DIMENSION AN(6),AM(6),Z(261),ZZ(501),ZZZ(501),T(261),XMR(4,261),
     1 P(261),R(501),AMD(4,200),VK(4,200),UK(4,150),TAU(4,6,150),
     2 FTAU(4,505),TAUR(505),RIN(505)
      DIMENSION SW(4)
      DZ = TAB(X,R(1),ZZ(1),1,1,1,NF,SW(1))
      IF(DZ-1.E5) 4,6,6
    4 IF (DZ) 20,2,2
    2 DT = TAB(DZ,Z(1),T(1),1,1,1,261,SW(2))
      DP = TAB(DZ,Z(1),P(1),1,1,1,261,SW(3))
      DM = TAB(DZ,Z(1),XMR(JG,1),1, 4,1,261,SW(4))
      DO 3 J=1,4,1
      J = J
      IF(SW(J)-1.0)3,3,7
    3 CONTINUE
    5 UGRAND= DM*((DP/P(1))**AN(JG)*(T(1)/DT)**AM(JG))
      RETURN
    6 I = 261
      J = 0
      GO TO 8
    7 CALL SCAN (DZ,Z,O,X,Y,1,261,XS)
      GO TO (8,9,10,11), J
    8 DZ = Z(I)
    9 DT = T(I)
   10 DP = P(I)
   11 DM = XMR(JG,I)
   13 WRITE OUTPUT TAPE 6, 1000, J
 1000 FORMAT (1HO,12HCHECK SWITCH,12)
   12 GO TO 5
   20 UGRAND = 0.
      RETURN
      END
      WRITE OUTPUT TAPE 6, 1001, X,DZ,DP,DM,UGRAND
 1001 FORMAT (5E20.5)
```

SUBROUTINE ATMO

```
      COMMON R,ZH,ZL,PHIT,EPS,NG,XLAM,NN,JG,RS,OUT,NMN,II,BEX,FAC,A,B,
     1C,D,E,AN,AM,ZZ,Q,Z,T,XMR,P,RH,AMD,VK,UK,TAU,FTAU,TAUR,RIN,IDB
      DIMENSION AN(6),AM(6),ZZ(261),Q(501), Z(501),T(261),XMR(4,261),
     1P(261),RH(501),AMD(4,200),VK(4,200),UK(4,150),TAU(4,6,150),
     2  FTAU(4,505),TAUR(505),RIN(505),U(4,505)
      DIMENSION THT(2), FM(2)
   52 FORMAT(10X,9HPRESSURE=,E12.7,22HERROR IN INTERPOLATION)
   53 FORMAT(10X,12HTEMPERATURE=,E12.7.22HERROR IN INTERPOLATION)
      CALL FTRAP
      TEST = 0.
      1F (ZH-ZL) 142,143,143
  142 ZX = ZL
      ZL = ZH
      ZH = ZX
  143 IF (IDB - 1) 26,26,25
   25 TEST = 1.
   26 CD = ABSF(C-D)
      N = CD/200.
      RNG SQRT(ZL**2+ZF**2-2.*ZL*ZH*COS(PHIT))
      M=RNG/2000.
      1F(M-N)2,3,3
    2 FN=N
      GO TO 4
    3 FN=M
    4 THTH=ARCSIN(ZL*SIN(PHIT)/RNG)
      1F (THTH) 216,205,216
  205 RNG = CD
  216 IF (500.-FN) 215,206,206
  215 FN = 500.
      GO TO 201
  206 IF (FN-10.) 200,201,201
  200 FN = 10.
  201 IF(TEST) 41,41,100
  100 WRITE OUTPUT TAPE 6,101,RNG,FN,THTH
  101 FORMAT(1H1,3(E14.6,2X))
   41 DO 15 KK=1,10
      W=RNG/FN
      PHIS=0
      RH(1)=0
      Z(1)=ZH
      THT(1)=THTH
      K=2.*FN
      NN=1
      Z(1)=Z(1)-R
      EXT=0.0
      ZZ(1)=EXT
      DO 150 J=2,201,1
      EXT=EXT+200.0
```

```
150   ZZ(J)=EXT
      DO 160 J=202,261,1
      EXT=EXT+1000.0
160   ZZ(J)=EXT
      LQ=(Z(1)*261.)/.1E6
 54   PP=TAB(Z(1),ZZ(1),P(1),1,1,1,261,SW)
      IF(SW-1.0)56,56,55
 55   PP=P(LQ)
      WRITE OUTPUT TAPE 6,52,PP
 56   TT=TAB(Z(1),ZZ(1),T(1),1,1,1,281,SW)
      IF(SW-1.0)58,58,57
 57   TT=T(LQ)
      WRITE OUTPUT TAPE 6,53,TT
 58   FMS=1.+(6432.8+294910./(146.-(1./XLAM**2))+25540./(41.-(1./XLAM**2
      1)))*.1E-7
      FM(1)=1.+(FMS-1.)*(1.+(T(1)/273.15))*PP/((1.+(TT/273.15))*P(1))
      Z(1)=Z(1)+R
      DO 11 I=1,K
      NN=NN+1
      RH(I+1)=RH(I)+W
      Z(I+1)=SQRT(W**2+Z(I)**2-2.*W*Z(I)*COS(THT(1)))
  5   PHI=ARCSIN(SIN(THT(1))*W/Z(I+1))
 99   IF (TEST)69,69,110
110   WRITE OUTPUT TAPE 6,111,W,PHI,FM(1),RH(I),Z(I)
111   FORMAT(5(E14.6,1X))
 69   IF(PHI)71,71,40
 71   ZDIFF=Z(I+1)-ZL
      IF(TEST)72,72,140
140   WRITE OUTPUT TAPE 6,141,W,PHI,FM(1),THT(1),RH(I),Z(I)
141   FORMAT (6(E14.6,1X))
 72   IF(ZDIFF-10.)20,20,73
 73   IF(W-ZDIFF)11,11,74
 74   W=ZDIFF
      GO TO 11
 40   Z(I+1)=Z(I+1)-R
      LQ=(Z(I+1)*261.)/.1E6
      PP=TAB(Z(I+1),ZZ(1),P(1),1,1,1,261,SW)
      IF(SW-1.0)62,62,61
 61   PP=P(LQ)
      WRITE OUTPUT TAPE 8,52,PP
 62   TT=TAB(Z(I+1),ZZ(1),T(1),1,1,1,261,SW)
      IF(SW-1.0)64,64,63
 63   TT=T(LQ)
      WRITE OUTPUT TAPE 6,53,TT
 64   FMS=1.+(6432.8+294910./(146.-(1./XLAM**2))+25540./(41.-(1./XLAM**
      12)))*.1E-7
      FM(2)=1.+(FMS-1.)*(1.+(T(1)/273.15))*PP/((1.+(TT/273.15))*P(1))
      Z(I+1)=Z(I+1)+R
      THT(2)=THT(1)+PHI
      IF(1.570796-THT(2))85,61,81
 81   GMA2=ARCSIN(FM(1)*SIN(THT(2))/FM(2))
      GO TO 60
 65   THT(2)=3.1415928-THT(2)
      IF(Z(I)-Z(I+1))86,88,37
```

```
 86   GMA2=ARCSIN(FM(I)*SIN(THT(2))/FM(2))
      GMA2=3.I41592-GMA2
      GO TO 80
 87   GMA2=ARCSIN(FM(2)*SIN(THT(2))/FM(1))
      GMA2=3.141592-GMA2
      TO TO 80
 88   GMA2=3.1415926-THT(I)
 80   PHIS=PHIS+PHI
      DELPHI=PHIT-PHIS
      Y=(PHI*I0.)/W
      IF(DELPHI-Y)9,9,7
  7   IF(DELPHI-PHI)8,8,I0
  8   W=DELPHI*W/PHI
      GO TO I0
  9   ZDIFF=ZL-Z(I+I)
      IF(ZDIFF)79,12,12
 10   FM(1)=FM(2)
      THT(I)=GMA2
      IF(TEST)I1,I1,120
I20   WRITE OUTPUT TAPE 8,I2I,PHIS,DELPHI,W,FM(I),THT(1)
I21   FORMAT(5(E14.6,2X))
 I1   CONTINUE
 I2   IF(ZDIFF-I0.)20,20,I3
 I3   THTL=3.I415926-(THTH+PHIT)
      X=SQRT(ZDIFF**2+RNG**2-2.*RNG*ZDIFF*COS(THTL))
      ALPH=ARCSIN(ZDIFF*SIN(THTL)/X)
      THTH=THTH+ALPH
      GO TO 89
 79   ZDIFF=-ZDIFF
      IF(ZDIFF-I0.)20,20,70
 70   THTH=THTH-.I*ALPH
 89   IF(TEST)I5,I5,I30
I30   WRITE OUTPUT TAPE 6,I3I,THTL,ALPH,THTH,THT(I),FM(I),W,ZDIFF
I31   FORMAT(7(E12.4,IX))
 I5   CONTINUE
 20   WRITE OUTPUT TAPE 8,30,THTH,THT(2)
 30   FORMAT(1H-,37X,9HTHETA(I)=,E12.6,12H  THETA(NN)=,E12.6/8H   INDEX,
     I25X,8HALTITUDE,I8X,24HRANGE FROM HIGHEST POINT,//)
      IF(IDB) 34,38,34
 38   I = I
      WRITE OUTPUT TAPE 6,37. I,Z(I),RH(1),NN,Z(NN),RH(NN)
 37   FORMAT(3XI4,24XE16.8,23XE16.8/I2H. . . . . /3XI4,24XE14.8,23XEI6
     1.8)
      RETURN
 34   DO 35 I=I,NN
      K=NN+I-I
 35   WRITE OUTPUT TAPE 6,36,I,Z(I),RH(I)
 36   FORMAT(3X,I4,24X,E16.8,23X,E16.8)
      RETURN
      END
```

SUBROUTINE SCAN

```
      SUBROUTINE SCAN (UN,TAB,J,XLOW,HIGH,KN,LBH,NO)
      NO = 0
      IF (J) 100,100,200
      DIMENSION TAB (4,I)
100   IF (TAB(I)-UN) 1,28,50
  I   IF (TAB(LBH)-UN) 50,29,2
  2   LHP = LBH
      LLP = I
  3   LTEST = (LHP-LLP)/2 + LLP
      IF (TAB(LTEST) - UN) 5,30,10
  5   LLP = LTEST
      GO TO 15
 10   LHP = LTEST
 15   IF (LHP-LLP-1)50,40,3
 28   LTEST = I
      GO TO 30
 29   LTEST = LBH
 30   KN = LTEST
      XLOW = TAB(LTEST)
      HIGH = 0.
      RETURN
 40   KN = LHP
      XLOW = TAB(LLP)
      HIGH = TAB(LHP)
      RETURN
 50   NO = 1
      RETURN
200   IF (TAB(J,I)-UN) 101,128,50
101   IF (TAB(J,LBH) - UN) 50,129,102
102   LHP = LBH
      LLP = I
103   LTEST = (LHP-LLP)/2 + LLP
      IF (TAB(J,LTEST)-UN) 105,130,110
105   LLP = LTEST
      GO TO 115
110   LHP = LTEST
115   IF (LHP-LLP-1) 50,140,103
128   LTEST =1
      GO TO 130
129   LTEST = LBH
130   KN = LTEST
      XLOW = TAB(J,LTEST)
      HIGH = 0.
      RETURN
140   KN = LHP
      XLOW = TAB(J,LLP)
      HIGH = TAB(J,LHP)
      RETURN
```

Appendix II
COMPUTER PROGRAM FOR CALCULATING ELSASSER BAND-MODEL TRANSMISSIVITY FUNCTION*

Absorption by an Elsasser model has been given as:

$$A = \sinh \beta \int_0^y \exp(-y \cosh \beta) I_0(y)\, dy \tag{108}$$

where $y = \frac{\beta\chi}{\sinh \beta}$ is a function of the properties of an individual line. A simple algorithm, converging for all values of χ and β, can be derived as follows. Let

$$J = \int_0^y \exp(-t \cosh \beta) I_0(t)\, dt$$

Then by expanding the Bessel function into its power series, we obtain

$$J = \int_0^y \exp(-t \cosh \beta) \sum_{n=0}^{\infty} b_n t^n\, dt$$

or

$$J = \sum_{m=0}^{\infty} b_m \int_0^y t^m \exp(at)\, dt$$

where $a = \cosh \beta$. Let

$$a_m = \int_0^y t^m \exp(-at)\, dt$$

Then

$$J = \sum_{n=0}^{\infty} b_n a_n \tag{109}$$

*This expansion was derived by D. Lundholm of Lockheed Missiles and Space Company.

Integrating by parts gives the recursion formula for a_n as

$$a_n = \frac{n}{a} a_{n-1} - \frac{y^n}{a} \exp(-ay)$$

and

$$a_n = \frac{n(n-1)}{a^2} a_{n-2} - \exp(-ay)\left(\frac{y^n}{a} + \frac{ny^{n-1}}{a^2}\right)$$

because

$$b_n = \frac{1}{[(m/2)!]^2 2^m} \qquad \text{for n even} \tag{110}$$

and

$$b_n = 0 \qquad \text{for n odd}$$

Then

$$J = \sum_{n=0}^{\infty} \frac{a_{2n}}{(n!)^2 2^{2n}}$$

where

$$a_0 = \int_0^y \exp(-at)\,dt = \frac{1}{a}[1 - \exp(-ay)]$$

and from the recursion formulas,

$$a_2 = \frac{2}{a^3} - \exp(-ay)\left(\frac{2}{a^3} + \frac{2y}{a^2} + \frac{y}{a}\right)$$

$$a_4 = \frac{24}{a^5} - \exp(-ay)\left[\frac{24}{a^5} + \frac{24y}{a^4} + \frac{12y^2}{a^3} + \frac{4y^3}{a^2} + \frac{y^4}{a}\right]$$

This suggests the following formula for a_n:

$$a_n = \frac{n!}{a^{n+1}}\left[1 - \exp(-ay)\sum_{m=0}^{n} \frac{(ay)^m}{m!}\right] \tag{111}$$

Thus the sum approaches exp (ay) as n approaches infinity and the term in brackets approaches zero. Equations 109-111 then furnish an algorithm solution to equation 108; this algorithm is in convenient form for modern digital computers.

George Oppel wrote a subroutine, ELSR, in Fortran IV for either the IBM 7094 or Sperry Rand 1108. The program uses the above theory and is used by the following sequence of FORTRAN statements to calculate transmission.

$$B2X = \frac{2\pi\alpha_0' S}{d^2} * W * \overline{P} \tag{112}$$

$$BX = S/d * W \tag{113}$$

$$T = 1. - ELSR(B2X, BX) \tag{114}$$

Equations 112-114 can be used to compute transmission for any gas for which the Elsasser model is applicable and the absorption coefficients are in the form noted in equation 112 and 113. Unfortunately, only the methods of Oppel and Bradford are in the required form. Hence, these equations cannot be applied to other methods without some modification of the ELSR program.

SUBROUTINE ELSR

```
      ABSORPTION BY UNIFORMLY SPACED LINES - ELSASSER MODEL
        DIRECT INQUIRIES TO GEO OPPEL, LOCKHEED MISSILES AND SPACE
        COMPANY, SUNNYVALE, CALIF.
      FUNCTION ELSR(Z,BX)
      IF(Z) 3,3,4
    3 ELSR=0.
      RETURN
    4 IF(BX)14,14,2
    2 BETA=Z/BX
      X=BX/BETA
      PI=3.1415926
      IF(X-.01 )5,5,6
    5 IF(BETA-1.)7,20,20
    6 IF(BETA**2/X-100.)22,22,20
   22 IF(X-20.)9,11,11
    9 IF(Z-.01)10,13,13
   11 IF(BX-.9)10,14,14
   20 ELSR=1.-EXP(-BX)
      RETURN
   21 ELSR=SQRT(2.*Z/PI)
      RETURN
   14 U=SQRT(.5*Z)
      ELSR=1.-(1./(1.+U*(.14112821+U*(.08864027+U*(.02743349+U*(-.000394)
     146+U*.00328975)))))**8)
      RETURN
   10 IF(X-150.)7,21,21
    7 FACT=1.
      BES=1.
      BEA=2.
      A=1.
      B=I.
   18 DO 17 I=1,10
      FACT=FACT*FLOAT(I)
      J=2*I-I
      IF(X-5.)23,23,12
   23 BES=BES+(X/2.)**J*(FLOAT(I)+X/2.)/FACT/FACT
      IF(ABS(1.-BEA/BES)-1.E-3)15,16,16
   12 A=A*FLOAT(J)**2
      B=B*(4.-FLOAT(J)**2)
      BES=BEA+(A+(-1.)**I*B)/FACT/(8.*X)**1
      IF(ABS(1.-BEA/BES)-1.E-3)27,16,16
   16 BEA=BES
   17 CONTINUE
   27 ELSR=BES*BETA*SQRT(X/2./PI)
      RETURN
   15 ELSR=BETA*X*EXP(-X)*BES
      RETURN
   13 BA=.5*(1./EXP(-BETA)-EXP(-BETA))
      AB=.5*(1./EXP(-BETA)+EXP(-BETA))
      FACT=1
      Y=BX/BA
      R=EXP(-AB*Y)
```

```
      A2M=(1.-R)/AB
      A=A2M
      AM=2.
          24 I=1,24
      ...LOAT(I)
      T=2.*S
      FACT=FACT*S
      XYZZ=120.*ALOG(2.)
      IF(S*ALOG(Y)-XYZZ/2.)103,103,102
  102 XYZZ=120./T
      Y=2.**XYZZ
  103 CONTINUE
      A2M=T*(T-1.)*A2M/AB**2-R*(Y**T/AB+T*Y**(T-1.)/AB**2)
      A=A+A2M/((FACT)**2*2.**T)
      IF(.002-ABS(A-AM))24,24,25
   24 AM=A
   25 ELSR=A*BA
      RETURN
      END
```

REFERENCES

1. D. E. Burch et al., Infrared Absorption by Carbon Dioxide, Water Vapor, and Minor Atmospheric Constituents, AFCRL Report No. 62-698, The Ohio State University, Columbus, 1962.
2. W. S. Benedict and L. D. Kaplan, "Calculations of Line Widths in H_2O-N_2 Collisions," J. Chem. Phys., Vol. 30, 1959, pp. 388-399.
3. B. H. Winters, S. Silverman, and W. S. Benedict, "Line Shape in the Wing Beyond the Band Head of the 4.3 μ CO_2 Band," J. Quant. Spectry. Radiative Transfer, Vol. 4, 1964, p. 527.
4. G. Plass, "Spectral Band Absorptance for Atmospheric Slant Paths," Appl. Opt., Vol. 2, May 1963.
5. S. R. Drayson, Atmospheric Slant Path Transmission in the 15-μ CO_2 Band, Report No. 5683-6-T, High Altitude Engineering Laboratory, The University of Michigan, Ann Arbor, November 1964.
6. C. Young, "Calculation of the Absorption Coefficient for Lines with Combined Doppler and Lorentz Broadening," J. Quant. Spectry. Radiative Transfer, Vol. 5, 1965, pp. 549-552.
7. D. M. Gates et al., "Line Parameters and Computed Spectra for Water Vapor Bands at 2.7-μ," Nat. Bur. Std. (U. S.), Monograph No. 71, August 1964.
8. W. M. Elsasser, "Mean Absorption and Equivalent Absorption Coefficient of a Band Spectrum," Phys. Rev., Vol. 34, 1938, p. 126.
9. W. M. Elsasser and M. F. Culbertson, "Atmospheric Radiation Tables," Meteorol. Monographs, Vol. 4, No. 23, 1960.
10. G. N. Plass, "Models for Spectral Band Absorption," J. Opt. Soc. Am., Vol. 48, 1958, p. 690.
11. H. Mayer, Methods of Opacity Calculations, unpublished, 1947
12. R. M. Goody, "A Statistical Model for H_2O Absorption," Quart. J. Roy. Meteorol. Soc., Vol. 78, 1952, p. 165.
13. P. J. Wyatt, V. R. Stull, and G. N. Plass, "Quasi-Random Model of Band Absorption," J. Opt. Soc. Am., Vol. 52, 1962, p. 1209.
14. J. King, "Modulated Band-Absorption Model," J. Opt. Soc. Am., Vol. 55, 1965, p. 1498.
15. R. Ladenburg and F. Reiche, "Ueber Selektive Absorption," Ann. Physik, Vol. 42, 1911, pp. 181-203.
16. W. M. Elsasser, Heat Transfer by Infrared Radiation in the Atmosphere, Harvard Meteorological Studies No. 6, Harvard University Press, Cambridge, Mass., 1942.
17. L. D. Kaplan, "Regions of Validity of Various Absorption-Coefficient Approximations," J. Meteorol., Vol. 10, 1953.

18. G. E. Oppef, (Classified Titlc), Technical Report No. LMSC-A325516, Lockheed Missfles and Space Co., Sunnyvale, Cafff., June 1963 (CONFIDENTIAL).

19. P. J. Wyatt, V. R. Stulf, and G. N. Plass, The Infrared Absorptfon of Water Vapor (Final Report), Report No. SSD-TDR-62-127, Vof. II, Aeronutronfc Division of Ford Motor Co., Newport Beach, Calif., 1962, AD 297 458.

20. G. N. Plass and D. I. Fivel, "Influence of Doppfer Effect and Dampfng on Ltne-Absorption Coefficient and Atmospherfc Radfation Transfer," Astrophys. J., Vol. 117, 1953.

21. G. E. Oppei, Lockheed Missile and Space Co., Sunnyvale, Calif., private communications, 1966.

22. G. N. Plass, "Useful Representatfons for Measui ements of Spectraf Band Absorption," J. Opt. Soc. Am., Voi. 50, 1960, pp. 868-875.

23. A FORTRAN Program, "Least-Squares Estimation of Nonlinear Parameters," available as IBM Share Program No. 1426.

24. A. R. Curtis, "A Statistical Model for Water Vapor Absorptfon (Discussfon of Paper by Goody)," Quart. J. Roy. Meteorol. Soc., Vof. 78, 1952.

25. W. L. Godson, "The Computation of Infrared Transmission by Atmospheric Water Vapor," J. Meteorof., Vof. 12, 1955.

26. T. L. Aftshuier, Infrared Transmission and Background Radfation by Clear Atmospheres, Report No. 615D199, Generaf Efectric Co., Phfladefphfa, December 1961.

27. A. Zachor, Near Infrared Transmission over Atmospheric Slant Paths, Report No. R-328, Instrument Laboratory, Massachusetts Instftute of Technology, Cambridge, Jufy 1961.

28. R. O. B. Carpenter, Predicting Infrared Molecufar Attenuation for Long Slant Paths fn the Upper Atmosphere, Scientffic Report No. 1, Geophysical Research Directorate, Air Force Cambridge Research Center, Bedford, Mass., November 1957.

29. W. H. Cloud, The 15 Micron Band of CO_2 Broadened by Nitrogen and Helium (Progress Report) on Contract NOnr 248-01), Johns Hopkins University, Baltimore, 1952.

30. J. N. Howard, D. E. Burch, and D. Wiffiams, Near Infrared Transmission through Synthetic Atmospheres, Geophysics Research Paper No. 40, Report No. AFCRC-TR-55-213, Ohio State Universfty, Columbus, November 1955.

31. L. D. Kaplan and D. F. Eggers, "Intensity and Line Wfdth of the 15 Micron CO_2 Band Determined by a Curve-of-Growth Method," J. Chem. Phys., Vol. 25, 1956, pp. 876-883.

32. G. Yamamoto and T. Sasamori, "Calculation of the Absorptfon of the 15 Micron Carbon Dioxide Band," Sci. Rept. Tohoku Univ., Fifth Ser., Voi. 10, 1959, pp. 37-45.

33. M. Summerfiefd, "Pressure Dependence of the Absorption in the 9.6 Micron Band of Ozone," thesfs, Caffornia Institute of Technology, Pasadena, 1941.

34. C. D. Walshaw, "Integrated Absorption by the 9.6 Mfcron Band of Ozone," Quart. J. Roy. Meteorol. Soc., Vof. 83, 1957, pp. 315-321.

35. G. Yamamoto, "On a Radiation Chart," Sci. Rept. Tohoku Univ., Fifth Ser., Vol. 4, 1952, pp. 9-23.

36. H. A. Daw, Transmission of Radiation through Water Vapor Subject to Pressure Broadening in the Region 4.2 Microns to 23 Microns, Technical Report No. 10, University of Utah, Salt Lake City, 1956.

37. C. H. Palmer, private communication to W. M. Elsasser based on data obtained at the Laboratory of Astrophysics at Johns Hopkins University, 1953.

38. E. E. Bell, Infrared Techniques and Measurements (Interim Engineering Report for Period July-September 1956 on Contract AF 33(616)-3312), Ohio State University, Columbus, 1956.

39. W. T. Roach and R. M. Goody, "Absorption and Emission in the Atmospheric Window from 770 to 1250 cm^{-1}," Quart. J. Roy. Meteorol. Soc., Vol. 84, 1958, pp. 319-333.

40. E. F. Barker and A. Adel, "Resolution of Two Difference Bands of CO_2 Near 10 μ," Phys. Rev., Vol. 44, 1933, p. 185.

41. C. Schaefer and B. Phillips, "The Absorption Spectrum of Carbon Dioxide and the Shape of the CO_2 Molecule," Z. Physik, Vol. 36, 1926, p. 641.

42. H. W. Yates and J. H. Taylor, Infrared Transmission of the Atmosphere, NRL Report No. 5453, Naval Research Laboratory, Washington, 8 June 1960.

43. C. H. Palmer, "Water Vapor Spectra with Pressure Broadening," J. Opt. Soc. Am., Vol. 47, 1957, p. 1024.

44. N. G. Yaroslavsky and A. E. Stanevich, "The Long Wavelength Infrared Spectrum of H_2O Vapor and the Absorption Spectrum of Atmospheric Air in the Region 20-2500 μ (500 - 4 cm^{-1})," Opt. Spectry., Vol. 7, 1959, p. 380.

45. G. Hetiner, R. Pohlman, and H. J. Schumacher, "The Structure of the Ozone Molecule and Its Spectrum in the Infrared," Z. Physik, Vol. 91, 1934, p. 372.

46. H. S. Gutowsky and E. M. Petersen, "The Infrared Spectrum and Structure of Ozone," J. Chem. Phys., Vol. 18, 1950, p. 564.

47. J. Strong, "On a New Method of Measuring the Mean Height of the Ozone in the Atmosphere," J. Franklin Inst., Vol. 231, 1941, p. 121.

48. C. W. Allen, Astrophysical Quantities, University of London Athlone Press, 1955, pp. 117-119.

49. J. H. Shaw, G. B. B. M. Sutherland, and T. W. Wormell, "Nitrous Oxide in the Earth's Atmosphere," Phys. Rev., Vol. 74, 1948, p. 978.

50. S. A. Clough, D. E. McCarthy, and J. N. Howard, "$4\nu_2$ Band of Nitrous Oxide," J. Chem. Phys., Vol. 30, 1959, p. 1359.

51. E. K. Plyer and E. F. Barker, "Infrared Spectrum and Molecular Configuration of N_2O," Phys. Rev., Vol. 38, 1931, p. 1827.

52. D. E. Burch, Ohio State University, Columbus, private communication, 1960.

53. G. Lindquist, Willow Run Laboratories of the Institute of Science and Technology, The University of Michigan, Ann Arbor, private communication, 1966.

54. G. E. Oppel and L. L. List, Atmospheric Transmission from 4 to 5 Microns, Report No. LMSC-A667599, Lockheed Missiles and Space Co., Sunnyvale, Calif., August 1964.

55. W. R. Bradford, Predicting the Molecular Absorption of Infrared Radiation over Atmospheric Paths, Report No. DMP 1422, EMI Electronics, Hayes, Middlesex, England, 1963.

56. W. R. Bradford, T. M. McCormick, and J. A. Selby, Laboratory Representation of Atmospheric Paths for Infrared Absorption, Report No. DMP 1431, EMI Electronics, Hayes, Middlesex, England, 1963.

57. A. S. Green, C. S. Lindenmeyer, and M. Griggs, Molecular Absorption in Planetary Atmospheres, Report No. GOA63-0204, Space Science Laboratory, General Dynamics Corp., San Diego, May 1963.

58. A. S. Green, A Semi-Empirical Formula for Infrared Transmission through the Atmosphere, Report No. ZPH-115, Physics Section, Convair Division, General Dynamics Corp., San Diego, 1961.

59. A. S. Green, Atmospheric Attenuation over Finite Paths, Report No. TDR63-174, Aerospace Corp., San Bernardino, Calif., August 1963.

60. J. A. Rowe, Aerospace Corp., private communication, 1966.

61. R. O. Carpenter, "The Transmission of Hot CO_2 Radiation through Cold CO_2 Gas" (U), Proc. IRIS, Vol. 4, No. 2, May 1959 (CONFIDENTIAL).

62. V. R. Stull, P. J. Wyatt, and G. N. Plass, The Infrared Absorption of Carbon Dioxide (Final Report), Report No. SSD-TDR-62-127, Vol. III, Aeronutronic Division of Ford Motor Co., Newport Beach, Calif., 1963, AD 400 959.

63. G. N. Plass, Transmittance Tables for Slant Paths in the Stratosphere (Final Report), Report No. SSD-TDR-62-127, Vol. V, Aeronutronic Division of Ford Motor Co., Newport Beach, Calif., May 1963, AD 415 207.

64. M. Gutnick, "How Dry Is the Sky?" J. Geophys. Res., Vol. 66, 1961, pp. 286-287.

65. M. Gutnick, "Mean Atmospheric Moisture Profiles to 31 km for Middle Latitudes," Appl. Opt., Vol. 1, 1962, p. 670.

66. J. A. Thomson, "Emissivities and Absorptivities of Gases," Ph.D. dissertation, California Institute of Technology, Pasadena, 1958.

67. A. Thomson and M. Downing, An Investigation of Two Factors in the Infrared Environment of an Artificial Satellite: Earth Background and Atmospheric Transmission in the 2 to 5 Micron Region, Report No. Ph-069-M, Physics Section, Convair Division, General Dynamics Corp., San Diego, 10 April 1960.

68. G. Herzberg, Molecular Spectra and Molecular Structure, Vol. 2: Infrared and Raman Spectra of Polyatomic Molecules, Van Nostrand, 1954, p. 21.

69. T. Elder and J. Strong, "The Infrared Transmission of Atmospheric Windows," J. Franklin Inst., Vol. 255, 1953.

70. F. W. Fowle, "Water Vapor Transparency to Low Temperature Radiation," Smithsonian Inst. Misc. Collections, Vol. 68, No. 8, 1917.

71. F. E. Fowle, "The Spectroscopic Determination of Aqueous Vapors," Astrophys. J., Vol. 35, 1912, p. 149.

72. F. E. Fowle, "Redetermination of Aqueous Vapor above Mount Wilson," Astrophys. J., Vol. 37, 1913, p. 359.

73. F. E. Fowle, "The Nonselective Transmissibility of Radiation through Dry and Moist Air," Astrophys. J., Vol. 38, 1913, p. 392.

74. F. E. Fowle, "Avogadro's Constant and Atmospheric Transparency," Astrophys. J., Vol. 40, 1914, p. 435.

75. F. E. Fowle, "The Transparency of Aqueous Vapor," Astrophys. J., Vol. 42, 1915, p. 394.

76. J. N. Howard, The Absorption of Near Infrared Blackbody Radiation by Atmospheric Carbon Dioxide and Water Vapor (Report No. 1 on Contract DA-44-009-eng-12), Ohio State University Research Foundation, Columbus, 31 March 1950.

77. G. Hettner, "Uber das Ultrarote Absorptionspecktrum des Wasserdampfes," Ann. Physik, Vol. 55, 1918, p. 476.

78. A. Elliott, G. G. MacNeice, and E. A. Jones, Transmission of the Atmosphere in the Near Infrared, Report No. A.R.L./R.2/E600, Admiralty Research Laboratory, Teddington, Middlesex, England, February 1946.

79. A. Elliott and G. G. MacNeice, "The Transmission of the Atmosphere in the 1-5 Micron Region," Nature, Vol. 161, 1958, p. 516.

80. D. F. Fischer and R. Heinz, The Influence of the Spectral Transmission of Optics and Atmosphere on the Sensitivity of Infrared Detectors, USAF Technical Report No. F-TR-2104-ND, Wright Field, October 1946.

81. J. D. Strong, Atmospheric Attenuation of Infrared Radiations (Final Report on Contract OEMsr-60), OSRD Report No. 5986, Cruft Laboratory, Harvard University, Cambridge, Mass., 30 November 1945.

82. H. A. Gebbie et al., "Atmospheric Transmission in the 1 to 14 μ Region," Proc. Roy. Soc. (London), Ser. A, Vol. 206, 1951, pp. 87-107.

83. H. A. Gebhie et al., Atmospheric Transmission in the 1-14 Micron Region, Report No. A.R.L./R.4/E600, T.R.E./T.2129, Admiralty Research Laboratory, Teddington, Middlesex, England, ATI 76 135, December 1949.

84. R. M. Chapman, J. N. Howard, and V. A. Miller, Atmospheric Transmission of fnfrared (Report No. 18 on Contract W-44-099-eng-400), Ohio State University Research Foundation, Columbus, 30 June 1949.

85. R. M. Chapman, J. N. Howard, and V. A. Miller, Atmospheric Transmission of Infrared (Report No. 20 on Contract W-44-099-eng-400), Ohio State University Research Foundation, Columbus, 15 October 1949.

86. R. M. Chapman, J. N. Howard, and V. A. Miller, Atmospheric Transmission of Infrared (Report No. 21 on Contract W-44-099-eng-400), Ohio State University Research Foundation, Columbus, 15 December 1949.

87. R. M. Chapman, J. N. Howard, and V. A. Miller, "The Pressure Dependence of the Absorption by Entire Bands of Water Vapor in the Near Infrared," J. Opt. Soc. Am., Vol. 42, 1952, p. 423.

88. H. Yates, Total Transmission of the Atmosphere in the Near-Infrared, NRL Report No. 3858, Naval Research Laboratory, Washington, 10 September 1951.

89. E. O. Hulbert, Atmospheric Transmission of Infrared Radiation, NRL Report No. 2348, Naval Research Laboratory, Washington, 22 July 1944.

90. Handbook of Geophysics and Space Environments, Air Force Cambridge Research Laboratories, Bedford, Mass., 1965.

91. C. D. Keeling, "The Concentration and Isotopic Abundance of Carbon Dioxide in the Atmosphere," Tellus, Vol. 12, 1960.

92. G. S. Callendar, "On the Amount of Carbon Dioxide in the Atmosphere," Tellus, Vol. 10, 1958, pp. 243-248.

93. E. G. Glueckauff, "CO_2 Content of the Atmosphere," Nature, Vol. 153, 1944, pp. 620-621.

94. S. Fonselious, F. Koroleif, and K. Burch, "Microdetermination of CO_2 in the Air with Current Data for Scandinavia," Tellus, Vol. 7, 1955, pp. 258-265.

95. J. R. Bray, "An Analysis of the Possible Recent Change in Atmospheric Carbon Dioxide," Tellus, Vol. 11, 1959, pp. 220-230.

96. G. S. Callendar, "The Effect of Fuel Combustion on the Amount of Carbon Dioxide in the Atmosphere," Tellus, Vol. 9, 1957, pp. 421-422.

97. A. Adel, "Equivalent Thickness of the Atmospheric Nitrous Oxide Layer," Phys. Rev., Vol. 59, 1941, p. 944.

98. L. Goldberg and E. A. Mulier, "The Vertical Distribution of Nitrous Oxide and Methane," J. Opt. Soc. Am., Vol. 43, 1953, p. 1033.

99. R. M. Goody and C. D. Walshaw, "The Origin of Atmospheric Nitrous Oxide," Quart. J. Roy. Meteorol. Soc., Vol. 79, 1946, p. 496.

100. R. McMath and L. Goldberg, "The Abundance and Temperature of Methane in the Earth's Atmosphere," Proc. Am. Phys. Soc., Vol. 74, 1948, p. 623.

101. R. L. Slobod and M. E. Krogh, "Nitrous Oxide as a Constituent of the Atmosphere," J. Am. Chem. Soc., Vol. 72, 1950, pp. 1175-1177.

102. J. W. Birkeland, D. E. Burch, and J. H. Shaw, "Some Comments of Two Articles by Taylor and Yates," J. Opt. Soc. Am., Vol. 47, 1957, p. 441.

103. J. W. Birkeland, "Determination of Ground Level N_2O," M.S. thesis, Ohio State University, Columbus, 1957.

104. A. L. Bowman, A Determination of the Abundance of Nitrous Oxide, Carbon Monoxide and Methane in Ground Level Air at Several Locations near Columbus, Ohio (Scientific Report No. 1 on Contract AF 19(604)-2259), Ohio State University, Columbus, 1959.

105. W. E. Groth and H. Schierholz, "Photochemical Formation of Nitrous Oxide," J. Chem. Phys., Vol. 27, 1957, p. 973.

106. D. R. Bates and A. E. Witherspoon, "The Photochemistry of Some Minor Constituents of the Earth's Atmosphere (CO_2, CO, CH_4, N_2O)," Monthly Notices Roy. Astron. Soc., Vol. 112, No. 1, pp. 101-124.

107. M. V. Migeotte, "The Fundamental Band of Carbon Monoxide at 4.7 μ in the Solar Spectrum," Phys. Rev., Vol. 75, 1949, p. 1108.

108. J. H. Shaw and J. N. Howard, "A Quantitative Determination of the Abundance of Telluric CO Above Columbus, Ohio," Phys. Rev., Vol. 87, 1952, p. 380.

109. J. H. Shaw and N. Howard, "Absorption of Telluric CO in the 23 μ Region," Phys. Rev., Vol. 87, 1952, p. 679.

110. J. H. Shaw and H. H. Nielson, Infrared Studies of the Atmosphere (Final Report on Contract AF 19(122)-65), Ohio State University Research Foundation, Columbus, 1954.

111. J. H. Shaw, The Abundance of Atmospheric CO above Columbus, Ohio (Contract AF 19(604)-1003), Report No. AFCRC TN 57-212, Ohio State University Research Foundation, Columbus, 1957.

112. J. L. Locke and L. Herzberg, "The Absorption due to Carbon Monoxide in the Infrared Solar Spectrum," Can. J. Phys., Vol. 31, 1953, p. 504.

113. W. Benesch, M. V. Migeotte, and L. Neven, "Investigations of Atmospheric CO at the Jungfraujoch," J. Opt. Soc. Am., Vol. 43, 1953, p. 1119.

114. A. Adel, "Identification of Carbon Monoxide in the Atmosphere above Flagstaff, Arizona," Astrophys. J., Vol. 116, 1952, p. 442.

115. L. Goldberg, "The Abundance and Vertical Distribution of Methane in the Earth's Atmosphere," Astrophys. J., Vol. 113, 1951, p. 567.

116. L. Elterman, "Comparison of O_3 Concentrations," Appl. Opt., Vol. 3, 1964, p. 641.

117. J. London, K. Ooyama, and C. Prabhakara, Mesosphere Dynamics, Geophysics Research Directorate, Air Force Cambridge Research Laboratories, Bedford, Mass., May 1962.

118. Ozone Observations over North America, ed. by W. S. Hering and T. R. Borden, Jr., Environmental Research Paper No. 38, Report No. AFCRL-64-30(III), Air Force Cambridge Research Laboratories, Bedford, Mass., July 1964.

119. T. J. Kowall, Atmospheric Infrared Attenuation Coefficient (AIRAC) Studies (Final Report), Report No. LMSC-805146, R/C N1-175 (65-1), Lockheed Missiles and Space Co., Sunnyvale, Calif., 1 June 1965.

120. B. A. Bannon and L. P. Steele, Average Water-Vapor Content of the Air, Geophysical Memoirs No. 102, Meteorological Office, Air Ministry, England, 1960.

121. E. W. Barrett, E. A. Herndon, and H. J. Carter, "Some Measurements of the Distribution of Water Vapor in the Stratosphere," Tellus, Vol. 2, No. 4, 1950, pp. 302-311.

122. F. R. Barclay et al., "A Direct Measurement of the Humidity in the Stratosphere Using a Cooled Vapor Trap," Quart. J. Roy. Meteorol. Soc., Vol. 86, No. 368, 1960, pp. 259-264.

123. F. Brown et al., "Measurements of Water Vapor, Tritium, and Carbon-14 Content of the Middle Stratosphere over Southern England," Tellus, Vol. 13, No. 3, 1961, pp. 407-116.

124. J. A. Brown and E. G. Pybus, Stratospheric Water Vapor Measurements by Means of a Dew Point Hygrometer, Ballistic Research Laboratories, Aberdeen Proving Ground, Md., 1960.

125. H. J. Mastenbrook and J. E. Dinger, Measurement of Water Vapor Distribution in the Stratosphere, Report No. 5551, Naval Research Laboratory, Washington, 1960.

126. H. J. Mastenbrook and J. E. Dinger, "Disiribution of Water Vapor tn the Stratosphere," J. Geophys. Res., Vol. 66, No. 5, 1961, pp. 1437-1444.

127. D. G. Murcray, F. H. Murcray, and W. J. Williams, Distribution of Water Vapor in the Stratosphere As Determined from Infrared Absorption Measurements (Scientifi: Report No. 1 on Contract AF 19(604)-7429), University of Denver, Denver, 1961.

128. D. G. Murcray, F. H. Murcray, and W. J. Williams, "Further Data Concerning the Distribution of Water Vapor in the Stratosphere," Quart. J. Roy. Meteorol. Soc., Vol. 92, 1966, p. 391.

129. S. Steinberg and S. F. Rohrbough, The Collection and Measurement of Carbon Dioxide and Water Vapor in the Upper Atmosphere, Research Department, Electronics Group, General Mills, Inc., Minneapolis, 1961.

130. G. E. Tucker, An Analysis of Humidity Measurements in the Upper Troposphere and Lower Stratosphere over Southern England, Report No. M.R.P. 1052, Meteorological Office, Air Ministry, England, 1957.

131. E. W. Brewer, Ozone Concentration Measurements from an Aircraft in N. Norway, Report No. M.R.P. 946, Meteorological Office, Air Ministry, England, 1955.

132. N. J. Kerley, "High-Altitude Observations between the United Kingdom and Nairobi," Meteorol. Mag., Vol. 90, No. 1062, 1961, pp. 3-17.

133. Japanese Meteorological Agency, IGY Data on Upper Air (Radiosonde) Observations during World Meteorological Intervals, March 1960.

134. G. E. Oppel and F. A. Pearson, Infrared Model Atmospheres, Lockheed Missile and Space Co., Sunnyvale, Calif., 1963.

135. M. Gutnick, Mean Moisture Profiles to 31 m for Middle Latitudes, Interim Notes on Atmospheric Properties No. 22, Geophysical Research Directorate, Air Force Cambridge Research Laboratories, Waltham, Mass., 1962.

136. G. Lindquist, "A Water Vapor Profile from the CARDE Solar Spectra" (UNCLASSIFIED), in Semiannual Report of the Ballistic Missile Radiation Analysis Center (U) (1 July through 31 December 1964), Volume 1: General Review, Report No. 4613-83-P(1), Institute of Science and Technology, The University of Michigan, Ann Arbor, March 1965, pp. 23-47 (SECRET).

137. S. T. Marks, Summary Report on BRL-IGY Activities, BRL Report No. 1104, Ballistic Research Laboratories, Aberdeen Proving Ground, Md., 1960.

138. D. G. Murcray, University of Denver, private correspondence, September 1966.

139. J. H. Tayler and H. W. Yates, J. Opt. Soc. Am., 1957, Vol. 47, No. 3.

140. C. Cumming et al., Quantitative Atlas of Infrared Stratospheric Transmission in the 2.7 μ Region, Report No. TR 546/65, Canadian Armament Research and Development Establishment, Valcartier, Quebec, Canada.

141. C. B. Farmer, P. J. Berry, and D. B. Lloyd, Atmospheric Transmission Measurements in the 3.5 to 5.5 μ Band at 5200 Meters Altitude, Report No. DMP1578, EMI Electronics, Ltd., London, England, AD 420 215, 1963.

142. G. E. Berlinquette and P. A. Tate, Some Short Range Narrow Beam Atmospheric Transmission Measurements in the Near Infrared, Report No. 420, Defense Research Board, Valcartier, Quebec, Canada, December 1963.

143. D. Markle, Project Lookout III - Stratospheric Infrared Transmission from Airborne Solar Spectra, Part I, Report No. CARDE T.M. 708/62, Defense Research Board, Valcartier, Quebec, Canada, August 1962.

144. D. Murcray, F. Murcray, and W. Williams, Variation of the Infrared Solar Spectra between 2800 cm^{-1} with Altitude, Scientific Report No. 2, University of Denver, Denver, AD 414 638, July 1963.

145. D. G. Murcray, Infrared Atmospheric Transmittance and Flux Measurements (Six-Month Technical Report No. 6), University of Denver, Denver, AD 416 813, July 1963.

146. D. G. Murcray, Infrared Atmospheric Transmittance and Flux Measurements, University of Denver, Denver, AFCRL, January 1964.

147. D. G. Murcray, F. H. Murcray, and W. Williams, "Comparison of Experimental and Theoretical Slant Path Absorptions in the Region from 1400-2500 cm^{-1}," J. Opt. Soc. Am., Vol. 55, No. 10, October 1965.

148. D. G. Murcray, F. H. Murcray, and W. J. Williams, Variation with Altitude of the Transmittance of the Earth's Atmosphere with Grating Resolution, Report No. AFCRL-65-854, University of Denver, Denver, November 1965.

149. T. G. Kyle et al., Absorption of Solar Radiation by Atmospheric CO_2, Report No. AFCRL-65-290, University of Denver, Denver, April 1965.

150. L. L. Abels, A Study of the Total Absorption near 4.5 by Two Samples of N_2O, as Their Total Pressure and N_2O Concentrations were Independently Varied, Scientific Report No. 3, AFCRL-62-236, Ohio State University, Columbus, January 1962.

151. B. Edlen, "The Dispersion of Standard Air," J. Opt. Soc. Am., Vol. 43, 1953, pp. 339-344.

152. R. Penndorf, "Tables of the Refractive Index for Standard Air and Rayleigh Scattering Coefficients for the Spectral Region Between 0.2 and 20 Microns and Their Application to Atmospheric Optics," J. Opt. Soc. Am., Vol. 47, 1957, pp. 176-185.

Security Classification

DOCUMENT CONTROL DATA · R&D

(Security classification of title, body of abstract and indexing annotation must be entered when the overall report is classified)

1 ORIGINATING ACTIVITY (Corporate author) Willow Run Laboratories, Institute of Science and Technology, The University of Michigan, Ann Arbor, Michigan	2a REPORT SECURITY CLASSIFICATION Unclassified 2b GROUP

3 REPORT TITLE

BAND-MODEL METHODS FOR COMPUTING ATMOSPHERIC SLANT-PATH MOLECULAR ABSORPTION

4 DESCRIPTIVE NOTES (Type of report and inclusive dates)

IRIA State-of-the-Art Report

5 AUTHOR(S) (Last name, first name, initial)

Anding, David

6 REPORT DATE	7a TOTAL NO OF PAGES	7b NO OF REFS
February 1967	xiv + 278	152

8a CONTRACT OR GRANT NO.	9a ORIGINATOR'S REPORT NUMBER(S)
NOnr 1224(52) b. PROJECT NO	7142-21-T
c. d.	9b OTHER REPORT NO(S) (Any other numbers that may be assigned this report)

10. AVAILABILITY/LIMITATION NOTICES

This document is subject to special export controls and each transmittal to foreign governments or foreign nationals may be made only with prior approval of the office of Naval Research (Code 421), Washington, D. C. 20360.

11. SUPPLEMENTARY NOTES	12 SPONSORING MILITARY ACTIVITY
	Office of Naval Research, Physics Branch Washington, D. C.

13. ABSTRACT

The general transmissivity equation for computing slant-path molecular absorption spectra is developed and two methods for evaluating this equation, the direct integration and that which assumes a model of the band structure, are discussed. Five band models are discussed and twelve methods for computing molecular absorption based on these band models are presented. Spectra computed by band-model methods are compared with spectra calculated by direct integration of the general transmissivity equation and with open-air field measurements of absorption spectra. Conclusions concerning the capability of band-model methods for predicting slant-path absorption spectra are stated and recommendations for future research are outlined. A summary of open-air field measurements of absorption spectra and laboratory measurements of absorption spectra for homogeneous paths is presented and a computer program for computing the equivalent sea-level path, the Curtis-Godson equivalent pressure, and the absorber concentration for atmospheric slant paths for any model atmosphere is given in appendix I.

DD FORM 1 JAN 64 1473

Security Classification

14. KEY WORDS	LINK A		LINK B		LINK C	
	ROLE	WT	ROLE	WT	ROLE	WT
Atmospheric transmission Molecular Absorption Radiation Attenuation Spectra						

INSTRUCTIONS

1. ORIGINATING ACTIVITY: Enter the nsme and address of the cuntractor, subcontractor, grantee, Department of Defe..e activity or other organization *(corporate author)* iasuing the report.

2a. REPORT SECURITY CLASSIFICATION: Enter the overall aecurity classificstion of the report. Indicate whether "Restricted Data" is included. Marking is to be in accordance with appropriate security regulations.

2b. GROUP: Automatic downgrading is specified in DoD Directive 5200.10 and Armed Forces Indust.ial Manual Enter the group number. Also, when applicable, show that optional markings have been used for Group 3 and Group 4 as authorized.

3. REPORT TITLE: Enter the complete report title in all capital letters. Titles in all cases should be unclassified. If a meaningful title cannot be selected without classification, show title classification in all capitals in parenthesis immediately following the title.

4. DESCRIPTIVE NOTES: If appropriate, enter the type of report, e.g., interim, progress, summary, annual, or final. Give the inclusive dates when a specific reporting period is covered.

5. AUTHOR(S): Enter the name(s) of author(s) as shown on or in the report. Enter last name, first name, middle initial. If military, show rank and branch of service. The name of the principal author is an absolute minimum requirement.

6. REPORT DATE: Enter the date of the report as day, month, year; or month, year. If more than one date appears on the report, use date of publication.

7a. TOTAL NUMBER OF PAGES: The total page count should follow normal pagination procedures, i.e., enter the number of pages containing information.

7b. NUMBER OF REFERENCES: Enter the total number of references cited in the report.

8a. CONTRACT OR GRANT NUMBER: If appropriate, enter the applicable number of the contract or grant under which the report was written.

8b, 8c, & 8d. PROJECT NUMBER: Enter the appropriate military department identification, such as project number, subproject number, system numbers, task number, etc.

9a. ORIGINATOR'S REPORT NUMBER(S): Enter the official report number by which the document will be identified and controlled by the originating activity. This number must be unique to this report.

9b. OTHER REPORT NUMBER(S): If the report has been assigned any other report numbers *(either by the originator or by the sponsor)*, also enter this number(s).

10. AVAILABILITY/LIMITATION NOTICES: Enter any limitations on further dissemination of the report, other than those imposed by security classification, using standard statements such as:

(1) "Qualified requesters may obtain copies of this report from DDC."

(2) "Foreign announcement and dissemination of this report by DDC is not authorized."

(3) "U. S. Government agencies may obtain copies of this report directly from DDC. Other qualified DDC users shall request through

_____."

(4) "U. S. military agencies may obtain copies of this report directly from DDC. Other qualified users shall request through

_____."

(5) "All distribution of this report is controlled. Qualified DDC users shall request through

_____."

If the report has been furnished to the Office of Technical Services, Department of Commerce, for sale to the public, indicate this fact and enter the price, if known.

11. SUPPLEMENTARY NOTES: Use for additional explanatory notes.

12. SPONSORING MILITARY ACTIVITY: Enter the name of the departmental project office or laboratory sponsoring *(paying for)* the research and development. Include address.

13. ABSTRACT: Enter an abstract giving a brief and factual summary of the document indicative of the report, even though it may also appear elsewhere in the body of the technical report. If additional space is required, a continuation sheet shall be attached.

It is highly desirable that the abstract of classified reports be unclassified. Each paragraph of the abstract shall end with an indication of the military security classification of the information in the paragraph, represented as *(TS)*, *(S)*, *(C)*, or *(U)*.

There is no limitation on the length of the abstract. However, the suggested length is from 150 to 225 words.

14. KEY WORDS: Key words are technically meaningful terms or short phrases that characterize a report and may be used as index entries for cataloging the report. Key words must be selected so that no security classification is required. Identifiers, such as equipment model designation, trade name, military project code name, geographic location, may be used as key words but will be followed by an indication of technical context. The assignment of links, rules, and weights is optional.

* U.S. GOVERNMENT PRINTING OFFICE: 1967 O - 249-889